Determination of dipole moments via thermochromic methods

Mathematisch - Naturwissenschaftliche Fakultät
Heinrich - Heine - Universität Düsseldorf

Inaugural - Dissertation

zur Erlangung des Doktorgrades
der Mathematisch - Naturwissenschaftlichen Fakultät
der Heinrich - Heine - Universität Düsseldorf

vorgelegt von

Matthias Heinrich Zajonz
geboren am 16.12.1993 in Recklinghausen

Düsseldorf, 04. Dezember 2024

aus dem Institut für Physikalische Chemie I
der Heinrich - Heine - Universität Düsseldorf

Gedruckt mit der Genehmigung der
Mathematisch - Naturwisselschaftlichen Fakültät der
Heinrich - Heine - Universität Düsseldorf

Referent:	Prof. Dr. Michael Schmitt
Koreferent:	Prof. Dr. Matthias Karg

Tag der mündlichen Prüfung: 10. Januar 2025

Meine Definition von Glück?
Keine Termine und leicht einen sitzen.
Harald Juhnke

Sólo un idiota puede ser totalmente feliz.
Mario Vargas Llosa

Jak to jest, że jest się tym, kim się jest?
Od czego to zależy?
I kim byłby, gdyby został kim innym?
Czesław Miłosz

Contents

Eigenständigkeitserklärung

Hiermit versichere ich, Matthias Heinrich Zajonz, die vorliegende Abschlussarbeit selbstständig und nur unter Verwendung der von mir angegebenen Quellen und Hilfsmittel verfasst zu haben. Sowohl inhaltlich als auch wörtlich entnommene Inhalte wurden als solche kenntlich gemacht. Die Arbeit hat in dieser oder vergleichbarer Form noch keinem anderem Prüfungsgremium vorgelegen.

Datum: _____ Unterschrift: _____

Acknowledgements

Sehr geehrte Damen und Herren es ist vollbracht. Endlich. Finalmente wie der Spanier sagt. Von daher möchte ich mich an dieser Stelle bei einigen Leuten, welche meinen Weg bis zu diesem Punkt begleitet haben, bedanken.

Allen voran möchte ich mich bei meinem Doktorvater Michael Schmitt bedanken, welcher mir die Möglichkeit gab, ganz nach meinem Gusto und in meiner Art und Weise, bei sich im Arbeitskreis zur Promovieren. Zudem danke ich Ihm für die Möglichkeit der Erfüllung eines kleinen Traumes, indem ich für drei Monate in Medellin forschen konnte und dadurch drei Monate am Stück in Südamerika verbringen konnte. Gracias. Besonderer Dank gebührt Michael Schmitt jedoch für seine Art und Weise wie er als Mensch ist - lass dich nicht verändern!

Prof. Dr. Matthias Karg danke ich für die Bereitschaft sich als Zweitgutachter zur Verfügung zu stellen.

Daniela Langer danke ich für die netten Gespräche und dafür, dass Du die perfekte Ergänzung zu Michael bist. Zudem bist Du die Verbündete aus dem Ruhrgebiet und verstehst wie die Dinge, betrachtet durch diese Brille, sind.

Andrea Lotzwick danke ich für die morgentlichen Gespräche und die wunderbare Erledigung aller organisatorischen Sachen.

Michael Schneider danke ich dafür, dass es während deiner Zeit hier niemals langweilig wurde und Du mir einige Male gezeigt hast wie die Dinge hier laufen und natürlich auch für den ganzen Schabernack.

Marie-Luise Hebestreit danke ich, dass Sie mich während der gesamten Zeit als beste Kollegin und als Freundin in diesem besonderen Arbeitskreis begleitet hat - ohne dich wäre es hier wohl nicht Auszuhalten gewesen.

Bedanken möchte ich mich auch beim "Büro der guten Laune" - somit bei Déborah, Mario (Marius) und Mario (Marco) - ihr seid immer für eine gute Ablenkung dagewesen und brachtet ein bisschen Normalität auf unseren Flur.

Spezieller und riesiger Dank gebührt Timon, welcher mich als seit etlichen Jahren als Freund begleitet und immer und in jeglicher Situation für mich da war - auch wenn Du öfters mit meiner Arbeit an der Uni gefremdelt hast.

Zudem gebührt Dank meiner Tante Danusia und auch ganz besonderer Dank - auch wenn er nicht mehr unter uns weilt - meinem Onkel Mi: Dziekujem za wszystko Michasiu.

Der größte Dank gilt meinen Eltern Irena Cecylia Barbara Zajonz und Heinrich Janus Zajonz. Danke dass ihr mich während der gesamten Zeit unterstützt habt und ihr mir viele Möglichkeiten gegeben habt mein Leben zu gestalten. Ohne euch wäre Vieles nicht möglich gewesen.

Übersicht

Dipolmomente repräsentieren die Ladungsverteilung in polaren Molekülen und sind ein Maß für die räumliche Ladungstrennung. Sie richten sich in einem äußeren elektrischen Feld entlang der Feldlinien aus. Dipolmomente von Molekülen sind seit langer Zeit Gegenstand eines regen wissenschaftlichen Interesses in einer Vielzahl von Forschungsgebieten und werden von zahlreichen Wissenschaftlerinnen und Wissenschaftlern untersucht. Während für die Bestimmung von Dipolmomenten im Grundzustand unterschiedliche Messmethoden existieren, die auch eine gute Genauigkeit liefern, stellt die Bestimmung von Dipolmomenten im elektronisch angeregten Zustand eine Herausforderung dar. Obgleich Dipolmomente im elektronisch angeregten Zustand in der Gasphase mit höchster Genauigkeit bestimmbar sind, offenbaren sich bei dieser Bestimmungsmethode rasch deren Limitationen, sobald die Molekülgröße erheblich zunimmt und eine Umsetzung der Untersuchung in der Gasphase nicht mehr möglich ist, da das zu untersuchende Molekül zuvor dissoziiert. An diesem Punkt setzt das zentrale Thema dieser Dissertation an, indem ein Phasenwechsel vorgenommen wird und die Bestimmung von Dipolmomenten im elektronisch angeregten Zustand in der flüssigen Phase erfolgt. Zu diesem Zweck wird der Ansatz der thermochromen Methoden gewählt, da dieser im Vergleich zum Ansatz der solvatochromen Methoden, die erstaunlicherweise, trotz einer Vielzahl von Problemen, nach wie vor eine hohe Verbreitung aufweisen, einige Vorteile bietet.

Als Grundlage der thermochromen Bestimmungsmethoden dienen die solvatochromen Bestimmungsmethoden, welche durch eine Vielzahl von theoretischen und experimentellen Studien mit dem Ziel der Quantifizierung der Lösemitteleffekte auf das gelöste Molekül und somit auf die Auswirkung der gegenseitigen Beziehung von Solvens und Solvat auf die Absorptions- und Emissionsspektren zu einer großen Anzahl von Gleichungen zur Beschreibung dessen führten. Die existierenden Gleichungen beschreiben die Korrelation zwischen der Änderung des Dipolmoments im Grundzustand hin zum Dipolmoment der elektronisch angeregten Zustände und deren Auswirkung auf die Absorption und Emission. In den am häufigsten verwendeten Gleichungen zur Beschreibung dieses Sachverhalts wird auf die lineare Korrelation zwischen dem Stokeshift und der sogenannten Lösemittelpolaritätsfunktion zurückgegriffen. Die zentralen Bestandteile dieser Lösemittelpolaritätsfunktionen sind der Brechungsindex und die Permittivität des verwendeten Lösemittels.

Unter Berücksichtigung der genannten Aspekte wird in der vorliegenden Dissertation ein Forschungsbeitrag geleistet. Im Folgenden erfolgt eine intensive Auseinandersetzung

mit der adäquaten theoretischen Beschreibung der Lösemittelpolaritätsfunktionen sowie der genauen Definition des Temperatureinflusses auf die maßgeblichen Parameter. Innerhalb des Arbeitskreises wurde bereits zuvor, unter Beteiligung des Autors, der invalide Parameter in Form des Onsager-Radius, welcher ein Bestandteil der originalen Lösemittelpolaritätsfunktionen ist, durch das reale Kavitätsvolumen ausgetauscht. Des Weiteren werden Dipolmomente in Lösung von Molekülen bestimmt, die eine gemeinsame Grundstruktur aufweisen, jedoch unterschiedliche Substituenten besitzen, sowie von größeren Molekülen, die in der Gasphase nicht leicht zugänglich sind. In der Gesamtschau dient das Vorgehen dem exakteren Verständnis der Bestimmung von Dipolmomenten im elektronisch angeregten Zustand über Methoden der Thermochromie, der methodischen Optimierung sowie der vertieften Einsicht in die Interaktion zwischen Solvens und Solvat, welche sich maßgeblich in der elektronischen Struktur des zu untersuchenden Moleküls manifestiert.

In Ergänzung zur theoretischen Auseinandersetzung bezüglich der Methode der Thermochromie und der darin enthaltenen Parameter, insbesondere dem Brechungsindex und der Permeabilität, sowie zur experimentellen Bestimmung von Dipolmomenten im elektronisch angeregten Zustand erfolgt eine Bestimmung der Molekülparameter über quantenchemische Rechnungen sowie über die hochauflösende laserinduzierte Fluoreszenzspektroskopie (**H**igh **R**esolution **L**aser - **I**nduced **F**luorescence, HRLIF), sofern die Moleküle durch diese Bestimmungsmethode zugänglich sind. Dies dient dem Zweck, Vergleichswerte zur Verifikation der Ergebnisse aus der Bestimmung in Lösung zu erhalten sowie dem Zweck der Bestimmung zusätzlicher Molekülparameter. Die Berücksichtigung dieser Daten verdeutlicht, dass zum gegenwärtigen Zeitpunkt unter Berücksichtigung des aktuellen Forschungsstandes eine verlässliche Interpretation der Ergebnisse der Dipolmomentbestimmung in Lösung lediglich unter Einbezug dieser Daten gewährleistet werden kann.

Abstract

Dipole moments represent the charge distribution in polar molecules and are a measure of the spatial charge separation. They align along the field lines in an external electric field. Dipole moments of molecules have been the subject of keen scientific interest in a variety of research areas for quite some time and are investigated by numerous scientists. While different measurement methods exist for determining dipole moments in the ground state, which also provide good accuracy, determining dipole moments in the electronically excited state is challenging. Although dipole moments in the electronically excited state can be determined with the highest accuracy in the gas phase, this method of determination quickly reveals its limitations as soon as the molecule size increases significantly and it is no longer possible to carry out the investigation in the gas phase because the molecule to be investigated dissociates beforehand. At this point, the central topic of this dissertation comes into play, in that a phase change is carried out and the determination of dipole moments in the electronically excited state takes place in the liquid phase. For this purpose, the approach of thermochromic methods is chosen because it offers some advantages over the approach of solvatochromic methods, which surprisingly are still widely used, despite of a large number of problems.

The basis of the thermochromic determination methods are the solvatochromic determination methods, which, through a variety of theoretical and experimental studies, have led to the quantification of the solvent effects on the dissolved molecule and thus on the effect of the mutual relationship between the solvent and solvate on the absorption and emission spectra of a large number of equations to describe it. The existing equations describe the correlation between the change in the dipole moment from the ground state to the dipole moment of the electronically excited states and their effect on absorption and emission. The most prominent equations for describing this phenomenon make use of the linear correlation between the Stokes shift and the so-called solvent polarity function. The central components of these solvent polarity functions are the refractive index and the permittivity of the solvent used.

Taking into account the aspects mentioned, a research contribution is made in the present dissertation. In the following, an intensive examination of the adequate theoretical description of the solvent polarity functions as well as the exact definition of the temperature influence on the relevant parameters is carried out. Within the working group, the invalid parameter in the form of the Onsager radius, which is a component of the original

solvent polarity functions, has already been replaced by the real cavity volume with the participation of the author. Furthermore, dipole moments are determined in solution for molecules that have a common basic structure but different substituents, as well as for larger molecules that are not easily accessible in the gas phase. The overall aim of the approach is to gain a more precise understanding of the determination of dipole moments in the electronically excited state using methods of thermochromy, methodical optimisation and a deeper insight into the interaction between solvent and solvate, which manifests itself significantly in the electronic structure of the molecule under investigation.

In addition to the theoretical discussion regarding the method of thermochromism and the parameters it contains, in particular the refractive index and the permeability, as well as the experimental determination of dipole moments in the electronically excited state, a determination of the molecular parameters using quantum chemical calculations and high-resolution laser-induced fluorescence spectroscopy, provided that the molecules can be accessed using this method. This serves the purpose of obtaining comparative values for the verification of the results from the determination in solution as well as the purpose of determining additional molecular parameters. The consideration of these data clarifies that at the present time, taking into account the current state of research, a reliable interpretation of the results of the dipole moment determination in solution can only be guaranteed by including these data.

1. Introduction

Natural sciences, in conjunction with socio-economic factors, constitute the bedrock of the humans civilisational success, and represent the endeavour of humankind, driven by curiosity, to elucidate the phenomena of our environment. The fact that this insatiable appetite for knowledge cannot be satiated is a consequence of the inherent nature of scientific inquiry, whereby with every question that is ostensibly resolved, new questions emerge. The natural sciences are traditionally divided into three distinct fields: biology, physics and chemistry. However, the boundaries between these individual fields are not always clear. It is also unnecessary to draw a clear distinction between the three major areas, since an interplay between all of them is ultimately required in order to answer the previously posed question. Although a question posed at the outset may be decomposed into discrete subcategories, this decomposition allows for precise categorization within a larger conceptual framework.

A closer examination of chemistry reveals that this field of natural science can be classified into three principal subcategories. The three subcategories are as follows: organic chemistry, which is the study of carbon-based compounds; inorganic chemistry, which is the study of compounds that do not contain carbon; and physical chemistry, which is the study of the physical interactions between chemical components. It is also important to note the growing significance of quantum and computational chemistry, which provides a foundation for the three classical fields.

Basic research constitutes an indispensable component of all fields of research. While the results of basic research may initially seem inconsequential, they are nevertheless a fundamental element of all research, providing the basis for the development of new methods, components, and innovations that have or may have a significant impact on our daily lives. Without basic research, it is often impossible to gain an accurate overview of the subject matter, and thus basic research constitutes an indispensable component of all research. A metaphorical comparison can be drawn with the construction of a house. Each individual component of the house, such as a stone, may appear to be of little

importance in isolation. However, it is of great significance when considered in the context of the overall composition of the house. This illustrates the importance of considering the interplay of small things for a large construct.

As a recent development, the concept of the dipole moment of an electron will be introduced at the outset, as the concept of parity will be used later in this work. The term is employed to delineate the spatial distribution of electrical charge, which is a consequence of the behaviour of the electron and its interaction with electromagnetic fields. Moreover, the electric dipole moment of an electron (**EDM**) represents a topic of ongoing investigation. The EDM represents an asymmetry in the electron's charge distribution, indicating that the electron is not perfectly spherically symmetrical. However, according to the Standard Model, this must result in a violation of CP - symmetry, which is the combination of charge conjugation symmetry **C** and parity symmetry **P**. The EDM must be colinear with the magnetic moment, i.e. the spin of the electron. According to quantum field theory (**QFT**) and the Standard Model of particle physics, the EDM is not zero, but extremely small. CP-symmetry is a concept that describes the conservation of physical laws in two dimensions. In the context of charge conjugation symmetry, this implies that the charge of all particles can be exchanged with their antiparticles. Similarly, in the case of parity symmetry, it suggests that physical systems can be observed as if in a mirror, whereby the spatial coordinates can be inverted or a system's behaviour remains unchanged when both symmetries are combined. The addition of time reversal symmetry **T**, which describes the behaviour of physical processes when reversed in time, leads to the CPT theorem. The existence of an EDM demonstrates that the CPT theorem is not wholly valid, as the parity symmetry P is breached due to the preferred orientation along a single axis in the context of space reflection. Furthermore, there is an additional breach of the T-symmetry, as the EDM determines how a particle behaves under time reversal. Furthermore, evidence of the violation of these three symmetries can be observed in nature. An illustration of the breach of C-symmetry can be observed in the decay of neutral pions. The neutral pion is C-symmetric, however, the generated photons violate this symmetry due to the inability to distinguish between a particle and its antiparticle. The violation of P-symmetry can be demonstrated by the decay of polarised ^{60}Co atomic nuclei, whereby the emitted electrons exhibit a preferred direction relative to the nuclear spin axis, and do not emit equally in both directions. The violation of T-symmetry can be demonstrated by the oscillation of kaons K^0 and $\bar{K}^0$, whereby the ratio of the probabilities of $K^0 \to \bar{K}^0$ and $\bar{K}^0 \to K^0$ exhibits an asymmetry [1], [2], [3], [4].

This dissertation is within the field of physical chemistry, specifically within the area of basic research concerning the determination of dipole moments in the in solution. Although the gas phase is commonly regarded as the optimal environment for measuring dipole moments, there are instances in which certain molecules or compounds cannot be accurately measured in this phase. In such cases, a change from the gas phase to a solution is necessary to obtain precise results. It is not possible to measure many molecules or compounds in the gas phase due to the risk of thermal decomposition prior to analysis. This is particularly relevant for large compounds, which require investigation in solution, since they decompose upon vaporization. The current research is specifically focused on determining dipole moments in liquids using thermochromic methods. The absorption and emission spectra are recorded using UV/Vis light in order to investigate the interaction between light and the molecules under investigation, where this interaction is dependent on temperature. The dipole moments in the electronically excited state can be determined with greater precision by recording temperature-dependent absorption and emission spectra and considering the temperature dependency of the parameters in the form of refractive index and dielectric constant. Alternatively, the method of solvatochromism, which remains a widely used approach, may not offer the same degree of accuracy. Moreover, the influence of wavelength dependence cannot be overlooked, as the values of the standard wavelength, which are typically employed, correspond to the $sodium - D\ line$. The molecules under investigation in this study absorb light at significantly lower wavelengths.

The current work's structure is derived from the previously mentioned points and the following overview is provided for the purpose of outlining that structure, starting here with this initial chapter (cf. 1) devoted to a concise introduction to the subject of matter and an elucidation of the reasons why the knowledge of dipole moments is regarded as a scientifically significant concept and why the phase change to the liquid phase is deemed essential, despite the fact that the determination in the gas phase is considered the gold standard in numerous sources. This is followed by a historical overview (cf. 2) of the determination of dipole moments, although it should be noted that this is not intended to be a comprehensive account. The objective is to concentrate on the subject matter encompassed by this dissertation.

Subsequently, a theoretical introduction (cf. 3) to the scientific context of this work is provided. Firstly, the general relationship between light and matter (cf. 3.1) is outlined, before the interaction between light and matter in the UV/Vis range is considered in

greater detail (cf. 3.1.1). As part of this discussion, a detailed consideration of the refractive index (cf. 3.1.2) is also provided, which plays an important role in this specific research area. After that a section outlines the imaging method, namely UV/Vis spectroscopy (cf. 3.2), and provides a general overview of the images and results obtained using this method (cf. 3.3). Moreover, a comprehensive yet accessible overview of the systems to be examined, namely the solutions (cf. 3.4), is provided, along with a detailed account of all pertinent aspects for a full understanding of these systems (cf. 3.4.1, 3.4.2, 3.4.3). Moreover, the influence of specific elements on the anticipated outcomes and the imaging techniques is evaluated (cf. 3.4.4). Next, the central quantity of this dissertation is defined, namely the dipole moments (cf. 3.5). Furthermore, the methods for determining dipole moments in solution are compared (cf. 3.6), which also marks the conclusion of the general theoretical introduction.

Subsequently, the quantum chemical calculation methods (cf. 4) pertinent to this research project are discussed. These represent a point of reference for the quality of the results, serve as comparative values and also provide previously unknown values that are relevant for the evaluation basis of the research results. Following this, an examination of the topic-specific calculation methods (cf. 5) is conducted, which can be considered the central point of this work.

The following chapter (cf. 6) provides a comprehensive account of the experimental setup and its constituent components. The description of the experimental setup is divided into two sections, where one refers to the determination of dipole moments in solution (cf. 6.1, 6.3, 6.4) and the other refers to the determination of dipole moments in the gas phase (cf. 6.5). The individual components of the experimental setups are also discussed in this chapter, separatly for the determination of dipole moments in solution (cf. 6.1.1 to 6.4.2) and separatly for the determination of dipole moments in the gas phase (cf. 6.5.1 to 6.5.6).

After that the next chapter addresses the chemical compounds (cf. 7.1) and the solvent (cf. 7.2) utilized, as the latter constitutes a pivotal element in the determination of the dipole moment in solution. Subsequently, the publications that are pertinent to this dissertation are presented (cf. 8, 9, 10, 11).

This is followed by a summary with an evaluation of the research conducted, and an outlook on the research area addressed in this work (cf. 12, 13). The literature that is

pertinent to this dissertation, along with the lists of graphical and tabular contents, are presented in the end. The work is concluded with an appendix, which contains information relevant to the publications. Technical abbrevations will be explained upon their first use. Additionally, causal connections between statements will be provided to ensure logical flow.

This section focuses on the significance of understanding dipole moments in the electrically excited state. It is a crucial aspect in comprehending fundamental processes and has several practical applications. Within this context, it is necessary to briefly discuss some application areas that rely on knowledge of dipoles in the electrically excited state. These areas include processes such as **F**luorescence / **F**örster **R**esonance **E**nergy **T**ransfer (**FRET**), **T**hermally **A**ctivated **D**elayed **F**luorescence (**TADF**), which can result in technologies like **O**rganic **L**ight **E**mitting **D**iodes Displays (**OLED** - Display), as well as **P**hoto-induced **E**lectron **T**ransfer (**PET**) [5], [6].

FRET is a range of applications used for medical diagnostics, **D**eoxyribo **N**ucleic **A**cid (**DNA**) analysis, and optical imaging. FRET is an electrodynamic phenomenon that happens between a donor molecule, abbreviated as (**D**), in the electrically excited state and an acceptor molecule, abbreviated as (**A**), in the ground electrical state. It should be mentioned that the term **R**esonance **E**nergy **T**ransfer (**RET**) is preferred for the processes mentioned, as these occur without the presence of photons. In this situation, the interaction of dipoles of the donor molecule and acceptor molecule over long distances plays a key role, leading to the donor molecule typically emitting at shorter wavelengths that result in overlapping with the absorption spectrum of the acceptor molecule. The amount of energy transferred relies on several factors, including the overlap of the emission and absorption spectra of the donor and acceptor, the quantum yield of the donor, the relative orientation of the transition dipoles of the donor and acceptor, and the distance between them, which enables RET to act as a tool for measuring distances. RET is commonly employed to determine the distance between two functionalities of a macromolecule, which serve as donor and acceptor. These donor and acceptor groups can be fluorescent moieties in the original macromolecule (intrinsic fluorescence). Nonetheless, extrinsic donors are frequently used due to the possibility to freely select the donor's location and to tailor D-A pairs according to the context [5]. Abeywickrama *et al.* [7] demonstrated the importance of understanding and determining dipole moments in the electrically excited state for modelling and enhancing the efficiency of various processes in the field of FRET/RET. Therefore, exploring methods to determine dipole moments in the electrically excited state

is crucial for improving these processes.

As previously stated, determining dipole moments in the electrically excited state is an important aspect of developing TADF emitters. To start with, it is necessary to mention the mechanism of molecular fluorescence, which is a two-step process from a classical perspective. Initially, absorption results in an electrically excited state, which subsequently relaxes to the ground state through radiation processes, specifically fluorescence. Other paths are not considered in this case. One possible alternative path is the complex **I**nter**S**ystem **C**rossing (**ISC**), which entails excitation of the ground state into the electronically excited triplet state. If the phosphorescence and excitation of the triplet state are very slow, and the energy gap between the excited singlet state and the triplet state is small enough, then a **r**everse intersystem crossing (**rISC**) occurs into the singlet state, followed by radiation process into the ground state. This phenomenon is referred to as **D**elayed **F**luorescence (**DF**) [8]. As shown in the publication by Penfold *et al.* [8], the mechanism of rISC leading to DF was revised by the work of Uoyama *et al.* [9] in 2012 and renamed thermally activated delayed fluorescence (TADF). Furthermore, this study presented high-efficiency electroluminescence employing organic molecules only, generating extensive interest in research, as well as the development of new emitters and comprehension of TADF processes [10], [11], [12], [13]. Despite the prior discovery of OLEDs, this could be labelled as the birth of OLEDs. Understanding and determining dipole moments in the ground state and electronically excited state, as well as their environmental influence, is essential to create new TADF emitters and understand intramolecular absorption and emission processes. These facts and the surrounding material highlight this importance [8].

This section provides a concise overview of the relationships between the dipole moment in the ground state, the dipole moment in the electronically excited state, and the transition dipole moment. This will facilitate a clear understanding of these relationships from the outset. The dipole moment in the ground state, μ_g, describes the distribution of the electrical charge of a molecule in the electronic ground state and is largely determined by the geometry and electron density of the molecule. The dipole moment of the electronically excited state, μ_e, describes the distribution of electrical charge in the molecule subsequent to electronic excitation. The rearrangement of electrons in the excited state gives rise to a change in the dipole moment in the ground state, which may be either more or less pronounced. Furthermore, this process can also result in a significant alteration to the geometry of the molecule. The transition dipole moment (**TDM**) is defined as

the vector representing the interaction of a molecule with electromagnetic fields during a transition between two electronic states. It describes the change in electron density distribution between the ground state and the electronically excited state. Furthermore, the TDM exerts a considerable influence on the probability of radiative transitions, such as absorption and emission. The discrepancy between μ_g and μ_e quantifies the extent of the electron rearrangement in the molecule following excitation. A high TDM signifies a increased probability for radiative transitions. Furthermore, the discrepancy between μ_g and μ_e affects the stability of the excited state and the interaction with the surrounding molecular environment. In the context of FRET processes, a pronounced dependence on these quantities is evident. In the context of non-radiative energy transfer (FRET), the transition dipole moment of the donor and acceptor molecules assumes a pivotal role. The efficiency of the energy transfer is contingent upon the alignment of the two transition dipole moments, which is described by the orientation factor κ^2. The maximum efficiency is achieved when the two TDM are aligned in parallel. Furthermore, the spectral overlap between the emission of the donor (i.e. the excited state μ_e) and the absorption of the acceptor (i.e. the ground state μ_g) is of central importance. It is therefore necessary to match these to each other, which, as a logical conclusion, requires knowledge of the acceptor's μ_g and the donor's μ_e. Furthermore, FRET processes are highly sensitive to the distance between the donor and acceptor, with the transfer probability exhibiting a proportionality of r^{-6} [14], [15]. In the case of thermally activated delayed fluorescence (TADF), it has been demonstrated that knowledge of the dipole moment sizes can enhance the efficiency of organic light-emitting diodes (OLEDs) by minimising non-radiative processes. In the context of TADF materials, it is crucial to ensure that the singlet state S_1 and the triplet state T_1 exhibit a minimal energy difference, ΔE_{ST}. This is achieved by maintaining a spatial separation between electrons and holes, which in turn results in a reduced transition dipole moment, TDM. If the difference between μ_g and μ_e is minimal, the reverse conversion of T_1 to S_1 is facilitated via intersystem crossing, which occurs using the thermal energy kT, which represents the central point of TADF emitters. Moreover, the processes of TADF emitters, in terms of colour rendering and efficiency, are closely related to the influence of the environment on the aforementioned dipole moments [16], [17], [18].

The knowledge of dipole moments in the excited state has a number of applications, which will be discussed in the following paragraphs. Firstly, there is the fundamental property of the interaction with electric fields, which can be described with greater precision by virtue of knowledge of the dipole moment in the excited state. Consequently,

the spectroscopic analysis of molecular structures can be conducted by exploiting the Stark effect, with the knowledge of the dipole moment in the excited state. Furthermore, knowledge of the dipole moments in the excited state facilitates more accurate electrostatic manipulation of molecules. Furthermore, the knowledge of the excited state dipole moment enables the interaction with solvents to be considered in advance, thus allowing the stabilisation of the molecule in polar solvents to be determined. This, in turn, permits conclusions to be drawn about the energetic shift of absorption and emission spectra [19].

In the field of nonlinear optics, an understanding of the dipole moments present in the excited state of molecules is crucial for comprehending their response to intense light fields. In the process of two-photon absorption, whereby two photons are simultaneously absorbed by a molecule in order to reach the excited state, the probability of this process is dependent upon the change in the dipole moment. Moreover, knowledge of the dipole moment in the excited state is crucial for understanding the polarizability of a molecule, which is dependent on the aforementioned dipole moment. This is particularly relevant in the context of nonlinear scattering processes, such as Raman scattering and Hyper - Raman scattering. Moreover, knowledge of the excited-state dipole moment is instrumental in the advancement of third-harmonic generation (**THG**), a nonlinear optical process whereby photons interact with a nonlinear material to produce photons with an energy exceeding that of the initiating photon. This phenomenon is contingent upon the occurrence of higher harmonic vibrations in molecules, which necessitate a modification in the dipole moment. The processes of nonlinear optics, in which excited-state dipole moments play a central role, are employed in the development of optical switches, laser technology and detectors [20], [21].

Furthermore, knowledge of dipole moments in the excited state is of significant importance when working with or investigating reactive intermediate states and chemical reactivity. The distinct electron distribution of molecules in their electronically excited state, which also results in a unique reactivity, offers a promising avenue for the development of novel reactions. By precisely determining the dipole moment of the excited state, it is possible to design reactions that exploit this difference in reactivity. To illustrate, it can be posited that molecules exhibiting a substantial dipole moment in their electronically excited state are inclined to undergo selective reaction with polar reagents. Moreover, knowledge of dipole moments in the excited state is of central importance in the context of photo-induced electron transfers within the field of photochemistry, as well as in the area of photosynthesis. It is also pertinent to mention internal conversion within photochemical processes, whereby

a change in the dipole moment in the excited state can facilitate transitions between states. Furthermore, knowledge of the dipole moment in the excited state is pertinent to the quenching process, whereby one molecule interacts with another and undergoes relaxation, as indicated by a change in the dipole moment [22].

Furthermore, knowledge of excited-state dipole moments is beneficial in the design of materials for optical and electronic applications. To illustrate, the OLEDs previously referenced, along with materials exhibiting a discernible alteration in dipole moment between the ground and electronically excited states, can be calibrated for enhanced light emission and precise coloration. Furthermore, knowledge of the dipole moment in the excited state is of central importance in the design of solar cells, as molecules with a large dipole moment in the excited state facilitate charge separation, thereby enabling electrons and holes to repel each other more strongly. Furthermore, the knowledge of excited-state dipole moments is of great importance in the production of sensors. The objective is to create sensors that are highly sensitive and can undergo significant changes in dipole moment when exposed to external factors such as electric fields, pH levels, and so forth. Such examples include dyes that exhibit alterations in fluorescence intensity or colour in response to external stimuli [23], [24], [25].

Moreover, an in-depth examination of charge separation and exciton formation can be conducted in conjunction with the knowledge of dipole moments in the excited state. Molecules with a high dipole moment tend to maintain the separation of electrons and holes, thereby facilitating the formation of free charge carriers. In organic solar cells, for instance, electrons can be transferred from an excited molecule to an acceptor, which is supported by a high dipole moment. Therefore, knowledge of the dipole moment is of great utility in the design of corresponding molecules. In the field of photovoltaics, as well as in luminescent materials, exciton formation, which is a bound electron-hole pair, plays a central role. Therefore, it is possible to design molecules that have a suitable dipole moment in the excited state, which requires the knowledge of this. This enables excitons to be generated and transported efficiently [26], [27], [28].

The significance of accurate knowledge regarding the dipole moment in the excited state can be classified into four primary categories. It constitutes fundamental research in the field of the interaction between light and matter, material design in the development of sensors, solar cells and OLEDs, chemical control, that is to say, the optimisation of photochemical processes, and technological applications in the field of optical technology and

nonlinear optics. A precise understanding of the dipole moment in the excited state allows for the targeted utilisation of molecular properties, thereby facilitating the development of solutions that are tailored to specific requirements.

2. Historical Background

The determination of dipole moments in solution has a long and varied history, spanning several decades. The process commences with theoretical considerations, subsequently progressing to experimental methodologies and ultimately culminating in the advent of quantum chemical calculations. At the outset of research into dipole moments, the interactions between molecules and an electric field were the primary focus. In this context, Maxwell's theoretical considerations [29] can be regarded as the theoretical foundation for the comprehension of electric dipoles. Although Max Reinganum [30] and Peter Debye [31] both defined the concept of the dipole moment in molecular physics around the same time, Debye is regarded as the founder of the electric dipole moment within molecules. Debye established a correlation between the dielectric constant of a substance and the dipole moment of the molecules it contains, and developed a model to determine the polarizability and the dipole moment as a function of molecular structure.

In the publication [32], Debye posits the theory that the dipole moment is indicative of the asymmetry inherent in the charge distribution of a molecule. Debye devised experimental techniques that enabled the determination of the aforementioned charge distribution through the utilisation of dielectric measurements. The underlying principle of this consideration is that molecules within an electric field experience an alignment that is proportional to the field strength and the dipole moment. This resulted in significant advancements in dielectric measurements for determining dipole moments in solution during the 1920s and 1930s. This principle is primarily based on the measurement of the change in capacitance of a capacitor with the liquid to be examined positioned between the two plates. Consequently, the dipole moment can be calculated by utilising the dielectric constants and the molecular mass. It is important to note that this method of determination was only capable of accessing dipole moments in the ground state.

The scientific description of the Stark effect, which was carried out practically simultaneously by Stark [33] and Lo Surdo [34], initially provided the potential for determining dipole moments in the gas phase and also for determining dipole moments in the electroni-

cally excited state. The transfer of the influence of an electric field on the dipole moment of a dissolved molecule, including mutual interaction and the dependent absorption and emission of the dissolved molecule, was defined almost simultaneously by Kirkwood [35] and Onsager [36]. This, in effect, marks the advent of the determination of the dipole moment in the electronically excited state in solution.

In the 1950s, this prompted a surge of interest within the scientific community, leading to an in-depth examination of the impact of the solvent on the optical properties of the molecules dissolved in it. This investigation culminated in the discovery of the solvatochromic effect and the development of solvatochromic methods for determining dipole moments in solution, utilising this effect. Based on Ooshika's theoretical description and methodology [37], Lippert [38] and Mataga [39] developed the basic solvatochromism equation to describe the relationship between the Stokes shift and the polarity of the solvent, and thus the dipole moment of the dissolved molecule. More precisely, this equation was developed independently by both researchers, but due to its practical similarity, it is commonly referred to as the Lippert and Mataga equation.

Despite its status as a fundamental equation for describing the mutual relationship between the absorption and emission spectra and the polarity of the solvent, the Lippert and Mataga equation has been the subject of criticism regarding its inaccuracy since its inception. Consequently, a multitude of equations have been devised to elucidate this relationship, with the Lippert and Mataga equation serving as a foundation. The most prominent of these are the Bayliss [40], McRae [41], Backshiev [42], Bilot [43], Kawski [44] and Chamma-Vialett [45] equations. However, more recent equations have also been proposed, including the Reichardt [46] equation. In addition to this method of determination, namely solvatochromism, other methods were also developed, including the method of dichroism [47]. However, this latter method did not become widely accepted. The foundation for the methods of thermochromism, which may be considered a modification of the methods of solvatochromism, was initially established by Gryczyński [48] and subsequently elaborated upon by Suppan [49].

In the 1970s, further developments of experimental methods were followed by new theoretical approaches, in particular through the advent of computer simulations and quantum chemical calculations. Among the spectroscopic methods, time-resolved fluorescence techniques are of particular note, as they enabled the determination of the change in the dipole moment between the ground state and the excited state in real time [50], [51]. Furthermore,

the enhanced computing capabilities enabled the inaugural quantum chemical simulations utilising early Hartree-Fock and ab initio methodologies, thereby facilitating the theoretical calculation of dipole moments [52].

From a spectroscopic standpoint, the 1980s and 1990s witnessed a steady advancement in existing techniques, coupled with a heightened precision in the examination of solvent polarity functions and an endeavour to delineate the optimal equation for specific systems, namely polar or non-polar solvents. Furthermore, the precise characterisation of the interactions between the solvent and the solvate, and the state of the dissolved molecule, whether in the ground or an excited state, was also investigated [53]. The potential of computational theoretical determination also saw significant advancement with the advent of density functional theory (**DFT**) [54], [55], time-dependent density functional theory (**TD-DFT**) [56], and the polarizable continuum model (**PCM**) [57] for the theoretical determination of molecular parameters, obviously including dipole moments.

In the field of dipole moment determination in solution, the 2000s can be divided into two main areas according to the method of determination. In the field of computer simulation and quantum chemistry, the DFT method established in the previous decades led to a more precise determination of dipole moments in the ground state and in the excited state through improvements in the calculation method, and was used particularly for complex solvent systems. At the same time, the TD-DTF method was further improved, so that it was increasingly used to understand solvatochromism and to investigate absorption and emission spectra of molecules in different solvents. In parallel, continuum-based solvation models such as PCM were refined. Ultimately, the collective advancement of these methods led to a synergistic outcome [58], [59]. In the experimental field, time-resolved fluorescence spectroscopy has been further refined, with the utilisation of faster detectors and laser pulses enabling the attainment of sub-picosecond time scales. This has facilitated the investigation of the dynamics of excited states [60]. Furthermore, novel spectroscopic techniques based on nonlinear optics have emerged, including femtosecond time-resolved spectroscopy, which has enabled the direct quantification of the interaction between solvents and solvates [61].

As was the case in the preceding decade, the 2010s may be divided into two distinct areas: theoretical calculation and experimental determination, in terms of the advancement of determining dipole moments in solution. In the theoretical determination, this can be observed, on the one hand, in the growing prevalence of multiscale modelling, which

enables the simulation of the microscopic intricacies of the interaction between solvent and solvate while simultaneously accounting for the global solvent effects on the dipole moment to be determined [62]. Moreover, there has been an increase in the combination of quantum chemical and molecular dynamics approaches. This has enabled a realistic modelling of the system, as the quantum chemical calculation of the dissolved molecule and the molecular dynamics simulation of the solvent behaviour have been used to calculate dipole moments with greater accuracy [63], [64]. Significant experimental progress has been made in the field of femtosecond time-resolved spectroscopy, which has greatly increased interest in this experimental method of determination. New experimental methods in the field of nonlinear optics and Raman spectroscopy have provided a further experimental approach to the determination of dipole moments in solution. For example, Hyper-Rayleigh Scattering (**HRS**) can probably be used to determine dipole moments in solution [65]. At the same time, time-resolved Raman spectroscopy has made it possible to shed more light on molecular transitions and the interaction with the solvent [66], [67]. The precise quantification of the solvent environment using fluorescence spectroscopy has allowed the development of tailor-made solvents or the targeted composition of solvents, so that the mutual interaction between solvent and solvate may be more precisely controlled [68], [69].

Although the 2020s are currently in progress and thus cannot be considered as a historical period, the development of a relativly new spectroscopic method for the determination of dipole moments in solution, single-molecule spectroscopy, in recent years merits brief discussion. This spectroscopic method enables the study of the behaviour and interaction of individual molecules under defined conditions. The method can be employed to quantify minute alterations in the dipole moment through the utilisation of ultrashort laser pulses for excitation. This enables the direct tracking of the transition between the ground and electronically excited states, with the corresponding fluorescence changes providing information about the change in the dipole moment during this process. The advantage of this method is that it allows for the identification of heterogeneous effects, which ultimately leads to a more accurate description of the interaction between solvent and solvate. Moreover, this method enables the measurement of dipole moment behaviour in the vicinity of interfaces, such as cells or nanostructured materials [70], [71], [72].

3. Theoretical Background

This section focuses on the theoretical background essential for this dissertation to enhance its comprehension. The structure of this section follows the principle of starting from small to large, with some additional information, where important components of the calculation methods (cf. 5) are also discussed. At the beginning, the interaction between light and matter (cf. 3.1) is briefly discussed, followed by a specification of this consideration with regard to UV- / Vis - spectroscopy (cf. 3.2). Subsequently, absorption and emission spectra (cf. 3.3), as a central component of this work, are discussed, followed by a discussion of solutions (cf. 3.4). Finally, the central topic of dipoles (cf. 3.5) is discussed and a comparison is made between thermochromic and solvatochromic methods (cf. 3.6).

3.1. Behavior of light vs. matter

In order to provide an overview of the subject matter, the interaction between light and matter can be classified into four principal categories, each of which can be further delineated into more detailed subcategories. These categories are defined as refraction, reflection, scattering and absorption. If this interaction is considered from the perspective of the intensity of the incident light at a 90° angle, the four aforementioned blocks can be combined with one another using the following equation 3.1, which is the rough simplification of the intensity reduction equation.

$$I = I_0 - I_{refraction} - I_{reflection} - I_{scattering} - I_{absorption} \tag{3.1}$$

In this context, the variable I represents the intensity of the light following the interaction, while I_0 denotes the initial intensity of the irradiated light and I_i the intensity of the respective interaction i.
Absorption represents the process by which light energy is absorbed by matter, whereby electrons are excited to a higher energy state. This is subsequently associated with the

phenomenon of emission, whereby light energy is released by matter as electrons return from the excited state to a lower energy state. Reflection is defined as the process by which light waves are reflected back from a material surface, with the angle of incidence corresponding to the angle of reflection. The phenomenon of refraction describes the process by which the direction of light waves is altered due to the differing optical densities of the materials involved. The deflection of light waves in different directions as a consequence of their interaction with minute particles of matter is referred to as scattering. Diffraction may be defined as the deflection of a light wave due to an obstacle. Polarisation describes the specific orientation of the light wave subsequent to its interaction with matter. In light of these diverse interactions, it is possible to view light as a collection of photons, which quantize energy and exhibit the characteristics of waves. In conclusion, the diverse interactions of light with matter result in a quantum mechanical description of light, characterised by a wave-particle duality. The wave character of light is exemplified by phenomena such as diffraction, interference, and wavelength. On the other hand, the particle character of light is evidenced by the photoelectric effect and the Compton effect. The wave-particle duality gives rise to the Heisenberg uncertainty principle, which states that certain pairs of physical quantities, exemplified by position and momentum in the classical context, cannot be determined simultaneously with arbitrary precision. All this can be demonstrated experimentally by the double slit experiment, whereby photons, for example, traverse the double slit in a manner analogous to particles, yet exhibit an interference pattern consistent with a wave when detected [5], [73].

Given that light constitutes a component of the electromagnetic spectrum, it is imperative to include an examination of the properties of electromagnetic waves in order to provide a comprehensive description. Electromagnetic waves are defined as propagating disturbances of the electromagnetic field, whereby the electric and magnetic fields oscillate perpendicular to each other. This wave carries energy, which in the case of light are photons. Photons are the fundamental units, quanta, of the electromagnetic field. Some of the key properties of electromagnetic waves can be employed to characterise them. It is first necessary to mention the fact that electromagnetic waves are transverse waves, whereby the oscillations of the electric and magnetic fields are perpendicular to the direction of propagation of the wave. In a vacuum, the speed of electromagnetic waves is equivalent to the speed of light c. However, this value is reduced when the medium is altered, as discussed in section 3.1.2. The spectrum of electromagnetic waves encompasses a range from low-frequency radio waves to high-frequency gamma rays, with the visible light spectrum situated within the wavelength range of approximately 400 to 700 nm. The wavelength of a wave is defined as the distance between two identical consecutive points. The energy of a photon is directly

proportional to the frequency of the wave, as described by the equation $E = h \cdot f$, where E is the energy, f the frequency and h the Planck constant. The term frequency is used to describe the number of oscillations that occur in a given period of time, typically expressed in hertz Hz. Furthermore, light or electromagnetic waves may be polarised, whereby the oscillation of the electric field is preferably aligned in one direction. The polarisation may be linear, circular or elliptical [73].

3.1.1. Absorption and Fluorescence

A more detailed examination of the absorption processes is now to be given, as this constitutes one of the principal topics of this dissertation. Furthermore, the processes of fluorescence will be considered, but the discussion will commence with absorption, as this precedes the processes of fluorescence. The absorption of electromagnetic waves by molecules results in a reaction that corresponds to the energy of the electromagnetic wave in question. This reaction can be identified through the measurement of alterations in specific parameters. The fundamental principle that underlies this phenomenon is the principle of energy conservation. The following relationships can be demonstrated as examples, considered in accordance with the energy introduced by the light. In the initial stages, with the absorption of microwaves by molecules, the rotation of the corresponding molecules is initiated. Furthermore, the excitation of molecules by infrared radiation results in the excitation of the vibration of the corresponding molecule. In this instance, the return of both excitations to the optimum of the respective molecule is facilitated by the release of heat energy. The presence of a permanent electric dipole moment within the molecule is a prerequisite for microwave excitation, as this enables the molecule to interact with the microwave's electric field. This results in the excitation of rotational transitions in the molecule, which thus alternates between different rotational transitions. The prerequisite for excitation by infrared radiation is the presence of vibratory bonds within the molecule, which can interact with the electric field of the infrared radiation during the vibration, thus initiating a change in the dipole moment and resulting in vibrational transitions. Moreover, the frequency of the radiation must correspond with the natural vibration frequency of the molecular bond. At the opposite end of the electromagnetic spectrum, X-rays serve as an illustrative example. In this instance, the excitation of inner core electrons results in their ionisation or promotion into higher-energy unoccupied orbitals. Subsequently, the excitation may result in either X-ray fluorescence or the Auger effect. In the case of X-ray fluorescence, an electron from a higher orbital falls into the gap that has been created and emits energy in the form of a photon. In contrast, in the Auger effect this energy is

transferred to another electron, enabling it to also leave the atom.
The UV/Vis range occupies a position approximately midway along the electromagnetic energy scale. This range can be defined in terms of the wavelength of light that is visible to the human eye. As an electromagnetic wave, UV/Vis radiation induces an excitation of the valence electrons of the corresponding molecules. The valence electrons transition from a ground state to an electronically excited state, which necessitates that the absorbed light energy be specific to each molecule and must at least correspond to the distance of the energy gap between the ground state S_0 and the first excited state S_1. The absorbed energy is the potential energy of the respective molecule and is responsible for the characteristic absorption spectra of molecules. Excitation in the UV/Vis range is contingent upon the presence of electrons occupying either the π or the n orbitals. Following excitation in the π orbitals, the π electrons undergo a transition into the antibonding $\pi*$ orbitals, which is known as the $\pi \rightarrow \pi$ transition. Concurrently, the n electrons transition from the n orbitals into the antibonding $\pi*$ orbitals, which is referred to as the $n \rightarrow \pi$ transition. Excitation of the σ electrons is a relatively uncommon occurrence, as this phenomenon occurs in the ultraviolet range of high energy, which consequently gives rise to an $\sigma \rightarrow \sigma$ transition.

The absorption A of a molecule, can be described by the Beer-Lambert law. This is done by utilising equation 3.2, where the intensity of the incoming light I_0 is correlated with the intensity of the outgoing light I. Furthermore, the absorption, reflection and scattering losses associated with the apparatus are considered in that equation.

$$A = log\left(\frac{I_0}{I}\right) = \epsilon \cdot c \cdot I \tag{3.2}$$

In the case of high-precision absorption measurements, however, this fact is expressed as the probability of photon absorption. Consequently, the quantity I_0 represents the intensity of the light observed in the reference measurement, whereas the quantity I represents the intensity of the light observed in the sample measurement. This results in the probability of photon absorption by the molecule under examination, represented by the number of molecules in the sample, $[S]$, and the distance travelled by the light through the sample, l. This probability is expressed by the proportionality factor κ.

$$\begin{aligned} \frac{dI}{dl} &= -\kappa \cdot [S] \cdot I \\ \frac{dI}{I} &= -\kappa \cdot [S] \cdot dl \end{aligned} \tag{3.3}$$

In light of the theoretical considerations, which assume the presence of infinitely thin layers, the previously listed equation is integrated in the practical application.

$$\begin{aligned} \int_{I_0}^{I} \frac{dI}{I} &= -\kappa \cdot \int_{0}^{l} [S] \cdot dl \\ ln\frac{I}{I_0} &= -\kappa \cdot [S] \cdot l \end{aligned} \tag{3.4}$$

In the context of UV/Vis measurements, the probability factor κ is replaced by the factor $\epsilon(\lambda)$, which is specific to the type of measurement. This results in the molar absorption coefficient, which is dependent on both the molecule and the wavelength. In accordance with the Beer-Lambert law, the following equation 3.5 is derived:

$$\frac{I}{I_0}(\lambda) = e^{-\epsilon(\lambda)\cdot[S]\cdot l} \tag{3.5}$$

In the context of this dissertation, the values of $[S]$ and l are known during the measurements, and the quantity to be determined is ϵ. However, it should be noted that this is not being calculated as an absolute value, but rather as the energy of the absorbed photon at the absorption maximum.

Given the preceding analysis of the absorption process in the UV/Vis range that precedes fluorescence, the following section will address the processes of fluorescence in this same range, occurring following excitation by electromagnetic waves in the form of light.
Fluorescence represents one of the physical processes that can occur in molecules subsequent to light excitation within the UV/Vis range. To be more precise, it is the emission of energy in the form of light, since the molecule is excited to an electronically excited

state after absorption, resulting in a transition from the ground state S_0 to the first excited state S_1. The emission of energy in the form of light, which returns the molecule to its ground state, typically occurs in a spectral range of longer wavelengths than that of the absorbed radiation. This phenomenon is referred to as a Stokes shift. In the excited state, the molecule possesses a greater degree of energy than it does in the ground state, which, however, results in increased instability. To release this excess energy, a series of processes ensue, including non-radiative transitions, fluorescence, and energy transfer. Within the excited state, the molecule undergoes rapid vibrational relaxation, which is non-radiative and occurs on a femtosecond to picosecond timescale. The energy released in this process is in the form of heat. According to the Kasha rule, fluorescence always occurs from the lowest vibrational level of the excited state. Furthermore, the energy release during vibrational relaxation results in a longer wavelength than the wavelength of the absorbed light. Consequently, the aforementioned Stokes shift is observed.

$$\begin{aligned} \Delta E_{photon} &= E_{out} - E_{in} \\ &= h(\nu_{out} - \nu_{in}) \\ &= hc\left(\frac{1}{\lambda_{out}} - \frac{1}{\lambda in}\right) \\ \lambda_S &= |\lambda_{out} - \lambda_{in}| \end{aligned} \tag{3.6}$$

The Stokes shift is a distinctive feature of each molecule. In addition, the fluorescence lifetime, defined as the time a molecule spends in the excited state prior to returning to the ground state and emitting a photon, represents another molecule-specific characteristic. The quantum yield is employed as an indicator of the efficiency of fluorescence, whereby the number of emitted photons is related to the number of absorbed photons. The process of fluorescence quenching refers to the reduction in the intensity of fluorescence. The quenching effects that occur can be classified into three main categories: dynamic quenching, which involves the collision of a fluorescent molecule with a quencher molecule, resulting in the release of energy in the form of heat; static quenching, which refers to the formation of a complex between the fluorescent molecule and the quencher molecule, leading to a reduction in the concentration of fluorescent molecules; and finally energy

transfer, or more precisely, resonance-energy transfer, which occurs in the non-radiative transfer of the energy of the excited state of the donating fluorescent molecule to a second accepting molecule and can be described by the phenomenon of Förster resonance energy transfer (**FRET**). Fluorescence can be influenced by external factors, including temperature, solvents and pH.

Fundamental principles of Kasha's rule were first articulated in 1950 by the eponymous chemist Michael Kasha and serve as a set of guidelines for processes of spontaneous emission. In essence, the Kasha rule states that the absorption of photons in the ground state S_0 into any excited state S_1 can occur, contingent upon the irradiated wavelength, followed by non-radiative internal conversion processes, which ultimately reach the lowest excited state. Once this lowest excited state is reached, complete relaxation to the ground state can occur through radiative processes, which can be either fluorescence or phosphorescence [74]. It is important to note that these conclusions are based on purely empirical observations. This means that there is a possibility that radiation processes may occur from the excited state S_2, if there is a large energy gap ΔE between the S_2 state and the S_1 state. This is in accordance with the findings presented in [75]. An extension to the Kasha rule was formulated by Sergei Vavilov and relates to the fluorescence quantum yield, which is independent of the irradiated excitation wavelength and thus has no influence on the emission wavelength. This extension is known as the Kasha-Vavilov rule [76]. However, as with the Kasha rule, there are exceptions to the Kasha-Vavilov rule, as determined by Robert J. Longfellow and others for benzene vapour [77]. The Kasha rule is derived as follows:

$$\frac{k_L}{k_{IC}} = \frac{I_{S^n} \rightarrow}{I_{S' \rightarrow S}} < 10^{-4}$$

$$\chi = \frac{\Phi_P}{\Phi_F} = \frac{k_{IS}}{k_F} \approx \frac{10^7}{10^8} = 0,1 \tag{3.7}$$

$$\int \epsilon dv = \frac{I}{8\pi c v^2 n^2} \cdot \frac{g_u}{g_l} \cdot \frac{I}{\tau_L}$$

From this consideration according to Kasha, the following time scales of the processes result: $\frac{I}{k_{IC}} < 10^{-4}\ s$, $\frac{I}{k_L} < 10^{-13}\ s$, $\frac{I}{k_{IS}} < 10^{6}\ s$ and $\frac{I}{k_{IC}} < 10^{-7}\ s$. The rate constant for spontaneous luminescence is represented by k_L, the rate constant for internal conversion by k_{IC}, the intensity of spontaneous emission by $I_{S^n} \rightarrow$, the intensity of fluorescence by

$I_{S' \to S}$, the ratio of intersystem crossing by χ, the ratio of phosphorescence to fluorescence ance under continuous simultaneous excitation by $\frac{\Phi_P}{\Phi_F}$, the ratio of the rate constants of intersystem crossing and fluorescence is represented by $\frac{k_{IS}}{k_F}$, the dielectric constant is represented by ϵ, the wavenumber is represented by ν, the speed of light is represented by c, the refractive index is represented by n and the lifetime of the luminescence is represented by τ_L.

The Jablonski diagram, initially conceptualised by Aleksander Jabłoński [78], is employed to visualise photophysical processes, encompassing the diverse electronic states of a molecule and the potential transitions between these states, such as those occurring during absorption and emission.

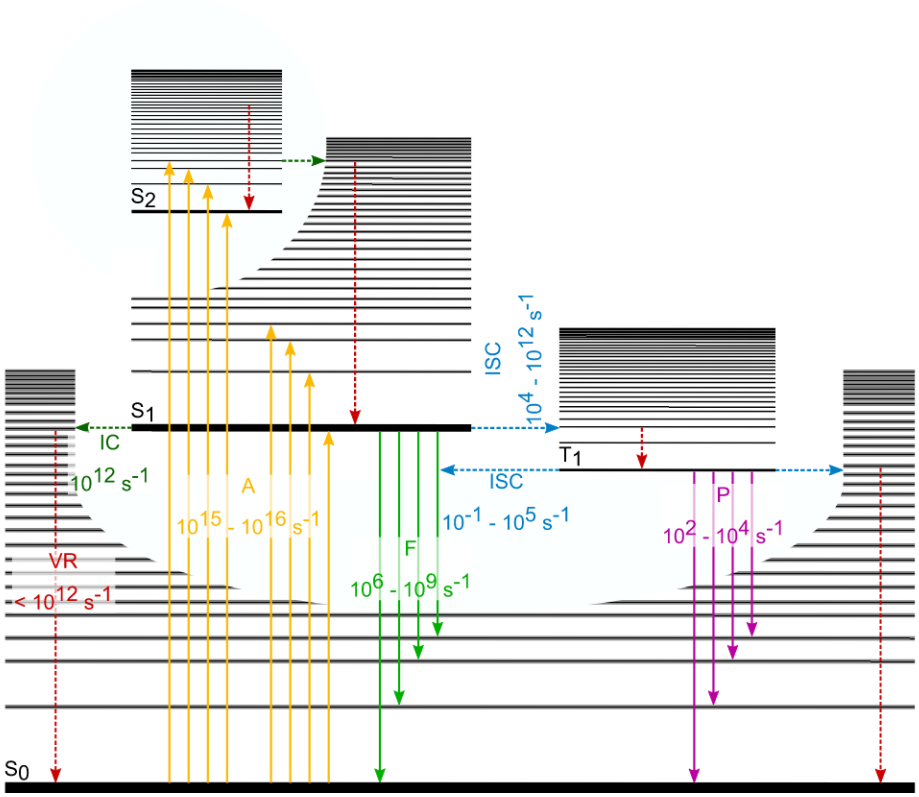

Figure 3.1.: Schematic representation of the Jabłoński diagram, a model for the representation of typical processes that occur following light excitation. The representation includes the approximate time scales of the respective processes. Solid lines indicate the occurrence of radiative processes, whereas dashed lines indicate the occurrence of non-radiative processes. Following abbreviations are used: S_0 represents the ground state, S_i the excited singlet state, T_1 the excited triplet state, A the process of absorption, F fluorescence, P phosphorescence, VR vibrational relaxation, IC internal conversion and ISC intersystem crossing.

In the following section, a more detailed analysis of the individual processes illustrated in Figure 3.1 will be presented, with the exclusion of any discussion on absorption processes, which were addressed in an earlier section.

Vibrational Relaxation

Vibrational relaxation is a pivotal process that typically supersedes all others. It occurs within a time frame of approximately $10^{-12}s^{-1}$ following light excitation. The reason of the vibrational relaxation process is to attain a lower vibrational state within the molecule. Energy transfer to the surrounding environment occurs via collisions and/or vibrational coupling, which is also referred to as collision relaxation. In formal terms, the transfer of heat energy is a consequence of this process. In consideration of the aforementioned rule of Kasha, this process is also pivotal for the return from an electronically excited state to the ground state.

Internal Conversion

Internal conversion is employed to describe isoenergetic, radiation-free transitions between two states of the same multiplicity and occurs within a time frame of approximately $10^{-12}s^{-1}$. This enables the higher vibrational states of an excited singlet state to initially decay into the vibrational ground state of the excited singlet state by vibrational relaxation, and subsequently transition to a higher vibrational state of a lower excited singlet state via internal conversion. This process also contributes to the fulfilment of the Kasha rule. To illustrate, excitation occurs in S_2 followed by vibrational relaxation into the ground state of S_2, whereupon a transition by internal conversion into S_1 occurs, and after subsequent vibrational relaxation into the ground state of S_1, the process of fluorescence into the ground state S_2 takes place. In the event of a minor energy disparity ΔE between the S_1 and S_0 states, the processes of internal conversion and fluorescence are in direct competition with one another. Consequently, the probability of internal conversion increases as the energy gap between the two states in question decreases.

Intersystem Crossing

The process of intersystem crossing represents an isoenergetic, non-radiative transition between two states of disparate multiplicity. The transition between the excited singlet state S_1 and the excited triplet state T_1 provides an illustrative example of transitions between different multiplicities. As intersystem crossing is a forbidden process (in the sense that it is not completely impossible, but very unlikely), this has an effect on its time constant, which is in the long-lasting range of approximately $10^4 - 10^{12}\ s^{-1}$. In order

for a transition between two different multiplicities to occur, a spin reversal must take place. This gives rise to an interaction between the magnetic moment of the spin and that of the associated orbital, namely spin-orbit coupling. Three possibilities exist for the relaxation of the triplet state to the ground state. A possibility is that another intersystem crossing into a high vibrational state of ground state can occur. Alternatively, when the energetic difference ΔE between the triplet state T_1 and the excited singlet state S_1 is minimal, an intersystem crossing into the S_1 state can occur, which is responsible for the phenomenon of delayed fluorescence. Lastly, a radiative transition from T_1 to S_0 in the form of phosphorescence is a further possibility.

Fluorescence

Fluorescence is defined as the process of radiative depopulation of the excited singlet state to the ground state. The energy of the emitted photon is indicative of the specific energy gap between the two states. The energetic shift that occurs between the absorption of S_0 in S_1 and the emission of S_1 in S_0 is referred to as the Franck-Condon shift. In order to satisfy Kasha's rule, some of the aforementioned processes of internal conversion must precede the phenomenon of fluorescence. Fluorescence is the slowest process following the photoelectric excitation of a molecule, occurring on a timescale of approximately $10^6 - 10^9\ s^{-1}$.

Phosphorescence

The phenomenon of phosphorescence is simultaneous to that of fluorescence. However, the transition occurs from the excited triplet state T_1 to the ground state S_0. In the majority of cases, an intersystem crossing occurs prior to the onset of phosphorescence, as direct excitation from the ground state to the triplet state is a possibility, albeit an exceedingly rare one. Given that the excited triplet state is typically less energetic than the excited singlet state, the wavelengths of the emitted radiation also differ. The longer lifetime of the excited triplet state allows for more sustained fluorescence processes, which can persist for up to several seconds.

In light of the elucidations pertaining to the rule of Kasha and the qualitative synopsis of the individual processes within the Jabłoński diagram, the decay of the excited state can be discerned through the decay of S_1. Following the absorption of light, the temporal development of the excited state S_1 can be described in most cases by a first-order kinetic model, whereby the population n of S_1 at the time t is considered.

$$n(t) = n_0 \cdot e^{-k_{S_1} \cdot t} \tag{3.8}$$

The rate constant, designated as k_{S_1}, is the primary determinant of the observed decay. This rate constant is comprised of additional rates, which can be derived from the Jablonski diagram. These are the rates of competing processes, namely fluorescence, internal conversion and intersystem crossing.

$$k_{S_1} = k_F + k_{IC} + k_{ISC} \tag{3.9}$$

Subsequently, the lifetime of the excited state can be calculated by the following equation.

$$\tau_{S_1} = \frac{1}{k_{S_1}} \tag{3.10}$$

Based on the aforementioned rate constants, the fluorescence quantum yield, defined as the ratio of emitted to absorbed radiation, can also be calculated.

$$\Phi_F = \frac{k_F}{k_F + k_{IC} + k_{ISC}} \tag{3.11}$$

A more exact analysis of the pure transitions involved in the processes of absorption and/or fluorescence can be conducted on the basis of the Franck-Condon principle. The principle describes the probability of transitions between the electronic states of a molecule and is based on the assumption of vertical transitions. The foundation of the Franck-Condon principle is the Born-Oppenheimer approximation, which pertains to the substantial mass disparities between atomic nuclei and electrons. This mass difference gives rise to the fact that the speed of movement of atomic nuclei is significantly lower than that of electrons. Consequently, atomic nuclei are unable to respond to electronic transitions and thus remain in their initial state, which is nevertheless modified by the newly established force field. This adjustment occurs through a change in distance and through vibration, resulting in a

shift in the equilibrium state of the excited state towards the ground state.

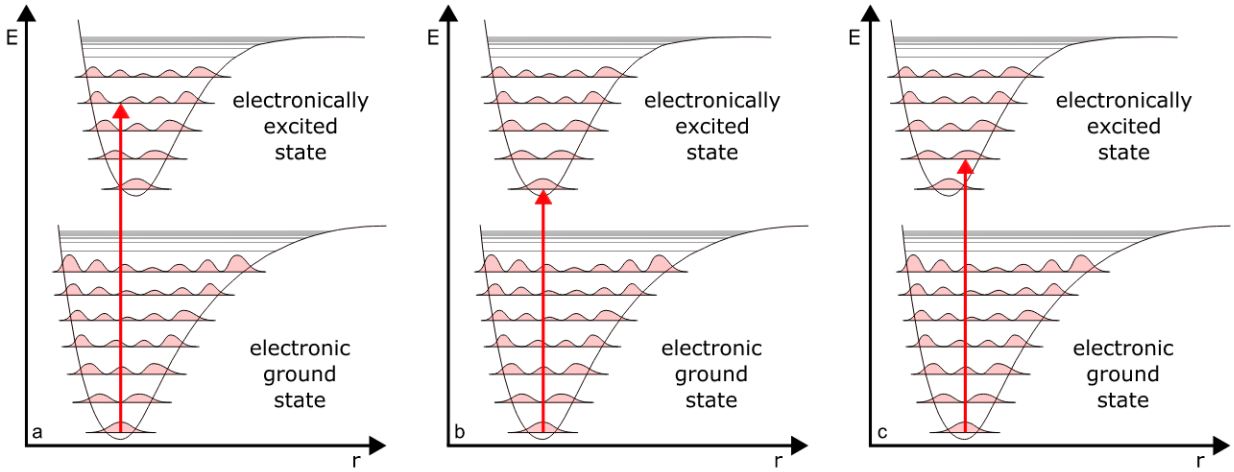

Figure 3.2.: Geometries of a electron transition and the associated probability densities from the Ψ^2 - equations, employing the Franck-Condon principle. The anharmonic oscillator is used as the basis for molecular vibration and the first vibrational states, S_0 and S_1, are shown. Part **a** depicts the Franck-Condon principle in the context of bond relaxation, Part **b** in the same equilibrium core distance, and Part **c** in the strengthening of bonds in the electronically excited state relative to the ground state. In accordance with [73].

The Franck-Condon principle is exemplified in Figure 3.2 by the depiction of potential curves in relation to the nuclear distance, represented by the variable r. The probability of a transition is contingent upon the relative positioning of the states in question. As previously stated, the transitions in question occur perpendicularly from the vibronic ground state, thereby enabling the determination of the vibrational state of the final state of a transition. The illustration demonstrates that the molecule is most probable to transition to this vibrational state where the convergence of the wave function or probability densities of the initial and final states are the highest. Nevertheless, this does not preclude the possibility of other transitions, although these have a markedly reduced probability and thus a correspondingly diminished intensity. In reference to Figure 3.2, the vibrational states in question are designated as **a:** $\nu' = 3$, **b:** $\nu' = 0$, and **c:** $\nu' = 1$ [73].

These considerations can be encapsulated in the Franck-Condon factor, which postulates that the intensity of an electronic transition is proportional to the overlap integral of the vibrational wave functions of the electronic states involved. Therefore, the overlap factor is equal to the Franck-Condon factor. In order to calculate the Franck-Condon

factor, it is necessary to consider the electronic ground state $|\Psi_g\rangle$ and its associated vibrational wave function $|\Phi_{\nu_g}\rangle$, as well as the excited state $|\Psi_e\rangle$ and its corresponding vibrational wave function $|\Phi_{\nu_e}\rangle$. The transition between the ground state and the excited state is described by a transition matrix element, which is augmented by the addition of the transition dipole operator, $\hat{\mu}$. The Born-Oppenheimer approximation allows for the decoupling of the electronic integral from the vibrational integral.

$$\langle \Psi_e \Phi_{\nu_e} | \hat{\mu} | \Psi_g \Phi_{\nu_g} \rangle \approx \langle \Psi_e | \hat{\mu} | \Psi_g \rangle \cdot \langle \Phi_{\nu_e} | \Phi_{\nu_g} \rangle \tag{3.12}$$

The Franck-Condon factor FC is defined as the square of the overlap integral of the vibrational wave functions with the specified nuclear coordinate Q.

$$\begin{aligned} \langle \Phi_{\nu_e} | \Phi_{\nu_g} \rangle &= \int \Phi_{\nu_e}(Q) \Phi_{\nu_g}(Q) dQ \\ FC_{\nu_g,\nu_e} &= |\langle \Phi_{\nu_e} | \Phi_{\nu_g} \rangle|^2 \end{aligned} \tag{3.13}$$

In consideration of the aforementioned aspects, the theoretical absorption and fluorescence spectra can be determined. The position of the potential curves in relation to one another determines the shape of the absorption and emission bands and their respective spectra. The phenomenon of a Stokes shift, which refers to the shift of the emission to higher and thus lower-energy wavelengths, can be explained by processes, as illustrated in the Jablonski diagram. It should be noted, however, that in the liquid phase, solvent effects (cf. 3.4.3, 3.4.4) also contribute to this phenomenon. Moreover, it is important to acknowledge that the sharpness and, consequently, the width of the individual transition lines within the resulting spectra are contingent upon the phase in which the absorption or emission spectrum was recorded. Consequently, the transition lines within the spectra are most distinct in the gas phase. This is attributable to the methodology and conditions of measurement (cf. 6.5). In contrast, line broadening occurs in the liquid and solid phases. In the liquid phase, this is due to solvent interactions (cf. 3.4.3, 3.4.4), temperature-dependent effects (cf. 3.6), and other effects. In the solid phase, it is due to lattice vibrations, lattice effects, and electronic dephasing.

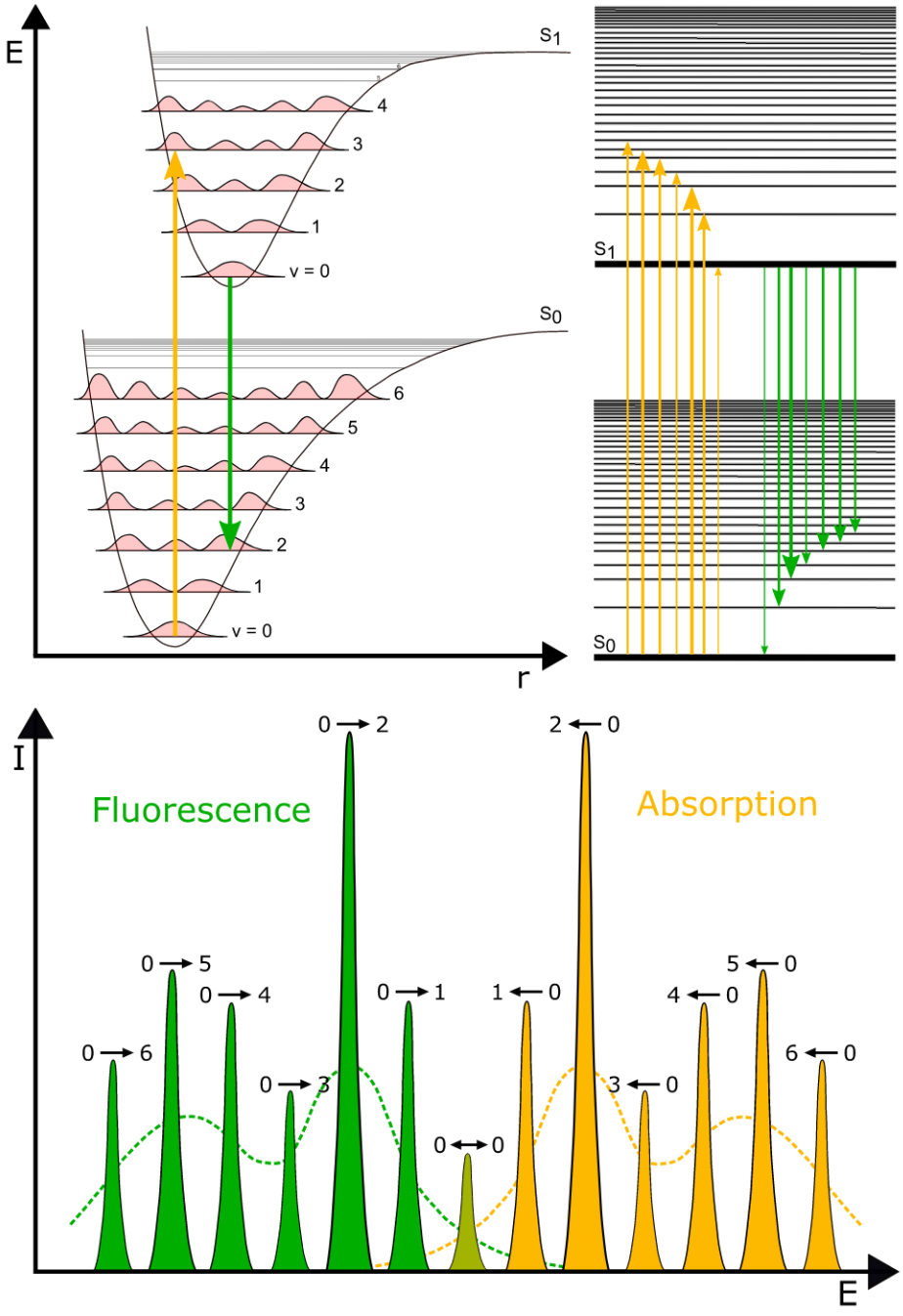

Figure 3.3.: Combining the Franck-Condon principle, the Jabłoński diagram and the theoretically resulting vibronic structure of the absorption and fluorescence spectrum in the gas phase, with a dashed line to represent the transitions shown in the liquid or solid phase. The phase change causes a broadening of the individual transition lines. The most probable transitions can be identified by the peak height and thickness of the arrow.

3.1.2. Refractive Index

Given the prevalence of publications in the specialist literature that neglect the influence of wavelength dependence in their calculations of refractive indices, while consistently considering the effect of temperature, this section will first examine the refractive index in detail [79]. It will then proceed to elucidate the dependence of refractive indices on temperature and wavelength, as well as the mutual influence between these two factors.

It is important to begin by noting that the refractive index is a dimensionless quantity. This is defined as the ratio of the wavelength of light in a vacuum to the wavelength of light within the corresponding medium. The standard wavelength for this is the Fraunhofer sodium - D - line at 589,2938 nm, which is the mean value of the sodium - D_1 - line and the sodium - D_2 - line. This value is commonly used as the n_D value in scientific literature [80].

$$n = \frac{c_0}{c_M} \tag{3.14}$$

In this context, the term n represents the refractive index, c_0 denotes the speed in a vacuum, and c_M signifies the speed within the medium under consideration. Given that light is an electromagnetic wave, it is necessary to consider the frequency, f, of the waves in order to make a special reference to electromagnetic waves. In general, the phase velocity, designated as c, and the wavelength, designated as λ, are linked by the following equation:

$$f = \frac{c}{\lambda} \tag{3.15}$$

In this equation, the variable c is defined as $c = \frac{c_0}{n}$ and the variable λ is defined as $\lambda = \frac{\lambda_0}{n}$. This makes it clear that the frequency f remains constant when passing from one medium to another, since the determining factors are equally dependent on n. This illustrates the relationship between the refractive index and the wavelength. Furthermore, a distinction is drawn between the phase refractive index and the group refractive index. The latter describes the refractive index for the envelope of a wave packet and corresponds to the phase refractive index in a vacuum. In contrast, the phase refractive index describes the refractive index of each individual wavelength and, as would be expected, differs from the

group refractive index under conditions outside a vacuum [80].

The following sections address the aforementioned indices, namely the phase refractive index n and the group refractive index n_g. Both indices describe the propagation of a light wave within a medium. The phase refractive index, represented by the ratio of the speed of light in a vacuum to the phase velocity in the medium $n = \frac{c}{v_{phase}}$, is influenced by the dispersion of the medium. The group refractive index, represented by the ratio of the speed of light in a vacuum to the group velocity of a light packet in the medium $n_g = \frac{c}{v_{group}}$, is influenced by the phase refractive index. Given that both indices pertain to disparate rates of light propagation within the medium, a more nuanced differentiation can be made at this juncture. Therefore, the term v_{phase} at n denotes the velocity of the individual wave fronts, whereas v_{group} at n_g represents the speed of energy propagation of a light pulse [81]. The physical meaning of both refractive indices can be divided as follows, despite their interdependence. The phase refractive index n determines the angle of refraction in accordance with the law of Snell and exerts an influence on the interference pattern. In contrast, the group refractive index n_g exerts an influence on the delay of a light pulse and thus also on the propagation of the pulse and the delay thereof. Both refractive indices are employed in the field of optics, with n being pertinent for the calculation of refraction angles, reflection, and interference, and n_g being relevant in the field of fibre optics and telecommunications for the evaluation of signal propagation [81], [82].

The determination of refractive indices is based on three principal measurement principles, which differ from one another with regard to the origin of the light. These principles are based on the principles of transmitted light, grazing incidence and total reflection. All of these measurement principles are based on a prism with a known refractive index and the refractive index of the sample to be investigated [83].

In the transmitted light measurement principle, the light is transmitted through a medium and the change in direction of propagation is examined. This method is predominantly employed in the domain of classical optics to ascertain the refractive indices of transparent liquids and solids. The principal advantage of this method is its simplicity of experimental setup, high degree of accuracy, and suitability for examination of thin layers. However, this method is not optimal for samples with high refractive indices and for strong scattering. In this method, the angle of incidence and the angle of refraction are typically measured, after which Snell's law $n_1 \; sin \; \theta_1 = n_2 \; sin \; \theta_2$ is applied [81], [83].

In the case of the grazing incidence method, the light is directed to the medium under examination at an extremely flat angle, approaching 90°. The diffraction or refraction of the light is then observed. This method is employed for the examination of refraction at exceedingly flat angles and in materials exhibiting markedly elevated refractive indices. This measurement method is pertinent to technical applications where light incidence from an extremely flat angle is of significance. Furthermore, it can be employed to ascertain the minutest details of light propagation. The principal disadvantage of this method is that it is technically challenging to implement, as it necessitates the precise alignment of the light incidence direction. The mathematical background is a variation of Snell's law, which is applicable in the case of a flat angle of incidence [81], [83].

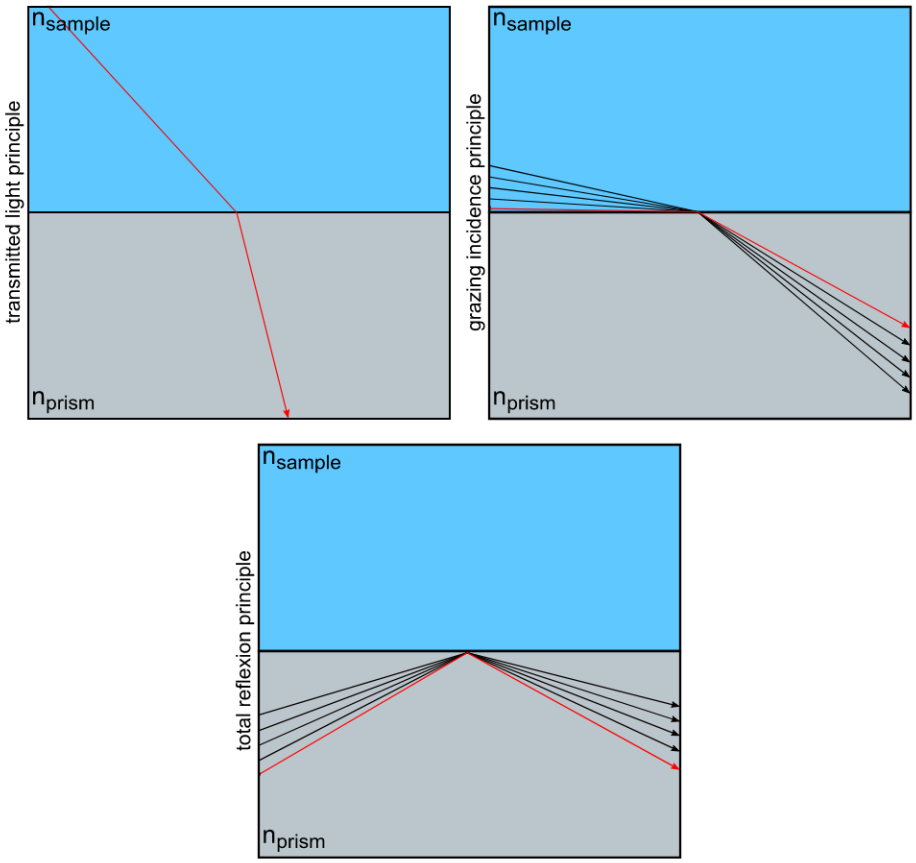

Figure 3.4.: A graphical depiction of the three measurement principles for determining refractive indices. The three measurement principles are illustrated in a clockwise sequence: the transmitted light principle, the grazing incidence principle and the total reflection principle.

In the scenario of total reflection, the light is directed towards the interface between the prism and the sample to be examined at an angle exceeding the critical angle. This method

is employed to ascertain the refractive indices of prisms and in the field of fibre optics. The principal advantage of this measurement principle is its high degree of accuracy, even when applied to samples with a high refractive index. The principle of total reflection is also employed in the field of optical communication technology. A limitation of this measurement principle is that the refractive index of one medium must be known and that it must be greater than that of the other medium. In this measurement method, the refractive index is determined directly by measuring the critical angle of total reflection $n = n_2 \; sin \; \theta_{critical}$, where $\theta_{critical}$ corresponds to the critical angle [81], [83].

In order to establish a link between the beginning of this section and the subsequent discussion, the following paragraphs will address the temperature dependence of refractive indices and the wavelength dependence of refractive indices.

Given that the refractive index is a variable dependent on temperature, it is evident from the preceding section that it is, in principle, the ratio of the speed of propagation of an electromagnetic wave between two different media. Consequently, the consideration of Brownian molecular motion and density change, which are also dependent on temperature, also flow into it [81], [84]. From a mathematical perspective, this can be expressed as follows through the use of a linear approximation:

$$n(T) = n_0 - \alpha(T - T_0) \tag{3.16}$$

In this context, the temperature-dependent refractive index is represented by the symbol $n(T)$, while the refractive index at the reference temperature T_0 is represented by the symbol n_0. The symbol α represents the substance-specific temperature coefficient.

In general, of course, exceptions do exist, the refractive index decreases with increasing temperature. This is due to the fact that the density of the medium in question is reduced. This reduction in density is caused by the fact that the molecules within the medium exhibit stronger thermal molecular motion when the temperature is increased. As a result of this increased motion, the speed of the electromagnetic wave within the medium is also increased. This can be applied to the classic three-phase states. Nevertheless, exceptions to this rule do exist. For example, in certain liquid crystals displays an increase of the refractive index is given as temperature rises. A complex interplay of interactions

occurs at the molecular level. Such phenomena are exemplified by phase transitions and anisotropy in liquid crystals [81], [84].

The dependence of the refractive index on both temperature and wavelength can be attributed to the seminal work of Christiaan Huygens [85] and Sir Isaac Newton [86]. Huygens established the foundation for the wave theory of light, which led to the conclusion that refraction and, consequently, the refractive index are dependent on wavelength [85]. In his publication Opticks from 1704, Sir Isaac Newton developed this concept further, conducting experiments to demonstrate that refraction at a prism occurs differently for different wavelengths of light, resulting in varying degrees of refraction for each wavelength. This led him to conclude that the refractive index is dependent on wavelength [86].

The general trend is for the refractive index to decrease as the wavelength increases. This is due to the fact that shorter wavelengths are refracted more strongly, as they can interact more strongly or more often with the electrons of the refractive medium. This phenomenon is referred to as normal dispersion. However, the situation is distinct in the case of anomalous dispersion. In this case, the refractive index may increase with rising wavelength at specific wavelengths proximate to the absorption bands. This phenomenon can be attributed to the enhanced interaction occurring near the resonance frequency of the material [81], [83], [84].

The foundation for the mathematical description of the wavelength dependence was established by Augustin-Jean Fresnel, who was able to describe dispersion in a mathematically precise manner [81], [84]. This was subsequently developed by Cauchy, who expressed it in the form of an empirical formula, which is known as the Cauchy equation [87]. Furthermore, the formulation of Maxwell's equations significantly advanced the comprehension of the interdependence.

$$n(\lambda) = A + \frac{B}{\lambda^2} + \frac{C}{\lambda^4} + \cdots \tag{3.17}$$

The parameters in 3.17 are the refractive index at a given wavelength $n(\lambda)$, λ the wavelength and A, B, C empirically determined material-dependent constants. The points delineate the potential for extending the equation to encompass additional empirical parameters.

In light of the observations made by other researchers and the inherent inaccuracy of the Cauchy equation, see Figure 3.5, Wolfgang von Sellmeier developed the Sellmeier equation in 1871 with the aim of describing the wavelength dependence of refractive indices. In essence, it constitutes an extension of the Cauchy equation [88].

$$n^2(\lambda) = 1 + \sum_{i=1}^{n} \frac{B_i \lambda^2}{\lambda^2 - C_i} \tag{3.18}$$

The parameters B_i and C_i, as listed in equation 3.18, are empirical in nature and may be extended by the addition of as many as desired, indicated by the suffix i. However, in the majority of cases, the agreement with the measured values is satisfactory for $i = 3$, as evidenced by Pedrotti [83]. In equation 3.18, the wavelength is expressed in μm.

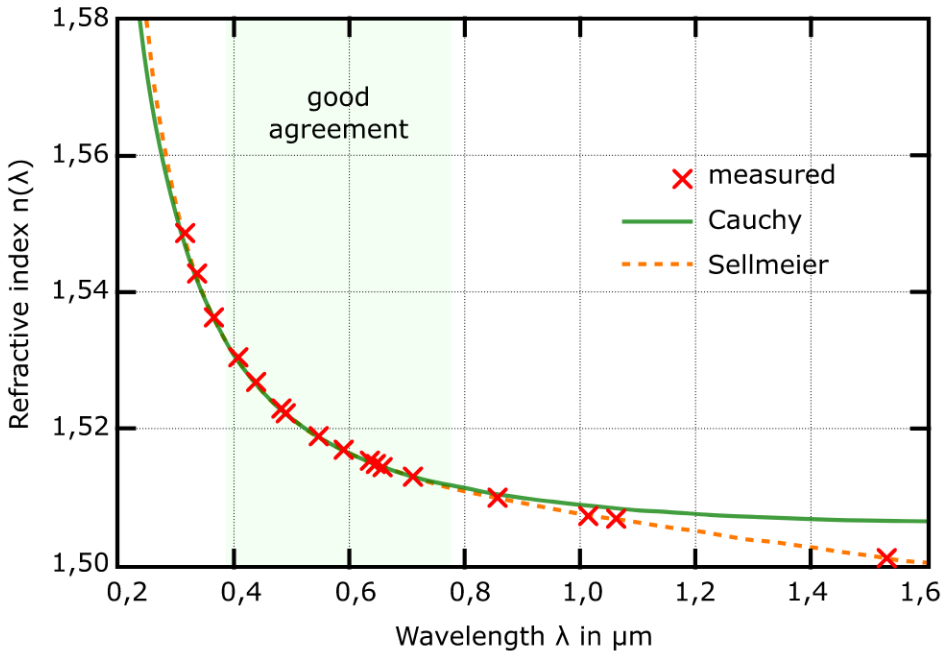

Figure 3.5.: Illustration of the agreement in calculating the wavelength dependence of refractive indices between Sellmeier, Cauchy, and measured values for a borosilicate glass [88].

In light of the aforementioned considerations, the following section elucidates the methodology employed to ascertain the refractive indices, encompassing the facets of temperature dependence and wavelength dependence, in addition to the interdependence of these dependencies.

The Sellmeier equation, with the coefficients B_i and C_i, as shown in equation 3.18, is used as the basis for the following equation, as this provides sufficient accuracy, as previously described. Furthermore, it is assumed that a constant temperature is present at the outset.

$$\sqrt{n^2(\lambda)} = \ n(\lambda) \ = \sqrt{1 + \sum_{i=1}^{3} \frac{B_i}{1 - \frac{C_i}{\lambda^2}}} \tag{3.19}$$

Furthermore, an equation is formulated that reflects the temperature dependence. In this instance, the behaviour is approximated by a third-degree polynomial, however, it should be noted that, as previously demonstrated, a sufficient approximation could also be achieved by a linear dependence.

$$n_\lambda(T) = p_0 + p_1\left(\frac{T}{K}\right) + p_2\left(\frac{T}{K}\right)^2 + p_3\left(\frac{T}{K}\right)^3 \tag{3.20}$$

In this context, the variable T represents temperature, p_i denotes the weighting of the respective term of the i-th order, and p_0 signifies the refractive index extrapolated to $T = 0\ K$ at a specified wavelength λ.

The two equations that establish the respective dependencies of the refractive indices are linked by multiplication, given that if a quantity z is proportional to two other quantities x and y, then it is also proportional to the product of the two quantities, i.e. $z \propto x \ and \ z \propto y$ so $z \propto x \cdot y$. In this instance, the refractive index n is the dependent variable, with the wavelength λ and temperature T serving as influencing variables. Consequently, it can be stated that: $n \propto = Model\ Function(\lambda) \ and \ n \propto = Model\ Function(T)$ which means $n \propto Model\ Function(\lambda) \cdot Model\ Function(T)$. The following equation can be derived from the aforementioned principles to describe the dependencies of the refractive indices.

$$n(\lambda, T) = \sqrt{1 + \sum_{i=1}^{3} \frac{B_i}{1 - \frac{C_i}{\lambda^2}}} \cdot \left(p_0 + p_1\left(\frac{T}{K}\right) + p_2\left(\frac{T}{K}\right)^2 + p_3\left(\frac{T}{K}\right)^3\right) \tag{3.21}$$

However, this supposition is contingent upon the assumption that the Sellmeier coefficients are temperature-independent, which also allows for an alternative description. In this instance, the Sellmeier coefficients B_i are defined as a function of temperature, thereby obviating the necessity to introduce a distinct polynomial for the temperature dependence. A similar approach is described in the literature by Wei [89], from which the following underlying equation can be derived.

$$n(T,\lambda) = \sqrt{B_0(T) + \sum_{i=1}^{2} \frac{B_i(T)}{1 - \frac{C_i}{\lambda^2}}} \tag{3.22}$$

Accordingly, the coefficients B_i in the aforementioned equation are modified as quadratic functions. This is equivalent to a multiplication of the Sellmeier equation, in which only two elements are employed instead of three, with a linear function that reflects the temperature-dependent behaviour of the refractive indices. This results in the following, where $(p_0 + P_1 \cdot T)^2$ is later summarizsed to $B_0(T)$:

$$\begin{aligned}
n(\lambda,T) &= \sqrt{1 + \sum_{i=1}^{2} \frac{B_i(T)}{1 - \frac{C_i}{\lambda^2}} \cdot (p_0 + p_1 \cdot T)} \\
&= \sqrt{(p_0 + p_1 \cdot T)^2 \cdot \left(1 + \sum_{i=1}^{2} \frac{B_i(T)}{1 - \frac{C_i}{\lambda^2}}\right)} \\
&= \sqrt{(p_0 + p_1 \cdot T)^2 \cdot \left(1 + \frac{B_1}{1 - \frac{C_1}{\lambda^2}} + \frac{B_2}{1 - \frac{C_2}{\lambda^2}}\right)} \\
&= \sqrt{(p_0 + p_1 \cdot T)^2 + \left(1 + \frac{B_1 \cdot (p_0 + p_1 \cdot T)^2}{1 - \frac{C_1}{\lambda^2}} + \frac{B_2 \cdot (p_0 + p_1 \cdot T)^2}{1 - \frac{C_2}{\lambda^2}}\right)} \\
&= \sqrt{B_0(T) + \left(1 + \frac{B_1(T)}{1 - \frac{C_1}{\lambda^2}} + \frac{B_2(T)}{1 - \frac{C_2}{\lambda^2}}\right)}
\end{aligned} \tag{3.23}$$

Ultimately, a temperature-dependent Sellmeier coefficient is derived in the numerator of the fraction, which can be abbreviated as $B_i(T)$. Therefore, the fundamental concept underlying the formula presented is analogous to that proposed by Wei [89]. The distinction lies in the fact that the temperature-dependent Sellmeier coefficients in Wei's cited work are not modelled with the same parameters for the polynomial in the aforementioned case, namely p_0 and p_1. Instead, individual polynomials are employed for $B_1(T)$ and $B_2(T)$.

3.2. UV/Vis Spectroscopy

As the name implies, UV/Vis spectroscopy, also designated as electron excitation spectroscopy, pertains to the examination of molecules through the utilisation of light within the ultraviolet range, spanning from approximately 200 to 400 nm, and in the visible light range, extending from approximately 400 to 800 nm. The underlying principle is based on the excitation of light within the aforementioned range of the electromagnetic spectrum, or alternatively, the emission of light, which is primarily characterised by fluorescence or phosphorescence (cf. 3.1.1). A direct correlation exists between the electronic transitions, the energy levels and, in particular, the molecular orbitals, with the emission investigations providing information about the electronically excited state.
It is postulated that molecules possess discrete energy levels which are superimposed by vibrational and rotational states. In the context of UV/Vis spectroscopy, the electronic energy levels and their associated states are of particular significance. The ground state, designated as S_0, is the lowest in terms of energy. Upon absorbing a photon, the molecule is promoted to an electronically excited state, which can be represented by the symbols S_1, S_2, and so on. This excited state can then be left, for instance, by emitting light. The photon emitted during a radiative transition is in accordance with the energy difference between the excited state and the ground state. An energy difference, $\Delta E = \gamma_{absorbtion} > \gamma_{emission}$, exists between the absorbed and emitted photon due to non-radiative processes that precede the emission, the so-called Stoke shift.

> In the context of quantum systems, energy levels are defined as metastable quantum-chemical states of a system, expressed in terms of energy. However, energy is not distributed continuously, but rather in discrete units, with only one energy level being occupied at a time. Consequently, the lowest-lying level is designated as the ground state, while higher-lying levels are referred to as excited states. Transitions between two levels are typically referred to as quantum chemical transitions. These can be

represented graphically using level schemes, as illustrated in Figure 3.1. In quantum chemical calculations, the states are represented as eigenvalues of the Hamiltonian operator, which provide further information about, for example, internal structure or angular momentum. This enables the indication of characteristic properties of the eigenvalues by quantum numbers or term symbols. The corresponding level width is a consequence of spontaneous changes, such as transitions between levels, and therefore does not permit the definition of a sharply delineated energy. If multiple quantum chemical states are present within a single energy level, this is referred to as degeneracy. Nevertheless, this degeneracy can be resolved, resulting in the subdivision of the level into a greater number of finer levels. Notable examples of this phenomenon include the Zeeman effect, which occurs when a magnetic field is applied, and the Stark effect, which occurs when an electric field is applied [90].

Typical electronic transitions observed in UV/Vis spectroscopy can be classified into three main categories. The transfer of an electron from a bonding π orbital to an antibonding π^* orbital, which typically occurs in conjugated systems, is referred to as a $\pi \rightarrow \pi^*$ transition. Transitions of the $n \rightarrow \pi^*$ type involve the transfer of an electron from non-bonding electrons n in antibinding π^* orbitals. This phenomenon is frequently observed in molecules containing heteroatoms. In contrast, $\sigma \rightarrow \sigma^*$ transitions entail the transition of an electron from a σ bonding orbital to an antibinding σ^* orbital. However, this transition is rarely observed in the visible range, and it is more prevalent in the UV range. In the majority of cases, the transitions involved are identical for both absorption and emission. Nevertheless, it is possible for emitted photons to be coupled to vibrational states, which can result in the emergence of fine structure in the emission spectrum.
Molecular orbital theory is employed for the purpose of elucidating the distribution of electrons within a molecule. The most prevalent molecular orbitals engaged in UV/Vis spectroscopy are the bonding, σ, π, and the antibonding, σ^*, π^*, molecular orbitals. σ - Orbitals originate from the overlap of atomic orbitals along a bond axis and are mostly present in single bonds. π - Orbitals are the result of a lateral overlap of p orbitals, which is typical for double bonds and conjugated systems. Antibonding orbitals are higher-energy orbitals that arise due to the overlap of atomic orbitals, but have a destabilising effect. In the end, transitions occur between the highest occupied molecular orbital (**HOMO**) and the lowest unoccupied molecular orbital (**LUMO**), with electrons moving from HOMO to LUMO. The effect of conjugated systems is that, due to the many conjugated double bonds, they reduce the energetic distance between HOMO and LUMO and thereby shift the absorption and emission into the visible range of the electromagnetic spectrum.

Molecular orbital theory describes the electronic structure of molecules on the assumption that electrons are distributed over the entire molecule and can be described by the corresponding molecular orbitals in which they reside. Molecular orbitals are constructed from the superposition of the individual atomic orbitals involved using the linear combination of atomic orbitals (**LCAO**), whereby the atomic orbitals are mathematically combined using the Slater-Condon rules, expressed as $\Psi_{MO} = c_1\Psi_A + c_2\Psi_B$. In this instance, the corresponding atomic orbitals are represented by Ψ_A and Ψ_B, with their respective weightings expressed by c_1 and c_2. Within the molecular orbital theory, a distinction is made between bonding, $\Psi_{bonding} = \Psi_A + \Psi_B$, and antibonding, $\Psi_{antibonding} = \Psi_A - \Psi_B$, molecular orbitals. Bonding molecular orbitals are formed as a result of two atomic orbitals that are interfering constructively, with the electrons in these orbitals exerting a stabilising influence on the molecule. This is due to an increase in electron density within the molecule. In contrast, antibonding molecular orbitals emerge from atomic orbitals that are interfering destructively, with the electrons in these orbitals exerting a stabilising influence on the molecule. This is due to a reduction in electron density between the nuclei. The occupation of the molecular orbitals is governed by the Pauli principle [91] and the Hund's rule [92], whereby each molecular orbital can accept a maximum of two electrons, with opposite spins. The occupation of molecular orbitals is in accordance with the increasing energy levels, commencing with the bonding orbitals and concluding with the antibonding orbitals. In the context of UV/Vis spectroscopy, it is crucial to consider the σ and π orbitals. The σ orbitals are formed by the overlapping of atomic orbitals along the bond axis, resulting in a rotationally symmetrical configuration. The formation of π orbitals is a consequence of the lateral overlap of p orbitals, which results in the distribution of electron density above and below the bond axis. The HOMO-LUMO gap is of great importance with regard to the optical properties. From the calculated and occupied molecular orbitals, molecular orbital diagrams can be generated that illustrate the comparative positions of the bonding and antibonding molecular orbitals within the context of the participating atomic orbitals. Furthermore, the number of bonding and antibonding molecular orbitals can be employed to indicate the bond order by using the equation: $BO = \frac{(n_{bonding} - n_{antibonding})}{2}$. So also the number of effective bonds can be discerned. A value exceeding one signifies the stability of a molecule. [19], [93].

In the context of UV/Vis spectroscopy, the selection rule governing the phenomenon

of transition is that of the electric dipole. This rule stipulates that a transition is only permitted if there is a change in the dipole moment. Furthermore, the Laporte rule, also referred to as the parity rule, is identified as a selection rule within the field of UV/Vis spectroscopy. This rule states that transitions between states of equal parity, such as $g \rightarrow g$ or $u \rightarrow u$, are prohibited, whereas transitions between states of different parity, such as $g \rightarrow u$, are permitted. As a consequence of symmetry breaking, Laporte forbidden transitions may be subject to weakening as a result of molecular distortion or interaction with the solvent. Moreover, the spin selection rule is applicable, whereby electronic transitions are only permitted if there is no alteration in the total spin. Consequently, transitions between states of the same multiplicity are permitted, whereas transitions between different multiplicities are prohibited. Notably, transitions between different multiplicities may be permitted via the phenomenon of spin-orbit coupling. These selection rules are equally applicable to both absorption and emission processes.
It is important to note that selection rules determine whether transitions between two energy levels are allowed or forbidden. The terms 'allowed' and 'forbidden' do not refer to the general possibility of a transition, rather, they pertain to the probability of the transition occurring and thus ultimately to whether the transition is intense or weakly visible. To illustrate, permitted transitions, exemplified by $\pi \rightarrow \pi^*$, are characterised by high intensity, whereas prohibited transitions, such as $n \rightarrow \pi^*$, are less intense due to the constraints imposed by spin and symmetry.

Spin-orbit coupling is used to describe a relativistic interaction between the spin of an electron and its orbital angular momentum. This phenomenon can be attributed to the special theory of relativity, which dictates that the electron moves in the electromagnetic field of the nucleus. From the electron's perspective, instead, it appears as if the nucleus is moving, thereby generating a magnetic field that interacts with the electron's spin and exerts an influence on it. This gives rise to an interaction between the spin S and the orbital angular momentum L. When considered in conjunction with the total angular momentum J, i.e. the J-coupling, this results from the sum of the spin and the orbital angular momentum. Therefore, the result is expressed as $J = L + S$. The quantum numbers L, S and J are employed to express the intrinsic states of an electron, with J representing the quantised value situated between $|L-S|$ and $|L+S|$. The effect of spin-orbit coupling can be observed, among other phenomena, in the fine structure splitting, which results in the separation of energy levels due to the differing energies associated with states with distinct J values. In the context of molecules, the phenomenon of strong spin-orbit coupling

gives rise to the splitting of molecular orbitals. Additionally, it can result in the partitioning of vibrational and rotational levels, a phenomenon that finds application in electron spectroscopy [90].

The fundamental possibility of splitting energy levels is employed in the field of UV-Vis spectroscopy in order to gain deeper insights into the electronic structure of molecules and thus their electrical properties. Additionally, this process enables the shifting of absorption and emission ranges into the visible range and the determination of the size of dipole moments in the ground and excited states. The latter is achieved through the utilisation of the Stark effect in high-resolution UV laser spectroscopy.

Stark Effect

The Stark effect, as described in [33] and [34], is the splitting and/or shifting of energy levels of molecules as a result of an external electric field. This leads to a partial lifting of the M-quantum number degeneracy. The Stark effect represents the electric counterpart to the magnetic Zeeman effect (cf. [94], [95]). Furthermore, the Stark effect can be classified into two distinct categories: the linear Stark effect and the quadratic Stark effect. It should be noted that the aforementioned terms can be used synonymously with those denoting the first-order Stark effect, which corresponds to the linear Stark effect, and the second-order Stark effect, which corresponds to the quadratic Stark effect. In the context of formal descriptions, the terms 'first-order' and 'second-order' are employed in the mathematical or quantum chemical portrayal of the Stark effect, whereas the terms 'linear' and 'quadratic' are utilized in the chemical or spectroscopic depiction of the Stark effect. In the following sections, the terms 'linear' and 'quadratic Stark effect' will be used. In the linear Stark effect, the energy shift is proportional to the strength of the electric field, with $\Delta E \propto E$, and can result in a splitting of the spectral lines. In contrast, in the quadratic Stark effect, the energy shift is proportional to the square of the strength of the electric field, with $\Delta E \propto E^2$, and it does not necessarily lead to a splitting of those. The linear Stark effect can only occur if a molecule has a permanent dipole moment that interacts directly with the applied electric field. The prerequisite for the quadratic Stark effect is the polarizability of a molecule, which induces the displacement. This does not require a permanent dipole moment and can also be achieved in symmetrical molecules. However, this is subject to change due to the polarizability and thus the interaction with the electric field.

In the field of quantum mechanics, the Stark effect is described using the Hamiltonian operator $\widehat{H}_S$, with the addition of a perturbation-theoretical approach that combines the

Hamiltonian operator of the undisturbed system, $\widehat{H}_{rot}$, with the associated perturbation, $\widehat{H}_E$ [6], [96].

$$\widehat{H}_S = \widehat{H}_{rot} + \widehat{H}_E \tag{3.24}$$

The operator of the perturbation designated as $\widehat{H}_E$ is constituted by three fundamental components: firstly, the electric field E_i, which is oriented along a fixed axis i within the three-dimensional space; secondly, the dipole moment components μ_α, which are aligned with the fixed molecular axes $\alpha = a, b, c$; and thirdly, the directional cosine $\Phi_{\alpha i}$, which quantifies the orientation relationship between the electric field and the aforementioned axes of the dipole moment components.

$$\widehat{H}_E = -E_i \sum_{i,\alpha} \mu_\alpha \Phi_{\alpha i} \tag{3.25}$$

This implies that the energies of the rotational states in the presence of an electric field E_S can be calculated using the field-free zero-order energy E^0, the induced first-order energy E^1 and the induced second-order energy E^2 [6], [96].

$$E_S = E^0 + E^1 + E^2 \tag{3.26}$$

To calculate the energy of the first-order Stark effect, the first-order correction is taken, which is obtained from the matrix elements of $\widehat{H}_E$ over the unperturbed wave functions $|JKM\rangle$.

$$H_{Stark} = -E_i \mu_\alpha \langle JKM|\Phi_{\alpha i}|JKM\rangle \tag{3.27}$$

In the case of a symmetrical rotor, the axis of symmetry is situated on the a-axis in the prolate case ($B = C$) and on the c-axis in the oblate case ($A = B$). According to equation 3.27, the first-order corrected energy $E^{(1)}_{Stark}$ can be obtained by evaluating the μ

component along the axis of symmetry.

$$E^{(1)}_{Stark} = E\mu\frac{KM}{J(J+1)} \tag{3.28}$$

This evidence demonstrates the linear dependence between the applied electric field, the dipole moment and the quantum number K, which explains why the latter disappears for $K = 0$. For the energies associated with the Stark effect of the second order $E^{(2)}_{Stark}$ equation 3.29, all of the aforementioned parameters are squared within the equation. With regard to the quantum number M, the consequence is that the degeneracy is partially lifted, resulting in a splitting that is no longer into $2J+1$ components but rather into $J+1$ components. This leads to the observation that the states with $+M$ and $-M$ exhibit the same energy [6], [96].

$$E^{(2)}_{Stark} = \frac{E_i^2\mu_\alpha^2}{2B}\left[\frac{(J^2-K^2)\,(J^2-M^2)}{J^3(2J-1)(2J+1)} - \frac{\left[(J+1)^2-K^2\right]\left[(J+1)^2-M^2\right]}{(J+1)^3\,(2J+1)\,(2J+3)}\right] \tag{3.29}$$

In the case of asymmetric rotors, the degeneracy in K is lifted, resulting in the Stark effect and second-order energies becoming the dominant factors. Furthermore, it is important to note that the dipole moment is oriented along three distinct axes. Accordingly, the complete Hamiltonian operator, in conjunction with the asymmetric rotor wave functions $|J\tau M\rangle$, must be employed for the calculation. This is achieved in a manner analogous to that described in equation 3.27, wherein two distinct wave functions, namely $|J\tau M\rangle$ and $|J'\tau' M\rangle$, which are subject to mutual mixing, are taken into consideration [96].

$$H_{Stark} = E_i^2\sum_\alpha \mu_\alpha^2 \sum_{J'\tau'}{}' \frac{|\langle J\tau M|\Phi_{\alpha i}|J'\tau' M\rangle|^2}{E_{J\tau} - E'_{J'\tau}} \tag{3.30}$$

Subsequently, a restructuring can be performed so that only the matrix elements $J' = J-1$, J and $J+1$ are included. Similarly, a quadratic dependence on the quantum number M is observed, indicating that the degeneracy occurs exclusively in the case of $J+1$. The second-order corrected energy of the Stark effect of the second order for asymmetric rotors is obtained [96].

$$E^{(2)}_{Stark} = E_i^2 \sum_{\alpha} \mu_\alpha^2 \left[\frac{(J^2 - M^2)}{J^2 (4J^2 - 1)} \sum_{\tau'} \frac{\langle J\tau | \Phi_{\alpha i} | J-1, \tau' \rangle^2}{E^0_{J\tau} - E^0_{J-1_{\tau'}}} \right.$$

$$+ \frac{M^2}{J^2 (J+1)^2} \sum_{\tau'} \frac{\langle J\tau | \Phi_{\alpha i} | J\tau' \rangle^2}{E^0_{J\tau} - E^0_{J_{\tau'}}} \tag{3.31}$$

$$\left. + \frac{(J+1)^2 - M^2}{(J+1)^2 (2J+1)(2J+3)} \sum_{\tau'} \frac{\langle J\tau | \Phi_{\alpha i} | J+1, \tau' \rangle^2}{E^0_{J\tau} - E^0_{J+1_{\tau'}}} \right]$$

As illustrated in figure 3.6, the splitting of energy levels in a rigid rotor (in this case, a linear rotor) as a function of the applied electric field and the oscillation of the corresponding electromagnetic wave exemplifies the Stark effect.

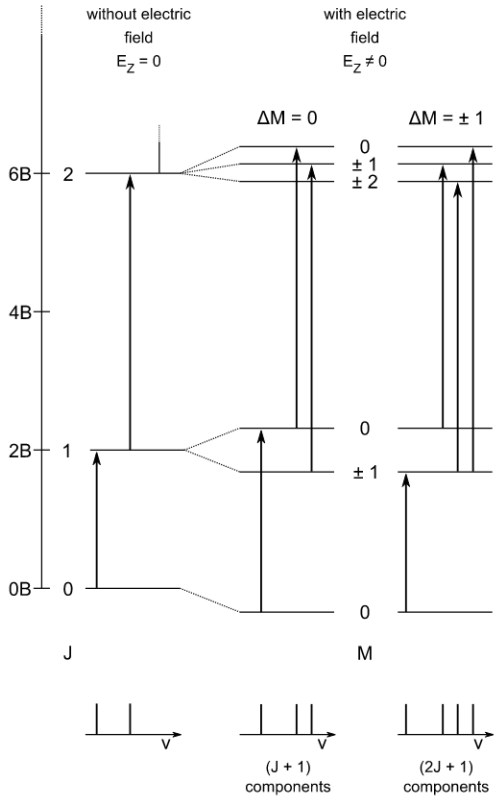

Figure 3.6.: Transitions between $J = 0$, $J = 1$ and $J = 2$ levels of linear rotor according to zero-field conditions on the left, following $\Delta M = 0$ in the middle and $\Delta M = \pm 1$ on the right, according to [6].

In this case, the only remaining quantum number that is applicable is M. The Stark splitting for $J = 1 \rightarrow 2$ is demonstrated, from which the transitions originate due to the disparate selection rules in M. Furthermore, a distinction is made between two cases: firstly, the light vector is parallel to the vector of the electric field, thus $\Delta m = 0$, and secondly, these vectors are perpendicular to each other, thus $\Delta M = \pm 1$ [6], [96].

In principle, UV/Vis spectroscopy offers a wide range of potential applications. In addition to the fundamental possibilities of investigating molecular parameters with regard to electronic structure, molecular geometry, and so forth, UV/Vis spectroscopy also offers applications in both quantitative and qualitative analysis.

3.3. Absorbtion and Emission Spectra

To provide an initial overview, the following figure 3.7 presents an outline of the terminology employed in the description of absorption and emission spectra. It is important to note that an increase in intensity is referred to as a hyperchromic shift, whereas a decrease in intensity is referred to as a hypochromic shift. A blue shift, that is to say, a shift towards shorter and more energetic wavelengths, is referred to as a hypsochromic shift. Conversely, a red shift, that is to say, a shift towards longer and less energetic wavelengths, is referred to as a bathochromic shift.

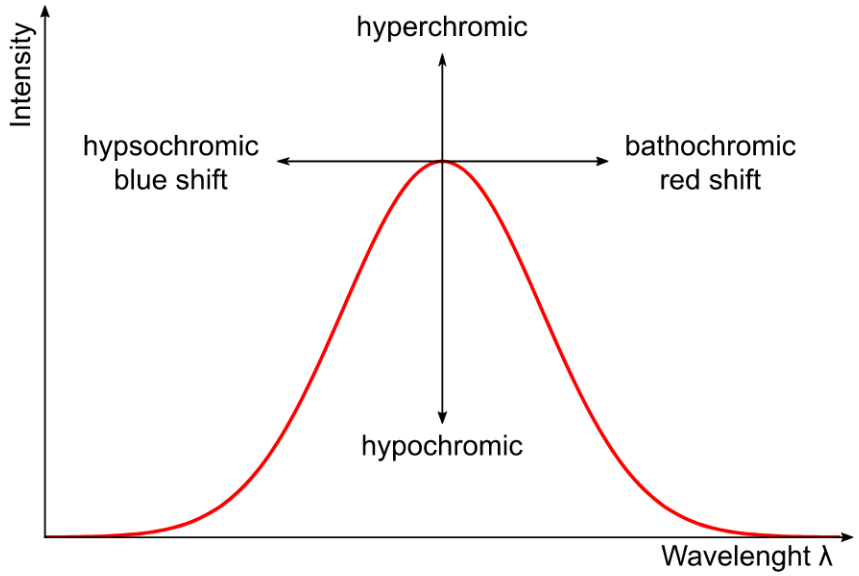

Figure 3.7.: Overview of the terminology used for absorption and emission spectra based on a fictitious spectrum within a coordinate system.

Moreover, a correlation exists between the molecular structure and the resulting absorption and emission spectra. An extension of the conjugated system results in a reduction in the energy differences between the π and π^* states, thereby causing a bathochromic shift. Functional groups that exhibit transitions within the UV/Vis spectrum are referred to as chromophores, and thus, as part of the molecular structure, exert an influence on the spectra. One such example is that of the carbonyl groups. Auxochromes are functional groups that are responsible for bathochromic or hyperchromic shifts. For example, this may include hydroxyl or amine groups. Hypochromic shifts may be caused by the formation of hydrogen bonds or aggregation.

Absorption and emission spectra are recorded in the unit of wavelengths nm due to the experimental setup and practical considerations. However, a conversion to wavenumbers cm^{-1} is necessary because this unit represents the general unit in spectroscopy. This is assumed by the calculation methods used in [4] and [5]. Furthermore, the use of the unit of wavenumbers allows for a linear representation of the energy differences, as wavenumbers are proportional to the energy of the photons. The conversion is performed using the general formula, $\widetilde{\nu} = \frac{\nu}{c} = \frac{1}{\lambda}$, which establishes a relationship between wavelength and wave number. The absorption and emission spectra in wavelengths are, in fact, mirror images of the spectra in wave numbers, and vice versa.

In order to convert wavelengths into wave numbers for emission spectra, it is necessary to correct the measured intensities, since when recording the emission spectra, the detection monochromator continuously scans the set wavelength range and thus detects the number of photons in this range. This results in different distances between the measuring points in wavelengths and wave numbers, which must be accounted for in order to obtain accurate conversion values. The intensities of the emission spectra are converted using the function $I_i^{\widetilde{\nu}} = \frac{I_i^{\lambda}}{\lambda_i^2}$ in order to facilitate the corresponding conversion. Conversely, a conversion of the intensities of the absorption spectra is not applicable, given that the irradiated light serves as the reference for the intensity.

Furthermore, the spectra are normalised, whereby all intensities of the individual spectra are scaled to 1. This has the effect of compensating for variations in sample concentrations, instrumental differences, varying experimental conditions, and so forth, thus creating a superior comparability of the individual spectra and facilitating the detection of trends or deviations.

In consequence of Kasha's rule, the emission spectra are also independent of the excitation wavelength, provided that, in the majority of cases, the excitation occurs above the S_1 state. As previously stated, this phenomenon is attributed to internal conversion, whereby fluorescence emission originates from the lowest excited state, namely S_1. It should be

noted that there are exceptions to this rule, such as in the case of fluorophores that emit from the S_2 state or those that exist in two ionised states.
Moreover, an examination of absorption and emission spectra reveals the existence of the so-called mirror rule, which posits that the two spectra of a molecule are typically mirror images of one another. This phenomenon can be attributed to the fact that the transitions from the ground state to the excited state and back again are highly analogous. It should be noted, however, that the aforementioned mirror image of absorption and emission spectra does not apply to the entire spectrum, but only to the absorption of $S_0 \rightarrow S_1$ and the emission of $S_1 \rightarrow S_0$. It should be acknowledged that exceptions to this rule do exist. This phenomenon occurs in molecules that undergo a significant geometric alteration in their excited state, or in molecules where disparate electronic transitions are preferred in this state. An illustrative example is that of azulenes [5], where the transition $S_2 \rightarrow S_0$ is favored over $S_1 \rightarrow S_0$.
In order to filter instrumental noise within the recorded absorption and emission spectra and obtain smooth fitting curves that allow for a precise determination of the maxima of the corresponding absorption or emission curves, a discrete Fourier transform including a low-pass filter is applied using the Fast Fourier Transform (FFT) algorithm. Prior to this, the data must be converted into equidistant data, as required by the method in question. The discrete Fourier transform via FFT enables the decomposition of a discrete-time signal into frequency components for subsequent analysis, resulting in a reciprocal function with the dependent variable of the circular frequency. This has the consequence of rendering the wave functions of the original function visible, thereby enabling the removal of interference frequencies, which are known as harmonics. Subsequently, a transformation is performed to return the data to the time domain [97].

In conclusion, it can be stated that a detailed analysis of absorption and emission spectra resulting from UV/Vis spectroscopy can be used to determine numerous physical and chemical properties of molecules, including the determination of concentration. The analysis of absorption spectra provides information regarding the type and intensity or probability of specific electronic transitions within the molecule under investigation. Furthermore, the assessment of absorption spectra provides valuable assistance in the structural elucidation of organic compounds. In many analyses, the emission spectrum is used to complement the absorption spectrum. Moreover, the examination of the excited state lifetime enables the elucidation of the molecule's relaxation dynamics. A joint evaluation of both spectra allows the determination of band gaps and is instrumental in elucidating the electronic structure of molecules. From the analysis of characteristic emission signals, conclusions can

be drawn regarding the formation of excimers and exciplexes, which in turn elucidates the nature of molecular interactions. The application of time-resolved UV/Vis spectroscopy enables the investigation of dynamic and kinetic processes, as evidenced by the spectra of photoreactions and electron transfer reactions, among others.

3.4. Solutions

As solutions are a fundamental aspect of this study, the subsequent sections will cover the main aspects of solutions. In addition, the crucial aspects of determining dipole moments in solutions will receive more detailed attention and can be found in further subsections, such as cavity volume (cf. 3.4.1) and permittivity (cf. 3.4.2). The refractive index utilised in this study is an inherent property of the solvent and has been previously reviewed (cf. 3.1.2). The importance of the solvent in this study lies in the determination of solvent-dependent parameters, which are crucial in the calculation methods, and in the determination of dipole moments in solution.

First, it is necessary to briefly classify what is a solution. It is a homogeneous mixture of two substances, one being a solid and the other a liquid. It forms a homogeneous phase. Based on the schematic classification of substances, this mixture can be divided into a solution and a dispersion. In a solution, the dissolved substance is homogeneously and statistically distributed in the solvent, in the form of molecules, atoms, or ions. In contrast, a dispersion is a heterogeneous mixture of at least two elements that do not dissolve in each other. Suitable examples for this phenomenon can be observed in common substances such as saltwater and milk. It should be noted for completeness that the solute may also take the form of a liquid or gas, and the solvent may also be a solid. However, these details are of secondary importance for this study, and the emphasis will rest on the liquid - solid configuration.

Solvents are substances that do not undergo a chemical reaction with the solute. Furthermore, solvents display considerable temperature dependency in numerous aspects, which is discussed subsequently all over in this chapter. On the one hand, solvents are categorised based on their physical properties, but the primary classification is between aprotic and protic solvents. Aprotic solvents lack a functional group and cannot dissociate protons (H^+). They are classified into two categories: aprotic-non-polar, such as alkanes, alkenes, or alkoxyalkanes, and aprotic-polar solvents, like ketones, nitriles, or sulphones. In contrast, protic solvents possess a functional group and can dissociate protons (H^+). Water, carboxylic acids, and short-chain alcohols are examples of protic solvents.

As this study examines a solid molecule in a liquid phase solvent, the topic of solubility

must also be addressed briefly. Solubility, as a general term, describes the capacity of a substance to dissolve homogeneously in a solvent. In general, there exists a differentiation between qualitative and quantitative solubility. The former denotes the capacity of a substance to dissolve in a solvent, whilst the latter specifies the highest proportion of dissolved substance to solvent. Upon closer examination of qualitative solubility, it is evident that polarity plays a crucial role. Polar substances tend to dissolve in polar solvents while non-polar substances dissolve in non-polar solvents. Hence, it is imperative to consider this factor when selecting the systems to investigate, given the underlying methodology of this study.
The process of solvation, occurring when molecules possessing a permanent dipole become immersed in polar solvents, shall be mentioned. Next, the intermolecular interactions between the solvent and the solute will briefly addressed. A more comprehensive understanding of the reciprocal impact of the solvent and solute, is given in section 3.4.3. Within this process, the solvent and solute molecules engage in electrostatic interactions that can be either attractive or repulsive. For instance, interactions such as dipole - dipole, van der Waals, or hydrogen bonding contribute to stabilising dissolved molecules and forming a solvation shell, which will be further elucidated in the subsequent section (cf. 3.4.1).

3.4.1. Cavity Volume

As discussed in the preceding section and reiterated in the subsequent sections, it is imperative to scrutinise the cavity volume in greater detail. A solvate shell is formed around the solute, leaving a cavity in which resides the solute. The size of this cavity depends on the size of the solute and of the solvent itself. Due to the influence of the resulting solvate shell on the molecule under investigation, the cavity volume is a variable within the methods utilized in this work (cf. 5).
When a solid is dissolved in a solvent through solvation, a solvation shell encircles a single, dissolved molecule. This occurs provided that attractive electrostatic forces surpass repulsive ones, thus allowing for solvation, and ensuring particle stabilization. During this process, solvent molecules uniformly arrange themselves around the dissolved molecule, ultimately forming the (first) solvation shell. The space between solute and solvent molecules is known as the dead volume. While the induced electric field during the formation of the solvate shell creates a mutual effect, its range is limited. Solvent molecules at a greater distance (outer solvation shell) remain unaffected, leaving the solute molecule as its primary focus. The size and shape of the resulting shell thus have two main influences, represented by the magnitude of the forces and the geometry of the solute molecule.

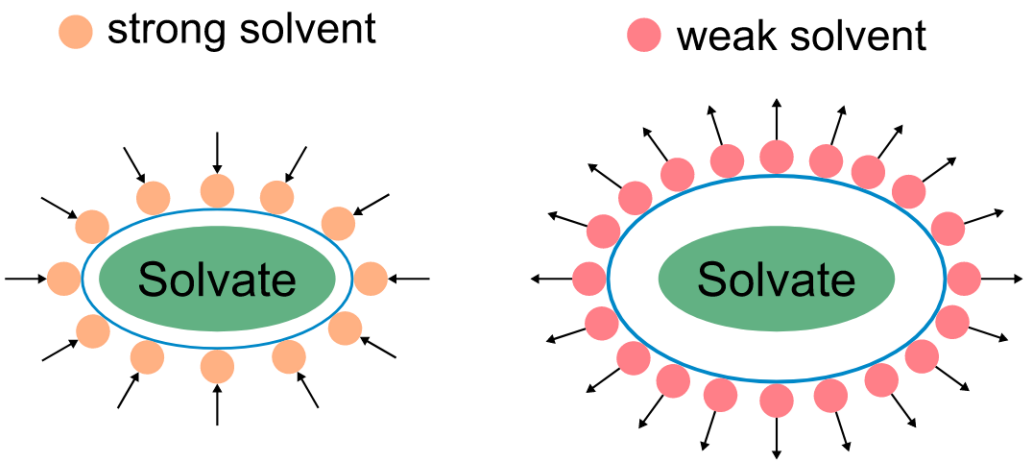

Figure 3.8.: Schematic comparison of the solvate shell formation using the same dissolved molecule in two distinct solvents.

As the cavity volume cannot be directly measured, it must be determined indirectly. The Onsager radius, derived from the Onsager reaction field theory, may be used for this purpose. However, it is an oversimplification, as pointed out by Onsager himself [36], and has been revisited by other researchers [98], [99], [100], [101]. As an oversimplification, a radius always implies a spherical solvate shell. However, this is not realistic due to various factors, such as charge distribution within the solute molecule and the size and geometry of this and other interactions. Furthermore, assuming a spherical solvation shell generally results in a significant overestimation of the cavity volume.

As previously highlighted by Onsager, the appropriate selection of the radius a represents a significant challenge and, at this stage, remains an ad hoc approach. In light of the veracity of the atomic model, it would be prudent and logical to identify an appropriate basis for the precise determination of the radius. Furthermore, Onsager observes that the molecular shape exerts an influence on the solvate shell, and that the radius a can only be applied to spherical solvate shells [36]. This criticism is also endorsed by Prabhumirashi [102] and others, who assert that the radius a lacks precise definition and that its determination is marred by significant irregularities. The methods of determination, for instance those based on the equivalent shell model, or the determination of a from the molar volume or the polarizability, demonstrate a significant overestimation of a. From a physical standpoint, it appears reasonable to ascertain the precise volume of the cavity, given that the factor a is incorporated into the calculation of the dipole moments to the third power and is more accurately

represented by an elipse. Prabhumirashi thus concludes that the radius a, which is determined from structural data, should be better determined by equating the volume equation for ellipses and spheres, as solved for a in [102]. In a subsequent publication, Prabhumirashi [103] responds to criticism from Suppan [104] by demonstrating, using aniline as an illustrative example, that the radius a is $1,9$ Å when the hydrogen atoms at the end are included and $1,46$ Å when they are not included. When determining the radius using the molar volume, the result would be $3,3$ Å. Ultimately, none of the aforementioned methods demonstrate sufficient accuracy. Furthermore, due to the irregular nature of the solvate shell, they do not accurately reflect reality and cannot be described by a simple geometric shape. Consequently, the cavity volume is employed, which neglects a necessity of the shape and only refers to the enclosed volume of the solvate shell, a methodology initially proposed by Demissie [101] in the context of dipole moment calculations in solution.

As previously discussed, the volume of an arbitrarily shaped cavity is not a directly measurable quantity. Nevertheless, the density of the solution can be utilized to establish a relationship with the cavity volume. The starting point for this is the definition of solution density which entails the ratio of mass to volume, as described in:

$$\rho = \frac{m}{V} \tag{3.32}$$

Upon introducing a substance to be dissolved, under the given conditions detailed in 3.4 and preceding this passage, the volume will remain constant while the mass of the solution will increase. This is due to the introduction of additional molecules and the coalescence of the solvent molecules to form the solvate shell.

$$\frac{1}{\rho} = \frac{1}{\rho^*} + \left(\frac{V_m}{M_w} - \frac{1}{\rho^*}\right) \cdot w \tag{3.33}$$

Where ρ is the measured density, ρ^* is the density at infinite dilution thus the density of the solvent, V_m the molar cavity volumen, M_w the mass of the dissolved molecule and w the mass fraction.

The molar cavity volume can be determined by converting the equation 3.33 to V_m, based on the linear relationship between the inverse density and mass fraction and their slope of the linear regression S. To determine the cavity volume of a molecule, division by the Avogadro constant is done.

$$V_m = \left(S + \frac{1}{\rho^*}\right) \cdot M_w \qquad with \qquad V_{molecule} = \frac{V_m}{N_A} \tag{3.34}$$

Naturally, the volume of the cavity varies with temperature, as temperature is a measure of kinetic energy and, for example, an increase in temperature, i.e. a transfer of thermal energy, is followed by an increase in kinetic energy, so that the particles move more strongly and therefore require more space. This correlation is founded on the law of energy conservation [105]. Therefore, in most cases, there is a rise in volume when mass remains constant, which consequently affects all dependent variables.

3.4.2. Permittivity

Permittivity, represented by the symbol ϵ, is a fundamental property of materials that demonstrates the interaction between and with electric fields. It reflects the potential for materials to become polarised by electric fields, as well as the capacity for them to exert an influence or attenuate an electric field. The dependence on frequency and temperature must be acknowledged. This indicates the extent to which electric field lines are affected by the medium. The permittivity of a material is indicative of the quantity of energy stored within an electric field within the material, and thus serves as a factor influencing the interaction between electric charges within the material. The SI unit (**Système international d'unités**) of permittivity is the Farad per metre, $F \cdot m^{-1}$. Two principal categories of permittivity exist, wherein the permittivity of a vacuum, designated as ϵ_0, serves as the electric field constant, $\epsilon_0 = 8,85418782 \cdot 10^{-12}\ F \cdot m^{-1}$, and functions as the reference point for comparative analysis of permittivities. The relative permittivity, ϵ_r, is a material constant that denotes the capacity of a material to store electrical energy within an electrical field. According to the definition, the value in a vacuum is $\epsilon_r = 1$ and is a dimensionless quantity. The relationship between permittivity, relative permittivity and dielectric constant is expressed by the following equation, which is used to describe the reduction in electric field strength through a material in comparison to a vacuum.

$$\epsilon_r = \frac{\epsilon}{\epsilon_0} \tag{3.35}$$

Furthermore, permittivity is employed as a metric for polarisation, whereby polarisation denotes the orientation of electric dipoles within a material in relation to the electric field. The various types of polarisation include ion polarisation, which refers to the relative displacement of anions and cations within a material, electronic polarisation, which concerns the relative displacement of the electron cloud in relation to the nucleus, and orientation polarisation, which is the alignment of dipole moments in an electric field. The latter two are of particular significance for the present investigations, however, in the context of these, only the orientation polarisation in relation to the permittivity is considered in greater detail, given that the description of the electronic polarisation is conducted via refractive indices, as explained in more detail in section 3.4.3. In principle, it can be stated that a high permittivity results in greater attenuation of the electric field lines than a low permittivity. Permittivity measurements may be conducted using a capacitor, whereby the capacitance of the capacitor is contingent upon the permittivity of the dielectric material situated between the capacitor plates.

If the permittivity is related to the solvent, or more precisely to the solvent polarity, then it can be said that the permittivity is a measure of its polarity. The high permittivity observed in polar solvents can be attributed to the presence of strong dipole moments within the solvent, which results in a pronounced reaction to electric fields. In contrast, nonpolar solvents exhibit a low permittivity and thus demonstrate a reduced responsiveness to electric fields. As permittivity is a solvent-specific quantity, it exerts an influence on the interaction between the solvent and the solvate, which is elucidated in greater detail in section 3.4.3. Four significant models are available for describing the permittivity of solvents, each employing a slightly different methodology. These are the Lorentz-Lorenz model [106], [107], the Debye model [32], the Onsager model [36] and the Kirkwood-Fröhlich model [108], [109].

The Lorentz-Lorenz model establishes a relationship between the refractive indices of the material under investigation and the molecular polarisation, thus establishing the permittivity of the material. It can be used to calculate the relationship between the dielectric constant and the refractive index. The fundamental premise of this model is the

representation of the permittivity as a function of the molecular density and the refractive index. This is predicated on the assumption of a direct correlation between the refractive index and electrical polarizability. It is important to note that this model does not take into account certain specific interactions and is therefore only applicable to electrically neutral and symmetrical molecules. The Lorentz-Lorenz equation, where ϵ_r is the relative permittivity, N is the number of molecules per unit volume and α is the polarizability of the molecule, is given by:

$$\frac{\epsilon_r - 1}{\epsilon_r + 2} = \frac{4\pi N\alpha}{3} \tag{3.36}$$

The Debye model is principally concerned with the description of the behaviour of polar molecules in solvents and their reaction to an oscillating electrical field. Its objective is to elucidate the frequency dependence of the dielectric properties of a solvent. The fundamental premise of this model is an investigation into the orientation of dipoles in response to an alternating electrical field, and the subsequent time delay in relaxation. Furthermore, the potential for thermal motion to disrupt the alignment of dipoles is considered, highlighting the limitations of their ability to fully adhere to the electric field. The relaxation time, designated as τ, emerges as a pivotal parameter. From these facts, it is possible to draw conclusions about molecular dynamics by considering the temperature dependence of the permittivity in relation to the relaxation time. One limitation of this model is that its description is only accurate for simple systems. The central equation in the Debye model is the equation for representing the frequency-dependent permittivity. The variables are as follows: $\epsilon(\omega)$ represents the complex permittivity at the frequency ω, ϵ_S denotes the static permittivity at low frequency, ϵ_∞ signifies the permittivity at high frequency, ω represents the angular velocity of the electric field and τ is the relaxation time of the polar molecule.

$$\epsilon(\omega) = \epsilon_\infty + \frac{\epsilon_S - \epsilon_\infty}{1 + (i\omega\tau)} \tag{3.37}$$

The Onsager model provides a more precise account of the dielectric polarisation of molecules within an electric field, with a particular focus on the interaction between a solvate, which possesses a dipole, and the surrounding solvent. This interaction gives rise

to a contribution to the overall dielectricity. The fundamental premise of the Debye model is the cavity space occupied by the dissolved molecule and the uniform distribution of the solvent's polarisation within this space. This distribution is calculated with consideration of the solvate's dipole moment and the solvent's permittivity. The resulting polarisation effects of the solvent are a consequence of the permittivity of the solvent and the position of the solvate within the electric field. The net effect of the solvate and the solvent is determined by the sum of their individual contributions. This model's primary focus is on dipole-dipole interactions, including the polarisation effects of a polar solvent, and is limited to small and spherical solvate molecules. One of the central equations of the Onsager model is the equation for determining the energy of the dipole in the electric field. This is given by the following equation, where μ is the dipole moment of the solvate, ϵ_r is the relative permittivity of the solvent and r is the radius of the cavity space.

$$E = -\frac{\mu^2}{(3\epsilon_r + 2)r^3} \tag{3.38}$$

The Kirkwood-Fröhlich model represents an extension of the Onsager model, whereby it is expanded to the interaction of neighbouring molecules in an electric field. Specific consideration is given to the mutual alignment of the dipoles, which should result in a correction of the permittivities predicted by the Onsager model. The introduction of the Kirkwood correlation factor, denoted as g, represents a pivotal aspect of this model. This factor describes the strength of the interaction between neighbouring molecules within the solvent field. In the event that a parallel alignment of the molecules is preferred, then is $g > 1$. Conversely, if an anti-parallel alignment is preferred, then is $g < 1$. The advantage of this model is that it can be used to analyse solvents in which the solvent molecules interact strongly with each other and cannot act independently. However, this necessitates an exact understanding of the molecular interactions and the geometry of the molecules. Moreover, it is only applicable to certain systems. The static permittivity is calculated using the following equation, where g corresponds to the Kirkwood correlation factor, μ to the dipole moment, N to the number of molecules, ϵ_0 to the permittivity of the vacuum, k_B to the Boltzmann constant and T to the temperature.

$$\epsilon_S = \frac{g\mu^2 N}{3\epsilon_0 k_B T} \cdot \frac{\epsilon_r - 1}{2\epsilon_r + 1} \tag{3.39}$$

Upon examination of the temperature dependence of the permittivity, it becomes evident that there is a negative correlation between permittivity and increasing temperature, resulting in a decline in permittivity. This is attributable to the enhanced thermal motion of the molecules, which renders it more challenging for the dipoles to align with the electric field. This, in turn, also results in a reduction in orientational polarisation, given that the alignment of the molecules is disrupted. It is important to note, however, that this is explicitly the interaction between the permittivity of a substance and an electric field. In considering the general case, the temperature dependence of the permittivity can be expressed using the following equation:

$$\epsilon(T) = \epsilon_0 - b \cdot T \tag{3.40}$$

where $\epsilon(T)$ is the permittivity at the corresponding temperature, ϵ_0 is the vacuum permittivity, b is a material-specific parameter that describes the decrease in permittivity with temperature and T is the temperature.

On the other hand, the relative permittivity of the solvent is a crucial property, and plays an even more significant role in the central equations of this work. Its variation with temperature is provided by the equation below, which differs a slightly from the general equation. It is dependent on the polarity of the solvent molecules, which is based on molecular interactions controlled by temperature.

$$\epsilon(T) = \epsilon_{T_0} + \alpha \cdot T \tag{3.41}$$

where $\epsilon(T)$ is the permittivity at the corresponding temperature, ϵ_{T_0} is the permittivity at laboratory conditions, α is the polarisation factor of the used solvent and T is the temperature.

In conclusion, it can be stated that permittivity represents a fundamental property of materials and is also a general measure of the extent to which materials are influenced by an electric field or exert influence themselves. With respect to solvents, permittivity is

also a parameter that indicates the extent to which a solvent can influence a dissolved molecule. In particular, it denotes the intensity of the electric field generated by the solvent in the vicinity of the dissolved molecule. This demonstrates that the permittivity of a solvent is a pivotal factor in the stabilization of dissolved molecules. Additionally, it influences the molecular structure and, consequently, the electronic transitions in solution by forming an electric field.

Since a solvent in which a substance is dissolved is effectively a dielectric, and the resulting electric field affects the dissolved molecule in its solvate shell, the following section (cf. 3.4.3) deals with the mutual influence between solvent and solvate.

3.4.3. Solvent and Solvate Interactions

Solvents can interact with the solute in a number of ways, which ultimately leads to a change in the electronic transitions. It is assumed that this is a complete solvation, whereby the solute is fully surrounded by the solvent, and that the solvent environment exerts a stabilising or destabilising effect on the electronic structure of the solute. A selection of potential interactions is provided next for reference. Such interactions may include dipole-dipole interactions, whereby polar molecules interact strongly with polar solvents, thereby stabilising both the ground state and the excited state. Another potential interaction is the formation of hydrogen bonds, which occurs predominantly in polar protic solvents, such as water or alcohols, and can therefore exert a profound influence on the electronic structure of the dissolved molecule. Furthermore, dispersion forces, which are present in non-polar solvents, also contribute to the interaction between the solvent and the dissolved molecule. Nevertheless, dispersion interactions that occur are typically weak in nature, yet they can nevertheless exert an influence on the existing energy levels of the dissolved molecules. From the aforementioned examples, it is evident that the interaction between the solute molecule and the solvent is predominantly electrostatic in nature. A comprehensive analysis will be presented in the following section.
A more detailed examination of the interaction between the solvent and the dissolved molecule reveals that the aforementioned electrostatic interactions can be described as intermolecular forces. These intermolecular forces can be classified into two categories. On the one hand, there are the category of directional, induction and dispersion forces, which are non-specific and cannot be fully saturated. Conversely, there are specific, directed forces, such as hydrogen bonds or charge transfer, which are capable of saturation. The following section will provide a more detailed examination of the aforementioned forces,

namely dipole-dipole interactions, hydrogen bonds and dispersion forces.
Dipole-dipole forces are directional forces based on the electrostatic interaction between two molecules with permanent dipole moments (cf. 3.5). In principle, there are two possible orientations in relation to each other. If the alignment is optimal at a given distance r from each other, the attractive force is proportional to r^{-3}, resulting in the two dipoles being aligned in a head-to-tail configuration. The second potential alignment is the anti-parallel alignment, which, with a few exceptions, is the more stable alignment (cf. for both alignements figure 3.9). However, both types of alignment can only exist exclusively if the attractive energy is greater than the thermal energy. This implies that the thermal energy causes the dipoles to align differently, although the statistical preference is for attractive alignments. As a consequence of this preferred alignment towards attraction, the quantity in question is strongly temperature-dependent. The Boltzmann-averaged dipole-dipole interaction is referred to as an orientation or Keesom interaction. It is important to note that the dipole-dipole interaction is only one of many interactions that can be considered under the assumption of an electric multipole. Consequently, other multipole-multipole interactions may also exist [110].

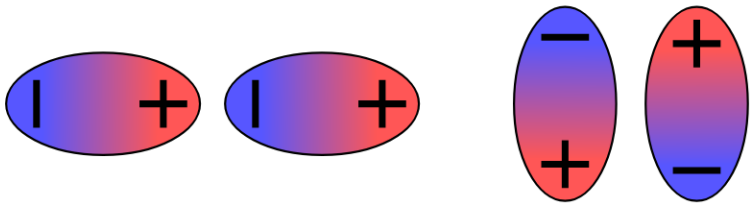

Figure 3.9.: Schematic representation of the alignment of two dipoles to each other. The configuration on the left represents a head-to-tail alignment. The right-hand illustration depicts an anti-parallel alignment. The figure is referenced in [110].

Dipole-induced dipole forces can be attributed to the phenomenon whereby molecules with a permanent dipole moment are capable of inducing a dipole moment in neighbouring molecules. The induced dipole moment is always aligned in the direction of the permanent dipole moment, thereby ensuring the presence of an attractive interaction. This type of interaction is independent of temperature. The magnitude of the induced dipole moment is contingent upon the polarizability, α, of the reactive molecule. This type of interaction is also referred to as induction or Debye interaction. This type of interaction is contingent upon the circumstances in which dipolar molecules are dissolved, either in non-polar solvents or in the opposite case [110].

Transient dipole-induced dipole forces, also known as dispersion forces or London interaction, result from the fact that even molecules devoid of a dipole moment can polarise an adjacent molecule as a consequence of the constant electrical movement, thereby leading to a dipole moment, albeit to a limited extent. Consequently, the electrical motion between the molecules in question is synchronised, resulting in a mutual attraction. Nevertheless, these forces are constrained in their range of applicability [110].
Hydrogen bonds represent one of the strongest intermolecular forces, and as a consequence, they play a significant role in the interactions between solvents and dissolved molecules. The formation of a hydrogen bond occurs when a hydrogen atom is bonded to a strongly electronegative atom, resulting in the exertion of a coordinative divalence. In general, a hydrogen bond is defined as a second bond formed between a covalently bonded hydrogen atom and another atom, as outlined in [111]. Nevertheless, the concept was first introduced in 1919 by Huggins [112], and the first publication on hydrogen bonds was made in 1920 by Latimer and Rodebush [113]. As a consequence of the formation of hydrogen bonds, in the event that such interactions should occur, and due to the inherent dipolar nature of the dissolved molecule, an impact on the distribution of charge is inevitable. The dipolar character of hydrogen bonds gives rise to a higher dipole moment upon formation than would be expected from a vectorial addition of the components involved. It is important to note, however, that the nature of the forces behind hydrogen bonds remains incompletely understood. There are compelling arguments for both the dipole-dipole and resonance interaction models to describe hydrogen bonds [110].

From the preceding brief examination of the most significant intermolecular interactions in terms of their impact on the electronic structure of the solute molecule, it is apparent that the existing interactions between the solvent and the solute represent a crucial consideration when determining dipole moments in solution. These interactions exert a profound influence on the charge distribution of a molecule of interest. In the following, a more detailed analysis with regard of the impact of solvent-solute interactions on the charge distribution within the molecule will be provided.

Figure 3.10 serves to illustrate the interaction between the dissolved molecule and the solvent in greater detail. For reasons of simplicity and comprehensibility, a spherical arrangement is used, based on the Onsager-Radius a [36]. $\mu_{G/E}$ represents the dipole moment in the ground state or in the excited state, whereas the symbol ϵ_r represents the permittivity of the solvent.

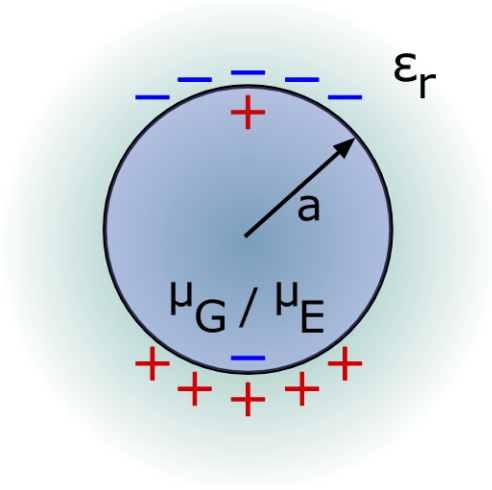

Figure 3.10.: Interaction of electrostatic forces of a dissolved molecule.

For an accurate description of the interaction depicted, the Onsager reaction field theory [36] is the preferred method, although more precise quantum chemical calculation techniques, which also consider the formation of irregular cavities, for instance in the form of the COSMO model (cf. [4]), are available today.
The assumption that the dipole moment of a dissolved molecule, and thus its electrical charge distribution, geometry, etc., remains unaffected by its environment has been rejected by Onsager at the outset of his publication, given that every molecule exhibits positive polarizability α and is a logical conclusion that can be drawn from the available scientific evidence.
Onsager's reaction-field theory, under the assumption of a spherical cavity shell, posits that the total electric field acting on a solute molecule can be decomposed into a cavity field, which is determined by the shape of the solute molecule and is proportional to the intensity of the external electric field. Furthermore, the total electric field is decomposed into a reaction field, which is proportional to the total electric moment and also dependent on the instantaneous orientation of the solute molecule. This implies that the average orientation of the solute molecule, and consequently the distribution of its charge, is determined by the coupled force couple comprising the cavity field and the electric moment of the solute molecule. As a consequence of the electrical deformability of each solute molecule, the reaction field invariably exerts an influence on the cavity field, and thus on the electrical moment of the solute molecule. It is important to note that the external and internal electric fields have opposite orientations, and that the medium surrounding the solute molecule is assumed to be homogeneous, polarizable, and of a constant dielectric constant [36].

The approach of a solvate shell, which encompasses the dissolved molecule and the subsequent interaction between the solvent and the dissolved molecule, along with the resulting impact on the charge distribution of the dissolved molecule, has been widely adopted. Consequently, all calculation methods for determining dipole moments in the liquid phase employ a solvent polarity function. In 1968, Suppan provided a more detailed discussion of the influencing variables and the intermolecular interactions that are crucial for this approach [114]. Of course, it should not go unmentioned that Lippert and Mataga, as well as Bilot and Kawski (cf. 5), also explicitly dealt with the construction of the solvent polarity functions.

In his publication, Suppan examines the primary interactions between solvents and solvates, including dispersion forces, dipole-induced dipole interactions, dipole-dipole interactions, higher multipole interactions, specific associations (such as hydrogen bonds), and solvent-cage strains and analyses these interactions in the context of Onsager's model. Firstly, it is observed that the only solvent parameters that demonstrate a correlation between transition energies and solvent properties that is both strong and linear are the parameters of the dielectric constant, denoted as D, and the refractive index, denoted as n [115], respectively, functions of the aforementioned parameters. From this, Suppan concludes that the description of the correlation via a function of D or n represents extreme cases and that a mixed function consisting of both functions should apply to intermediate cases, but that these differ from solvent to solvent [114].

Onsager's reaction field theory, following Suppan's argumentation, postulates that the solvent comprises molecules with dipole moments and isotropic polarizability, and that this reductionist approach is only applicable in limited circumstances. The solute molecule in the ground state is stabilised by the solvent-solvate system solely if the reaction field originates from the permanent dipole moment and the spherical cavity shell. In the event of dipole-dipole interactions being taken into consideration, and on the assumption that the dipole in question is non-polarizable, it is postulated that following the excitation of the system by light, the dipole moments of the solvent do not have sufficient time to reorientate, and thus the reaction field remains unaltered. Nevertheless, this scenario would result in a solvent cage tension, thereby increasing the energy of the excited state. In a more general consideration, however, it is not assumed that the reaction field is the same before and after light excitation. While the permanent dipoles of the solvent undoubtedly do not have time to realign, the induced dipoles can follow the light excitation due to the polarizability of the solvent [114].

According to Suppan, dipole-induced dipole interactions, that is to say the polarisation effect of the dissolved molecule, can be defined as a distinct term and are also independent

of the dipole-dipole interactions. Furthermore, Suppan notes that dispersion interactions are contingent upon the oscillation strength. However, empirical evidence indicates a tenuous correlation between the two variables, suggesting that the original London dispersion theory may offer a more comprehensive understanding. This theory posits that the energy of the interaction is contingent upon the polarizability of the solvent, which, in turn, is a function of the refractive index. The impact on the solute can be quantified in terms of the change in polarizability upon excitation, taking into account the number of molecules and the volume of the solvation shell [114].

Furthermore, Suppan makes reference to specific associations, which is why solvents and solvates cannot be considered from a purely dipole-dielectric interaction perspective. This can be observed, for instance, in the discrepancies from the functions of D or n, which were previously mentioned at the outset of this section. To illustrate this point, the role of hydrogen bonds is worthy of mention, given their status as one of the most significant specific associations, capable of fostering a robust bond between the solvent molecule and the solvate. Nevertheless, assuming certain simplifications, the interactions involved in the formation of hydrogen bonds can only be described in terms of their electrostatic nature [114]. Nevertheless, the utilisation of solvents with the capacity to form hydrogen bonds has considerably more far-reaching implications and should, wherever feasible, be eschewed in favour of more suitable solvents.

In conclusion, Suppan posits that the electron distribution of the electronically excited state is independent of the solvent, with only the energy of this state undergoing a shift. This has the consequence that the dipole moment of the excited state must be the same under the influence of any solvent, provided that the solvent effect is of a purely dielectric nature. In such cases, the corresponding equations can be applied. To enhance the solvent-solvate theory, it is observed that there is scope for refinement in only two parameters. On the one hand, this is the well-discussed (cf. 3.4.1) Onsager radius; on the other hand, it is the solvent polarity functions. With regard to the solvent polarity functions, it is found that the solvate shell cannot be regarded as a continuum; rather, it might be advantageous to consider it as a system of discrete point charges. However, experimental findings indicate that a macroscopic system comprising discrete point charges, which have been averaged over space and time, may appear as a static continuum. In light of these findings, it seems reasonable to conclude that the solvent polarity functions can be applied with a reasonable degree of plausibility [114].

A more detailed investigation of the impact of the solvent on the dissolved molecule was conducted in 1974 by Nicol [116], who examined the theories of spectral shifts resulting from solvent influence and developed a model for calculating them. Nicol's work is based

on a comparison between the absorption and emission spectra of dissolved molecules and isolated molecules. Additionally, mutual interactions, such as dipole-dipole interaction, dipole-induced dipole interaction and London forces, are examined by applying second-order perturbation theory. A methodology is developed that can calculate the solvent interactions and the resulting shifts of the spectra in different solvents, with the calculation method varying for each class of solvent. It has been demonstrated that Stark effects can occur as a consequence of the solvent, which is regarded as a source of fluctuation fields. It can therefore be seen that both Stark interactions and London forces play a pivotal role in the description of the interaction. The aforementioned approach is based on a combination of classical dielectric theories and quantum mechanical perturbation theories. Ultimately, the solvent exerts an influence on the electric field at the site of the solvate. The fundamental premise of this approach is that the energy states of the dissolved molecule in the absence of a solvent are known, and the impact of the solvent is regarded as a perturbation to these energy levels. The description of these levels is based on macroscopic quantities, such as the dielectric constant and refractive index. The aforementioned energy change is calculated on the basis of the interaction previously outlined by Suppan, with the addition of a multipole development to encompass higher-order contributions. In conclusion, it can be stated that the interaction between solvent and solvate affects not only the energy levels of the solvate molecules, but also the transition energies between different states [116].

In his publications [102] and [103], Prabhumirashi further criticises, also based on Nicol's results, that the interaction between solvent and solvate is described solely in terms of the effects of dielectric polarisation, and that this description does not differentiate between the classes of solvents. This assertion is erroneous because the bands of the solvate, including their attributes such as position, shape, intensity, and structure, exhibit significant variation across different solvents. As demonstrated by Nicol [116], the linear plots for distinct classes of solvents are distinctly disparate. It is therefore evident that the interactions between solvent and solvate should be based on their chemical nature, which may include factors such as functional groups, π or lone pair electrons, the affinity for hydrogen bonding, or even complexation. Moreover, only solvents belonging to a single solvent class should be considered collectively, and only solvents exhibiting weak and non-specific interactions should be employed for meticulous investigations into the impact of the solvent-solvate interaction on the absorption and emission spectra, where the determination of dipole moments in solution is addressed. From the preceding argument, it follows that the interaction between solvent and solvate is essentially limited to the effects of dielectric polarisation if that limitation is applied.

In light of the aforementioned points and further publications, such as [5], [53] and [117], it is possible to identify several key aspects of the interaction between solvent and solvate. When considering the influence of the solvent on the dissolved molecule, the polarity of the solvent represents a pivotal factor. However, it is evident that this interaction cannot be adequately described by a single theoretical framework. It is possible for excess vibrational energy to be readily donated to the solvent. Furthermore, solvent effects can lower the energy of the excited state through the stabilising effect of polar solvent molecules on the excited state. Following excitation, the solvent dipoles may reorientate themselves around the excited state or relax, which results in a reduction in the energy state. However, it has been demonstrated that polar solutes exhibit a higher degree of sensitivity to polar solvents than non-polar solutes. In consideration of the fluorescence lifetime, which typically falls within the range of $1 - 100\ ns$, it becomes evident that this lifetime exceeds the time required for solvent relaxation. Consequently, the fluorescence phenomenon occurs from the relaxed state of the solvent. The considerably faster processes of absorption, occurring in the range of $10^{-15}\ s$, demonstrate that the impact of the interaction on absorption processes is markedly diminished, given that these occur at a much faster rate. Figure 3.11 provides an overview of the aforementioned aspects.

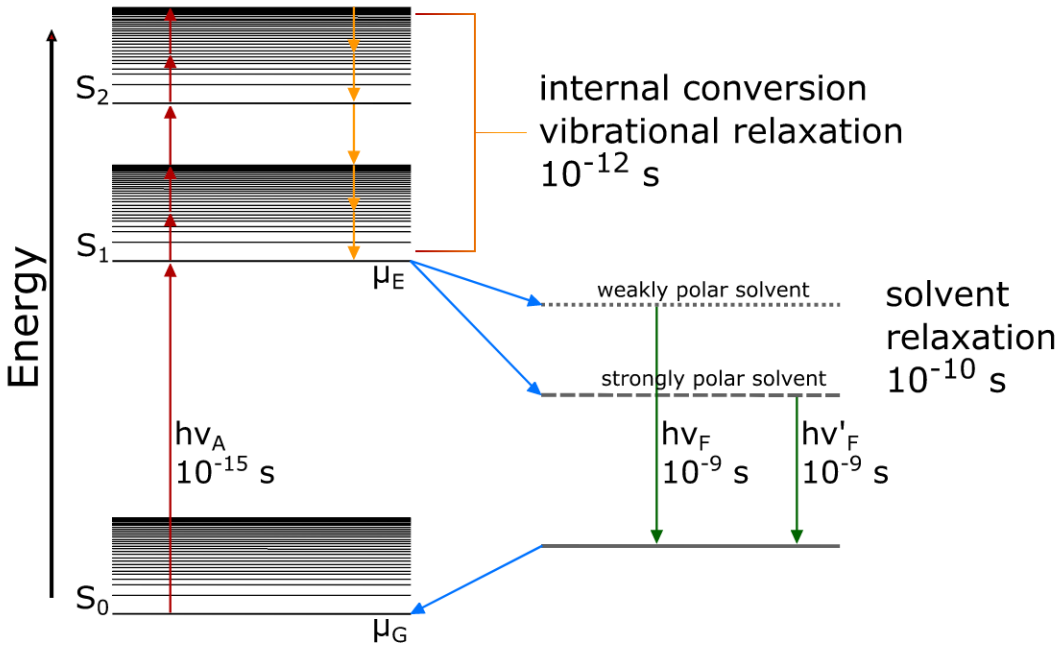

Figure 3.11.: Duration of processes following light excitation and the solvent's impact are illustrated in a Jablonski diagram. The red arrows illustrate absorption processes, while the yellow, green, and blue arrows depict emission processes.

Given the intricate nature of the interaction between the solvent and the solvate, it is essential to provide a concise overview of the other mechanisms that exert an influence. It is imperative not to overlook these particular effects, as even in the absence of a change in the polarity of a solvent, the introduction of an additive at low concentrations can result in a spectral shift, thereby reducing the corresponding energy levels. Figure 3.12 provides an overview of the specific solvent-solvate interactions.

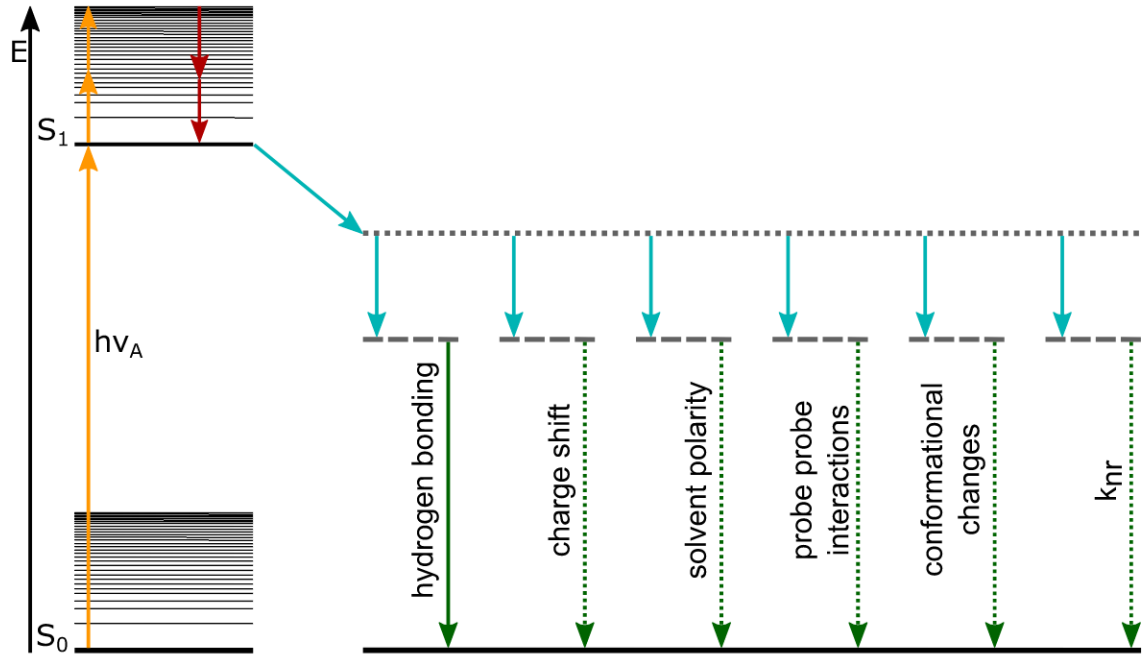

Figure 3.12.: Impact of solvent effects on the excited state, observing different effects. Teal-coloured arrows indicate the lowering of the energy level with the addition of solvent relaxation and the corresponding effect. Green arrows indicate fluorescence. The position of the energy levels is schematic and not qualitative.

These specific interactions include the formation of hydrogen bonds, as previously mentioned. Additionally, the possibility of an internal charge transfer state (**ITC**) forming due to the polarity of the solvent should be considered. This results in charge separation occurring after excitation, and the ITC state thus having the lowest energy level. An alternative possibility is that no separation occurs, resulting in the locally excited state (**LE**) having the lowest energy level. Furthermore, the interaction with the solvent can also facilitate non-radiative decay or alter the conformation of the solvate (cf. 3.12).
Upon returning to the general effects of polarisation via the refractive index n and the dielectric constant ϵ of the solvent on the solvate, it becomes evident that the energy

difference between the ground state and the excited state is influenced. A detailed examination of the effects of n and ϵ on the position of the absorption and emission bands reveals that while n reduces the energy loss, ϵ increases the difference. It can thus be seen that n responds at a higher frequency because n depends only on the electron motion, whereas ϵ represents a static quantity that depends on the electron motion but also on the molecular motion. The consequence of this is that the rise in the refractive index and the subsequent movement of electrons serve to stabilise both the ground state and the excited state simultaneously. This stabilisation also occurs when the dielectric constant increases, but only after the reorientation of the solvent molecules. This is because this process requires the movement of the entire solvent molecule, and thus this type of stabilisation has a time component. In anticipation of the subsequent elucidation, it is also pertinent to note that this process is contingent upon temperature and viscosity, occurring on a timescale commensurate with solvent relaxation (cf. 3.15). It is important to consider the influence of both variables separately due to the aforementioned differences, as this is also reflected in the solvent polarity functions derived from the applied calculation methods (cf. 5).

A more detailed examination of the temporal component necessitates a brief reiteration of the Franck-Condon principle (cf. section 3.1.1 and figure 3.2), which, as previously elucidated, postulates that there is no motion of the nuclei during electronic excitation. In contrast, however, the electrons of the solvent are capable of reacting to the dipole of the excited state generated by the excitation and realigning themselves with this excited state. Furthermore, solvent molecules have the potential to orientate themselves in an equilibrium position around the excited state, given that the lifetime of the excited state is relatively long, spanning a range of 10^{-8} s. In this instance, the polarizability is a consequence of the electron motion of the solvent and the dipole moment of the solvent. From this, and from the separate consideration of the components of the polarizability, the designations of the high-frequency polarizability for n and the low-frequency polarizability for ϵ are derived. The distinction between the two components is referred to as the orientation polarizability. These relationships permit the interaction between the solvent and the solvate to be considered via the dipole moments of the ground state μ_G and the electronically excited state μ_E of the solvate, with the addition of the reaction fields around these solvate dipoles. The reaction fields can be subdivided into two components, representing the electron motion $R_{el}^{G\ or\ E}$ and the solvent reorientation $R_{or}^{G\ or\ E}$. Figure 3.13, which provides a graphical illustration of the processes in question, is presented herewith for the purpose of elucidating the following operations in greater detail.

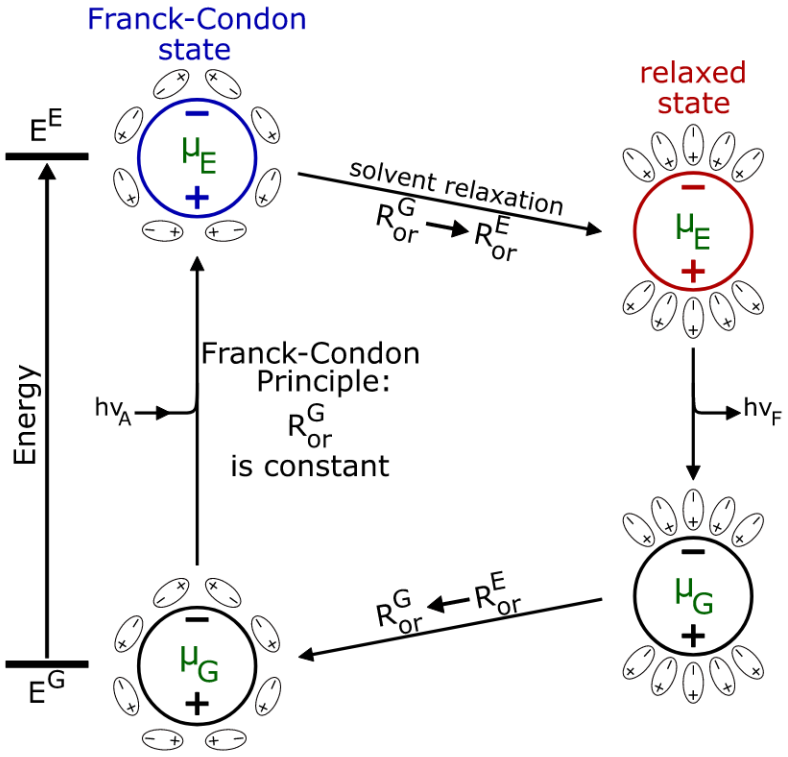

Figure 3.13.: Relaxation processes within the molecule and solvent during light excitation and the mutual influence. With: $E^{G/E}$ energy of state, μ_G ground state dipole moment, μ_E excited state dipole moment, hv_A absorption, hv_F fluorescence and $R_{or}^{G/E}$ solvent orientation electric field [5].

Figure 3.13 illustrates the behaviour of the aforementioned reaction fields during the processes of excitation and emission. The initial state is a dipole moment in the ground state, which is stabilized by the interaction of the solvent and solvate. Following light excitation, the Franck-Condon principle leads to the formation of the corresponding Franck-Condon state, whereby the electron motion has already been adapted, as this occurs practically simultaneously with the light excitation and thus also lowers the transition energy. The reorientation of the solvent molecules is not possible within the specified timeframe, resulting in the orientation reaction field aligning with that of the ground state. Assuming a rapid relaxation of the solvent and, consequently, the reorientation of the solvent molecules prior to emission processes, a relaxed state is attained, exhibiting a lower energy state, which is then the site of the emission process. Similarly, the reaction field of the electrons, or electronic motion, can occur directly and simultaneously with emission. This results in an elevated ground state due to the lack of reorientation of the solvent molecules. Subsequently, the reorientation of the solvent molecules occurs, which in turn gives rise to a reaction in the reaction field associated with the solvent reorientation.

Moreover, the impact of temperature on this interaction has yet to be considered in the context of the interaction between the solvent and solvate. Nevertheless, this aspect merits closer examination, given that all interactions are also temperature-dependent. As a natural consequence of the reduction in temperature, liquids typically exhibit an increase in viscosity, which results in a reduction in the mobility of solvent molecules. As a consequence of the increased viscosity, the time required for the reorientation of the solvent molecules following light excitation in response to the excited state of the solvate is also prolonged. If the solvate is in the Franck-Condon state following light excitation and the rate of relaxation of the solvent is slower than the emission rate of the excited state, the emission will occur from the Franck-Condon state. The opposite situation has been previously described. In the event that the rates are equal, or if the difference is minimal, emission processes from both the Franck-Condon state and the relaxed state occur concurrently. An illustration of the impact of temperature regarding relaxation processes can be found in figure 3.14.

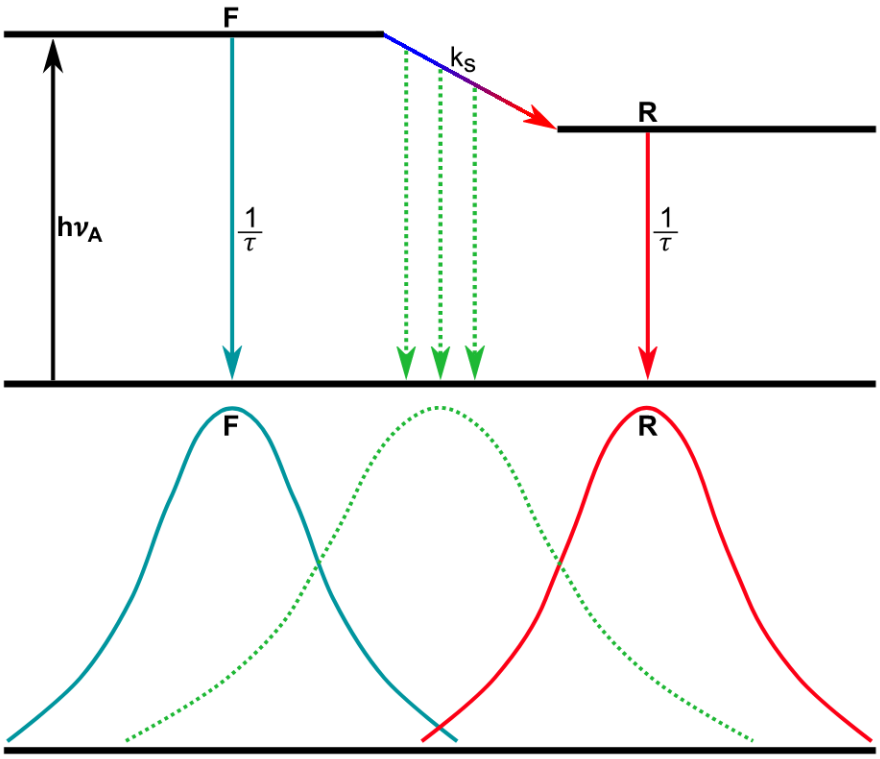

Figure 3.14.: Schematic representation illustrating the impact of temperature on solvent relaxation and its subsequent effect on theoretical emission spectra. With: F the Franck-Condon state, R the relaxed state, k_S the relaxation rate, $\gamma = \frac{1}{\tau}$ the decay rate, petrol when $\gamma > k_S$, green when $\gamma = k_S$ and red when $\gamma < k_S$. According to [5].

In sum, although this section is not a comprehensive delineation of solvent–solvate interactions — and is, moreover, circumscribed to those aspects salient to this dissertation — it can be asserted that a qualitative portrayal of solvent effects in the context of determining dipole moments in solution occupies a prominent position in science. Indeed, it represents one of the most challenging and, at the same time, most extensive subfields within this method of determination. The multitude of factors influencing the interaction between solvent and solvate precludes the application of a single theory to describe the complete interaction and the associated effect on a molecule with regard to its dipole moment. By eschewing the particular interactions and streamlining the complexity to a single or two variables, more precise descriptions of these interactions and the effects of these interactions, even in the context of high complexity, can be obtained. This also makes it evident that a variation of the solvent, and in particular a change between solvents from different solvent classes, cannot be considered a useful approach if the aim is to identify a superior alternative, since too many properties and parameters are altered as a result. With regard to the determination of dipole moments in solution, the reduction, as has already been done in the past, to the polarity variables, namely the refractive index and permittivity, and the use of cavity volumes, as well as the maintenance of the greatest possible constancy, whereby the required variation is obtained via the temperature, is a promising approach. The aforementioned variables, namely refractive index (cf. 3.1.2), permittivity (cf. 3.4.2) and cavity volume (cf. 3.4.1), are temperature-dependent quantities. By investigating their temperature dependence, it is possible to obtain a more accurate description of the polarity functions, which are related to the spectral shift. Ultimately, the aforementioned facts illustrate the determination methods via thermochromism.

Additionally, it is important to highlight that the reaction field, which is the consequence of the arrangement of solvent molecules around the solvate molecule, gives rise to an electric field of magnitude $10^7\ V/cm$. This field is capable of influencing the electronic structure of the solvate molecule in a manner analogous to that of a homogeneous externally applied electric field. This phenomenon is known as electrochromism [110].

It is evident that the interactions between the solvent and the solvate inevitably influence the absorption and emission spectra, as the logical conclusion necessitates. The following section addresses the effects of the aforementioned interaction on the spectra.

3.4.4. Solvent effects on molecular electronic spectra

Figure 3.15 illustrates the mean durations of the solvent relaxation processes, depicted in orange and the fluorescence lifetime processes, depicted in green, as well as the ratio of the two. Although the solvent relaxation process is observed to occur at a faster rate than the fluorescence processes, a certain degree of overlap between the two remains constant. It should be noted that the figure assumes that the two processes occur at room temperature. Consequently, it serves as a guide and a recap of the preceding section.

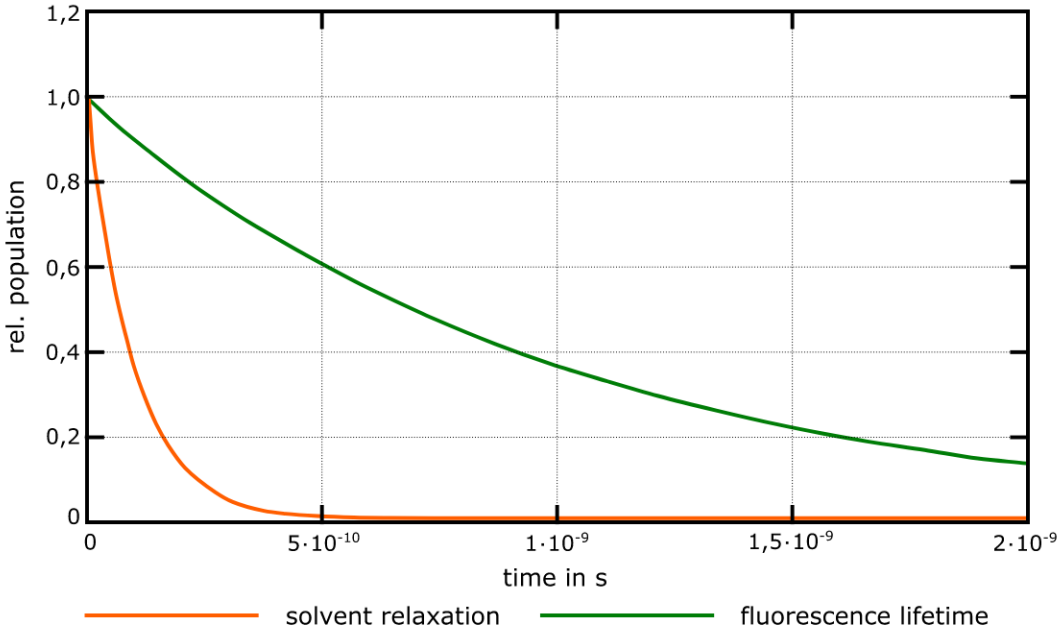

Figure 3.15.: Comparison of the time duration between the solvent relaxation processes and the fluorescence lifetime based on average values with the decrease of the population on $\frac{1}{e}$.

As a consequence of the aforementioned interaction between the solvent and the dissolved molecule, the solvent exerts a considerable influence on the absorption and emission spectra within UV/Vis spectroscopy in the liquid phase. This is primarily due to the fact that these interactions primarily affect the electronic transitions and change the energies of the energy levels, thus the ground state and the electronically excited state. These alterations have a direct impact on the absorption and emission spectra, influencing the width, structure and position of the curves and, consequently, the respective maxima.
The interaction between the solvent and the solvate can exert a significant influence on the absorption spectra, leading to alterations in the observed spectra. To illustrate, a bathochromic shift may occur, which can be attributed to a greater degree of stabilisation

of the excited state in comparison to the stabilisation of the ground state. This results in a reduction of the energy difference between the ground states. Examples of this phenomenon can be observed in molecules in which $\pi \rightarrow \pi^*$ transitions occur, whereby the excited state is more strongly stabilised by polar solvents due to the increased polarity of the excited state. In contrast, a hypsochromic shift occurs when the ground state is more strongly stabilised. This phenomenon is exemplified by molecules exhibiting a $n \rightarrow \pi^*$ transition, which, as previously discussed, involves the excitation of non-bonding electrons. This is attributable to the stabilisation of the ground state by the polar solvent, which possesses the non-bonding electron pair and is therefore more polar. Furthermore, effects can be observed with regard to the intensity of the absorption, whereby the interaction between the solvent and the solvate influences the transition probability. In the case of $\pi \rightarrow \pi^*$ transitions, the intensity of the transition is typically enhanced in the presence of polar solvents. Conversely, the intensity of $n \rightarrow \pi^*$ transitions is usually diminished due to the stabilisation of the ground state by a polar solvent, which consequently reduces the probability of the transition.

With regard to emission spectra, it can be observed that these spectra are also influenced by the interaction between the solvent and the solvate, albeit in a slightly different manner. This is because these are ultimately the result of the transition from the excited state to the ground state, and are therefore more strongly influenced by the interaction, due to the role played by relaxation processes. When the Stokes shift is initially considered, it becomes evident that an increase in solvent polarity results in a more pronounced shift, due to the relaxation of the excited state. The corresponding relaxation processes are elucidated in section 3.4.3. A bathochromic shift in the emission spectra is observed when the excited state is strongly stabilised by a polar solvent. The bathochromic shift of rhodamine 6G (cf. figure 6.16) as the polarity of the solvent increases serves as an illustrative example. In contrast, a hypsochromic shift occurs when the excited state is unable to be stabilised by the solvent to the same extent as the ground state, resulting in a larger energy difference between the two states. Such examples include molecules that exhibit a pronounced dipole-dipole interaction with the solvent, wherein the excited state also displays a lower polarity compared to the ground state. Fluorescent dyes, such as merocyanine or polymethine, serve as illustrative examples of this phenomenon. The observation of fluorescence intensity in relation to the effect of the interaction between solvent and solvate demonstrates that this can also be influenced. The presence of polar solvents often increases the probability of non-radiative transitions, such as ISC or IC, which ultimately results in a decrease in fluorescence intensity. This is due to the fact that the return to the ground state occurs more frequently via these processes. Also, quenching

effects may also result from the interaction. Moreover, the lifetime of the excited state can be affected by the promotion of non-radiative transitions by the solvent.

In principle, it can be stated that the type of transition is of interest with regard to its effect on the absorption and emission spectra. In light of the aforementioned transitions, it becomes evident that the most pertinent ones are the $\pi \rightarrow \pi^*$ and $n \rightarrow \pi^*$ transitions, while the $\sigma \rightarrow \sigma^*$ transitions can be disregarded, given that they predominantly occur in the UV range and solvent interactions typically exert minimal or even none influence on the spectra in question. An additional consequence of the interaction between the solvent and the solvate is the impact that the solvent has on the shape of the absorption band associated with the $\pi \rightarrow \pi^*$ transition, which is manifested in alterations to the vibronic interaction. It can therefore be concluded that the external solvent polarisation is responsible for the breaking of internal symmetry restrictions, which in turn results in the observation of new absorption bands within the spectrum [110].

Bayliss [40] and McRae [118], [119], [41] have already put forth a system for categorising the combinations and their effects on the spectra, with a particular focus on the combination of solvent and solvate. The classification is divided into four categories, as outlined below [110]:

1st. **A nonpolar solvate dissolved in a nonpolar solvent.**
In this instance, it can be stated that only dispersion forces are of consequence. The strength of the dispersion forces is contingent upon the refractive index, the intensity of the transition, and the dimensions of the solvate. The solvent exerts no discernible influence on the energy levels, however, the dispersion forces result in a slight bathochromic shift.

2nd. **A nonpolar solvate dissolved in a polar solvent.**
In this instance, the absence of the dipole moment of the solvate precludes the possibility of specific alignment between the solvate molecule and the solvent molecules. Nevertheless, it is necessary to consider the interactions of the quadrupole of the solvate with the solvent molecules in this case. The ground state is more strongly stabilised, resulting in a slight hypsochromic shift.

3rd. **A dipolar solvate dissolved in a nonpolar solvent.**
In this instance, dipole-induced dipole interactions and dispersion forces

are of consequence. Should the dipole moment of the solvate increase following electronic excitation, the Franck-Condon state will be more strongly stabilised, resulting in a bathochromic shift. A decrease in the dipole moment in the excited state results in a reduction in the stabilisation of the Franck-Condon state, leading to a hypsochromic or bathochromic shift. This shift is dependent on the bathochromic shift due to polarisation.

4th. **A dipolar solvate dissolved in a polar solvent.**
In this instance, the dipole-dipole interactions are of paramount importance. The ground state of the solvate is markedly stabilised as a consequence of these interactions. An increase in the dipole moment of the excited state results in a bathochromic shift due to the stabilisation of the excited state. A bathochromic shift also occurs when the dipole moment decreases in the excited state, although of less magnitude.

It should be emphasised that this categorisation into four distinct groups is intended as a broad framework and is not intended to be used as a comprehensive criterion for classifying the influence of solvent solvate interactions on absorption and emission spectra. This is due to the multitude of factors and exceptions that can potentially influence these interactions.

In principle, it can be stated that when considering absorption spectra alone and reducing the influence of the solvent to polarity alone, the solvent polarity or solvent polarity function ultimately serves as a function of the variables in the form of refractive index and permittivity, together with the angle of observation of increasing polarity the $\pi \rightarrow \pi^*$ transitions undergo a bathochromic shift. Similarly, the $n \rightarrow \pi^*$ transitions undergo a hypsochromic shift.

In the context of a summary, it can be stated that a sole consideration of the impact of solvent and solvate interaction on emission spectra is sufficient to conclude that solvent influence on emission spectra, as it's the case with absorption spectra, is dependent on solvent polarity, which is determined by the solvent polarity function. In this way, the effects on the position and shape of the spectrum, as well as the effect on the lifetime of the excited state, can be determined. In essence, it can be posited that in instances where the dipole moment of the excited state is greater than that of the ground state,

a bathochromic shift occurs, which mirrors the increasing polarity of the solvent. The converse scenario has already been elucidated. Furthermore, the relaxation time and the lifetime of the molecule in the excited state must be considered within the context of the emission spectra, as this has an impact on the bands of the emission spectrum, which may represent the unreleased state, the relaxed state, or a combination of the two. Furthermore, the close relationship between absorption and emission spectra is evidenced by the fact that the appearance of the emission spectra is also determined by the influence of the solvent on the ground state and thus the absorption spectra.

In conclusion, it can be stated that generalisations about the appearance of absorption and emission spectra, derived from the interaction between a solvent and a solvate, are possible. However, these should be treated with caution, given that the factors influencing the interaction between a solvent and a solvate are extremely diverse and complex. Nevertheless, there are a number of quantitative calculation methods that precisely link these aspects, namely the influence of the solvent on the solvate with the shift of the maxima in absorption and emission spectra. This enables the investigation of molecular properties, including the calculation of dipole moments in the ground state and in the electronically excited state.

3.5. Dipoles

Dipole moments, represented by the symbol μ, are a fundamental physical property of molecules. They exert a significant influence on a range of crucial physical properties, including boiling point, melting point and solubility. Moreover, dipole moments exert an influence on both intramolecular interactions and intermolecular interactions between molecules. This signifies that, in addition to its profound significance in the field of physics, it constitutes a fundamental concept in the discipline of chemistry. A molecular dipole moment is generated as a result of two opposite electrical charges, which are separated by a given spatial distance. It follows that the dipole moment is a vectorial quantity. The resulting electric field is represented in chemical notation as a vector arrow from the positive charge to the negative charge and in physical notation from the negative to the positive charge. The product of the charge and the distance between the charges serves as a measure of the strength of a dipole moment, which can be expressed mathematically as follows: $\mu = q \times d$. In this context, the charge is represented by the symbol q, while the distance between the charges is represented by the symbol d. The dipole moment is expressed in Debye units, D. For the purpose of conversion into SI units, the appropriate

formula is coulombs times metres, $C \cdot m$, which is, $1\ D = 3,33564 \cdot 10^{-30}\ C \cdot m$, in Debye units. Once determined, the dipole moment provides information regarding the polarity of a molecule and the resulting interactions. Furthermore, an understanding of the dipole moment is crucial for the aforementioned applications, as well as for comprehending the underlying mechanisms of various processes.

Due to the composition of atoms, which consist of positively charged cores in the form of protons and negatively charged shells in the form of electrons, and the composition of molecules, which consist of different atoms, enabling the formation of dipole moments, gives rise to numerous dependencies and influencing factors that determine the strength of dipole moments. One of the most significant factors influencing the strength of dipole moments is the degree of electronegativity disparity between the atoms involved in a molecule. To illustrate, substantial discrepancies in electronegativity result in augmented charge separation and, consequently, elevated dipole moments. An additional crucial factor is the molecular geometry, which concerns the spatial configuration of the atoms within a molecule. This determines whether the bonding dipoles either add up to a total dipole moment or cancel each other out. In the case of CO_2, the molecule serves as a negative example, exhibiting polar bonds that nevertheless cancel each other out due to its symmetrical geometry. Furthermore, the bond length and type of bond between the atoms influence the strength of the dipole moment, with longer bonds resulting in a higher dipole moment for the same charge distribution. A crucial aspect of the influence on dipole moment strength is the molecular environment, whereby the charge distribution within the molecule can be shifted, strengthened or even reduced. For example, this can be achieved by applying an external electric field or by dissolving the molecule, which ultimately corresponds to the application of an electric field, given that the solvent molecules that form the cavity of the dissolved molecule themselves constitute an electric field that influences the dissolved molecule and thus its charge distribution. As the aforementioned dependencies and influencing factors are also temperature-dependent variables, the temperature exerts a direct or indirect influence on the strength of the dipole moment.

Moreover, it is necessary to consider the dipole moments in the electronically excited state, where the electronically excited state have already been discussed in the previous section 3.1.1. Dipole moments in the electronically excited state pertain to the distribution of charge in an excited molecule, which may differ considerably from the charge distributions observed in the ground state. This discrepancy can be attributed to the alteration in the electron density distribution that occurs in the excited state. Such alterations are brought about by the differing polarisation of the orbitals during the excitation process, coupled with the movement of the excited electrons to higher-energy positions. Never-

theless, the mathematical representation remains identical to that of the ground state. The dependencies and influencing factors of the dipole moments in the electronically excited state can be divided into two categories: the type of excitation, which can be, for example, either $\pi \rightarrow \pi^*$ or $n \rightarrow \pi^*$ excitation, and the associated change in molecular structure and molecular geometry. This phenomenon allows for the development of a strong dipole moment in molecules that are symmetrical in their ground state, as a result of the formation of a strongly asymmetric electron configuration following excitation. A well-known example of this phenomenon is the aromatic hydrocarbon benzene, C_6H_6, which in its ground state is a symmetrical, planar molecule with an even distribution of electrons in a delocalised ring system. In the excited state, the electron density distribution becomes asymmetric due to the transition of electrons from a π orbital into a higher π^* orbital. This results in a change in the molecule's symmetry, causing the molecule to become asymmetrical. Similarly to the gorund state dipole moments, solvation and environmental effects occur in the electronically excited state dipole moments. These can alter the electron density distribution, but they can also stabilise it, leading to further changes in this electron density distribution. Furthermore, the polarizability of the solvent can impede or facilitate the relaxation and adjustment of the dipole moment.
Since the initial conceptualisation of dipole moments by Max Reinganum in 1903 [30] and the subsequent independent formulation of the concept by Peter Debye in 1905 [32], Debye became the pre-eminent researcher in the field of dipole moments. In 1912, Debye devised the initial methodology for quantifying dipole moments in the ground state through the utilisation of a capacitor, wherein the dielectric constant ϵ_r serves as the primary measurement parameter. The dipole moment is calculated using the following equation, which is known as the Debye equation:

$$P_m = \frac{\epsilon_r - 1}{\epsilon_r + 2} \cdot \frac{M}{\rho} = \frac{N_A}{3\epsilon_0} \cdot \left(\alpha + \frac{\mu_g^2}{3k_BT}\right) \tag{3.42}$$

By solving the equation 3.42 for the variable μ, results in the following expression:

$$\mu = \sqrt{3k_BT \cdot \left(\frac{\epsilon_r - 1}{\epsilon_r + 2} \cdot \frac{M}{\rho} \cdot \frac{3\epsilon_0}{N_A} - \alpha\right)} \tag{3.43}$$

Variables in 3.42 and 3.43: P_m corresponds to the molar polarisation, M to the molar

mass, ρ to the density, N_A to the Avogadro constant, ϵ_0 is the permittivity of the vacuum, α is the polarizability, k_B is the Boltzmann constant, T is the temperature and μ is the dipole moment.

Over time, further models and concepts were developed for determining dipole moments in the ground state, which addressed the increasing demand for greater precision and speed in the determination process. One initial approach was the measurement in the gas phase via microwave spectroscopy. The foundations of this method were developed in the 1930s and 1940s, and significant improvements were made in the 1950s. The fundamental premise of this methodology is the interaction of molecules with electromagnetic microwave radiation, whereby molecules with a dipole moment can undergo rotational absorption of these electromagnetic waves. The frequency of absorption is dependent on both the moment of inertia and the dipole moment. Subsequently, the dipole moment of the ground state can be determined directly through the analysis of rotational spectra [120], [121], [122], [123]. In the 20th century, there was a focus on developing measuring methods in the liquid phase due to the growing interest in studying large molecules that could not be brought into the gas phase due to their tendency to dissociate. These are electro-optical measurement methods that utilise the Kerr effect. This describes the induction of a dipole moment in molecules under the influence of a strong electric field, resulting in the emergence of birefringent properties. The variation in the refractive index in response to an applied electric field and its polarization furnishes insight into the dipole moment of the molecule [124], [125], [126], [127]. In the present era, the most reliable method for determining dipole moments in the ground state is high-resolution UV laser spectroscopy. This approach employs the Stark effect to shift and split the spectral lines of a molecule. The dipole moment can be calculated by measuring the line shift [128], [129], [130], [131], [132].
In contrast to the relatively straightforward determination of dipole moments in the ground state, the determination of dipole moments in the electronically excited state represents a complex and challenging task. This is due to the fact that the lifetimes of electronically excited states are relatively short and they are also energie dependent. The most significant methodologies for determining dipole moments in electronically excited states are UV/Vis spectroscopy techniques in solutions, which are based on solvatochromism and thermochromism. The fundamental premise is the examination of absorption and emission spectra following a modification of external parameters, a process that is elucidated in greater detail as the main topic of this dissertation. The foundations of this approach can be traced back to the 1950s and 1960s, with its principles initially established by

Ooshika [37], Lippert and Mataga [38], [133], [39], as well as Bilot and Kawski[43], [134], [135], [136]. An alternative approach for determining dipole moments in excited states is time-resolved spectroscopy utilising pump-probe techniques. This was made feasible by the advent of femtosecond spectroscopy in the 1980s. In this approach, an ultrashort laser pulse is employed to excite the molecule to the electronically excited state, i.e. pump pulse, which is then probed by a second laser pulse, designated as the probe pulse. The evaluation of the dipole moment is based on the analysis of changes in absorption and emission [137], [138], [139], [140], [141]. As with the determination of dipole moments in the ground state, the gold standard is the determination by high-resolution UV laser spectroscopy, employing the same methodology and with the same inherent limitations [6], [142], [143], [96]. An alternative approach for determining dipole moments in the excited state is through the determination of photostationary states and electroluminescence. This method relies on the interaction of molecules in the electronically excited state with an electric field during continuous excitation. The distinction in the response to the electric field between the ground state and the electronically excited state is employed in this instance.

Furthermore, a comprehensive analysis of dipole moments necessitates an examination of the distinction between permanent and induced dipole moments, which will be addressed in the subsequent section.

Permanent Dipole

A permanent dipole moment is defined as an unequal distribution of electron density and, consequently, of the charge distribution that persists over time. It persists in a state of permanence and exists independently of external electric fields, although not in terms of its strength. This enables molecules with a permanent dipole moment to orientate themselves in accordance with an external electric field.

Mathematically, a permanent dipole moment can be described by a general consideration of the potential energy of a known charge distribution outside the charge area. This potential energy can then be expanded using a Taylor series, which provides a detailed representation of the potential energy at each point in the charge distribution. This implies that the potential energy can be characterised at any point in terms of the reference point P. From this line of reasoning, the multipole expansion $V(r)$ is shown in equation 3.44 [32], [144], [145].

$$V(r) = \frac{1}{r}\int_V \rho(r')d\tau' + \frac{1}{r^2}\int_V \rho(r')r'cos\theta d\tau' + \frac{1}{r^3} \int_V \rho(r')r'^2\left(\frac{3}{2}cos^2\theta - \frac{1}{2}\right)d\tau' + \cdots \tag{3.44}$$

Figure 3.16 illustrates the graphical representation of the individual components of the quantities utilized in equation 3.44, with the charge density represented by the variable ρ.

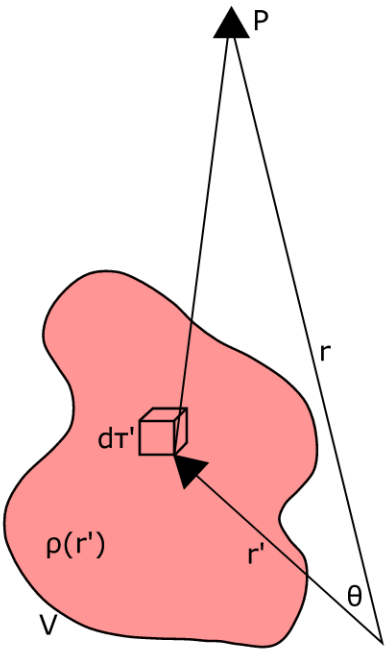

Figure 3.16.: Graphical representation illustrating the vector relations of a permanent dipole according to [6].

The individual terms of the multipole expansion, shown in equation 3.44, illustrate the progression of the individual charge conditions in ascending order, thereby demonstrating that the dipole moment can be adequately described by a single term within the context of a holistic consideration.

$$V_{monopole}(r) = \frac{1}{r}\int_V \rho(r')d\tau' = \frac{q}{r} \tag{3.45}$$

The initial term of the multipole expansion, as illustrated in equation 3.45, pertains to the description of a monopole, which is defined as a permanent charge, i.e. the net charge. The second term of the multipole expansion is the term for describing a dipole moment, as illustrated in equation 3.46. This approach permits the construction of additional multipoles, such as a quadrupole moment (cf. the final term in equation 3.44), from terms of lower order.

$$V_{dipole}(r) = \frac{1}{r^2}\int_V \rho(r')r'cos\theta d\tau' = \frac{\hat{r}}{r^2}p \tag{3.46}$$

In this instance, the dipole moment is represented by the variable p for point charges. Upon resolution of p, the subsequent equation, designated as 3.47, is derived for the dipole moment.

$$p = \sum_{i=1}^{n} q_i r_i' \tag{3.47}$$

Induced Dipole

In contrast to the permanent dipole moment, the induced dipole moment is a result of external influences. This can be achieved through the application of an external electric field, or alternatively, by the influence of a neighbouring dipole or an ion in the vicinity. The induction processes initiated by the external electric field prompt a shift in the electron density within the previously neutral molecule, enabling the formation of a transient dipole moment due to the prevailing unequal charge distribution. The strength of the resulting dipole moment is contingent upon the polarizability of the molecule, as expressed by the proportionality factor α, and the intensity of the indicated electric field. The induced dipole moment is described by the following equation:

$$\vec{\mu}_{ind} = \alpha \cdot \vec{E} \tag{3.48}$$

The proportionality factor, designated as α, is also referred to as polarizability. It serves

as a measure of the strength of the influence exerted by an external electric field on the polarizability of a molecule. This influence is proportional to the applied electric field, which is represented by the symbol E. In terms of the induced dipole moment, this factor describes the ease with which the electron cloud, and thus the charge density/distribution, within a molecule may be distorted in response to an applied electric field. Polarizability can be broadly classified into three principal categories. The first type of polarizability is electronic polarizability, which refers to the displacement of the electron cloud relative to the nucleus, and thus the positive charge. In comparison to the other two types of polarizability, this polarizability is frequently the dominant contribution to the total polarizability. The other is ion polarizability, which describes the displacement of the entire atoms or ions within a molecule relative to each other. The latter type of polarizability is orientational polarizability, which is predominantly observed in molecules with permanent dipole moments and describes the alignment of these dipole moments in response to an electric field. The polarizability of a molecule is influenced by a number of factors, including its size and structure. Larger molecules have a greater capacity for distortion due to their larger electron cloud. The electron configuration is another factor influencing polarizability. Molecules with loosely bound electrons, for example in the case of unsaturated compounds or anions, show a higher polarizability. The bond order is another factor influencing polarizability. Molecules with double bonds have a higher polarizability due to the easier delocalisation of the electrons. Finally, electronegativity is a factor influencing polarizability. With high electronegativity, there is a stronger electron bond to the positive nucleus, and thus the polarizability is reduced. It should be noted that polarizability is not always an isotropic quantity. The polarizability is expressed in SI units in cubic metres m^3.
If the three types of polarizability, namely the orientational polarizability P_O, the electronic polarizability P_E and the ionic polarizability P_I, are combined into a single equation 3.49, the total polarizability/molar polarizability P/P_m is obtained.

$$P/P_m = P_O + P_E + P_I \tag{3.49}$$

Subsequently, the separate determination of the displacement polarizability, comprising the electronic polarizability and the ionic polarizability, and the orientational polarizability can be carried out. This also has the consequence that the dipole moment μ and the polarizability α are also determined, as this is the application of the equation 3.42 according

to Debye [32]. This is made possible by determining the molar polarizability P_m as a function of temperature and plotting it as a function of $\frac{1}{T}$. This yields a straight line with the ordinate intercept corresponding to α and the slope corresponding to μ.

3.6. Thermo- vs. Solvatochromism

Solvatochromism and thermochromism are phenomena whereby the absorption and emission maxima of molecules undergo alteration as a consequence of their interaction with different solvents, in the case of solvatochromism, or temperature changes, in the case of thermochromism. This alteration is attributable to a modification in the energy differential between the ground state and the excited state as an result of external influence. Both phenomena can be employed to determine dipole moments in solution. This is ultimately attributable to alterations in the critical parameters that influence the solute molecule and its electronic structure, manifested in the form of the refractive index n and the permittivity ϵ. These two critical parameters are dependent on the solvent and temperature.
The classical method for determining dipole moments in solution was, and in some cases is still considered the standard method of determination, namely solvathochromism. Nevertheless, a more detailed examination of the interrelationships within this approach reveals that it is not without significant shortcomings. As previously stated, the absorption and emission maxima, and thus the energy gap between the ground state and the electronically excited state of the molecule under investigation, are influenced by the differentiation of the solvent used. The solvents employed exhibit disparate properties, primarily manifesting as variations in refractive index and permittivity. The term solvatochromism was first employed to describe this phenomenon in 1922 by the German chemist Arthur Hantzsch [146]. As a consequence of its uncomplicated application and execution, and the extensive range of potential applications reflected in the versatility of the solvent, the solvatochromic method gained rapid acceptance and proved highly successful [147], [148]. Nevertheless, a more detailed examination of the solvatochromic method, as previously noted, reveals that it encompasses a number of inherent disadvantages. This aspect was already considered by Mataga in 1956 [39]. It can be observed that although the requisite alteration in the parameters, namely the refractive index and permitivity, occurs when the solvent is replaced, the additional effects of the change in the solvent are disregarded [102]. To illustrate, the affinity for the formation of hydrogen bonds, which exerts a pronounced influence on the mutual interaction between the dissolved molecule and the solvent, is not taken into account. Such considerations are evident, yet they are not incorporated as variables in the calculation methodologies.

In order to circumvent the limitations of the solvatochromism method, Suppan initially proposed the thermochromism method in 1985 [149], based on Gryczyńskis and Kawskis work [79], a proposal that was subsequently validated by extensive research conducted by Kawski [150], [151], [152], [153], [154]. The fundamental premise of the thermochromism method is the utilisation of a consistent combination of the molecule under examination and the solvent employed. The requisite variation of the parameters, expressed in terms of refractive index and permittivity, which are temperature-dependent quantities, is generated through the measurement of samples at different temperatures. The advantage of this approach is that the other influencing variables are altered in a similar manner in response to temperature, thereby ensuring better comparability by maintaining the same solvent. The aforementioned relationships within the thermochromic method have resulted in a significant increase in the importance of accurately determining the temperature dependence of the variable sizes of the refractive indices and the permitivities. Consequently, these two parameters represent pivotal quantities for determining dipole moments in solution, as they constitute the primary components of the calculation methods (cf. 5) by Lippert [38], [133], Mataga [39] and Kawski [43], as well as Demissie [101].
It can thus be concluded that both methods, namely solvatochromism and thermochromism, are founded upon a change in polarity of the solvent, and its resultant effect upon spectroscopic measurements in terms of absorption and emission.
In addition, it is essential to consider an additional aspect, which is a crucial parameter for determining dipole moments in solution when employing solvatochromic or thermochromic techniques. This is the Onsager radius, denoted as a^3, which reflects the size of the solvate shell surrounding the solute molecule (cf. 3.4.1 and 3.4.3). The approximation of the Onsager radius, which postulates a spherical shell, is inherently imprecise, particularly for organic compounds, which often exhibit an ellipsoidal or irregular shape [102]. Consequently, the size of the solvate shell is significantly overestimated. This shortcoming has already been identified by Onsager himself [36] and by Mataga [39] as a significant limitation in the precise determination of dipole moments in solution. To address this limitation, the Onsager radius is replaced with the actual cavity volume, as proposed by Demissie [101], within the calculation methods. The practicality of this approach has been corroborated by a substantial body of published literature [155], [156], [157].
Due to the fact that the determination of dipole moments in solution initially took place using the method of solvatochromism, since the method of thermochromism was only established later, consequently all calculation methods (cf. 5) are based on the premise of calculation using the methods of solvatochromism. As both methods are fundamentally based on the variation of the refractive index and permeability, which results in a

change in the polarity function of the solvent, it is relatively straightforward to adapt the calculation methods for use with thermochromism. It should be noted that this variation occurs in two ways: firstly, in the case of solvatochromism, through the exchange of the solvent, and secondly, in the case of thermochromism, through the variation of temperature. Gryczyński and Kawski demonstrate in their publication [79] that this is feasible by determining the temperature dependence of the variables of interest and by establishing temperature-dependent equations to describe the corresponding values of the variables at each temperature. Furthermore, this is accomplished with the variable of the real cavity volume, introduced by Demissie [101], which also exhibits a temperature dependence, thus allowing for the determination of an equation describing this variable's temperature dependence. This approach allows the corresponding values of the temperature-dependent variables to be assigned to the corresponding measured values of the absorption and emission at the corresponding temperature. As a result, this enables the entire system comprising the dissolved molecule and solvent in question to be considered separately at that temperature.

In conclusion, it can be stated that thermochromic methods are more appropriate for determining dipole moments in the ground state and in the electronically excited state in the liquid phase when all the aforementioned aspects (cf. 3.4.3, 3.4.4) are taken into account. This is because this method maintain the system, comprising the solvent and solvate, in a consistent state, thereby preventing the fluctuations in parameters that are not fully within control. While the requisite spectral shifts are occasionally less pronounced than those achieved through solvent exchange, this can be offset by a broad temperature span and a substantial number of measurement points. In conclusion, the advantages of thermochromic methods are more significant than their disadvantages.

In the following, the equations according to Lippert and Mataga, Bilot and Kawski as well as Demissie are shown in their form for methods of thermochromism. In section 5, a comprehensive analysis of the theoretical foundations of these equations is presented, without delving into the transformation to methods of thermochromism.

Lippert and Mataga:

$$\Delta\vec{v} = \frac{2(\mu_e - \mu_g)^2}{4\pi\varepsilon_0 hca^3} \cdot \Delta F(T) + Const.$$
$$\Delta F(T) = \frac{\varepsilon(T) - 1}{2\epsilon(T) + 1} - \frac{1}{2} \cdot \left(\frac{n^2(T) - 1}{2n^2(T) + 1}\right) \tag{3.50}$$

Bilot and Kawski:

$$\Delta\tilde{\nu} = \frac{2(\mu_e - \mu_g)^2}{4\pi\varepsilon_0 hca^3} \cdot F(T) + Const.$$
$$F(T) = \frac{2n^2(T) + 1}{n^2(T) + 2}\left(\frac{\varepsilon(T) - 1}{\varepsilon(T) + 1} - \frac{n^2(T) - 1}{n^2(T) + 2}\right) \tag{3.51}$$

$$\sum\tilde{\nu} = \frac{2(\mu_e - \mu_g)^2}{4\pi\varepsilon_0 hca^3} \cdot \Phi(T) + Const.$$
$$\Phi(T) = F(T) + \frac{3(n^4(T) - 1)}{(n^2(T) + 2)^2} \tag{3.52}$$

Demissie:

$$\tilde{\nu}_{A/F}(T) = \tilde{\nu}^0_{A/F} - \frac{2\mu_{g/e}(\mu_e - \mu_g)}{3\varepsilon_0 hc} \cdot \Delta F_i(T)$$
$$F_1(T) = \frac{1}{V(T)}\left[\frac{\varepsilon(T) - 1}{2\varepsilon(T) + 1} - \frac{1}{2}\left(\frac{n^2(T) - 1}{2n^2(T) + 1}\right)\right] \tag{3.53}$$
$$F_2(T) = \frac{1}{V(T)}\left[\left[\frac{\varepsilon(T) - 1}{\varepsilon(T) + 2} - \frac{n^2(T) - 1}{n^2(T) + 2}\right]\frac{2n^2(T) + 1}{n^2(T) + 2} + \frac{3(n^4(T) - 1)}{(n^2(T) + 2)^2}\right]$$

4. Computational Methods

In this chapter, quantum chemical calculation methods as they offer significant reference values to evaluate the accuracy of determining dipole moments in the liquid phase will be discussed. This involves calculating the respective dipole moments in the ground and excited states. Moreover, precise dipole moment measurements of the ground state are a necessity in the computation approaches of thermochromic methods (cf. 5). These values can be obtained through quantum chemical calculations, provided that they are not attainable through gas phase determination experiments or literature sources. Furthermore, these calculations are highly significant in the field of determining dipole moments through the gas phase [6], [130], [129]. They serve as a crucial starting point in the assessment of the obtained rotation-resolved spectra using evolutionary algorithms. A vital aspect of this researchs quantum chemical calculation is the optimisation of the structure, which employs a correlation - consistent polarised Valenz - Tripelzeta basis set (**cc-pVTZ**) from the **TURBOMOLE** library [158]. The equilibrium geometry of the electronic masses and the lowest excited singlet state is optimised through the approximate coupled cluster singles and doubles model (**CC2**) employing the resolution - of - the - identity (**RI**) approximation [159], [160], [161]. Additional structural optimisation is achieved through modifications to CC2 using spin component scaling (**SCS**) [162]. Oscillation frequencies and zero - point corrections of the adiabatic excitation energy were obtained using the NumForce script [163] through the numerical second derivative. In addition, the Conductor - like Screening Model (**COSMO**) [164], [165], [166], which is included in the RI and CC2 (**ricc2**) module of the TURBOMOLE library [158], is considered, as it meets the requirements of dipole moment determination in solution.

Within quantum chemical post - Hartree - Fock ab initio methods, various techniques are available for approximating electron correlation. These include the configuration interaction of Møller - Plesset perturbation theory and density functional theory. However, this section focuses on the CC2 method mentioned above and used in the context of this work. One advantage of this method is that it considers the positions of other electrons, which can impact the behavior of the electrons. Therefore, the quality of the results is considerably enhanced when utilizing this technique [93].

Here, the ground state wave function Ψ is written with an exponential approach from the cluster operator $\widehat{T}$ and the Hartree - Fock wave function is formulated as a Slater determinant for the ground state Φ_0:

$$\Psi = e^{\widehat{T}}\Phi_0 \tag{4.1}$$

$$e^{\widehat{T}} = 1 + \widehat{T} + \frac{\widehat{T}^2}{2!} + \frac{\widehat{T}^3}{3!} + \cdots = \sum_{k=0}^{\infty} \frac{\widehat{T}^k}{k!} \tag{4.2}$$

The cluster operator represents the sum of all excitation operators $\widehat{T}$ and indicates the potential excitation from an occupied spin orbital $i, j, k, \ldots$ to a virtual spin orbital $a, b, c, \ldots$. $\widehat{T}_N$ corresponds to a complete system of N electrons at their maximum excitation. Excitation operators comprise the cluster amplitudes t and the exciting Slater determinants $\Phi_i^a, \Phi_{ij}^{ab}, \ldots$. The transition of the ground state Slater determinants Φ_0 into a linear combination of all n - fold excited Slater determinants is accomplished by a particular excitation operator $\widehat{T}_n$. If the equation 4.4 is taken into consideration, it is feasible to create a doubly excited Slater determinant $\widehat{T}_1^2\Phi_0$ utilizing quadratic and higher order terms for the excitation operator $\widehat{T}_1$:

$$\widehat{T} = \widehat{T}_1 + \widehat{T}_2 + \widehat{T}_3 + \cdots + \widehat{T}_N \tag{4.3}$$

$$\widehat{T}_1\Phi_0 = \sum_{a=n+1}^{\infty}\sum_{i=1}^{n} t_i^a \Phi_i^a \qquad \widehat{T}_2\Phi_0 = \sum_{b=a+1}^{\infty}\sum_{a=n+1}^{\infty}\sum_{j=i+1}^{n}\sum_{i=1}^{n-1} t_{ij}^{ab}\Phi_{ij}^{ab} \tag{4.4}$$

The wave function from the equation 4.1 is inserted into the Schrödinger equation and multiplied by $\langle\Phi_0 \mid$ to calculate the coupled cluster energy ($\mathbf{E_{CC}}$). The orthogonality of the spin orbitals $\langle\Phi_0 \mid e^{\widehat{T}}\Phi_0\rangle = \langle\Phi_0 \mid \Phi_0\rangle = 1$ is used as a tool. This results in the following equation [93]:

$$\widehat{H}\Psi = E\Psi \tag{4.5}$$

$$\widehat{H}e^{\widehat{T}}\Phi_0 = E_{CC}e^{\widehat{T}}\Phi_0 \tag{4.6}$$

$$\langle\Phi_0 \mid \widehat{H} \mid e^{\widehat{T}}\Phi_0\rangle = E_{CC}\langle\Phi_0 \mid e^{\widehat{T}}\Phi_0\rangle \tag{4.7}$$

$$\langle\Phi_0 \mid \widehat{H} \mid e^{\widehat{T}}\Phi_0\rangle = E_{CC} \tag{4.8}$$

Cluster amplitudes associated with the excitation operator $\widehat{T}_n$ can be obtained by multiplying the coupled - cluster vector function Ω_{μ_n} with $e^{-\widehat{T}}$ and the set of all respective n - fold excited Slater determinants $\langle\Phi_{\mu_n}\mid$. The method for calculating these amplitudes is outlined in [167]. These determinants can be determined using the Schrödinger equation. Consequently:

$$\Omega_{\mu_n} = \langle\Phi_{\mu_n} \mid e^{-\widehat{T}}\widehat{H}e^{\widehat{T}} \mid \Phi_0\rangle = 0 \tag{4.9}$$

Due to the disproportionately large amount of computation involved, it is impossible to obtain an exact solution to the Schrödinger equation. However, this can be overcome by selectively choosing excitation operators, allowing the Coupled - Cluster method to be applied. The simplest form of this is the Coupled - Cluster - Singles method (**CCS**). This uses the first term $\widehat{T}_1$ to calculate the parameters, but can increase the accuracy by including higher excitation operators, as seen in the Coupled - Cluster - Singles - and - Doubles method (**CCSD**) ($\widehat{T} = \widehat{T}_1 + \widehat{T}_2$) [167].

The next part focuses on the Approximate - Coupled - Cluster - Singles - and - Doubles method (**CC2**), a new coupled - cluster technique established in 1995 by Christiansen *et al.* and associated with the two previously described methods. Here, the equation for the single excitation remains in its original form. The equation for the double excitation is approximated through a perturbation - theoretical approach. The Hamilton operator $\widehat{H}$ is defined as the sum of the Fock operator $\widehat{F}$ and the fluctuation operator $\widehat{U}$ [167].

$$\widehat{H} = \widehat{F} + \widehat{U} \tag{4.10}$$

Thus, the CC2 - method results in a neglect of all $\widehat{T}_2$ - dependent terms of the vector function $\Omega_{\mu_2}^{CC2}$, which have a higher order than the first in the fluctuation potential $\widehat{U}$. Thereby, a reduction of the computational effort by one power, comparable to the CCSD - method, with a qualitative equation of the CC2 - energy with the Møller - Plesset - perturbation theory of second order (**MP2**). From this follows a hierarchy from CCS via CC2 to CCSD [167], [168]. However, it should be highlighted that the CC2 method's computational effort can only be significantly reduced by incorporating the RI approximation. Consequently, this method could been utilised for systems containing up to 15 atoms [169], [170]. In addition to the reduction of the computational effort and of the transformation of the two-electron integrals, it also reduces memory requirements, allowing molecules two to three times larger to be analysed [170], [160], [161]. To enhance precision in computing outcomes, the MP2- and CC2- methods utilize an SCS modification [171], [162] which assigns two distinct parameters, c_{OS} and c_{SS}, to the levels of correlation energy following equation 4.11.

$$E = c_{OS}E_{OS} + c_{SS}E_{SS} \tag{4.11}$$

These two parameters serve as scaling factors for the energy contributions of electron pairs with opposite (**OS**) and equal (**SS**) spin. This modification leads to the enhancement of short - range dynamical correlation due to the c_{OS} parameter, while the c_{SS} parameter reduces the long - range non - dynamical correlation [171]. According to Grimme [171], 51 reaction energies were calculated through SCS - MP2, and corresponding values were fit from Quadratic - Configuration Interaction with Singles and Doubles (non - iterative) (**QCISD(T)**) / Quadruple - Zeta - Valence (**QZV**) calculations. Consequently, an empiri-

cal optimization of the parameters $c_{OS} = 6/5$ and $c_{SS} = 1/3$ can be performed. This leads to a distinct alteration in the identification of electronically excited states after CC2 or SCS - CC2, as demonstrated by [157] for example.
To incorporate solvent effects into the calculated values, Klamt and Schüürmann developed the COSMO model [164]. This model was subsequently implemented in the ricc2 module of TURBOMOLE by Schäfer *et al.* [165] and later extended by Lunkenheimer and Köhn [166]. The COSMO model falls under the category of dielectric continuum models. It involves the solute molecule being enclosed in a cavity within a dielectric continuum of permittivity ϵ. The shell of the cavity is termed the solvent accessible surface (**SAS**). At this interface, there exists an interaction between the charge of the solute particle and the homogeneous dielectric continuum, which is expressed by the following equation:

$$4\pi\epsilon\sigma(r) = (\epsilon - 1)n(r)E^{-}(r) \tag{4.12}$$

The equation raises the problem of computing the screening charge density, as expressed in equation 4.12. Here, $n(r)$ denotes the normal vector of the surface at point r, and $E^{-}(r)$ denotes the electric field inside the cavity at that point. Here, the charge distribution of the solute molecule and the screening charges constitute $E^{-}(r)$. However, according to equation 4.12, it is not possible to solve this for cavities with arbitrary shapes [164]. However, it is noteworthy that the equation 4.12 holds the analytical solution for a spherical and ellipsoidal cavity, as previously demonstrated by Onsager [36], by incorporating an extension to the electric multipole moments. Nevertheless, this oversimplifies the problem and is heavily reliant on the choosen cavity size. Furthermore, the method of simplification is complicated by simultaneous cavity modifications. To address this issue, Klamt and Schüürmann [164] introduced a non - iterative method for solving equation 4.12 in cavities of arbitrary shape, based on a solution of a Green's function: the **Co**nductor - like **S**creening **Mo**del - **COSMO**.
In this model, the dielectric screening energies are assumed for specific geometries based on the parameter $(\epsilon - 1)/(\epsilon + x)$. The permittivity of the screening medium, denoted by ϵ, is also taken into account. The range is given be $0 \leq x \leq 2$. While screening effects in strong dielectric media correspond well to screening effects of infinitely strong dielectrics such as conductors, $\epsilon = \infty$, which are much easier to handle, the screening energy of a conductor of N point charges Q_i (in the following expressed as vector Q) at position r_i inside a spherical cavity of radius R can be expressed as follows for the total screening energy of the

system, where ΔE includes the energy gain of the source charges Q due to the screening as well as the positive energy due to the interaction of the screening charges on the sphere [164]:

$$\Delta E = -\frac{1}{2} QDQ \tag{4.13}$$

$$D_{ij} = \frac{R}{(R^4 - 2R^2 r_i r_j + r_i^2 r_j^2)^+} \tag{4.14}$$

While equation 4.13 provides a precise solution for conductors, it can be adjusted for many dielectrics by a small ϵ - dependent correction factor in form of $f(\epsilon) = (\epsilon - 1)/(\epsilon + \frac{1}{2})$. Similarly, by employing the dielectric operator D, the entire screening energy can be presented as a quadratic equation along with the inclusion of the charge vector Q, resembling the Coulomb interaction amongst the charges.

$$E_{Coulomb} = -\frac{1}{2} QCQ \tag{4.15}$$

$$C_{ij} = || \, r_i - r_j \, ||^{-+} \qquad\qquad C_{ii} = 0 \tag{4.16}$$

This quadratic fit simplifies the computation of a molecule's dielectric screening energy within a spherical cavity compared to Onsager's multipole expansion [36], and marks the initial step towards formulating the corresponding formula, based on the Green function, for irregularly shaped cavities [164].
Assuming a conductor at first, charges Q_i are enclosed by an irregular surface S. To determine the screening energy, S is divided into many small segments S_μ aligned to t_μ with constant surface charge density σ_μ for each segment. Under the assumption that $\mid S_\mu \mid$ describes the area, and $q_\mu = \mid S_\mu \mid \sigma_\mu$ describes the charge of each segment μ, then the following equation 4.17 gives the electrostatic interaction of each charge at point r_j with the charge at S_μ.

$$b_{i_\mu} = \frac{1}{\mid S_\mu \mid} \int_{S_\mu} \mid\mid r - r_i \mid\mid^{-1} d^2 r \qquad \approx \qquad \mid\mid t_\mu - r_i \mid\mid^{-1} \tag{4.17}$$

Where considering the electrostatic interaction between the units of charge at S_μ and S_ν, it is necessary to assume $\mu \neq \nu, a_{\mu\nu}$, as expressed by equation 4.18.

$$a_{\mu\nu} = \frac{1}{\mid S_\mu \mid\mid S_\nu \mid} \int_{S_\mu} \int_{S_\nu} \mid\mid r - r^t \mid\mid^{-1} d^2 r^t d^2 r \qquad \approx \qquad \mid\mid t_\mu - t_\nu \mid\mid^{-1} \tag{4.18}$$

It should be noted that a highly accurate approximation for the diagonal element $a_{\mu\mu}$ is given by $a_{\mu\mu} \approx 3.8 \mid S_\mu \mid^{-\frac{1}{2}}$. From these equations, the total energy of the total system is given by 4.19 [164].

$$E(q) = \frac{1}{2} QCQ + QBq + \frac{1}{2} qAq \tag{4.19}$$

Where vectors Q representing the N source charges Q_i, q representing the M surface charges q_j, and matrices A derived from $a_{\mu\nu}$, B derived from b_{i_μ}, and Coulomb matrix C (cf. equations 4.15, 4.16).

Furthermore, it is necessary to adjust the total energy in accordance with the current screening charge distribution q^*, which minimises that energy, to ensure that the evaluations of the screening energy in cavities of arbitrarily shaped objects are comparable to those of a sphere, where the Green function / dielectric operator becomes $BA^{-1}B$.

$$\nabla_q E(q) \mid_{q^*} = BQ + Aq^* = 0 \qquad with \qquad q^* = -A^{-1}BQ \tag{4.20}$$

$$E(\sigma^*) = \frac{1}{2} Q(C - BA^{-1}B)Q \tag{4.21}$$

$$\Delta E = -\frac{1}{2} QBA^{-1}BQ = -\frac{1}{2} QDQ \tag{4.22}$$

As of currently, only point charges have been taken into account and therefore an expansion to incorporate charge distributions resulting from the basis functions has to be made. This can be achieved through the application of the formula $\rho_{\kappa\lambda}(r) = P_{\kappa\lambda}\varphi_\kappa(r)\varphi_\lambda(r)$. $\varphi_\kappa(r)$ and $\varphi_\lambda(r)$ represent r_i, and Q_i is defined by matrix element $P_{\kappa\lambda}$. This ultimately results in [164]:

$$b_{\kappa\lambda,\mu} = \frac{1}{\mid S_\mu \mid} \int_{S_\mu} \int \frac{\varphi_\kappa(r)\varphi_\lambda(r)}{\mid\mid r^t - r \mid\mid} d^3r d^2r^t \qquad \approx \qquad \int \frac{\varphi_\kappa(r)\varphi_\lambda(r)}{\mid\mid t_\mu - r \mid\mid} d^3r \tag{4.23}$$

Therefore, the analytical gradient of the dielectric energy regarding the atomic position R_x can be computed using equation 4.24, based on the total dielectric screening energy equation 4.22.

$$\nabla_{R_x}\Delta E = -q^*(\nabla_{R_x}B)Q + \frac{1}{2}q^*(\nabla_{R_x}A)q^* \tag{4.24}$$

Assuming that each segment S_μ is bound to a single atom, the matrices of B and A in relation to R_x can be computed based on the subsequent equations, with $\nabla_{R_x}a_{\mu\mu} \approx 0$ as the diagonal component [164].

$$\nabla_{R_x}b_{i_\mu} \qquad \approx \qquad \nabla_{R_x} \mid\mid t_\mu - r_i \mid\mid^{-1} \qquad \approx \qquad \frac{t_\mu - r_i}{\mid\mid t_\mu - r_i \mid\mid^3}(\delta_{ix} - \delta_{\mu x}) \tag{4.25}$$

$$\nabla_{R_x}a_{\mu\nu} \qquad \approx \qquad \nabla_{R_x} \mid\mid t_\mu - t_\nu \mid\mid^{-1} \qquad \approx \qquad \frac{t_\mu - t_\nu}{\mid\mid t_\mu - t_\nu \mid\mid^3}(\delta_{\nu x} - \delta_{\mu x}) \tag{4.26}$$

With $\delta_{ix} = 1$ *or* 0 depending on whether point r_i belongs to atom x or not, and $\delta_{\mu x} = 1$ *or* 0

on whether segment S_ν belongs to atom x or not.

Additionally, it should be noted that the form of the equations 4.25 and 4.26 is the case of point charges and not the case of the charge distribution density, which is introduced by the equation 4.23, and that only the direct geometric dependence has been considered, leaving aside the indirect geometric dependence, which plays only a minor role in that case [164].
The following discussion briefly describes the incorporation of COSMO into TURBOMOLE, following the implementation by Schäfer *et al.* [165]. The first step in the implementation is the conductor boundary equation of vanishing total potential, where Φ^X denotes the electrostatic potential vector of the solvent X, while q^* represents the screening charges within a conductor of infinite dielectric strength ϵ.

$$0 = \Phi^{tot} = \Phi^X + Aq^* \tag{4.27}$$

Further follows the implementation of the finite value for ϵ for the screening charges over:

$$q = f(\epsilon)q^* \qquad with \qquad f(\epsilon) = \frac{\epsilon - 1}{\epsilon + \chi} \tag{4.28}$$

From the two equations shown above (cf. 4.27, 4.28) then follows the relation to the screening charges to the solute potential and the charge density of the solute.

$$Aq = -f(\epsilon)\Phi^X \tag{4.29}$$

The calculation of the matrix A is done via a Cholesky factorization instead of an inversion of the matrix, due to time and memory savings [165]. In order to implement COSMO in the self - consistency part of Hartree - Fock (**HF**) or density functional theory (**DFT**), the total electrostatic potential of the iteratively updated screening charges is added in the form of an external potential to the one - electron part, taking into account the polarization energy, and half of the solute - continuum interaction energy is subtracted in order to generate the screening charges. In the following, the scheme of a self - consistent field cycle

within HF or DFT calculations with COSMO according to Schäfer *et al.* [165] is shown.

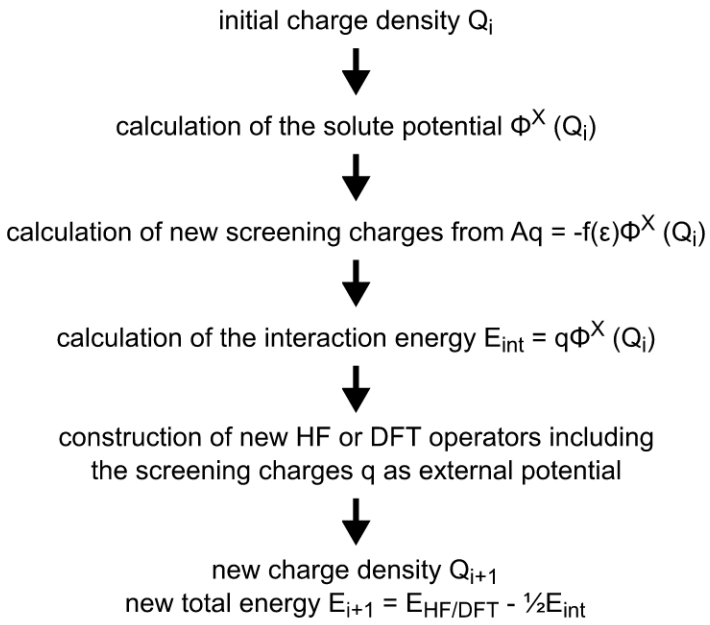

Figure 4.1.: Scheme of an SFC cycle in HF/DTF calculations with COSMO according to Schäfer *et al.* [165].

After completing the cycle, it is essential to adjust the total energy for the outlying charge error, as it was shown by A. Klamt and V. Jonas [172] before. To accomplish this, a stable and localized correction algorithm utilizes an auxiliary cavity located 0.85 Å outside the SAS. This permits the calculation of screening charges from the auxiliary cavity, which are then projected onto the original cavity [165].

5. Calculation Methods

This section of the dissertation discusses the calculation methods for dipole moments in solution used during the research work, which gave the best results in the context of their determination. Alternative techniques, including Bakhshiev [42], [173] and McRea [41], [174], were also considered. The methods mentioned in the previous sentence should not be overlooked. However, their limitations prevent a detailed discussion as their results lack accuracy and deviate considerably from the comparison values, such as those obtained through quantum chemical calculations or gas - phase determination. Fundamentally, all methods for calculating dipole moments in solution are based on the influence of the polarity of the solvent, represented by the corresponding solvent polarity function ΔF_i, where i is the notation of the solvent polarity function used, on the Stoke shift of the absorption and emission spectra. In contrast to Demissie [101], by the calculation methods of Lippert/Mataga [38], [39] and Bilot/Kawski [43], [135] only the dipole moment in the excited state μ_e can be determined, which requires the knowledge of the dipole moment in the ground state μ_g. However, the calculation method proposed by Demissie [101] has some weaknesses that will also be discussed later. Furthermore, it should be noted that the calculation methods mentioned previously were initially developed for solvatochromism, but can be easily applied to thermochromism as well due to the factors discussed in 3.6 and the reliance of solvent polarity.

5.1. Ooshika

As Ooshika's publication [37] is pivotal in establishing dipole moment calculation methods in solution, specifically those according to Lippert and Mataga [38], [39], and Bilot and Kawski [43], which are predominantly used in this work (cf. 5.2 and 5.3), as well as forming the basis for other notable calculation methods like McRea [41] or Bakhshiev [42], it shall be examined in greater depth below.
The aim of this publication is to establish a calculation theory to determine the absorption spectra of molecules in a solution using the perturbation theory. The shift can be calculated as a function of experimentally determinable quantities such as the dielectric constant,

refractive index, and the absorption wavelength of the solvent. This work assumes a uniform distribution of solvent molecules and categorizes various effects into distinct groups [37].
The categorization of these various effects is based on Sheppard's findings [175] and, from a theoretical point of view, leads to the following five categories [37]:

1st. Dielectric effects, which from the molecular perspective, take place in the dipole - dipole interaction between solute molecules and solvent molecules.

2nd. Specific short - range interactions occuring between dissolved molecules and solvent molecules, including solvation effects such as hydrogen bonds or electron transfer.

3rd. Association effects between dissolved molecules, which depend on concentration and may be disregarded in highly diluted solutions.

4th. Electrochemical phenomena like alterations in the dissociation degree of dissolved molecules and the inclusion of electrolytes.

5th. Long - range intermolecular resonance is insignificant for absorption effects, but it does play a part in quenching effects.

These five groups are similar to the five term groups described in the later section on the calculation method according to Lippert and Matage (cf. 5.2 and equation 5.23). However, they are not identical.
As an introduction, Ooshika [37] indicates that various approaches have been used by Sheppard [175], Bayliss [176] and Brooker [177] to explain the phenomena, although all of them had flaws. Thus, the approach proposed by Simpson [178], which is based on the valence bond method incorporating perturbation theory, is pursued.
To comprehend Ooshika's suggested methodology, certain assumptions must be made initially. Therefore, the solute molecule is fixed and a N molecular distribution function is described by the following equation:

$$f(1, 2, \ldots, N) = f_0 + f_1 \tag{5.1}$$

With f_0 representing the hypothetical distribution function of the solute molecule with the dipole moment set to 0, and f_1 representing the orientation of solvent molecules at the dipole of the solute molecule in its ground state. This function persists despite the solute molecule absorbing light, even when the solvent molecules take a much longer time to relax their orientation due to absorption processes (cf. figure 3.13).

The electronic wave function equations are formulated for the dissolved molecule by 5.2 and the solvent as a whole by 5.3.

$$H_0\psi_m = \varepsilon_m\psi_m \tag{5.2}$$

$$H\Psi_n = E_n\Psi_n$$

$$H = \sum_{i=1}^{N} H_i - \sum_i \sum_{j>i} \frac{\mu_i\mu_j}{r_{ij^3}}\ \Theta_{ij} \tag{5.3}$$

$$\Theta_{ij} = 2\ cos\ \theta_i\ cos\ \theta_j - sin\ \theta_i\ sin\ \theta_j\ cos\ \varphi_{ij}$$

With n representing the quantum number, H_i representing the Hamiltonian operator of the i - th solvent molecule, μ_i representing the dipole moment of the operator, r_{ij} representing the distance between the i - th and j - th solvent molecules, and Θ_{ij} representing the mutual orientation between μ_i and μ_j [37].

It is necessary to introduce the perturbation operator for the interaction between the solute molecule and the solvent molecules, with the proviso that the distances between the two components under consideration are of a larger nature, so that the problem under consideration can be reduced to the perturbation of the total energy of the system by V and can thus be expressed in terms of the change in the perturbation of the solvent molecules f. Where r_i and Θ_i denote the distance of mutual orientation between the solute molecule and the i - th solvent molecule.

$$V = -\sum_i \frac{\mu_0 \mu_i}{r_{j^3}} \Theta_i \tag{5.4}$$

The electronic wave function of the total system of the first - order can be deduced based on the following assumptions: the solute molecule is in state m, while the solvent molecules are in the ground state, labelled g. Furthermore, the distribution of solvent molecules is contingent upon the dipole moment of the ground state in solution, φ_g, and do not change by light absorption.

$$\Phi_{mn} = \varphi_m \Psi_n \tag{5.5}$$

In the following, Ooshika [37] first examines the energy of the first - order perturbation ΔE_1 under considaration of the mutual orientation between $(m|\mu_0|m)$ and $(\Psi_g|\mu_i|\Psi_g)$. This observation indicates a deviation from the Hamiltonian operator, where ΔE_1 is averaged over the molecular distribution. This consideration leads to the previously published result according to Onsager [36], which can be written as followed, where D is the dielectric constant and n represents the refractive index. Respectivly the solvent parameters.

$$(\Psi_g|\mu_i|\Psi_g) = \frac{(2D+1)(n^2+2)}{3(2D+n^2)} \mu_{gas} = \mu \tag{5.6}$$

From this, the approximation can be derived following Onsager 5.7 or Ooshika 5.8.

$$\begin{aligned} \vec{F} &= \left\{ \frac{2(D-1)}{2D+1} - \frac{2(n^2-1)}{2n^2+1} \right\} \frac{\vec{\mu_g'}}{a^3} \\ \vec{\mu_g'} &\approx \vec{\mu_g} + \frac{2(D-1)}{2D+1} \frac{2}{a^3} \sum_{m \neq g} \frac{\vec{\mu_g} \cdot (g|\vec{\mu_0}|m)(g|\vec{\mu_0}|m)}{\varepsilon_m - \varepsilon_g} \end{aligned} \tag{5.7}$$

$$\langle \Delta E_1 \rangle = -\left\{ \frac{2(D-1)}{2D+1} - \frac{2(n^2-1)}{2n^2+1} \right\} \left\{ \frac{\vec{\mu_g} \cdot \vec{\mu_m}}{a^3} + \frac{2(D-1)}{2D+1} \frac{2}{a^6} \sum_{m' \neq g} \frac{\left\{ \vec{\mu_g}(g|\vec{\mu_0}|m') \right\} \left\{ \vec{\mu_m}(g|\vec{\mu_o}|m') \right\}}{\varepsilon'_m - \varepsilon_g} \right\} \tag{5.8}$$

Next, the second order perturbation is considered, which according to Ooshika [37] can be classified into three different interactions. The first, $\Phi_{mg} - \Phi_{mn}$, characterises the average interaction between the dipole of solute molecule $\vec{\mu_m}$ and the induced dipole of the fixed i - th solvent molecule, as well as its orientation in the solution in the presence of $\vec{\mu_m}$ field. Described by:

$$\Delta E_{21} = \mu_{m^2} \sum_{n \neq g} \sum_{ij} \frac{(\Psi_g|\mu_i|\Psi_n)(\Psi_g|\mu_j|\Psi_n)\Theta_i\Theta_j}{(E_g - E_g) r_i^3 r_j^3} \tag{5.9}$$

under averaging this energy over f_0 it equals to:

$$\langle \Delta E_{21}^0 \rangle = -\frac{2(n^2-1)}{2n^2+1} \frac{\mu_{m^2}}{a^3} \tag{5.10}$$

The second, $\Phi_{ng} - \Phi_{m'g}$, can initially be defined as follows:

$$\Delta E_{22} = \sum_{m' \neq m} \sum_{ij} \frac{\mu^2 \Theta_i \Theta_j}{r_i^3 r_j^3} \frac{(m|\mu_0|m')^2}{\varepsilon_m - \varepsilon_{m'}} \tag{5.11}$$

under averaging ΔE_{22} over f_0:

$$\int \frac{\mu \mu_{eff} \Theta_i^2}{r_i^6} f_0^{(1)}(i) d\tau_i \qquad with \qquad \frac{\mu_{eff} \Theta_i}{r_i^3} = \sum_j \frac{\overline{\mu \Theta_j}^0}{r_j^3} \tag{5.12}$$

This equation (cf. 5.12) demonstrates, for μ_{eff}, that ensuring the i - th molecule's position and orientation are fixed permits the remaining molecules to polarise the solute molecule, provided a distribution other than the i - th is used. However, assuming independence of μ_{eff} from the i - th position and a solvent molecule possessing a point dipole within a spherical cavity, it can be concluded that the resulting surface charges are solely dependent on the orientation of the medium in relation to the correlation between solvent molecules. Therefore, the surface charges can be expressed by the dipole of the external environment.

$$-\frac{2(D-1)}{2D+1}\mu \qquad for \qquad \mu_{eff} = \mu - \frac{2(D-1)}{2D+1}\mu = \frac{3}{2D+1}\mu \tag{5.13}$$

Equation 5.13 demonstrates that the solvent molecules' polarizability D is accounted for, but μ_{eff} indicates that it constitutes only a portion of the permanent dipole. By employing $\frac{\mu^2}{kT} = \frac{(2D+1)^2(D-n)}{3(2D+n^2)D}d^3$, the dipole moment of the solvent molecules can be removed, resulting in the following expression for the second interaction's energy:

$$\langle \Delta E_{22}^0 \rangle = \frac{2(D+1)(D-n^2)}{3(2D+n^2)D}\frac{kT}{a^3}\sum_{m' \neq m}\frac{(m|\mu_0|m')^2}{\varepsilon_m - \varepsilon_{m'}} \tag{5.14}$$

Therefore, f_1 is utilised for averaging as it is a correction term. This ensures $\langle \Delta E_{22}^1 \rangle$ is obtained, representing the interaction energy between the reaction field and the mutual orientation of the solvent and solute molecules, and the energy of the induced dipoles in the solute molecules. In addition, the energy of the induced dipole moments of the solvent molecules is introduced [37].

$$\langle \Delta E_{22}^1 \rangle = \left\{\frac{2(D-1)}{2D+1}\right\}^2 \frac{1}{a^6}\sum_{m' \neq m}\frac{\{\vec{\mu_g}(m|\vec{\mu_0}|m')\}^2}{\varepsilon_m - \varepsilon_{m'}} \tag{5.15}$$

The third, $\Phi_{mg} - \Phi_{m'n}$, initially defined as follows:

$$\Delta E_{23} = \sum_{m' \neq m}\sum_{n \neq g}\sum_{i,j}(m|\mu_0|m') \times \frac{(\Psi_g|\mu_i|\Psi_n)(\Psi_g|\mu_j|\Psi_n)\Theta_i\Theta_j}{(\varepsilon_m - \varepsilon_{m'} + E_g - E_n)r_i^3 r_j^3} \tag{5.16}$$

Thus, the assumption is made that the polarizability of the solvent molecule is isotropic, so that averaging over f_1 is not required and only averaging over f_0 should be taken into account. Additionally, it is assumed that the excited states of the solvent are almost completely degenerate and that the absorption of the solute molecule takes place at much longer wavelengths than that of the solvent molecule, $|E_g - E_n| \gg |\varepsilon_m - \varepsilon_{m'}|$, so that the energy of the third interaction is given by the following equation:

$$\langle \Delta E_{23} \rangle = -\frac{2(n^2-1)}{2n^2+1}\frac{1}{a^3}\sum_{m' \neq m}(m|\mu_0|m')^2 \times \left\{1 - \frac{\varepsilon_m - \varepsilon_{m'}}{E_g - E_n}\right\} \tag{5.17}$$

Ultimately, the various effects illustrated earlier are analyzed in conjunction to determine the energy change in the state m, which leads to Ooshika's equation for absorption [37].

$$\begin{aligned}
\langle \Delta E \rangle_m = &-\frac{2(D-1)}{2D+1}\frac{\vec{\mu_g}\vec{\mu_m}}{a^3} - \frac{2(n^2-1)}{2n^2+1}\frac{\mu_m^2 - \vec{\mu_g}\vec{\mu_m}}{a^3} \\
&+ \frac{2(D-1)(D-n^2)}{3(2D+n^2)D}\frac{kT}{a^3}\sum_{m' \neq m}\frac{(m|\mu_0|m')^2}{\varepsilon_m - \varepsilon_{m'}} \\
&+ \left\{\frac{2(D-1)}{2D+1}\right\}^2 \frac{1}{a^6}\left\{\sum_{m' \neq m}\frac{\{\vec{\mu_g}(m|\vec{\mu_0}|m')\}^2}{\varepsilon_m - \varepsilon_{m'}}\right. \\
&\left. + 2\sum_{m' \neq m}\frac{\{\vec{\mu_g}(g|\vec{\mu_0}|m'\}\{\vec{\mu_m}(g|\vec{\mu_0}|m')\}}{\varepsilon_g - \varepsilon_{m'}}\right\} \\
&- \frac{2(n^2-1)}{2n^2+1}\frac{1}{a^3}\sum_{m' \neq m}(m|\mu_0|m')^2 \\
&\times \left\{1 - \frac{\varepsilon_m - \varepsilon_{m'}}{E_g - E_n}\right\}
\end{aligned} \tag{5.18}$$

5.2. Lippert and Mataga

The calculation methods of E. Lippert [38] and N. Mataga [39] were developed independently, and their combination forms the basis of the Lippert - Mataga plot. Common to both theories is the endeavour to regard the dissolved molecule and the solvent as a unified system and elucidate the ensuing interaction. Both refer to the general theory of the solvent's impact on the absorption spectrum, as proposed by Y. Ooshika [37] and others [176], [41].
In his paper, Lippert refers to Ooshika's equation for absorption 5.18 [37] and applies it analogously to fluorescence. It is assumed that the solvent completely relaxes before fluorescence processes occur. The following equation 5.19 is obtained by calculating the difference between the absorption and fluorescence maximum, where Δf denotes the polarity of the solvent.

$$\begin{aligned} \nu_A - \nu_F &= \frac{2}{hc_0} \cdot \Delta f \cdot \frac{(\mu_e - \mu_g)^2}{a^3} + Const. + smaller\ Terms \\ \Delta f &= \left(\frac{D-1}{2D+1} - \frac{n_D^2 - 1}{2n_D^2 + 1} \right) \end{aligned} \tag{5.19}$$

With $\nu_{A/F}$ the maximum of the absorption or fluorescence spectra, h the Planck constant, c_0 the speed of light in vacuum, a the Onsager radius, $\mu_{g/e}$ the dipole moments in the ground state or in the excited state, D the dielectric constant of the solvent, n_D the refractive index of the solvent at standard conditions.

Following Lippert's method, the spectral difference $\nu_A - \nu_F$ is plotted against the polarity of the solvent using Δf. This gives a linear equation (cf. 5.20) which can be used to calculate the difference in dipole moments $\Delta\mu$ between the ground state dipole moment and the excited state dipole moment, with m representing the slope of the plot. However, it should be noted that Lippert has already restricted the applicability of the demonstrated connections to predominantly strongly polar molecules in weakly polar solvents [133].

$$m = \frac{2 \cdot (\mu_e - \mu_g)^2}{hc_0 a^3} \tag{5.20}$$

Mataga presents an opposing perspective to Lippert's, highlighting that dipole - dipole interactions primarily stabilise the individual states of the molecule and solvent, shown and described in Figure 3.13, during the absorption and fluorescence processes. For this stabilization, Mataga introduces two terms which are expressed by equation 5.21 for absorption processes and by equation 5.22 for fluorescence processes [39].

$$hc\Delta\sigma_a = \langle\Delta E\rangle_f^e - \langle\Delta E\rangle_e^g \tag{5.21}$$

$$hc\Delta\sigma_f = \langle\Delta E\rangle_e^e - \langle\Delta E\ \rangle_f^g \tag{5.22}$$

Here, the four states (cf. 3.13), and their stabilization, are described using the following terms: $\langle\Delta E\rangle_e^g$ represents the equilibrium in the ground state, $\langle\Delta E\ \rangle_f^e$ represents the Franck - Condon state of the excited state, $\langle\Delta E\rangle_e^e$ represents the equilibrium in the excited state, and $\langle\Delta E\rangle_f^g$ represents the Franck - Condon state in the ground state.

Referring to Ooshika's theory [37], it is demonstrated that the stabilisation energy of solute molecules in the m - state transfers to the molecules in the excited state. This is expressed via the stabilisation energy $\langle\Delta E\rangle^m$ (cf. 5.23) of the solute molecule in the m - state [39].

$$
\begin{aligned}
\langle \Delta E \rangle^m = & -\left\{ \frac{2(D-1)}{2D+1} - \frac{2(n^2-1)}{2n^2+1} \right\} \\
& \times \left\{ \frac{\vec{\mu_e} \cdot \vec{\mu_g}}{a^3} + \frac{2 \cdot (D-1)}{2D+1} \frac{2}{a^5} \sum_{m' \neq e} \frac{\{\vec{\mu_e}(e|\vec{\mu_0}|m')\}\{\vec{\mu_m}(e|\vec{\mu_0}|m')\}}{\varepsilon_{m'} - \varepsilon_e} \right\} \\
& - \frac{1}{2} \cdot \frac{2(n^2-1)}{2n^2+1} \cdot \frac{\mu_m^2}{a^3} \\
& + \frac{2(D+1)(D-n^2)}{3(2D+n^2)D} \cdot \frac{kT}{a^3} \times \sum_{m' \neq m} \frac{(m|\vec{\mu_0}|m')^2}{\varepsilon_m - \varepsilon_{m'}} \\
& + \left\{ \frac{2(D-1)}{2D+1} \right\}^2 \cdot \frac{1}{a^3} \times \sum_{m' \neq m} \frac{\{\vec{\mu_e}(m|\vec{\mu_0}|m')\}^2}{\varepsilon_m - \varepsilon_{m'}} \\
& - \frac{1}{2} \cdot \frac{2(n^2-1)}{2n^2+1} \cdot \frac{1}{a^3} \times \sum_{m' \neq m} (m|\mu_0|m')^2 \left\{ 1 - \frac{\varepsilon_m - \varepsilon_{m'}}{E_g - E_n} \right\}
\end{aligned}
\tag{5.23}
$$

The variables introduced in the equation shown above refer with ε_m to the electronic energy of the solute molecule in the m - state, E_n to the electronic energy of the solvent molecule in the n - state, $\vec{\mu_m}$ to the dipole moment of the m - state and $\vec{\mu_0}$ to the dipole moment of the solute molecule.

Equation 5.23 can be separated into five distinct terms, with every term considering a different intermolecular interaction.

1st. Term: Orientation effect between both dipoles

2nd. Term: Interaction between the permanent and induced dipoles

3rd. Term: Polarisation of the solvate

4th. Term: Interaction between reaction field and orientation of the solvate molecules

5th. Term: Dispersion forces

Including the stabilization equations 5.21 as well as 5.22 and the equation 5.23 for the stabilisation of the m - state, the shifts of the absorption and fluorescence spectra by the solvent can be expressed by means of $hc\Delta\sigma_f$ and $hc\Delta\sigma_a$. If both relationships are set to each other, the total equation 5.24 is obtained from this [39].

$$\begin{aligned} hc(\Delta\sigma_f - \Delta\sigma_a) = &- \left[\frac{2\cdot(D-1)}{2D+1} - \frac{2\cdot(n^2-1)}{2n^2+1}\right] \times \frac{(\vec{\mu_e}-\vec{\mu_g})^2}{a^3} \\ &+ \left\{\frac{2\cdot(D-1)}{2D+1}\right\}^2 \cdot \frac{1}{a^3} \\ &\times \left[3\sum_{m\neq e}\frac{\{\vec{\mu_e}(e|\vec{\mu_a}|m)\}^2}{\varepsilon_e-\varepsilon_m} + 3\sum_{m\neq g}\frac{\{\vec{\mu_g}(g|\vec{\mu_0}|m)\}^2}{\varepsilon_g-\varepsilon_m}\right. \\ &- \sum_{m\neq g}\frac{\{\vec{\mu_g}(g|\vec{\mu_0}|m)\}^2}{\varepsilon_g-\varepsilon_m} - \sum_{m\neq e}\frac{\{\vec{\mu_g}(e|\vec{\mu_0}|m)\}^2}{\varepsilon_e-\varepsilon_m} \\ &- 2\sum_{m\neq e}\frac{\{\vec{\mu_e}(e|\vec{\mu_0}|m)\}\{\vec{\mu_g}(e|\vec{\mu_0}|m)\}}{\varepsilon_g-\varepsilon_m} \\ &\left. - 2\sum_{m\neq g}\frac{\{\vec{\mu_g}(g|\vec{\mu_0}|m)\}\{\vec{\mu_e}(g|\vec{\mu_0}|m)\}}{\epsilon_g-\varepsilon_m}\right] \end{aligned} \tag{5.24}$$

Upon closer examination, it becomes apparent that the variables $\Delta\sigma_f$ and $\Delta\sigma_a$ can be substituted with σ_f^m and σ_a^m, respectively σ_f^m is defined as the wavelength of the clearest peak of the fluorescence spectrum and σ_a^m is defined as the peak of the absorption with the longest wavelength. Moreover, a predominant number of terms from equation 5.23 become extremely small, so that they are neglected accordingly [39].

$$-hc(\sigma_f^m - \sigma_a^m) \cong \left[\frac{2\cdot(D-1)}{2D+1} - \frac{2\cdot(n^2-1)}{2n^2+1}\right]\cdot\frac{(\vec{\mu_e}-\vec{\mu_g})^2}{a^3} + Const. \tag{5.25}$$

By considering the equation 5.25 according to Mataga's approach, it is evident that the equation 5.19 proposed by Lippert yields the same results. When considering both equations collectively, the Lippert-Mataga equation 5.26 is obtained.

$$\vec{v}_A - \vec{v}_E = \frac{2(\mu_e - \mu_g)^2}{4\pi\varepsilon_0 hca^3} \cdot \Delta F + Const. \tag{5.26}$$

$$\Delta F = \frac{\varepsilon - 1}{2\epsilon + 1} - \frac{1}{2} \cdot \left(\frac{n^2 - 1}{2n^2 + 1} \right)$$

With the measured wavenumber $\vec{\nu}_{A/E}$, the permittivity of the vacuum ε_0, the permittivity of the solvent ε, and the refractive index of the solvent n.

5.2.1. Critique of Lippert and Mataga

The Lippert-Mataga method of calculation has been the subject of ongoing criticism since its publication. This is evident from critical comments in other publications, which will be examined in more detail below. However, it should be noted that by no means this list is complete. The primary critique of the Lippert-Mataga method of calculation is that it inadequately considers the distinctive interactions between the solvent and the solvate, as well as the polarizability of the solvate. Consequently, the calculated dipole moments according to Lippert and Mataga are frequently, or consistently, markedly higher than would be the case when employing alternative calculation methods [102]. Furthermore, the values obtained differ significantly from those obtained through quantum chemical calculations or in the gas phase. As early as the 1950s, when the Lippert and Mataga calculation method was first introduced, the first criticism was raised that the model presented was too simplistic [114]. This included the assumption of a spherical solvate shell and the reduction of the interaction between solvent and solvate to dipolar interactions. In the 1960s, the Lippert-Mataga model was expanded in order to address these shortcomings [42], [44], [136], [179]. However, it was subsequently discovered that the Lippert-Mataga calculation method was particularly ineffective when applied to highly polar solvents. The criticism persisted in the 1970s, but it was acknowledged that the Lippert and Mataga calculation method was likely applicable to simple, weakly polar molecules in non-polar solvents and, as previously mentioned, ineffective for more complex systems. These assumptions were further reinforced and confirmed by the advent of

quantum chemical calculations in the 1980s [180]. In the 1990s, the criticism primarily focused on the lack of consideration of molecular polarizability in the electronically excited state [53], [181], [182]. The criticism continued into the 2000s, 2010s and 2020s, yet the Lippert-Mataga calculation method remains in use, albeit with restrictions, for calculating excited state dipole moments in the liquid phase, whether according to solvachromism or thermochromism [5], [183]. The findings of this study corroborate the criticisms levied against the Lippert-Mataga calculation method (cf. 9).

5.3. Bilot and Kawski

The method for calculating according to Bilot and Kawski was established in their 1962 publication. Essentially, this method relies on quantum mechanical perturbation calculations and the Onsager model for liquid media [36]. This accounts for the shift in absorption and emission spectra due to the electrostatic contribution of the solvent's permittivity and refractive index [43]. The distinction between the calculation method as described by Lippert and Mataga (cf. 5.2) and the present one is the inclusion of the molecule's polarisability in the analysis. The starting point of the theory according to Bilot and Kawski is the consideration of the mutual electrostatic influence between the solvent and the dissolved molecule, considering the time duration of the individual processes that occur, such as the relaxation of the solvent or fluorescence, as already described in previous chapters (cf. figure 3.13).
Following Bilot and Kawski, the calculation method employs the equilibrium state as the starting point. The dipole moment, characterized by the matrix element $(m|M|m)$, aligns parallel with the reaction field of the solvent, described by E_m. As per [43], for the total dipole moment in the ground state, the equation 5.27 is valid by summing up the constant and induced dipole moment. With $(m|\alpha|m)$ representing the static electron polarizability of the solute molecule in its ground state.

$$(m|M^G|m) = (m|M|m) + (m|\alpha|m)E_m \tag{5.27}$$

Introducing Onsager's Reaction Field Theory [36], the electric field acting on the dissolved molecule changes due to its interaction with the dipole of the dissolved molecule, leading to the equation 5.28 [43]. Where a_m^3 represents the cavity volume based on the Onsager radius a_m of the solute molecule in its ground state and ε denotes the static dielectric constant of the solvent.

$$\begin{aligned} E_m &= f_m(\varepsilon) \cdot (m|M^G|m) \\ f_m(\varepsilon) &= \frac{2}{a_m^3}\frac{\varepsilon - 1}{2\varepsilon + 1} \end{aligned} \tag{5.28}$$

Thus, introducing the effect of the electric field on the dipole moment of the solution in

the ground state into the previous equation 5.28 for the total dipole moment gives the following equation 5.29 for the total dipole moment of the solution in the equilibrium state.

$$(m|M^G|m) = \frac{(m|M|m)}{1 - (m|a|m)f_m(\varepsilon)} \tag{5.29}$$

However, it is necessary to partition the reaction field into an orientation and induction part due to the alteration in the dissolved molecule's dipole moment during the transition to the excited state. The induction component of the reaction field, with the presence of the orientation component, can be achieved through an equation 5.30 based on the refractive index. This equation was extrapolated to the zero frequency [43]. With $E_{m(ind)}$ for the induction component.

$$\begin{aligned} E_{m(ind)} &= f_m(n_0^2)(m|M^G|m) \\ f_m(n_0^2) &= \frac{2}{a_m^3}\frac{n_0^2 - 1}{2n_0^2 + 1} \end{aligned} \tag{5.30}$$

Concurrently, the orientation component, equation 5.31, of the reaction field can be reproduced by the difference of equations 5.29 and 5.30. With $E_{m(or)}$ for the orientation component.

$$E_{m(or)} = [f_m(\varepsilon) - f_m(n_0^2](m|M^G|m) \tag{5.31}$$

From these relations the energy of the induction field in the Franck - Condon state $E^F_{k(ind)}$, the energy of the induction and orientation field in the ground state $E_{g(ind)/(or)}$ as well as the energy of the excited Franck - Condon state $E^F_{e(ind)}$ can be calculated taking into account the perturbation theory [43]. By determining the corresponding equations for the absorption as well as the emission shift and transforming them, the following equation 5.32 is obtained for the shift difference.

$$hc(\Delta\nu_a - \Delta\nu_f) = (M_e - M_g)^2 \left[\frac{f(\varepsilon)}{1-\alpha f(\varepsilon)} - \frac{f(n_0^2)}{1-\alpha f(n_0^2)}\right] + (M_e - M_g)^2 \frac{\alpha f(n_0^2)}{1-\alpha f(n_0^2)} \left[\frac{f(\varepsilon)}{1-\alpha f(\varepsilon)} - \frac{f(n_0^2)}{1-\alpha f(n_0^2)}\right] \tag{5.32}$$

Where: h is Planck's constant, c is the speed of light in vacuum, $\nu_{a/f}$ is the wavelength of absorption or fluorescence, $M_{g/e}$ is the dipole moment of the ground or excited state, $f(\varepsilon)$ the function of the dielectric constant of the solvent, $f(n_0^2)$ the function of the refractive index of the solvent, a the Onsager radius of the cavity shell and α the polarisability of the dissolved molecule.

The two summands of the equation 5.32 each represent the contribution of the Stark effect to the shift of the absorption and emission spectra, where the first summand represents the linear Stark effect and the second the quadratic Stark effect. The proportion of the quadratic Stark effect is negligibly small as compared to the linear Stark effect, which is evident through the relationship between $\frac{\alpha}{a^3} < 1$ and $\frac{[\alpha f(n_0^2]}{[1-\alpha f(n_0^2]} << 1$. Therefore, the second term could be excluded, shortening the equation 5.32 to the initial expression of the Bilot - Kawski plot 5.33 [43].

$$hc(\Delta\nu_a - \Delta\nu_f) = (M_e - M_g)^2 \frac{1}{1-\alpha f(n_0^2)} \left[\frac{f(\varepsilon)}{1-\alpha f(\varepsilon)} - \frac{f(n_0^2)}{1-\alpha f(n_0^2)}\right] \tag{5.33}$$

Further research by Bilot [135] and later by Kawski alone [152] resulted in minor adjustments to the equation 5.33, which ultimately led to its current form. Additionally, Bilot and Kawski devised two separate polarity functions of the solvent, denoted by F and Φ, which led to the development of the two equations 5.34 and 5.35 [152]. Where *const.* represents negligible components, as previously demonstrated by Lippert and Mataga 5.2, of the equations.

$$\tilde{\nu_A} - \tilde{\nu_F} = \frac{2(\mu_e - \mu_g)^2}{4\pi\varepsilon_0 hca^3} \cdot F + const.$$
$$F = \frac{2n^2+1}{n^2+2}\left(\frac{\varepsilon-1}{\varepsilon+1} - \frac{n^2-1}{n^2+2}\right) \tag{5.34}$$

$$\tilde{\nu_A} + \tilde{\nu_F} = -\frac{2(\mu_e - \mu_g)^2}{4\pi\varepsilon_0 hca^3} \cdot \Phi + const.$$
$$\Phi = F + \frac{3(n^4-1)}{(n^2+2)^2} \tag{5.35}$$

With the wave numbers of absorption or emission denoted by $\nu_{A/F}$, and the dipole moment of the ground state or excited state represented as $\mu_{g/e}$, the dielectric constant as ε_0, the Planck quantum of action as h, the speed of light in vacuum as c, the Onsager radius as a, the refractive index of the solvent as n, and the permittivity of the solvent as ε.

5.4. Demissie

Although the research findings obtained through Demissie's calculation method did not yield convincing outcomes during this study, the method is still discussed below as it offers an engaging approach. This method was considered for each molecule examined, and its dipole moments were determined using it.
In essence, Demissie [101] employed the calculation techniques outlined by Lippert and Mataga [38], [39], alongside those of Bilot and Kawski [43], as well as the earlier methods of Bakshiev [42] and McRea [41]. Significant adjustments were made to factor in the Onsager radius variables. Specifically, the Onsager radius was replaced with the actual cavity volume when using the calculation methods according to Lippert and Mataga, as well as Bilot and Kawski, for the purposes of this study.
By utilising the real cavity volume and the potential for autonomous calculation of the ground state dipole moment as well as the electronically excited dipole moment, where the calculation by Lippert and Mataga only calculate the difference $\Delta\mu$ between both states and the one by Bilot and Kawski only calculate the dipole moment of the electronically excited state μ_e, utilising any solvent polarity function, Demissie achieves the subsequent equations 5.36 [101]:

$$\tilde{\nu}_{A/F} = \tilde{\nu}^0_{A/F} - \frac{2\mu_{g/e}(\mu_e - \mu_g)}{3\varepsilon_0 hc} \cdot \Delta F_i$$

$$F_1 = \frac{1}{V}\left[\frac{\varepsilon - 1}{2\varepsilon + 1} - \frac{1}{2}\left(\frac{n^2 - 1}{2n^2 + 1}\right)\right] \tag{5.36}$$

$$F_2 = \frac{1}{V}\left[\left[\frac{\varepsilon - 1}{\varepsilon + 2} - \frac{n^2 - 1}{n^2 + 2}\right]\frac{2n^2 + 1}{n^2 + 2} + \frac{3(n^4 - 1)}{(n^2 + 2)^2}\right]$$

With $\nu_{A/F}$ representing the wavenumbers for absorption and emission, respectively, $\mu_{g/e}$ being the dipole moment of the ground state or excited state, ε_0 indicating the dielectric constant, h denoting Planck's constant, and c representing the speed of light in a vacuum, V the real cavity volume, n the refractive index of the solvent and ε the permittivity of the solvent and F_1 the polarity function of the solvent according to Lippert and Mataga as well as F_2 the polarity function of the solvent according to Bilot and Kawski.

Demissie [101] accomplishes independent calculation of state - dependent dipole mo-

ments by plotting absorption or emission wavenumbers against the corresponding solvent polarity function, utilizing equation 5.37, where $S_{A/F}$ corresponds to the respective slope.

$$S_{A/F} = \frac{2\mu_{g/e}(\mu_e - \mu_g)}{3\varepsilon_0 hc} \tag{5.37}$$

Consequently, the ratio of the slopes and thus the ratio of the dipole moments can be calculated from the two individual functions.

$$\begin{aligned} \frac{S_F}{S_A} &= \frac{\frac{2\cdot\mu_g\cdot(\mu_e-\mu_g)}{3\cdot\varepsilon_0\cdot h\cdot c}}{\frac{2\cdot\mu_e\cdot(\mu_e-\mu_g)}{3\cdot\varepsilon_0\cdot h\cdot c}} \\ &= \frac{2\mu_e(\mu_e - \mu_g)}{2\mu_g(\mu_e - \mu_g)} \\ &= \frac{\mu_e}{\mu_g} \end{aligned} \tag{5.38}$$

By converting the equation referenced in 5.38 into the corresponding dipole moment, the dipole moments can be computed separately as per Demissie's method [101].

$$\begin{aligned} \mu_g &= \mu_e \cdot \frac{S_A}{S_F} \\ &= \sqrt{\frac{3\varepsilon_0 hc S_A^2}{2(S_F - S_A)}} \end{aligned} \tag{5.39}$$

$$\begin{aligned} \mu_e &= \mu_g \cdot \frac{S_F}{S_A} \\ &= \sqrt{\frac{3\varepsilon_0 hcS_F^2}{2(S_F - S_A)}} \end{aligned} \tag{5.40}$$

5.4.1. Critique of Demissie

This distinct approach to calculating the dipole moments of the respective state, independent of the knowledge of the contrary dipole moment in the respective state, is an intriguing methodology. Nevertheless, this approach proves disadvantageous in every respect, yielding unsatisfactory results when compared with known values for the correspondingly calculated dipole moments or with other calculation methods. In the context of calculating the dipole moments of all molecules examined in the course of this work, as well as the molecules previously examined in this working group, for example see [184], using the method of Demissie, it can be observed that the dipole moment in the ground state is entirely underestimated according to the calculations of this method. Furthermore, the calculated dipole moment in the electronically excited state according to the approach of Demissie is markedly disparate from the corresponding reference values. This leads to the conclusion that, after considering the results, the calculation method according to Demissie can, at best, be used to calculate dipole moments in the electronically excited state, if at all. It should be noted that these conclusions are based on empirical data, and thus it is possible that the theoretical consideration is justified, but that its practical application has shown its limitations. One potential explanation for this discrepancy is the possibility that the influence of the solvent on the ground state of the molecule under examination is considerably weaker than its impact on the electronically excited state. Furthermore, the corresponding solvent polarity function from the calculation methods, where the effect of the solvent is set in relation to the dipole moment of the ground state and the dipole moment of the electronically excited state, is adopted without modification. Consequently, the effect of the solvent on the dipole moment in the ground state is overestimated, resulting in a significant underestimation of the dipole moment in the ground state. Consequently, the effect of the separate consideration on the dipole moments in the electronically excited state is comparatively minor, given that these are predominantly influenced by the solvent effects.

6. Experimental Setup

This chapter provides a detailed description and analysis of the experimental setup that is pertinent to this research project. It provides an overview of the measuring instruments employed and, in select instances, the functionality of specific components within these instruments, thereby facilitating a comprehensive understanding of the measurement technology utilized. The order of presentation is not of consequence, as the subject matter necessitates the interplay of diverse measuring instruments, methods, and techniques.

6.1. Spectroscopy

The following section provides an overview of the structural and functional characteristics of the spectrometers employed in this study to record absorption and emission spectra. In the case of absorption spectroscopy, an absorption spectrometer manufactured by Varian, designated as the Cary 50 Scan UV-Visible Spectrophotometer, was employed. In the case of emission spectroscopy, a device from the same manufacturer, Varian, was also employed: the Cary Eclipse Fluorescence Spectrophotometer.

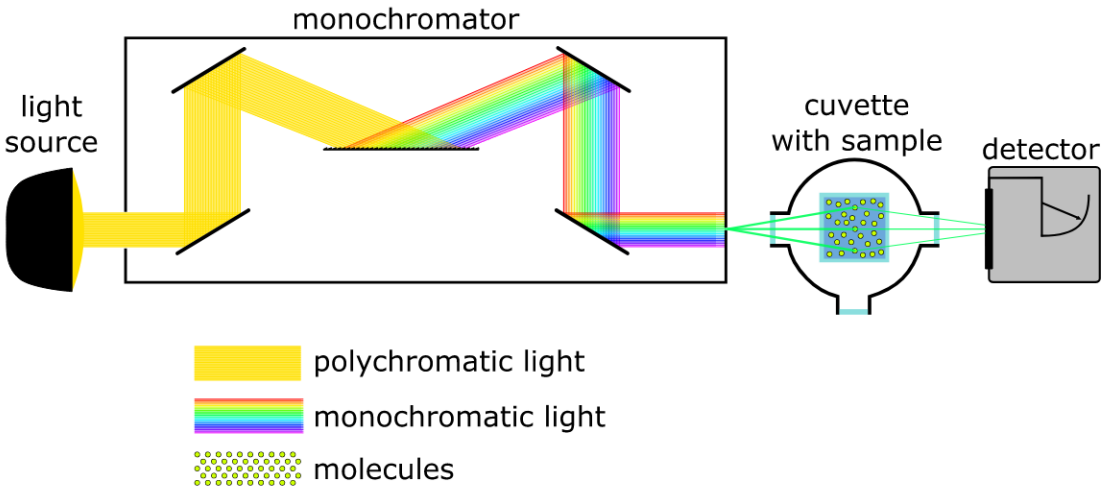

Figure 6.1.: Schematic illustration of a one - way absorption spectrometer with a sample in the sample chamber.

Absorption spectrometers can be broadly classified into two main categories, distinguished by the manner in which they are constructed. The two types of construction differ in the number of beam paths, with a distinction being made between single-beam and double-beam construction. In the course of this research, a spectrometer with a single-beam construction was employed. As illustrated in Figure 6.1, this absorption spectrometer is of a linear construction.

In regard to the light source, it is evident that the specifications for light sources utilized in spectrometers necessitate a high degree of stability in regard to their capacity for light generation. The light source should be capable of generating continuous or discrete light across a broad wavelength range. Moreover, the light spectrum should be readily definable and exhibit minimal fluctuations in emitted light within the defined wavelength range and at varying light intensities. In accordance with the aforementioned criteria, gas discharge lamps filled with xenon or mercury and also deuterium or tungsten lamps are utilised in the majority of contemporary spectrometers.
The generated light beam is introduced into the optical system via the coupling unit, which typically comprises mirrors and/or lenses and is thus capable of focusing the light. The polychromatic light is then directed onto an optical component, namely the monochromator. Prior to this, the light beam traverses a narrow adjustable slit, which serves to pre-select the transmitted light spectrum. The optical component is typically a prism or grating. The monochromator functions to divide the polychromatic light into its constituent spectral lines, thereby producing monochromatic light. The wavelength range to be transmitted is selected via a narrow adjustable slit, which defines the portion of the dispersed light spectrum to get in contact with the sample.
The monochromatic light beams of the specified wavelength range are directed into the sample chamber subsequent to the slit. The molecules of the sample to be analysed undergo a process of absorption, whereby a certain proportion of the light emitted at specific wavelengths is absorbed by the sample. Conversely, portions of the monochromatic light beams that are not absorbed are directed to a detector, where they are calibrated relative to the reference measurement, which is conducted prior to the sample measurement due to the single-beam design. During the detection phase, the light intensity of the transmitted light is measured and converted into an electrical signal, which is then forwarded to the read-out unit. The light intensity of the individual wavelengths is evaluated during the spectral analysis within the read-out unit.

As illustrated in Figure 6.2, the configuration of a fluorescence spectrometer is anal-

ogous up to the sample chamber and in the area of the evaluation unit to that of an absorption spectrometer.

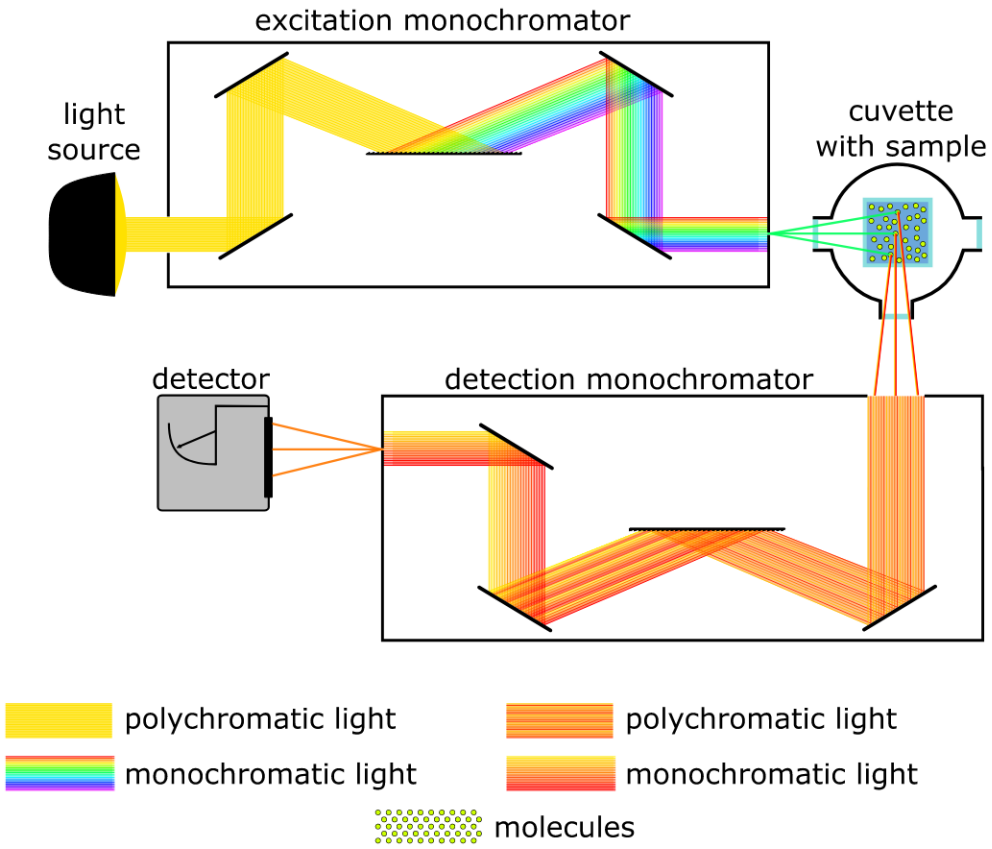

Figure 6.2.: Schematic illustration of an emission spectrometer measuring at a 90° angle with a sample inserted.

In the case of a fluorescence spectrometer, however, the sample chamber is followed by a detection monochromator, which is arranged at an angle of 90° to the sample chamber. The configuration of the apparatus is arranged at an angle of 90°, which serves to minimise the proportion of excitation light that is detected. The requisite excitation wavelength is established in advance through measurements conducted in the absorption spectrometer. The aforementioned minimisation of excitation light detection is a consequence of the fact that only a limited proportion of the light from the sample chamber is reflected at a right angle, with the majority of the light emitted by the sample molecules occurring at angles other than that of the excitation light.

Fluorescence measurements can be conducted using two distinct methodologies. These are fluorescence excitation spectroscopy and fluorescence emission spectroscopy, respectively. In fluorescence excitation spectroscopy, the excitation monochromator selects

a specific wavelength range from the polychromatic light emitted by the light source, thereby allowing only this wavelength range to pass through to the sample chamber, as in absorption spectroscopy. In contrast, the detection monochromator performs a scan of the emitted wavelength range. This indicates that the spectra of the absorption and emission measurements are highly similar. The distinction is made on the basis of the measured variable, which in the case of absorption measurements is the transmission and in the case of emission measurements is the intensity of the emission in relation to the absorbed wavelength. In fluorescence emission spectroscopy, in contrast, the excitation wavelength, typically the global maximum of the corresponding absorption spectra, is fixed, while the detection monochromator scans the specified wavelength range. This is the method by which the emission pattern of the molecule under investigation is obtained.

6.1.1. Monochromator

The utilisation of polychromatic light sources necessitates the decomposition of polychromatic light into monochromatic light. As previously stated, a monochromator is employed for this purpose, serving to isolate a specific wavelength within the spectrum. A monochromator is an optical component based on the principle of grating theory, specifically surface reflection by gratings. The gratings, which are grooved metallic surfaces, offer several advantages over prisms. These include a higher diffraction efficiency, a higher resolution and easier calibration. The wavelength employed is selected via an adjustable slit, which is then automatically controlled following the input of the requisite wavelength [80].
As previously stated, diffraction gratings are optical components with a surface that features a multitude of minute, parallel grooves. The grooves are positioned in such close proximity to one another that different wavelengths of the incident light are diffracted under different angles and subsequently spatially separated. The distance between the grooves is defined as the grating constant. The diffraction of light enables the respective light waves to interact with one another. This gives rise to two distinct types of interference, contingent on the angle of incidence of the light waves. In the case of constructive interference, the individual light waves are in phase, whereas in the case of destructive interference, the light waves are not in phase. The following diffraction equation 6.1 describes the relationship between the diffraction angle, wavelength and grating constant:

$$n\lambda = d \cdot (sin\ \theta_i + sin\ \theta_d) \tag{6.1}$$

In this context, the term diffraction order denoted by the symbol n refers to an integer value that characterises the various interference maxima. The wavelength is represented by the symbol λ. The grating constant is represented by the symbol d. The angle of incidence on the grating is represented by the symbol θ_i. Finally, the angle of deflection of the diffracted light is represented by the symbol θ_d. Furthermore, the equation demonstrates that for any given wavelength, there exists a specific angle that results in constructive interference [19], [185].

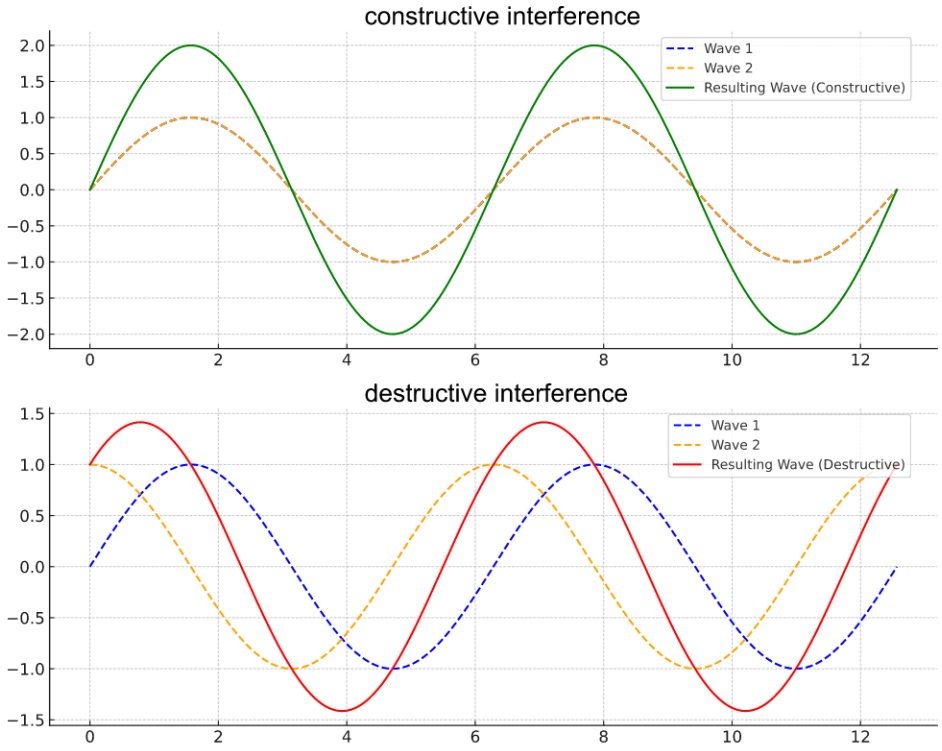

Figure 6.3.: A graphical representation of constructive and destructive interference.

The diagram 6.3 above illustrates the impact of the respective interferences with clarity. The upper part of the figure illustrates constructive interference, whereby the blue and yellow waves are in phase and therefore overlap, resulting in the green wave, which corresponds to an amplified wave from the blue and yellow. The lower part of the illustration depicts destructive interference, whereby both the blue and yellow waves are shifted at an angle of 90° to each other, resulting in the red wave. This illustrates how the shifted waves partially or completely cancel each other out.

6.1.2. Photodiode

In the majority of cases, photodiodes, in particular PIN photodiodes, are employed as detectors for spectroscopic measurements due to their ability to cover a broad spectral range for detection and react more rapidly to light changes than pn photodiodes. These photodiodes are based on the principle of the internal photoelectric effect, which, in contrast to the photoelectric effect, does not result in the emission of electrons but rather in the generation of electron-hole pairs [186]. A schematic representation of the processes occurring within a PIN photodiode is provided in Figure 6.4.

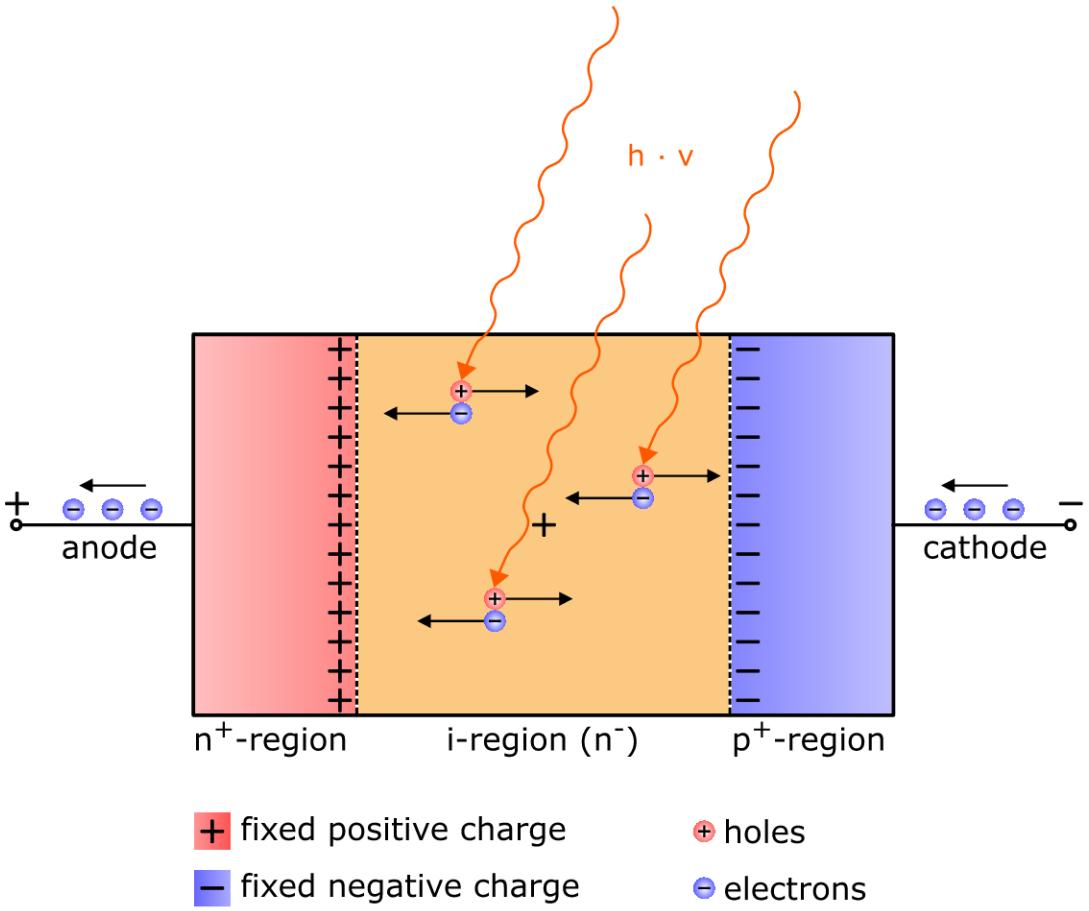

Figure 6.4.: Schematic representation depicts the processes occurring within a photodiode.

The fundamental constituents of photodiodes are distinct semiconductors, which are classified into three categories: the n^+-, n^--, and p^+ - region. This classification system allows for the identification of the specific region type, as illustrated in Figure 6.4. Additionally, the type of mobile charge carriers is illustrated. The diffusion of electrons from

an n-type semiconductor to a p-type semiconductor results in the formation of a fixed charge distribution at the respective boundary layer when the two types of semiconductor come into contact with one another. The i-region is an intrinsic layer that contributes to the sensitivity of the photodiode. When a photon with a higher energy than the band gap of the semiconductor material interacts with this region, electron-hole pairs are created. These can then propagate in different directions, generating an electric current. The corresponding charges are attracted by the oppositely charged boundary layer. In order to restore equilibrium, an electron from the n-region is conducted towards the anode, while an electron from the cathode is conducted into the p-region. This consequently gives rise to an electric current that is proportional to the number of incident photons [187].

6.2. Measuring Cell

A measuring cell was developed by the working group for the spectrometer mentioned in the previous section for the purpose of carrying out thermochromic spectroscopic measurements. This cell was subject to constant further development and optimisation over time [188], [156], [189]. The fundamental principle is based on a vacuum-sealed steel chamber with optical apertures at 90° (emission measurements) and 180° (absorption measurements) angles, in conjunction with two integrated cooling units. In order to prevent condensation of humidity at temperatures below 273.15 K at the optical ports and in the sample-containing cuvette, it is necessary to create a vacuum inside the measuring cell. The optical ports are constructed from double-glazed quartz glass windows. In addition to the connection for the oil-slide pump, which is used to generate a vacuum, the cell has an input and an output connection for an external circuit cooler. This is employed to cool the internal cooling element, which is comprised of two Peltier devices. Furthermore, the measuring cell is equipped with an external access point to the sample holder, the cuvette, thereby facilitating the replacement of samples during operation without breaking the cooling or vacuum. In order to enhance efficiency, all temperature-controlled constructional components are situated as distally as possible from the outer shell. In order to achieve this, the internal structure of the measuring cell is mounted on a **PTFE** block - (**P**oly - **T**etra - **F**luoro - **E**thylen). The cooling liquid of the external cooling circuit is introduced into a copper block, which, as previously stated, serves to cool the warm side of the Peltier device. To enhance the efficiency of the external cooling circuit, thin rods are integrated within the hollow space of the copper block, which generate turbulence and thereby facilitate more effective heat exchange. A smaller copper block is affixed to the Peltier devices, along with an extension that serves to enhance the contact surface area

between the cuvette and the copper block. This is the primary factor responsible for the maximum transfer of heat between the cooling unit and the cuvette. All contact points are coated with a heat-conducting paste to enhance the transfer of heat, and all apertures in the external casing are sealed with sealing rings. Furthermore, the temperature is recorded at two points within the structure of the measuring cell. This is achieved by monitoring the copper block of the cuvette holder to regulate the Peltier devices and by gauging the temperature of the sample within the cuvette itself. The temperature is determined through the use of PT100 sensors.

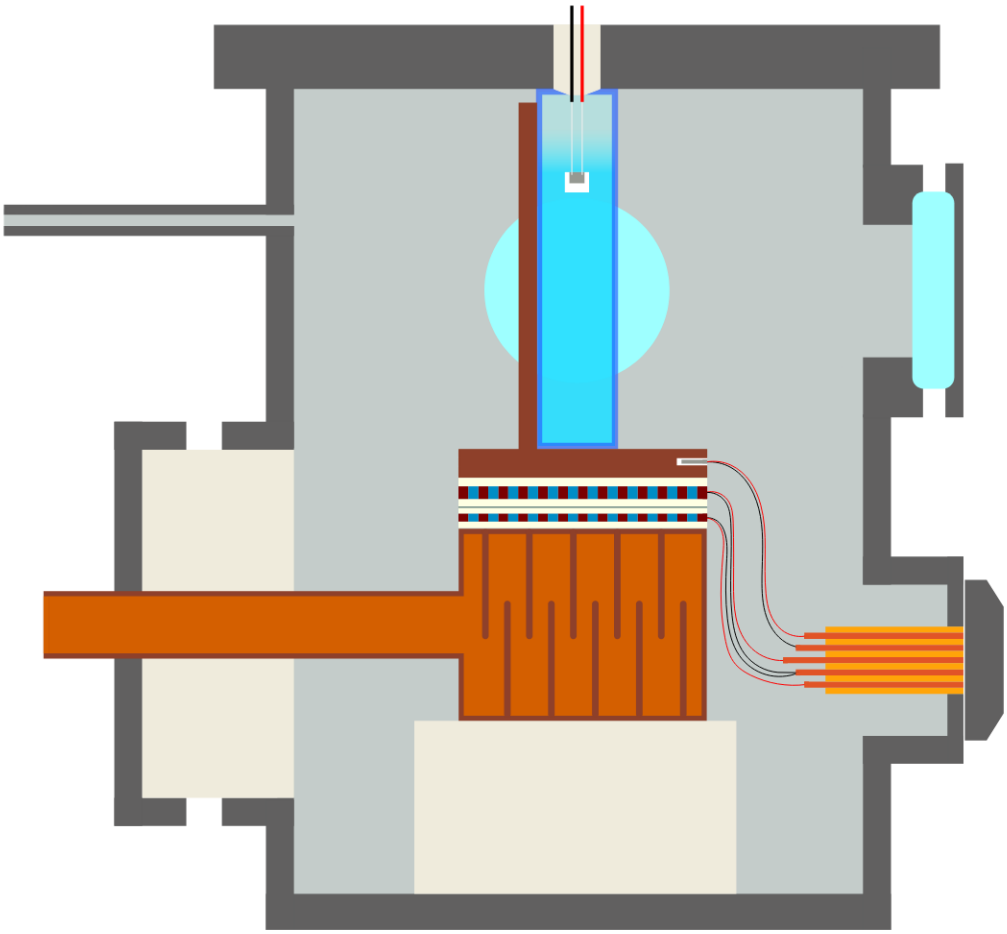

Figure 6.5.: Schematic representation depicts the cross-section of the constructed measuring cell, which includes optical windows, a sample-filled cuvette, a vacuum pump connection, two temperature sensors per PT100, Peltier devices, and the copper block for external cooling and the electronic connection point for the internal electronics, as in [189].

A PT100 sensor is a resistance thermometer that is distinguished by its high degree of accuracy and stability. A PT100 sensor is based on the electrical resistance of platinum,

which exhibits highly stable and linear behaviour over a wide temperature range, typically between -200 $°C$ and 850 $°C$. Given the sensitivity of platinum, a protective sheath made of thermally conductive material is incorporated into the design of the sensor. The measuring principle is based on the measurement of the voltage drop as a function of temperature, which is proportional to the temperature in question. The Callendar-Van-Dusen equation is typically employed to elucidate this relationship, which can be expressed as follows: $R(T) = R_0 \cdot (1 + A \cdot T + B \cdot T^2 + C \cdot (T - 100) \cdot T^3)$ with $R(T)$ representing the resistance at a given temperature T, R_0 denotes the resistance at 0 $°C$, which is therefore 100 Ω, and the constants A, B and C are contingent upon the specific platinum wire utilized.

The two Peltier devices installed inside the measuring cell are of a different design and serve distinct functions. This is due to the fact that the temperature differential ΔT between the hot and cold sides of the Peltier device establishes the upper temperature limit for the corresponding Peltier device. It thus follows that the function of one Peltier device is to facilitate cooling of the hot side of the Peltier device responsible for tempering the measuring cell. The function of the other device is, therefore, to temper the sample within the sample holder. The two Peltier devices are distinguished by their respective internal resistances. The Peltier device responsible for tempering the measuring cell exhibits a low internal resistance, which results in a considerable temperature differential ΔT between its hot and cold sides. In contrast, the Peltier device used to temper the hot side of the other Peltier element has a high internal resistance, which serves to reduce its ΔT while simultaneously increasing the precision of the temperature to be achieved. This set up indicates that lower temperatures can be attained with greater precision.

6.2.1. Peltier Device

Peltier devices comprise two distinct semiconductors that are coupled via a metallic conductor. A schematic representation of a Peltier device is provided in Figure 6.6. The outer structure is comprised of a thin ceramic outer plate or shell, which serves to provide shielding for the inner components. The interior comprises multiple semiconductor elements, assembled in pairs to form small blocks. These blocks consist of N- and P-doped semiconductor materials. In many instances, these are bismuth tellurides. The flow of electrical current is enabled via the conductor path, which is a metallic connection between the individual blocks. In order to provide additional stability to the structure, further ceramic layers are placed between the semiconductor layers. The structure and composition of the individual blocks permit the design of Peltier devices without limit [190].

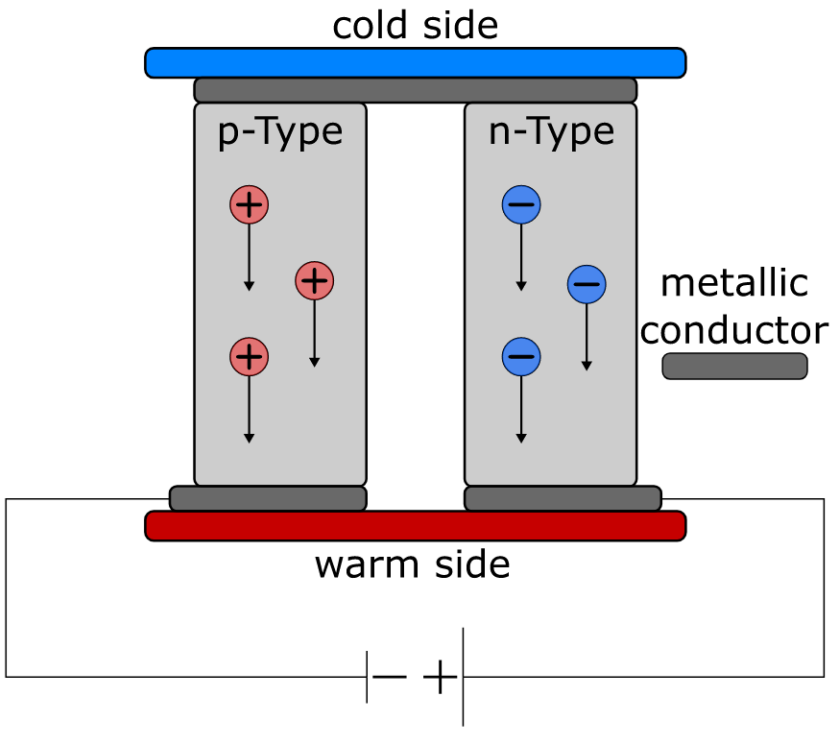

Figure 6.6.: Internal structure of a Peltier device demonstrating the building block.

The current flow within the Peltier device necessitates the absorption of heat energy by a semiconductor, enabling the electron to occupy the energetically higher conduction band of the other semiconductor. This results in the formation of the cold side of the Peltier element. Conversely, the electron of the other semiconductor must release heat energy in order for it to occupy the energetically lower conduction band of the other semiconductor. This results in the formation of the warm side of the Peltier element. The respective n- and p-doping processes are responsible for the observed difference in the energy level of the conduction bands of the respective semiconductor. The conduction bands of n-doped semiconductors are characterised by a lower energy level in comparison to the conduction bands of p-doped semiconductors [190].

The Peltier effect is a phenomenon within the field of thermoelectricity, which describes the interaction between electrical and thermal energy within materials. The interaction of thermoelectricity is primarily described by two effects: the Peltier effect and the Seebeck effect. The interaction of thermoelectricity can be expressed by a matrix equation 6.2 when Ohm's law and thermal conduction are taken into account [191].

$$\begin{pmatrix} \Delta V \\ \dot{Q} \end{pmatrix} = \begin{pmatrix} R & S \\ \Pi & -\kappa \end{pmatrix} \begin{pmatrix} I \\ \Delta T \end{pmatrix} \tag{6.2}$$

Figure 6.7 was created for the purpose of enhancing clarity and providing a graphical illustration of the relationships resulting from the matrix shown in equation 6.2. The figure demonstrates that the Peltier effect is the inverse of the Seebeck effect. The Seebeck effect is defined as the generation of voltage through thermo-diffusion currents. In contrast, the Peltier effect describes the generation of temperature differences through the application of voltage. The two effects can be linked via the Thomson effect, which describes the generation or absorption of heat in a homogeneous conductor when an electric current passes through it and a temperature gradient exists along this conductor [191].

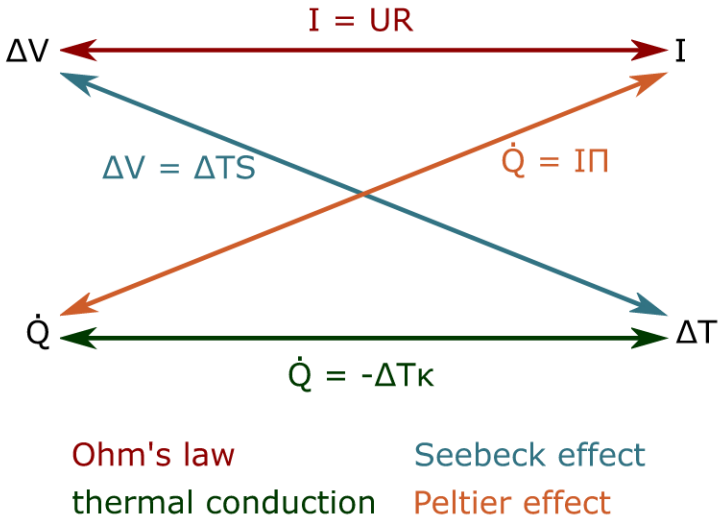

Figure 6.7.: Overview of the thermoelectric relations.

The aforementioned three effects are interrelated via the Thomson relation, which is represented by the equations $\Pi = S \cdot T$ and $\mu = T \cdot \frac{dS}{dT}$. In this equation, Π denotes the Peltier coefficient, S represents the Seebeck coefficient, μ is the Thomson coefficient, and T is the absolute temperature. This is feasible due to the fact that all three effects delineate disparate facets of thermoelectricity, which is founded upon the universal phenomenon of the migration of charge carriers, specifically electrons or holes, in response to temperature disparities and electric fields. The movement thus results in the generation of voltage (Seebeck), in cooling or heating (Peltier), or in additional heat generation (Thomson) [192], [193].

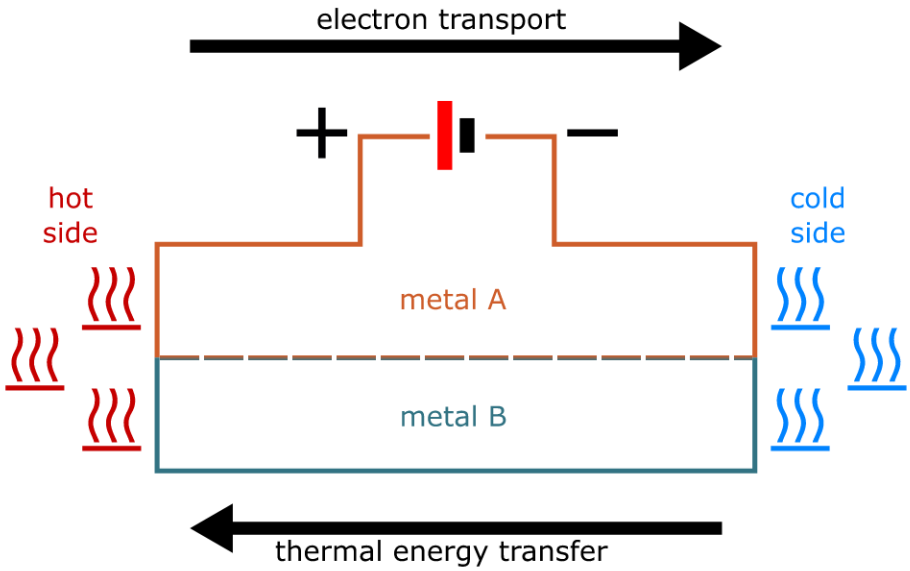

Figure 6.8.: Schematic representation of the Peltier effect.

From a mathematical perspective, the Peltier effect is defined by the equation 6.3, representing the production of a heat source represented by $\dot{Q}$, where I corresponds to the electric current and Π_A and Π_B are material- and temperature-dependent Peltier coefficients associated with the transported energy. The sign of the equation is indicative of whether heat energy is being withdrawn or added.

$$\dot{Q} = \Pi_{AB} I = (\Pi_A - \Pi_B) \cdot I \tag{6.3}$$

Figure 6.8 is used to illustrate the Peltier effect. The illustration demonstrates that when electrons are in motion within a conductor, they not only transport charge but also energy. The energy level of the conduction band of the semiconductor is also subject to change when electrons are transferred between two different and alternately arranged semiconductors. In order to maintain the principle of energy conservation, energy in the form of thermal energy must be released when electrons move from a conduction band with a higher energy level to one with a lower energy level. Conversely, the same principle of energy conservation applies to the absorption of thermal energy [194].

6.3. Density measurements

A variety of techniques exist for determining density. However, the approach utilising a frequency oscillator, as proposed by H. Stabinger [195], is regarded as the most accurate. The schematic structure of the density meter employed in the present study is illustrated in Figure 6.9. This is a high-precision density meter from Anton Paar, model DMA 4500 M, which incorporates built-in cooling and heating by Peltier elements and a controllable temperature range of minus 10 to 100 $°C$.

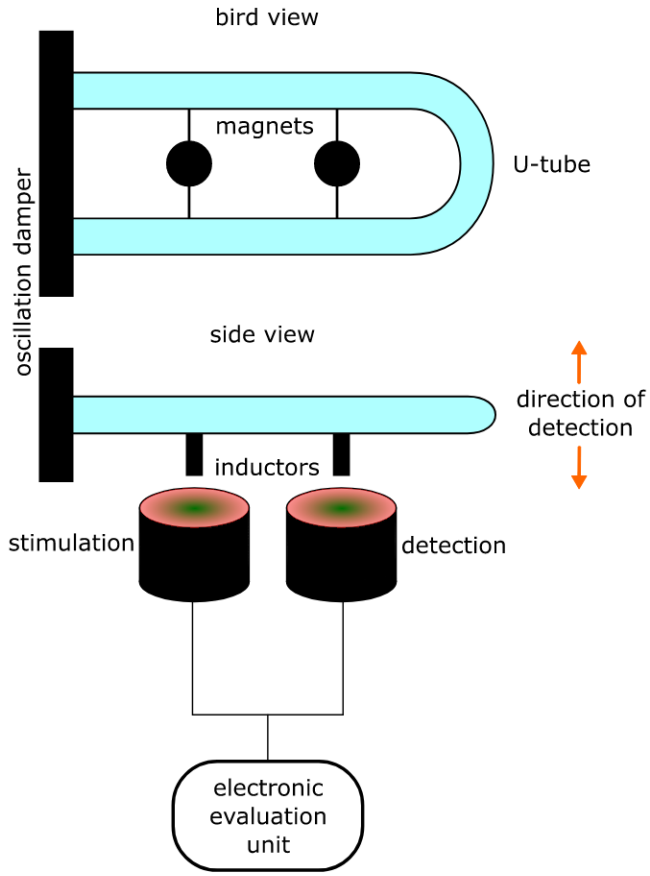

Figure 6.9.: Schematic representation of a density meter based on the oscillating U - tube principle.

The configuration illustrated in Figure 6.9 comprises a glass U-tube that serves as a sample chamber and is surrounded by a gas with high thermal conductivity, thereby facilitating temperature control. The frequency oscillator is constituted of two magnetic inductors, one of which is responsible for excitation and the other for detection. Furthermore, a light barrier may be employed for the purpose of detection. The signals are then conveyed to the evaluation unit and display module via an amplifier.

The laws of the anharmonic oscillator provide the foundation for the measurement principle utilising a frequency oscillator. In order to fully describe an anharmonic oscillator, it is sufficient to consider only two parameters: the natural frequency and damping. The latter helps to reduce the overall complexity of the model. Furthermore, the model of mass oscillation is also a fundamental component in this determination. The data points are generated from the recording of the frequency and duration of the vibration. This relationship allows for the plotting of the oscillation frequency as a function of density, with a constant sample volume, thus obtaining the oscillation period τ, as demonstrated in equation 6.4.

$$\tau = 2\pi \cdot \sqrt{\frac{\rho V + m}{D}} \tag{6.4}$$

The parameters are defined as follows: In this context, the variable ρ corresponds to the density of the sample to be analysed, V to the cell volume of the sample chamber and, in this case, to the volume of the U-tube, m to the mass of the measuring cell, and D to the field constant. If equation 6.4 is squared, the resulting equation is solved for the density, with the terms $\frac{4\pi^2 V}{D}$ substituted by G and $\frac{4\pi^2 m}{D}$ substituted by H.

$$\rho = \frac{(\tau^2 - H)}{G} \tag{6.5}$$

From these relationships, it can be observed that a shift in the natural frequency of oscillation occurs as a consequence of the specific density of a given sample. Moreover, it can be theorised that the measuring cell volume will increase as a result of the oscillation node shift. When all the effects are considered together, it can be seen that the error k in kg/m^3 is of the same order of magnitude as $k \approx 0,05 \cdot \sqrt{\eta}$. In this context, the term η represents the viscosity in $mPa \cdot s$.

$$\rho = A \cdot \tau + B \tag{6.6}$$

In light of these considerations and the attenuation resulting from the density of the sample,

the density of the sample can be determined by comparing it with the determination from a two-point adjustment of samples of known density, which are typically the values of water and air. This ultimately yields the final equation 6.6 for determining the density, where the parameters A and B are known from the aforementioned adjustment [195], [196].

6.4. Measurements of the refractiv index

The following section elucidates the configuration of the refractometer employed to ascertain the refractive indices, as illustrated in Figure 6.10, including the beam path. The refractometer employed is a multi-wavelength refractometer from Anton Paar, specifically the Abbemat MW model. It is also important to note that the refractometer employed can be tempered and is capable of measuring refractive indices at varying wavelengths. The configuration of the refractometer permits the selection of five distinct wavelengths. The following wavelengths are available for selection, categorised according to the Fraunhofer lines: H - F line at 486,1 nm, Ar - Ion line at 513,2 nm, Nd - YAG line at 531,9 nm, Na - D line at 589,3 nm and He - Ne line at 632,9 nm. The device is capable of functioning within a temperature range of 10 to 70 degrees Celsius. The temperature is regulated by two integrated Peltier elements. In accordance with the three measuring principles of refractive indices outlined in the theoretical section, the refractometer utilized in this instance employs the principle of total reflection.

In the initial stage, a light source, specifically a white LED, is employed to generate polychromatic light. A wavelength filter is employed to filter out the desired measuring wavelength from the polychromatic light, focusing it onto the boundary surface between the prism, comprising yttrium aluminium garnet, and the sample to be analysed. The light of the total reflection is then directed onto a detector, in this case a CCD detector, by means of a further lens and thus detected.

6.4.1. Wavelength Filter

The wavelength filters utilised in the refractometer are of a dichroic design. This design is based on the principle of reflecting wavelengths that are not desired and allowing wavelengths that are desired to pass through. The structure and operational principles of this type of filter are illustrated in Figure 6.11.

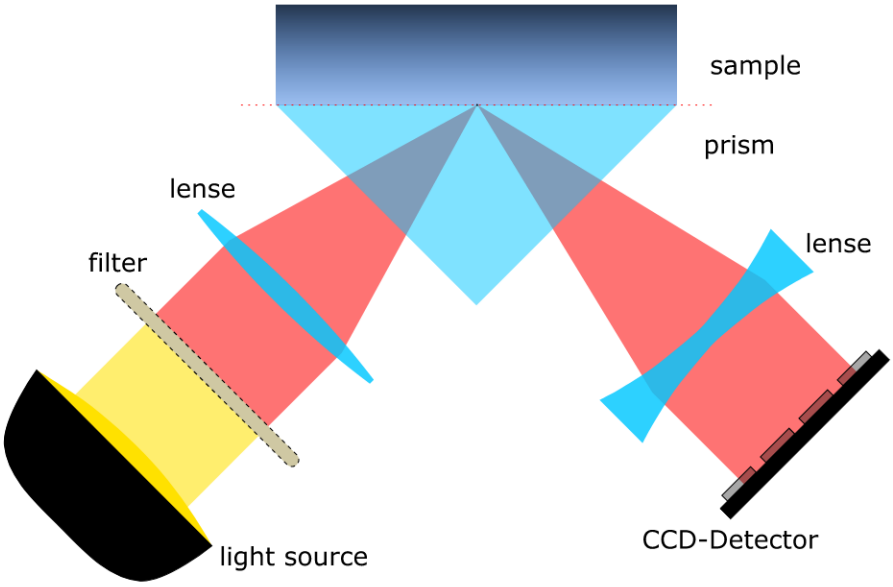

Figure 6.10.: Schematic presentation of the construction of a refractometer based on the principle of total internal reflection.

As illustrated in the figure 6.11 above, the reflection of distinct wavelengths is accomplished through the coating of discrete layers with varying refractive indices, thereby allowing only those wavelengths without the corresponding refractive index to pass through. The variation in refractive index is achieved through the utilisation of disparate coating materials. It is of particular importance to maintain the angle of incidence of the light on the dichroic wavelength filter, as the theoretical layer thicknesses, and thus the refractive indices of the respective layer, change at a different angle of incidence. This results in the wavelengths being filtered incorrectly. The parameter $\lambda/4$ represents the path difference and thus describes the rotation of the polarisation direction, in this case by $\pi/4$ to the main axis. This results in a phase shift that is proportional to the rotation, which is equal to a quarter of the wavelength [83].

6.4.2. CCD Detector

The physical principle underlying the operation of CCD sensors is based on the internal photoelectric effect. Figure 6.12 illustrates the band model of a CCD sensor, which elucidates the behaviour of electrons and holes in a semiconductor material, typically silicon.

In accordance with the illustration depicted in Figure 6.12, the valence band represents the highest fully occupied energy band within a semiconductor. However, its electrons

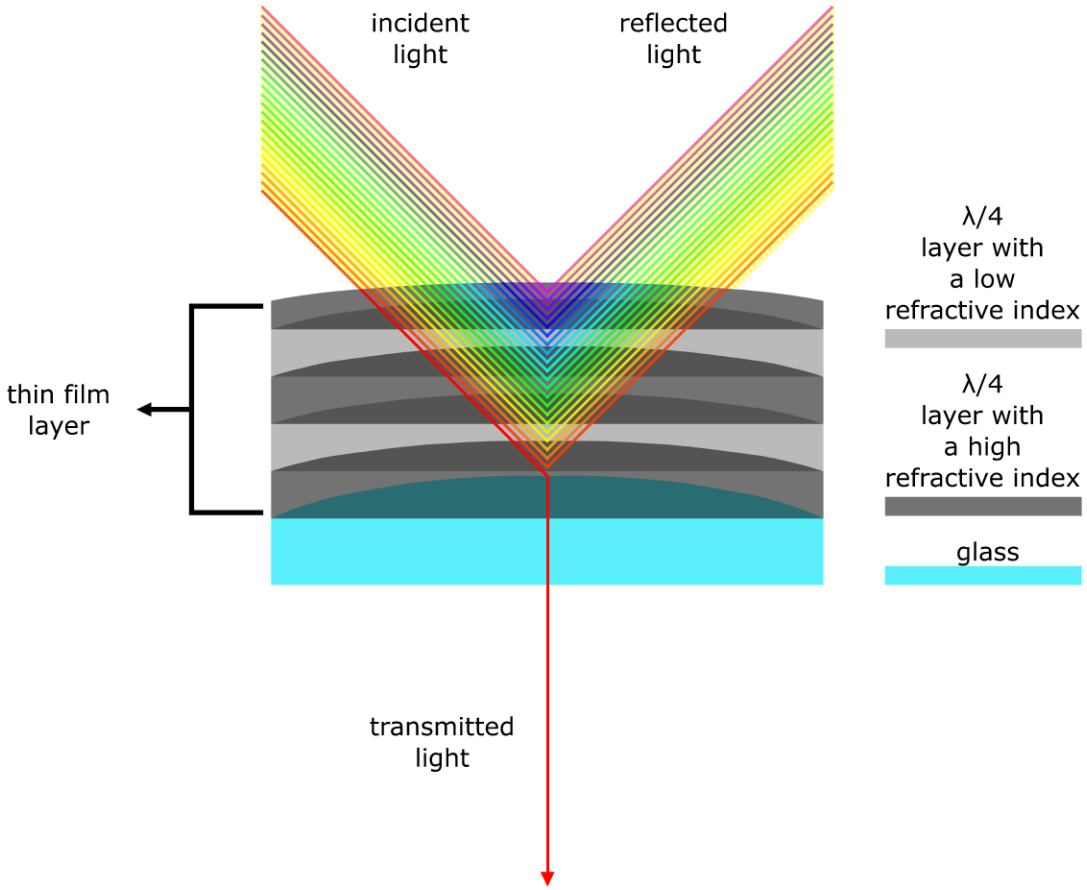

Figure 6.11.: Schematic description of the structure and function of a wavelength filter in the refractometer used.

are firmly bound to the corresponding atoms and thus do not contribute to electrical conductivity. In contrast, the conductor band represents the lowest unoccupied energy band, and its electrons contribute to electrical conductivity due to their capacity for free movement. A band gap exists between the two bands, representing the energy difference between the valence band and the conductor band. In order for electrons to be lifted from the valence band into the conductor band, this energy difference must be overcome. Additionally, there are holes in the valence band, which are defined by the absence of electrons and behave as positive charge carriers. These are displaced as soon as electrons move in the valence band. This results in the formation of electron-hole pairs, which are created by photon energy exceeding the prevailing band gap. In this process, a photon excites an electron from the valence band to the conductor band, thereby creating a hole in the valence band.

The generation of electron-hole pairs is a consequence of the interaction between photons

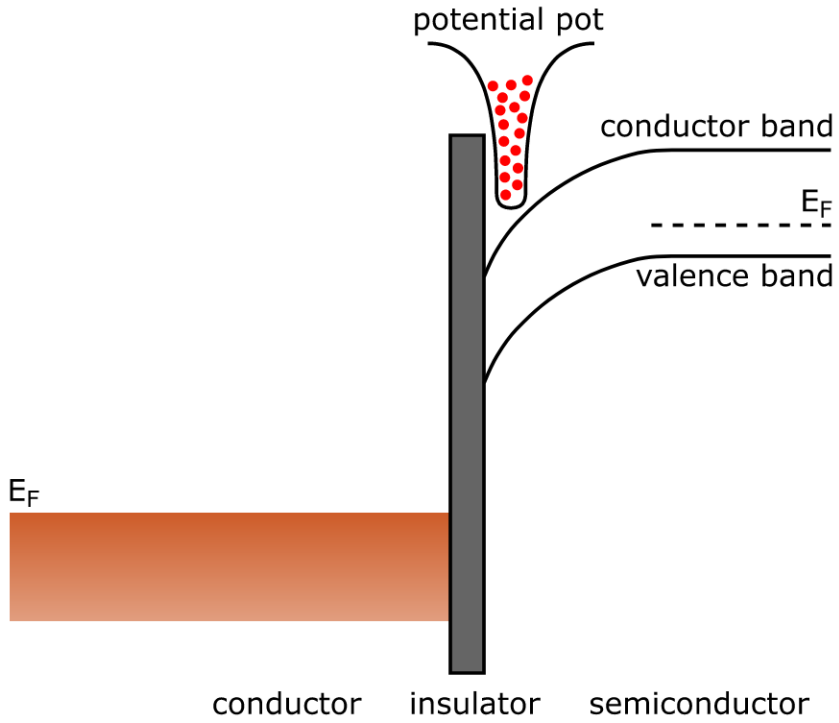

Figure 6.12.: Band model of a CCD sensor.

and the CCD sensor. The number of pairs generated is proportional to the light intensity. The electrons raised by the photons also generate a minority charge, which is collected in a potential pot, that is to say, a pixel, while the holes move in the opposite direction. A potential pot is defined as a locally lowered potential region within a semiconductor that is capable of trapping the minority charge. This implies that each potential pot is associated with a specific pixel in the recorded image, or when evaluating the light intensity. The read-out process entails the sequential transfer of the collected minority charge via neighbouring pixel rows to a read-out register and subsequently to an amplifier. The processes described are illustrated in Figure 6.13, which depicts the schematic structure of the surface of a CCD sensor. The layer designated as SiO_2 serves the function of providing an electrically insulating, optically transparent barrier, while the layer labelled $p - Si$ represents the outer surface of the semiconductor. The aforementioned potential pots are created through the application of a voltage, which enables the collection of the minority charges associated with the resulting electron-hole pairs. The alteration in the area subjected to an applied voltage can result in a corresponding shift in the charge. The factors that cause background noise can be divided into two categories: leakage current and dark current. Leakage current refers to the flow of electrons into the conduction band due to thermal excitation. Dark current, on the other hand, describes the current

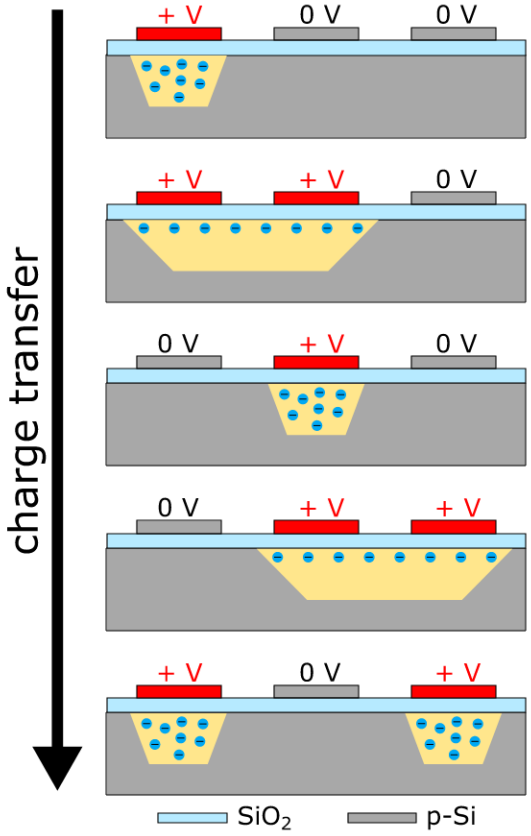

Figure 6.13.: A schematic representation of the processes occurring within a charge-coupled device (CCD) sensor.

that flows through the sensor even when it is not exposed to light. Quantum efficiency is employed as a metric for the efficacy of CCD sensors, quantifying their capacity to transform photons into electrons [197].

6.5. HRLIF Measurements

One objective of the present work is to determine the dipole moments in the excited state in the gas phase, with the aim of establishing reference values for the calculated dipole moments in the liquid phase. As previously stated, the dipole moment of the ground state is also required for the calculation method, which can be obtained from dipole moment determinations in the gas phase. The method employed for this purpose is known as **h**igh-**r**esolution **l**aser-**i**nduced **f**luorescence (**HRLIF**). The experimental setup for conducting these measurements is also illustrated, comprising three principal components. These comprise the laser system, the apparatus for generating a molecular beam and the vacuum system.

6.5.1. Pump Laser

The pump laser is a diode laser from Newport Spectra Physics, specifically the Millenna eV, 15W model. This laser emits light at a wavelength of 532,0 nm and reaches a maximum power of 15 W. The experimental setup of this laser is illustrated in Figure 6.14.

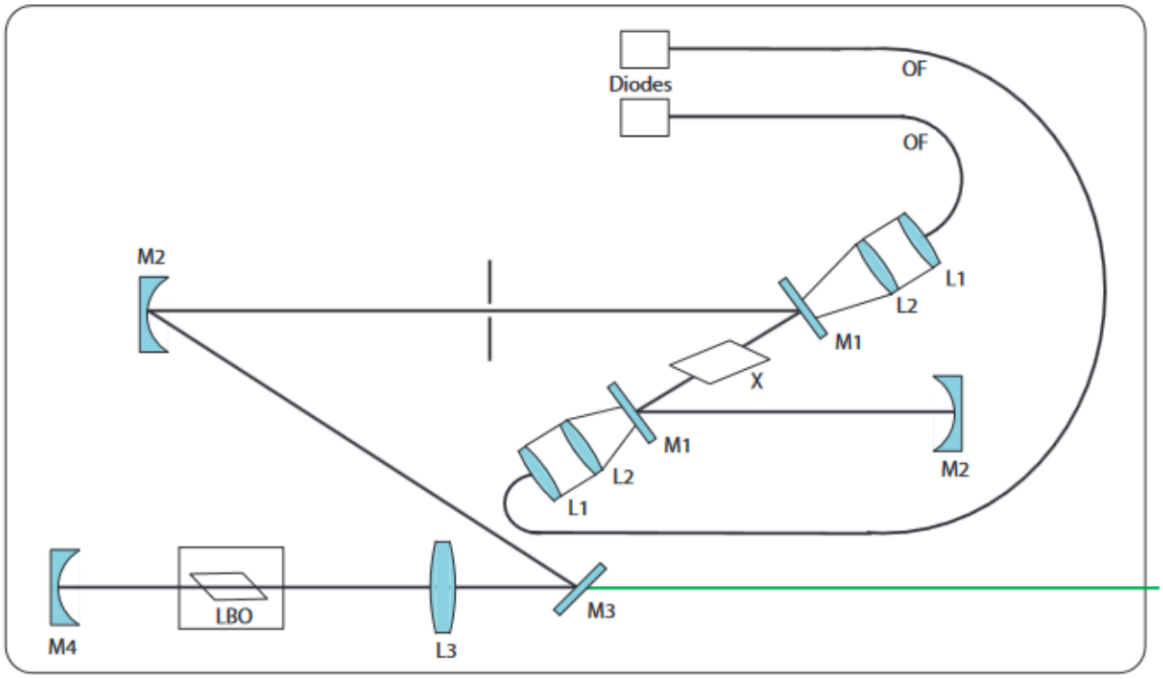

Figure 6.14.: The diagram illustrates the structure of the pump laser that is used. The letters OF, L, M, X and LBO represent the following components: OF is an optical fibre; L is lenses; M is mirrors; X is the yttrium vanadate crystal; and LBO is the lithium triborate crystal [131], [96], [198].

Two diodes emit light at a wavelength of 809,0 nm, which is then guided via optical fibres. The light is subsequently focused by lenses $L1$ and $L2$ onto a neodymium-doped yttrium-vanadate crystal, designated $X = Nd : YVO_4$. The light absorbed by the crystal is subsequently re-emitted at a wavelength of 1064,0 nm, whereupon it is amplified in the resonator via the mirrors $M1$. These materials are transparent to the wavelength of 809,0 nm and highly reflective to the wavelength of 1064,0 nm. The light is then directed to a non-linear lithium triborate crystal via the highly reflective mirror $M2$, where frequency doubling occurs. This process of doubling the wavelength results in the desired wavelength of 532,0 nm. Subsequently, the light beam traverses the highly reflective mirror $M4$, which

allows for the transmission of wavelengths of 532,0 and 1064,0 nm, before exiting the setup via the output mirror $M3$ and entering the ring dye laser [96], [199].

6.5.2. Ring Dye Laser

This section will provide a schematic demonstration and explanation of the functioning of the ring dye laser Matisse DS, produced by Sirah Lasertechnik GmbH as shown in Figure 6.15. The process continues after the light beam has departed from the previously described pump laser. This process facilitates the transfer of the dye molecules of the ring dye laser to the first electronically excited state. Subsequently, these molecules undergo a transition to the lowest vibrational level via non-radiative processes. Subsequently, broadband fluorescence occurs, whereby the dye molecules transition to different vibrational states of the electronic ground state.

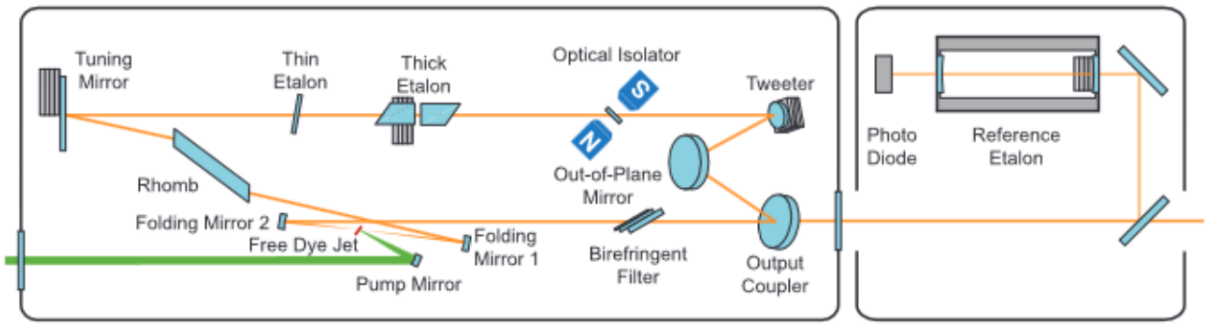

Figure 6.15.: Schematic overview of the Matisse DS ring dye laser and the reference cell by Sirah Lasertechnik GmbH [142].

The dye solution is subjected to impact processes with solvent molecules, which are then reduced or inhibited by means of permanent cooling. It is imperative to prevent the non-radiative transition of the dye molecules into the triplet state by electronic excitation, as this can impede or suppress the laser process due to the longer lifetime of these processes. One potential solution to this issue is to continuously pump the dye through a nozzle at a pressure of 20 bar.

As previously described, the measure results in the formation of a laminar dye beam, which is indicated in Figure 6.15 as a red line. To circumvent the formation of standing waves and guarantee that all active molecules participate in the amplification process, an optical diode is employed that exclusively amplifies waves propagating in a single direction. This is made possible by exploiting the Faraday effect. The polarisation vector of the electric field undergoes a rotation of a few degrees following its passage through a terbium-gallium-

garnet crystal situated within a strong magnetic field. Subsequently, the wave impinging upon the out-of-plane mirror induces a further rotation of the polarisation vector. This implies that the two effects mutually cancel each other out for the counter-clockwise mode and add up for the clockwise mode, which results in a loss of intensity at the optics situated at the Brewster angle to the laser beam [96], [200].

This results in a broad fluorescence spectrum that must then be reduced to the required wavelength in the particular case. In order to achieve this, a total of three wavelength-selecting elements are employed, beginning with the coarsest. This is the birefringent or double-refracting filter, which is composed of three quartz plates in a ratio of 1:3:15 to each other. In this process, linearly polarised light is split into two partial beams by the birefringent quartz crystal, which are referred to as the ordinary beam, perpendicular to the optical axis of the crystal, and the extraordinary beam, along the optical axis of the crystal. Given that the two beams have disparate refractive indices, their phase velocity also differs, which in turn gives rise to a rotation in the polarisation of the incident light contingent on the wavelength. The orientation of the optical axis determines whether the polarisation of the outgoing beam is again linearly polarised for some wavelengths, while other wavelengths experience significant losses during passage through the laser cavity. The wavelength is selected by the arrangement of the crystal, whereby the use of quartz plates with thicknesses of 325 μm, 975 μm and 4,55 nm can narrow the transmission range to less than 2 cm^{-1} [96], [200], [201].

Subsequently, the second wavelength-selective element is the thin etalon. This is analogous to a Fabry-Pérot etalon. The structure comprises two parallel, partially transparent mirrors situated at a fixed distance apart. The reflection between the two mirrors generates a number of partial waves, the transmission of which through the etalon is contingent upon their phase alignment. The wavelength is selected by modifying the angle of inclination [96], [200].

The third and final wavelength-selective element is the thick etalon, which corresponds to a Fabry-Pérot interferometer. This is constituted by two prisms positioned in parallel with an air layer situated between them. The transmitted wavelength can be modified by adjusting the thickness of the air layer, which is accomplished through the use of piezoelectric motors.

This structure achieves an internal linewidth of 250 kHz, and the addition of matching mirrors allows for the adjustment of the optical path length of the cavity, thereby enabling the scanning of a range of one wavenumber. In order to stabilise the set wavelength of the laser, the light emitted by the dye laser is coupled into a reference cell with a confocal resonator. During the scanning process, a spectrum comprising an Airy function

is generated by the transmitted light of the reference resonator. In the event of laser instability, the intensity of the reference signal undergoes a change. The tweeter, which is mounted on a fast-acting piezo motor, serves to counteract the disturbance by means of the error signal [96].

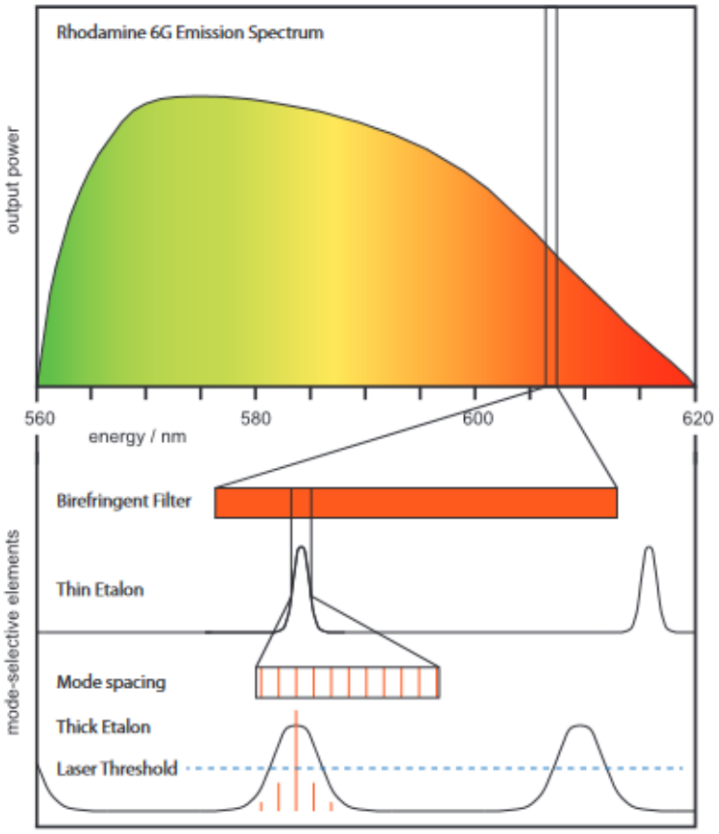

Figure 6.16.: The emission spectrum of rhodamine 6G in ethylene glycol and a representation of the mode of action of the three wavelength-selective elements [142], [202].

6.5.3. Frequency Doubler

The subsequent figure 6.17 illustrates the configuration of the frequency doubler integrated into the apparatus. At the outset, the laser beam impinges upon the phase modulator, which is linked to a fibre coupler via an optical fibre, with the objective of stabilising the cavity. The beam properties, specifically diameter, divergence, precise height and position of the laser beam to be coupled into the cavity, are adjusted using two lenses, the beam shifter and two deflection mirrors. The resonator comprises two mirrors, a nonlinear

crystal and a prism, and is capable of being moved using piezoelectric elements. This enables the beam path within the cavity to be closed and the length to be adjusted in accordance with varying fundamental wavelengths. In order to prevent reflection losses of the fundamental frequencies, the crystal and the prism are cut at the Brewster angle. Once the frequency doubling process is complete, the elliptical beam is converted into a non-astigmatic beam through the use of a cylindrical lens and a prism expander. The detectors for the fundamental and the harmonics are employed for the purpose of evaluating the quality of the alignment, whereby the intensity of the respective light is assessed.

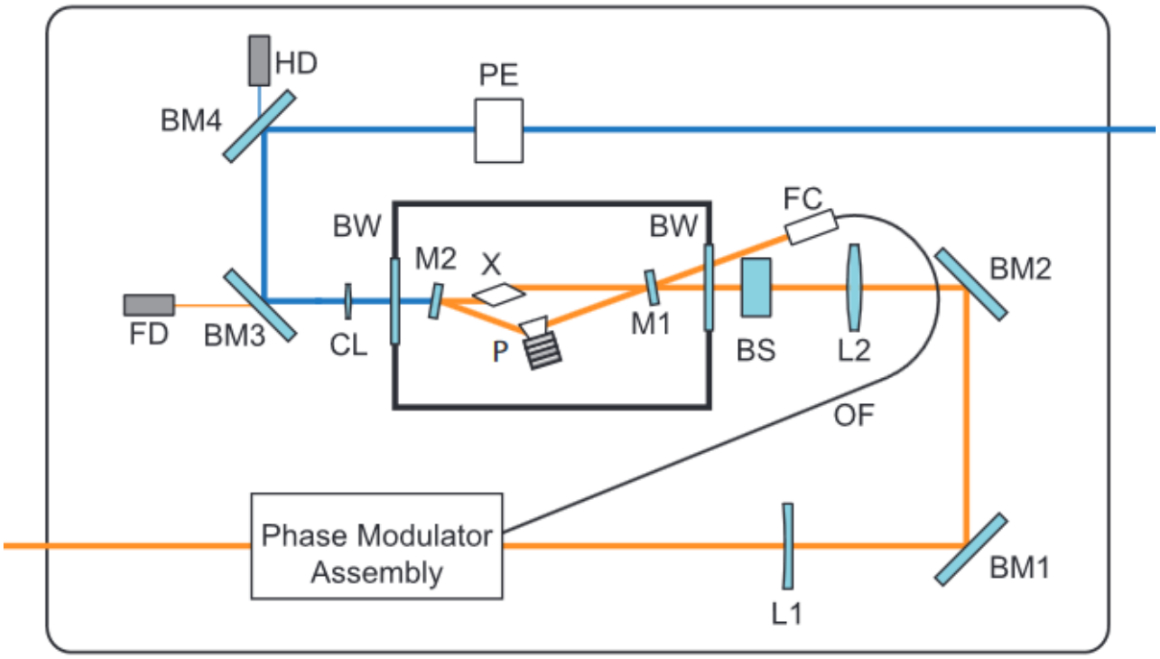

Figure 6.17.: Above the schematic structure of a frequency doubler is illustrated. **L** - lens, **BM** - beam mirror, **BS** - beam shifter, **BW** - Brewster window, **M** - mirror, **X** - doubling crystal, **P** - prism, **OF** - optical fibre, **FC** - fibre coupler, **CL** - cylindrical lens, **FD** - fundamental detector, **HD** - harmonic detector, **PE** - prism expander [142].

When the optical properties of a material are altered by the action of extremely intense laser beams, resulting in a reduction of the wavelength of the light by a factor of two upon passage through the medium, this phenomenon is designated as the nonlinear process of frequency doubling. This leads to a distinction between nonlinear optics and classical linear optics, where the polarization of light P is defined as the sum of several components.

$$P = \epsilon_0 \chi^{(1)} E + \epsilon_0 \chi^{(2)} E^2 + \epsilon_0 \chi^{(3)} E^3 + \cdots \tag{6.7}$$

The variables P represent the polarisation of light, E the electric field strength, ϵ_0 the permittivity of the vacuum, and χ the susceptibility.

In order to adequately describe the frequency doubling, it is sufficient to utilise the initial two terms of the power series. To achieve this, the variable $E = E_0\ cos(\omega t)$ is substituted for a monochromatic light wave in equation 6.7, with the assistance of the function $cos^2(x) = \frac{(1+cos(2x))}{2}$, which transforms the equation into equation 6.8.

$$P = \epsilon_0 \chi^{(1)} E_0\ cos(\omega t) + \frac{1}{2}\epsilon_0 \chi^{(2)} E_0^2 + \frac{1}{2}\epsilon_0 \chi^{(2)} E_0^2\ cos(2\omega t) \tag{6.8}$$

This transformation implies that the resulting equation comprises a constant term in addition to terms that depend on the excitation frequency ω and on twice the frequency $2\ \omega$, which demonstrates that each molecule in the medium emits two waves at both frequencies.
A prerequisite for the generation of a sufficiently high intensity frequency-doubled light is the attainment of identical phase velocities for both the incident wave and the harmonic generation. This may be accomplished through the utilisation of a compatible medium, exemplified by β - barium borate crystals [96], [203], [204], [205].

6.5.4. Determination of the Relative and Absolute Frequency

In order to ascertain the relative and absolute frequency, it is necessary to utilise a portion of the light emitted by the dye laser, employing a reference etalon for the determination of the relative frequency. This is necessary because while the desired wavelength of the dye laser can be precisely adjusted, it is not precise enough to determine the absolute frequency. The aforementioned reference etalon is analogous in structure to a Fabry-Pérot etalon. The necessity for the reference etalon is due to the fact that the speed of the adjustment mirror during the scanning process is not constant, which can result in shifts within the recorded rotation-resolved spectrum. To address this issue, the transmitted light from the reference etalon is recorded with an exact distance of 149,9434(54) MHz between the transmission

lines. This indicates that the rotation-resolved spectrum can be linearised on the basis of the reference spectrum. Moreover, the determination of the absolute frequency necessitates the utilisation of an additional external standard. To achieve this, the absorption spectrum of iodine is recorded and compared with the excitation transitions of iodine recorded in a table. This enables the position to be determined with an accuracy of 0,1 cm^{-1} [206].

6.5.5. Molecular Beam

The excitation and subsequent measurement of the fluorescence emission of the molecules under examination is conducted within a molecular beam. In order to create a molecular beam, it is necessary to transfer the molecules into the gas phase and expand them into a vacuum through a nozzle. A molecular beam is defined as a collimated supersonic nozzle beam, created by the expansion of molecules from a nozzle into a vacuum [207], [208].

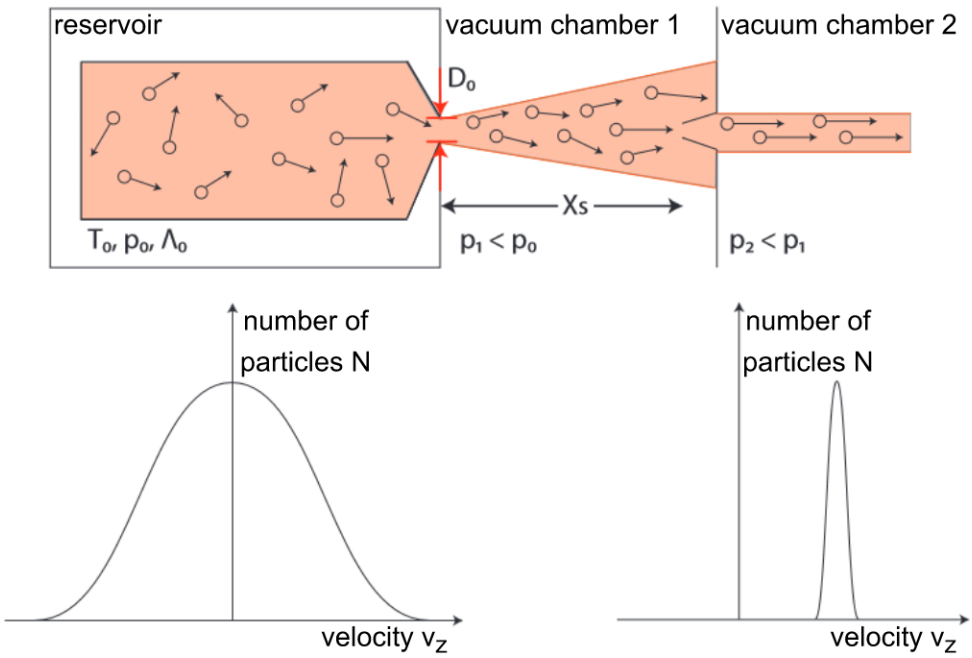

Figure 6.18.: Schematic diagram of the adiabatic expansion and subsequent collimation of the resulting supersonic jet by a skimmer, with additional representation of the velocity distributions before and after the expansion process [204].

In accordance with the illustration depicted in Figure 6.18, the initial configuration of molecules is situated within a reservoir characterised by an initial temperature of T_0 and an initial pressure of p_0. This results in the emergence of the mean free path, represented by the symbol Λ_0. Given that the mean free path is many times smaller than the diameter

of the nozzle, an adiabatic expansion is possible. This results in the conversion of the non-directional thermal motion of the molecules into directional thermal motion as they exit the nozzle. Due to the exceedingly high pressure within the reservoir, a significantly greater number of collisions occur in the vicinity of the nozzle, resulting in the transfer of translational energy and a notable narrowing of the velocity distribution in the direction of the jet [204].

$$n(\nu_z) = C_1 e^{\frac{-m(\nu_z - u)^2}{2kT}} \tag{6.9}$$

With the following variables: C_1 the pre-exponential factor, m the mass of the molecules, u the flow velocity, T the temperature, and k the Boltzmann constant.

As previously described, the conversion of energy into directed flow results in a reduction of translation, rotation and oscillation energy to low Kelvin ranges. Consequently, following expansion, only the lowest rotational oscillation states of the molecules remain occupied. To minimise the formation of clusters, a carrier gas, typically an inert gas, is added in high concentration, thereby reducing the likelihood of cluster formation [204], [209].

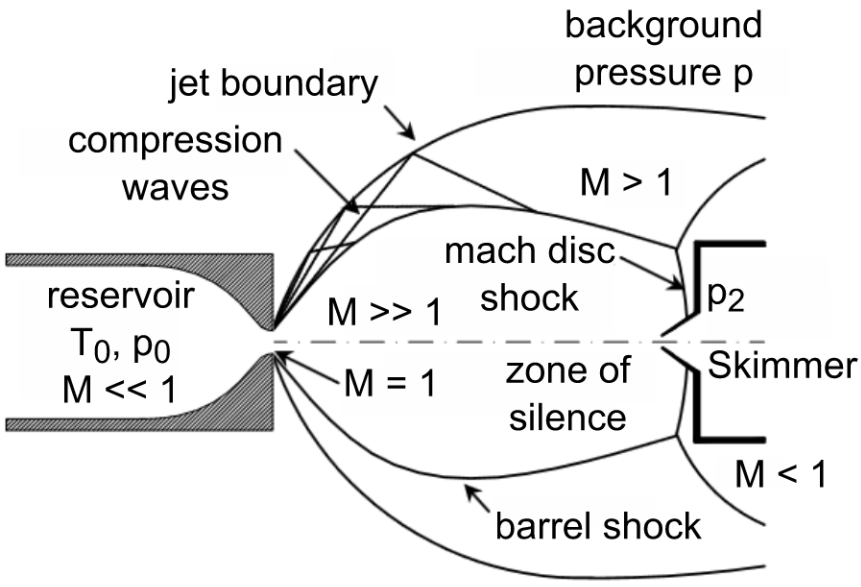

Figure 6.19.: A schematic representation of the supersonic expansion and skimmer is provided. With M relate to the Mach number, T to the temperature and p to the pressure [210].

The maintenance of the molecular beam following supersonic expansion is contingent upon the utilisation of skimmers. These are conical hollow cones with sharp edges and extremely small openings at their apex. As a consequence of the expansion and propagation of the molecular beam, shock fronts are formed within the vacuum chamber. These are spatially standing and act in a manner that is counterproductive to the maintenance of the molecular beam when it passes through, see figure 6.19. The shock front X_M, which is referred to as the Mach disc, encompasses the area in which the desired molecular beam properties are located. In order to maintain the molecular beam, it is necessary to mount the skimmer at a distance $X_1 < X_M$ from the nozzle opening. This distance must be calculated with due consideration of the nozzle operating pressure p_0 and the pressure of the vacuum chamber p_1 [131], [96], [211]. The following equation is employed as the foundation for calculating X_M:

$$X_M = 0,67 \cdot D_0 \sqrt{\frac{p_0}{p_1}} \tag{6.10}$$

The subsequent trajectory of the molecular beam is illustrated in Figure 6.20 and complemented by a depiction of the imaging detector and the apparatus employed for Stark measurements.

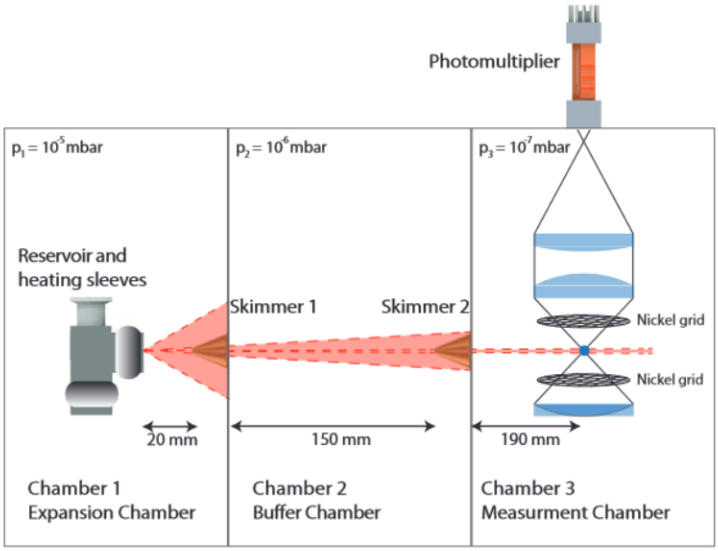

Figure 6.20.: Schematic representation of the path of the molecular beam through the individual chambers within the apparatus, as well as the imaging detector and the Stark setup [142], [128].

The UV laser beam generated by the laser assembly strikes the molecular beam at an angle of 90°, thereby causing the molecules to become electronically excited. The fluorescent molecules emit fluorescent light, which is directed to the photomultiplier via a spherical mirror and two plano-convex lenses, collectively referred to as the imaging optics. In order to facilitate the implementation of Stark measurements, two nickel grids are positioned in a manner that is above and below the point of intersection between the molecular beam and the laser beam. The circular nickel grids have a diameter of 50 mm and a grid density of 28 threads per centimetre, which permits the transmission of 95% of the fluorescent light. A total voltage up to 10000 V can be applied, with the maximum of 5000 V each distributed to the two grids. Given the distance between the grids of 2,349(5) cm, this results in an electric field strength of up to 4,200 V/cm [128].

6.5.6. Vacuum device

The apparatus depicted in Figure 6.21 comprises three vacuum chambers arranged in a linear configuration, interconnected via skimmers.

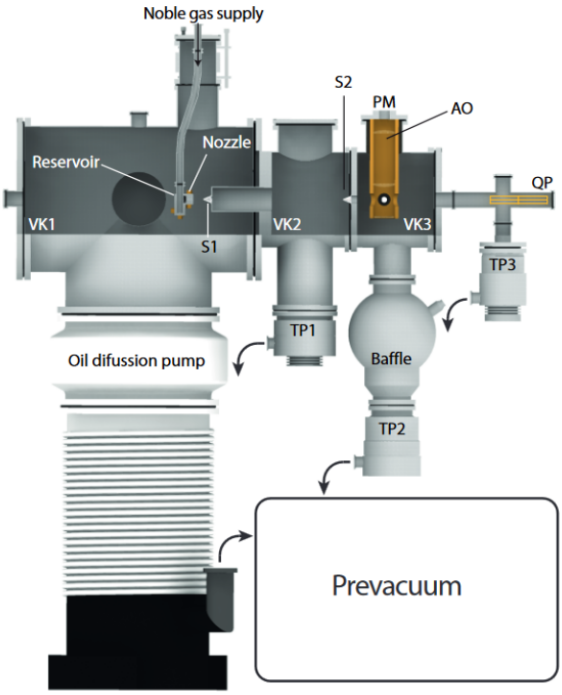

Figure 6.21.: Schematic structure of the molecular beam apparatus, with a particular focus on the design of the vacuum apparatus. **VK** represents the vacuum chamber, **S** the skimmer, **TP** the turbomolecular pump, **AO** the imaging optics, **PM** the photomultiplier and **QP** the quadrupole [142].

Each vacuum chamber within the apparatus has a distinct function, the initial chamber is employed for the expansion of the sample, the second acts as a buffer, and the final chamber is utilized for the measurement. The pressure declines in a stepwise manner from one chamber to the next, while the diameter of the skimmer opening increases from 1 mm to 3 mm. Furthermore, all vacuum chambers are linked to a pre-vacuum system, which is powered by three oil rotary vane pumps and a roots pump. In order to generate the main vacuum, an additional oil diffusion pump is utilised in the initial chamber, with the subsequent two chambers employing turbomolecular pumps for this purpose. Furthermore, a liquid nitrogen-cooled spherical cold trap (baffle) is employed in the third vacuum chamber to achieve a pressure of 10^{-6} to 10^{-7} $mbar$. A quadrupole mass spectrometer, which is coupled to the oil rotary vane pump and the turbomolecular pump, is installed at the end of the last vacuum chamber. Its function is to align the molecular beam so that it can pass through the skimmer with optimal precision [128].

6.6. Preparation of the Preparations

All molecules and solvents were procured from commercial manufacturers and utilized without additional purification. When preparing the individual solutions, great care was taken to ensure that the concentrations were maintained within the same range. One batch from one system, that is to say, from one solvent and one solvate, was prepared at the outset of each series of measurements. The same batch was then used for each subsequent sub-measurement, thus ensuring the highest possible degree of similarity between the samples to be examined and excluding any potential effects of different concentrations. Furthermore, each batch was analysed with minimal delay. Density measurements and spectroscopic measurements were conducted concurrently to the greatest extent feasible to minimise the time the batch was left standing and to minimise changes to the batch due to the time it was left standing. Furthermore, new bottles of solvent were employed for each batch to circumvent any hygroscopic effects. The sample containers were always cleaned in accordance with the same procedure and with the utmost care to ensure that no residues remained on the containers.

7. Systems

This chapter provides a classification of the investigated molecules and highlights potential areas of application for the molecule being discussed. Furthermore, a concise explanation of the solvent used, along with its fundamental characteristics, is presented.

7.1. Molecules

As indole C_8H_7N is the primary building block of the molecules and compounds that are crucial to this study, they will be discussed in further detail below. This significance is supported by the reality that indole serves as a building block for numerous biological molecules [212], [213], [214], [215], as well as for molecules involved in TADF processes [216], [217] ,[218], besides being the fundamental building block of two molecules examined in this research.

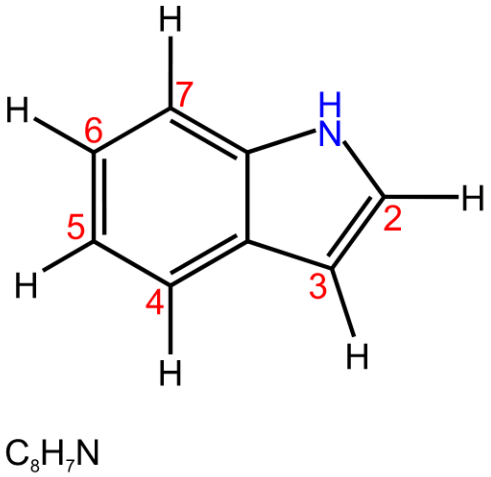

Figure 7.1.: Structural formula of indole, with markers indicating possible substituent positions.

Indole is a heterocyclic organic compound comprising a benzene ring fused with a pyrrole ring, resulting in an aromatic structure. This feature provides the compound with high

stability due to the delocalised electrons within the conjugated π - system. The nitrogen atom of the pyrrole ring endows indole with weak basicity in several reactions. Due to its aromaticity resulting in high electron density, indole is highly susceptible to electrophilic substitutions. Additionally, it can undergo nucleophilic substitutions which provide the opportunity to introduce functional groups to the ring system.

In order to underscore the significance of indole as an ingredient, the following sections elaborate on its areas of application [219]. In chemical synthesis, indole is widely used as a starting reagent for numerous complex organic compounds. Indole is found in several pharmaceutical derivatives, which are utilized for the treatment of mental dysfunctions or cancer, as stated previously. For instance, the neurotransmitter serotonin, which has a crucial role in mood regulation, features indole as a structural component [220], [221], [222]. Furthermore, indole or its derivatives are employed in the food industry for adding flavour and enhancing taste. The production of perfumes also utilizes indole derivatives [223], [224], [225]. Notably, indole derivatives are employed in the textile industry as dyes and pigments, but it should be clarified that these pigments are not solely restricted to textile use [226], [227], [228]. Indole derivatives are present within the agrochemical sector, with uses in pesticides and growth regulators. Analytical chemistry also utilises indole derivatives as indicators or reagents for chemical analysis, due to their capacity to form coloured complexes [229], [230], [231]. Additionally, these derivatives play a substantial role in microbiology, where they are used to detect individual bacterial species, as the production of indole by bacteria can be used as a diagnostic tool [232], [233], [234].

7.1.1. Cyanoindoles

Cyanoindoles $C_9H_6N_2$ (**n - CI**) are a class of organic molecules, where the basic building block is an indole ring, as suggested by the name. The indole ring is a bicyclic aromatic structure formed by the fusion of a benzene and a pyrrole ring. A cyano group (**CN**) is substituted onto this ring system. The ring structure of the indole results in aromaticity, which stabilises the system and enables the delocalisation of electrons. The structure of the central ring enables the cyano group to be positioned in seven different locations, resulting in seven constitutional isomers of the n - cyanoindole. As a result of this structure, cyanoindoles possess diverse chemical reactivity and serve as key components in the synthesis of various organic compounds. These compounds are employed in pharmaceutical products among other applications [235].

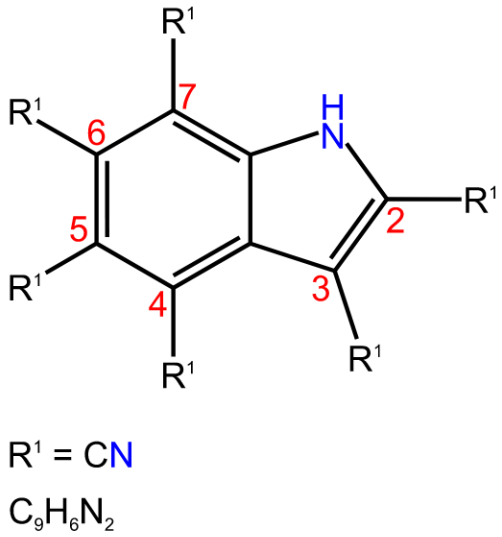

Figure 7.2.: Structural formula of n - cyanoindole presenting the respective location of the cyano group.

The chemical properties of n - CI are manifold. n - CIs are practical for electrophilic substitution reactions due to the electron richness of the indole ring. The CN group can be transformed into various reactions such as halogenation, nitration, or a Friedel-Crafts reaction. Additionally, the nitrogen atom of the indole ring can be protonated due to the free electron pairs, acting as a weak base. Moreover, the CN group can exert an electron-withdrawing effect, influencing the reactivity of the indole ring towards nucleophilic addition and leading to hydrolysis reactions, among others. However, the impact of the cyano group will be addressed at a later stage.

This section will briefly discuss the mesomeric effect (**M - effect**) and the inductive effect (**I - effect**) of n - CI. The M - effect is the influence of a substituent on an aromatic ring, which can affect the distribution of electrons within the ring system via mesomerism. This effect, which can be positive (donating electrons: +M - effect) or negative (withdrawing electrons: -M - effect), influences the reactivity and stability of the aromatic ring system. The I-effect directly influences the electron distribution within a molecule due to the substituent's properties. This effect can also exert a positive (+I - effect) or negative (-I - effect) influence. This influence affects both the reactivity and the sterics of the system.

The CN group of the n - CI has both a +M - effect and a -M - effect. The nitrogen atom in the cyano group increases the carbon atom's electronegativity and can withdraw electron density from the attached ring system through mesomerism. Consequently, electrons within

the aromatic ring system decrease in density. On the other hand because the nitrogen atom has free electron pairs, the cyano group can also increase the electron density of the ring system through mesomerism. Nevertheless, the cyano group is predominantly characterized by its -M - effect.

Considering the inductive effect, it is clear that the cyano group has a strong negative inductive effect (-I - effect). This effect is due to the high electronegativity of the carbon and nitrogen atoms present in the cyano group, which results in a prominent electron-withdrawing impact of this substituent group.

7.1.2. Methylindoles

As explained in the previous section, the basic structure of methylindoles C_9H_9N (**n - MI**) comprises an indole ring, and hence, it is not elaborated further. The substituent in n - MI is the methyl group (**Me**), as suggested by its name. Similar to n - CI, the Me group can be placed in seven different positions, resulting in seven constitutional isomers of n-methylindole. N-methylindole finds a wide range of applications in fields such as pharmacy, agrochemistry, and materials chemistry. Because of the high similarity to biological molecules, n - MI exhibits a high level of biological activity.

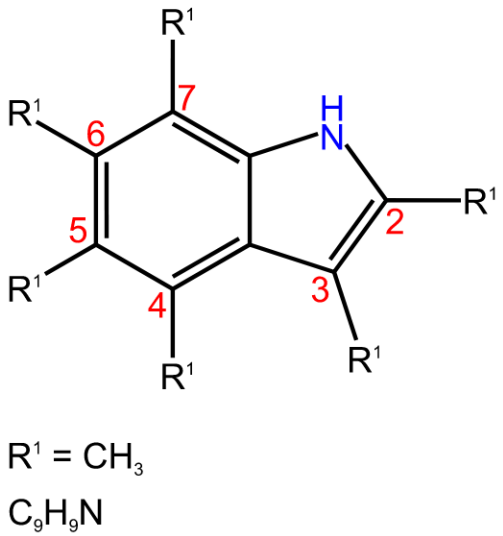

Figure 7.3.: Structural formula of n - methylindole presenting the respective location of the methyl group.

The chemical properties of n - MI are as diverse as those of n - CI. Therefore, this section presents the main chemical properties of n - MI. For instance, methylindoles can un-

dergo electrophilic aromatic substitution, such as halogenation, nitration, or sulphonation. Moreover, they can undergo nucleophilic substitution or act as weak bases due to their acid - base properties and form salts in the presence of strong acids. These properties resemble the properties of n - CI because they are founded on the shared building unit of indole. Moreover, the functional group offers the potential for a chemical conversion that can manifest through oxidation or reduction. Owing to their similarity to biological molecules, n - MI compounds can interact with biological receptors and enzymes, granting them significant importance in pharmaceutical research. When present with Lewis bases, methylindoles initiate complex formation, causing a change in both their behaviour and reactivity.

Given that the mesomeric effect and inductive effect have already been explained in the previous section (cf. 7.1.1), the following part will deal with these two effects of the methyl group.

In comparison to the CN group, the mesomeric effect of the Me group is relatively weak. It is generally assumed that the mesomeric effect of the methyl group is a +M - effect. This is because the effect of hyperconjugation happens due to the overlap of the σ - electrons of the C - H bond with the π - electrons of the aromatic ring. Such overlaps result in an increase in electron density through delocalisation within the aromatic ring, specifically at the ortho and para positions in relation to the Me group.

Similar to the mesomeric effect, the inductive effect of the Me group is also an electron - donating effect, namely the +I - effect. In this case too, the sigma bonds of the methyl group contribute, as they result in weaker binding of the group's electrons. Similarly to the aforementioned +M - effect, this causes a slight rise in the electron density of the aromatic ring in the ortho and para positions relative to the Me group. This increase in electron density makes these positions more reactive.

7.1.3. Dicyanobenzene

The fundamental structure of dicyanobenzene $C_6H_4(CN)_2$ (**n,n - DCB**) is a benzene ring that has been substituted with two cyano groups, resulting in three possible constitutional isomers: 1,2 - DCB (*ortho* - dicyanobenzene), 1,3 - DCB (*meta* - dicyanobenzene) and 1,4 - DCB (*para* - dicyanobenzene). Dicyanobenzene is employed in a multitude of fields due to its two cyano groups and distinctive electronic properties. For instance, DCBs

function as precursors for dyes and pigments, representing an intriguing foundation for the advancement of organic dyes. Furthermore, DCBs are employed in the fabrication of organic semiconductors, organic solar cells, and optoelectronic devices for the production of displays and sensors. Moreover, they are employed in the pharmaceutical industry, polymer chemistry and as a reagent in chemical reactions.

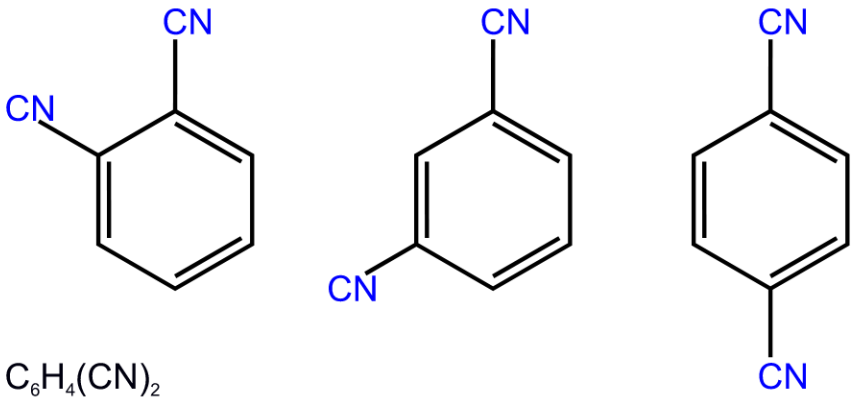

Figure 7.4.: Structural formula of the constitutional isomers of dicyanobenzene. From left: 1,2 - dicyanobenzene, 1,3 - dicyanobenzene and 1,4 - dicyanobenzene.

As with the preceding molecules, the chemical properties vary in accordance with the constitutional isomer of the respective DCB. At room temperature, DCBs exist in a solid state and have melting points that range from approximately 130 $°C$ for 1,2-DCB to over 220 $°C$ for 1,4-DCB, with 1,3-DCB exhibiting a melting point intermediate to these values. DCBs exhibit high solubility in organic solvents, yet display low solubility in water. With regard to reactivity, DCBs are capable of undergoing nucleophilic substitution as a consequence of the cyano group, thereby facilitating further functionalisation. The presence of the aromatic ring enables DCBs to undergo electrophilic aromatic substitution, albeit with a markedly diminished reactivity compared to benzene, which can be attributed to the electron-withdrawing cyano group. In the presence of acids or bases, DCBs undergo hydrolysis, resulting in the formation of corresponding carboxylic acids. Furthermore, DCBs are capable of forming complexes with transition metals, thereby facilitating their utilisation in coordination chemistry.

Given that the substituents of DCBs are cyano groups, the behaviour of DCBs with regard to the -/+I - effect and with regard to the -/+M - effect is analogous to that of the n - cyanoindoles. The cyano group's strong electron-withdrawing property gives rise to an -I - effect, whereby electron density is drawn away from the carbon atom of the

aromatic ring via the σ bonds. The inductive effect is additive due to the presence of two cyano groups in DCBs. However, it is essential to consider the relative positioning of the two cyano groups in order to gain a comprehensive understanding of the observed behaviour. With regard to the electron-withdrawing effect of the cyano groups, this indicates that the inductive effect is more cooperative in nature when the substituents are in the *ortho* and *meta* positions and more competitive in nature when they are in the *para* position. Nevertheless, this results in a significant reduction in electron density within the benzene ring. This effect results in a reduction in the affinity for an electrophilic aromatic substitution, thereby increasing the affinity for a nucleophilic attack on the electron-deficient aromatic ring.

If the corresponding DCB, or its substituents, are considered in terms of the mesomeric effect, the initial situation is identical to that which is observed when the inductive effect is considered. The two cyano groups result in an -M - effect, which also has electron-withdrawing properties and, due to the presence of two cyano groups, has an additive effect akin to the -I - effect. The -M - effect is exemplified by the potential formation of mesomeric resonance structures, wherein a double bond is removed from the aromatic ring. This has a particular impact on the reduction of electron density in the *ortho* and *para* positions relative to the cyano group. The -M - effect enhances the stability of the intermediates in the event of a nucleophilic attack, thereby increasing the affinity for this type of attack.

In conclusion, it can be stated that both effects work in conjunction to significantly reduce the electron density within the aromatic ring. This ultimately results in an increase in reactivity with regard to nucleophilic aromatic substitutions and a decrease in reactivity with regard to electrophilic aromatic substitutions. The position of the substituents in relation to each other is also of consequence due to the two equally decisive substituents. An examination of the constitutional isomers of DCB in terms of dipole moments reveals that, in the case of 1,2-DCB and 1,3-DCB, the presence of a dipole moment is not precluded. Conversely, 1,4-DCB should, in theory, exhibit no dipole moment due to its symmetry. However, this assertion is not entirely accurate, as demonstrated by Exner and Mach [236]. It was demonstrated that 1,4-DCB exhibits a modest dipole moment of approximately 0,45 D when evaluated in solution. This phenomenon can be attributed to anomalous solvent effects, such as donor-acceptor complex formation 3.4.3. These findings reiterate the challenges inherent in measuring dipole moments in solution.

7.2. Solvents

Ethyl acetate $C_4H_8O_2$ (**EtHac**) is an ester ($CH_3COOCH_2CH_3$) that is employed extensively as a solvent in numerous industrial sectors and in research. The most prominent illustration of ethyl acetate's utilisation as a solvent is its substitution for acetone in the production of nail varnish remover. Additionally, ethyl acetate is employed as a flavoring agent in perfumes and food products due to its aromatic, albeit not aromatic in the chemical sense, fruity-sweet odor. Consequently, ethyl acetate has been approved as a food additive within the European Union under the FLAVIS number (**FL - number**) 09.001.

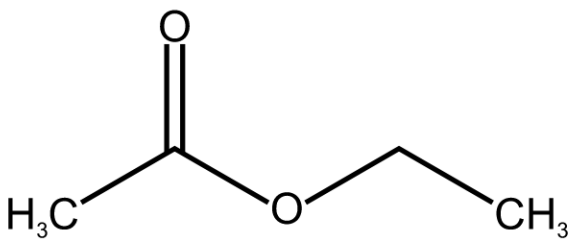

Figure 7.5.: Structural formula of the used solvent ethyl acetate.

The melting point of ethyl acetate is approximately -83 $°C$ [237], the boiling point is approximately 77 $°C$ [238], the refractive index is approximately 1,3724 (n_D - value) [239], and the density is approximately 0,9003 $\frac{g}{cm^3}$ [240], [241] under laboratory conditions. The permittivity is 6,02 at 25 $°C$ [242], and the dipole moment is around 1,78 D [243], [244]. With regard to the polarity scale for solvents, ethyl acetate has an $E_T(30)$ value of 38,1 $kcal \cdot mol^{-1}$ [46].

The determination of the solvent polarity over a certain value or characteristic value is not a straightforward process, and many empirical parameters also reach their limits. In 1963, Dimroth and Reichardt proposed the solvent polarity parameter $E_T(30)$ [245]. This parameter is based on the transition energy of the longest wavelength of the solvatochromic absorption band of a pyridium-N-phenolate-betaine dye. The advantage of this dye is that it exhibits negative solvatochromism of the $\pi \rightarrow \pi^*$ absorption band and, furthermore, that solvatochromic absorption can be observed over a broad range, from $\delta = 810\ nm$ to $\delta = 453\ nm$.

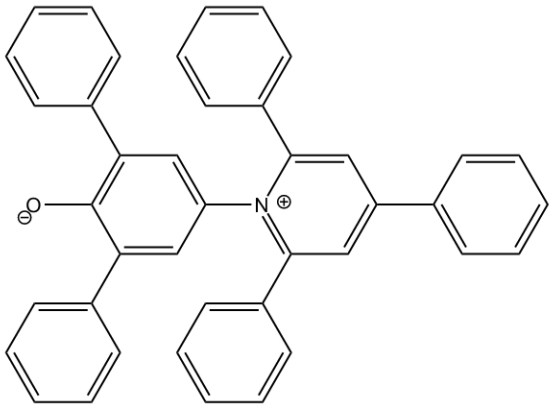

Figure 7.6.: Structural formula of the pyridinium-N-phenolate betaine dye used for the purpose of determining the $E_T(30)$ value.

The parameter $E_T(30)$ is calculated using the formula for calculating the Z-values and provides an indication of the transition energy of the dissolved betaine dye (cf. equation 7.1). This demonstrates that elevated $E_T(30)$ values are indicative of elevated solvent polarity, whereas diminished values are indicative of the opposite [46].

$$E_T/(kcal \cdot mol^{-1}) = h \cdot c \cdot \tilde{\nu} \cdot N_A = 2,859 \cdot 10^{-3} \cdot \tilde{\nu}/cm^{-1} \equiv Z$$
$$E_T/(kcal \cdot mol^{-1}) = 1,196 \cdot 10^{-2} \cdot \tilde{\nu}/cm^{-1} \tag{7.1}$$

Where: h represents Planck's constant, c denotes the speed of light, $\tilde{\nu}$ signifies the wave number of the photon of the electronic excitation, N_A represents Avogadro's constant and 1 $kcal \cdot mol^{-1} = 4,184\ kJ \cdot mol^{-1}$.

Ethyl acetate is classified as a moderately polar compound and is miscible with a wide range of organic solvents. With regard to reactivity, ethyl acetate is capable of undergoing acid-catalysed or base-catalysed hydrolysis. Furthermore, it can participate in nucleophilic substitution reactions due to the presence of the ester function. With regard to its solvent behaviour, ethyl acetate exhibits excellent properties, as it is capable of dissolving both polar and non-polar substances.

Given its favourable properties, accessibility and cost-effectiveness, ethyl acetate was selected as the optimal solvent for determining dipole moments in solution, as part

of this research project. The temperature range encompassed for the measurement of thermochromic shifts is sufficiently extensive in view of the capabilities of the available measuring setups and the solubility of all the molecules to be examined in the ethyl acetate employed. Moreover, the investigation of the solvent parameters with regard to ethyl acetate does not present any significant challenges. Moreover, previous publications, in particular [156], have demonstrated the efficacy of ethyl acetate in similar contexts.

8. Publication on Dicyanobenzene

Excited State Dipole Moments of Two Dicyanobenzene Isomers from Thermochromic Shifts.[†]

Matthias Zajonz[a], Tim Oberkirch[a], Marie-Luise Hebestreit[a], Mirko Matthias Lindic[a], Christof Hättig[b], and Michael Schmitt[a*]

[a]Heinrich-Heine-Universität, Institut für Physikalische Chemie I, D-40225 Düsseldorf, Germany, E-mail:mschmitt@hhu.de
[b] Ruhr-Universitaet Bochum, Lehrstuhl für Theoretische Chemie, D-44780 Bochum, Germany

8.1. Abstract

The excited state dipole moments of two positional isomers of dicyanobenzene have been determined from thermochromic shifts of the absorption and fluorescence emission spectra in ethyl acetate solution and compared to the results of *ab initio* calculations. It is shown that the dipole moments of the two cyano groups add up vectorially for both the ground and excited states.

8.2. Introduction

The concept of dipole moments as measure of charge density distributions in molecules has been successfully used in chemistry for over 100 years [144], [30]. One key to this success story is that dipole moments in electronic ground states follow the laws for summation of vectors, which are directed along individual chemical bonds. This enables intuitive assessment of molecular dipoles from increment rules. While this procedure has entered basic chemistry textbooks [19], [246] and works well in numerous cases, the situation for electronically excited states is far more complex. Dipole moments in electronically excited states provide a good hint to the electronic nature of the excited state. The excited states

of aromatic molecules can be classified, using the nomenclature of Platt as L_a, L_b, B_a and B_b states, depending on the position of the wave functions' nodal planes. The lowest two excited singlet states, L_a and L_b are degenerate in benzene, their degeneracy is lifted upon substitution. Depending on the substituent(s) and their relative position, they can be energetically close, making a straightforward assignment difficult. However, since their excited state dipole moments differ considerably, these can be used for an unequivocal assignments of the states.

Recently, several aromatic species bearing cyano groups, have been detected via radio astronomy in the interstellar medium, among them aromatics as benzonitrile (BN) [247], 1,2-dicyanobenzene, 1,3-dicyanobenzene [248] and 1- and 2-cyanonaphthalene [249].

Electronic Stark spectroscopy of benzonitrile (BN), performed in the group of Pratt yielded the dipole moments in the ground and first excited singlet state [250]. Since their ground state dipole moment differs considerably from a value of 4.14(5) D, which was determined by microwave Stark spectroscopy [251], Wohlfart *et al.* used Fourier transform microwave spectroscopy in a supersonic jet, to determine the dipole moment of benzonitrile precisely. They found a value of $\mu_a = 4.5152(68)$ D, in good agreement with the value determined by Borst *et al.* of 4.48(1), which settled the dispute about the dipole moment of benzonitrile. Sato-Toshima *et al.* determined the ground state dipole moments of 1,2-dicyanobenzene (12-DCB) and 1,3-dicyanobenzene (13-DCB) in benzene and dioxan solutions using the method of Guggenheim [252]. Chitarra *et al.* measured the rotational spectra of 12-DCB and 13-DCB in the centimeter- and millimeter-wave domains and determined their ground state rotational constants, the quartic and sextic centrifugal constants and the nuclear quadrupole coupling constants [248].

In the present contribution we will show, how the dipole moments of the cyano groups sum up vectorially in the two dicyanobenzenes for both the ground and the electronically excited states. Since both molecules have C_{2v} symmetry in both states, the direction of the dipole moment does not change upon excitation, just the modulus, which makes them ideal candidates for the thermochromic determination of their excited state dipoles.

8.3. Computational Methods

8.3.1. Quantum chemical calculations

Structure optimizations were performed with TURBOMOLE, version 7.5.1 [253] employing a Dunning's correlation-consistent polarized valence triple zeta (cc-pVTZ) basis set from the TURBOMOLE library [158], [254]. The equilibrium geometries of the electronic ground

and the lowest excited singlet states were optimized using the approximate coupled cluster singles and doubles model (CC2) employing the resolution-of-the-identity (RI) approximation [170], [160], [161]. For the structure optimizations spin-component scaling (SCS) modifications to CC2 were taken into account [162]. Additionally, ground state properties have been calculated at the RI-MP2 level of theory [255] for the isolated molecules and compared to those from the Conductor-like Screening Model (COSMO) [164]. Similarly, for the excited states gas phase values from the ADC(2) method [256] are compared to the respective solvation values from COSMO. Vibrational frequencies and zero-point corrections to the adiabatic excitation energies were obtained from numerical second derivatives using the NumForce script [163].

8.4. Experimental Methods

The cavity volumes of the cyanoindoles and benzonitrile, dissolved in ethyl acetate were determined using a high-precision density meter from Anton Paar (model: DMA 4500). For this purpose, a concentration series was prepared and measured in a temperature range from 265.15 to 343.15 K with an increment of 2 K. The spectroscopic measurements were carried out in a self-constructed cell using two spectrometers from Varian. A Varian Cary 50 Scan UV-Visible was used for absorption measurements and a Cary Eclipse Fluorescence for emission measurements. The measurements were performed between 225.15 K and 343.15 K with an increment of 2 K. For the determination of the refractive indices of the solvent, a refractometer from Anton Paar (model: Abbemat MW) was used, whereby measurements were made on a temperature scale from 283.15 K to 343.15 K with an increment of 1 K. At each temperature refractive indices were determined at 5 different wavelengths. The permittivity of the solvent was determined using a Keysight E4990A Impedance Analyzer in combination with the capacitor of a Keysight 16452A Test Fixture.

8.5. Results and Discussion

8.5.1. Computational Results

The structures of BN, 12-DCB, and 13-DCB in the ground and the lowest two excited singlet states have been optimized at the SCS-CC2/cc-pVTZ level of theory, using the Turbomole program suite [253]. The ground state geometries are shown in Figure 8.1. All Cartesian coordinates of the optimized structures are given in the online supporting material. The calculated rotational constants and inertial defects of the lowest two singlet

states and dipole moment components on the main inertial axes for each molecule are presented in Table 8.1. The calculated inertial defects in the ground state of the three molecules are small and numerical artefacts of a planar structure. All three molecules possess C2v-symmetry in the electronic ground state, with the C_2-axis being the inertial a-axis for BN and 12-DCB and the b-axis for 13-DCB. The dipole moments are consequently oriented along the a-axis for BN and 12-DCB and along the b-axis for 13-DCB, cf. Figure 8.1. The symmetry is preserved in the excited state, thus the orientation of the permanent dipole moment stays like in the ground state and only the modulus changes upon electronic excitation.

In order to compute dipole moments in solution, the conductor-like screening model (COSMO) [164] was used. Since COSMO for RI-CC2 calculations of the excited states is not implemented, we switched the dipole moment computations to (RI-)ADC(2) for the excited states and to (RI-)MP2 for the ground state. At first, we compared the dipole moments from the respective CC2 calculations to those from MP2 (S_0) and ADC(2) (S_1 and S_2). This comparison is shown in Table 8.3. Very close agreement shows, that the values from ADC(2) can indeed be used for the excited states in the COSMO model.

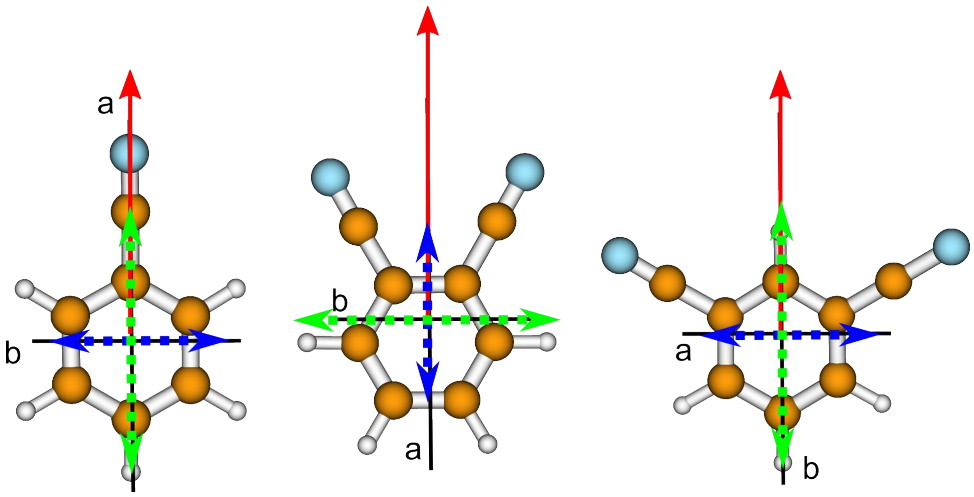

Figure 8.1.: SCS-CC2/cc-pVTZ optimized ground state geometries of benzonitrile, 12-DCB, and 13-DCB along with inertial axes a and b, the permanent dipole moment vector (red straight arrow), the transition dipole moment to the S_1-state (blue dotted double arrow), and the TDM to the S_2-state (green dotted double arrow).

Table 8.1.: SCS-CC2/cc-pVTZ calculated rotational constants A, B, C and inertial defects in the ground state (doubly primed values) and the excited state (primed values) of BN, 12-DCB, and 13-DCB. The inertial defect ΔI is defined as: $\Delta I = I_c - I_b - I_a$, where the I_g are the moments of inertia with respect to the main inertial axes $g = a, b, c$.

	BN		12-DCB		13-DCB	
	calc.	exp. [250]	calc.	exp. [248]	calc.	exp. [248]
A''/MHz	5656	5656.7(1)	2004	2000.710452(98)	2705	2723.018609(46)
B''/MHz	1535	1547.4(1)	1335	1346.325041(27)	899	906.419893(21)
C''/MHz	1208	1214.8(1)	801	804.503123(25)	675	679.859840(15)
$\Delta I''$ / amuÅ^2	0.00	0.07(5)	0.00	0.211(1)	0.00	0.207(1)
μ''_a/D						
μ''_b/D						
μ''_c/D						
A'/MHz	5470	5474.7(1)	1937	-	2633	-
B'/MHz	1495	1510.2(1)	1310	-	886	-
C'/MHz	1174	1183.9(1)	781	-	663	-
$\Delta I'$ / amuÅ^2	0.00	0.08(6)	0.00	-	0.00	-
μ'_a/D						
μ'_b/D						
μ'_c/D						
$\Delta A'$/MHz	-186	-182.0(1)	-68	-	-72	-
$\Delta B'$/MHz	-40	-37.2(1)	-25	-	-13	-
$\Delta C'$/MHz	-34	-30.9(1)	-20	-	-12	-

Table 8.2.: Adiabatic excitation energies $\tilde{\nu}_{ad.}$, vertical excitation energies $\tilde{\nu}^{exc.}_{vert.}$, vertical emission energies $\tilde{\nu}^{em.}_{vert.}$, and transition dipole moment orientation θ of the lowest two excited singlet states of BN, 12-DCB, and 13-DCB. θ is defined as the angle between the TDM and the inertial a-axis.

	BN		12-DCB		13-DCB	
	S_1	S_2	S_1	S_2	S_1	S_2
$\tilde{\nu}_{ad.}$/cm^{-1}	37162	43347	35835	42798	35958	44142
$\tilde{\nu}^{exc.}_{vert.}$/cm^{-1}	40802	49166	38982	46081	39272	47640
$\tilde{\nu}^{em.}_{vert.}$/cm^{-1}	36755	43912	35228	34307	35464	36029
θ/°	90	0	0	90	90	0
LUMO ← HOMO	´-	0.95	-	0.94	-	0.97
LUMO ← HOMO-1	0.75	-	0.75	-	0.72	-
LUMO+1 ← HOMO	0.63	-	-0.62	-	0.65	-

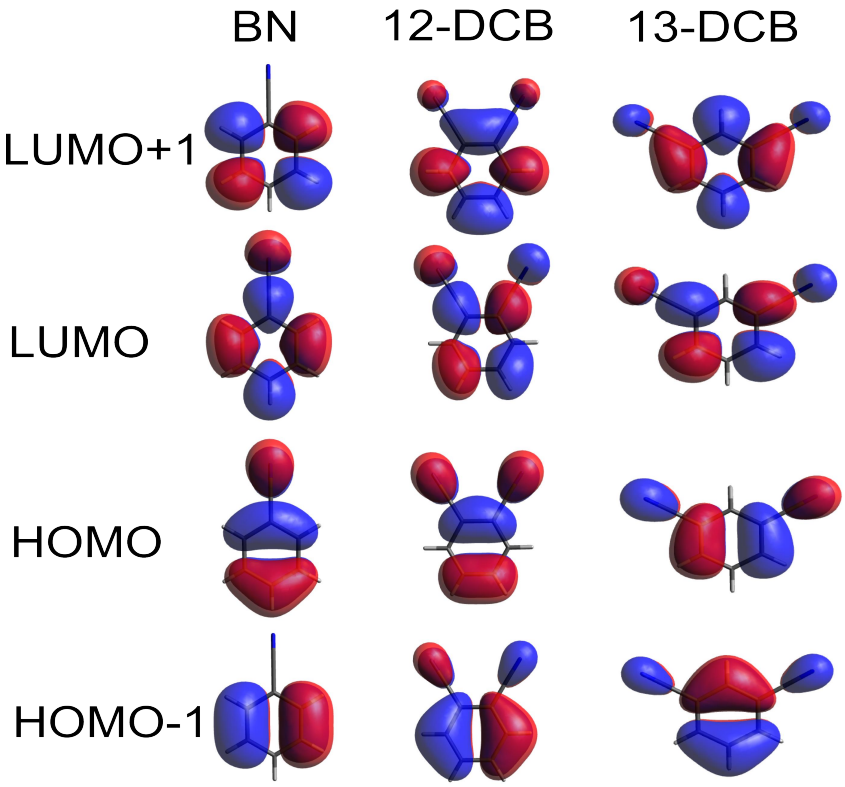

Figure 8.2.: Frontier orbitals of BN, 12-DCB, and 13-DCB. Orientation as in Figure 8.1.

Adiabatic excitation energies and transition dipole moment orientation of the lowest two excited states of BN, 12-DCB, and 13-DCB have been calculated, including zero-point-energy correction at the level of optimization. These results are presented in Table 8.2 along with the vertical absorption and emission energies to and from the respective states. In all cases, the S_1-state, which is of $\pi\pi^*$ nature, is the L_b state ($^1B_2$) in Platt's notation [257], while the S_2-state can be described as L_a-state ($^1A_1$). The respective frontier orbitals are shown in Figure 8.2. For BN, the transition dipole moment (TDM) of the S_1-state is oriented along the inertial *b*-axis, as has been confirmed experimentally and thus runs through the **b**onds, while that of the S_2-state is oriented along the inertial *a*-axis and runs through the **a**toms in agreement with Platt's L_a-L_b notation. The S_1 TDM of 12-DCB is oriented along the *a*-axis and runs though the bonds (L_b), while that of the S_2-state is parallel to the *b*-axis and runs through the atoms (La). For 13-DCB the S_1-TDM is again along the *a*-axis, running through the bonds and the S_1-TDM along *b*, running through the atoms. Mind the fact, that the molecules in Figure 8.1 are oriented in such a way, that the C_2-symmetry axis and the permanent dipole moment vector are pointing upwards, which causes the inertial axes *a* and *b* to switch in 13-DCB compared to BN and 12-DCB.

8.5.2. Experimental Results

First, the cavity volume of 12-DCB and 13-DCB in EA, which is used to replace the Onsager radius [101], [184] has been determined from the relation between the weight fraction w and the molar cavity volume V_m:

$$\frac{1}{\rho} = \frac{1}{\rho^*} + \left(\frac{V_m}{M} - \frac{1}{\rho^*}\right) \cdot w \tag{8.1}$$

where ρ is the density of the solution, ρ^* is the density of the solvent, V_m is the molar cavity volume, and M is the molar mass of the solute.

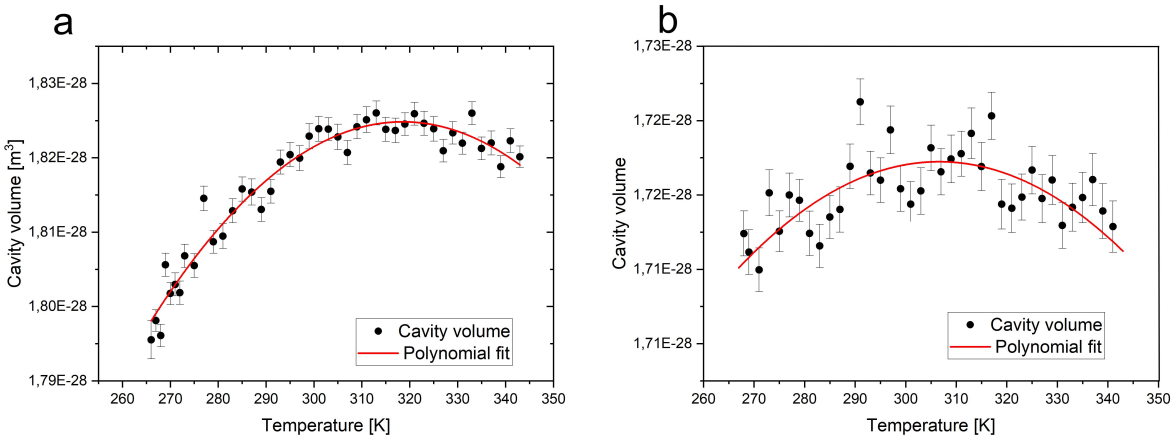

Figure 8.3.: Dependence of the cavity volume of 12-DCB (a) and 1,3-DCB (b) in EA from the temperature of the solution.

According to equation (8.1) the molar cavity volume can be calculated from the slope of a linear fit of the plot of the inverse density $\frac{1}{\rho}$ versus the weight fraction w. This procedure was repeated for all temperatures, which are used for the thermochromic shifts, cf. Figure 8.3.

The absorption and fluorescence maxima shift upon changing the solvent index of refraction and permittivity, what can be introduced by a variation of the solvent (solvatochromic shifts). Since both index of refraction and permittivity are functions of the temperature this shift can also be induced by a temperature variation (thermochromic shifts).

The shift of the fluorescence and absorption spectra of 12-DCB (a) and 13-DCB (b) with varying temperature is shown in Figure 8.4.

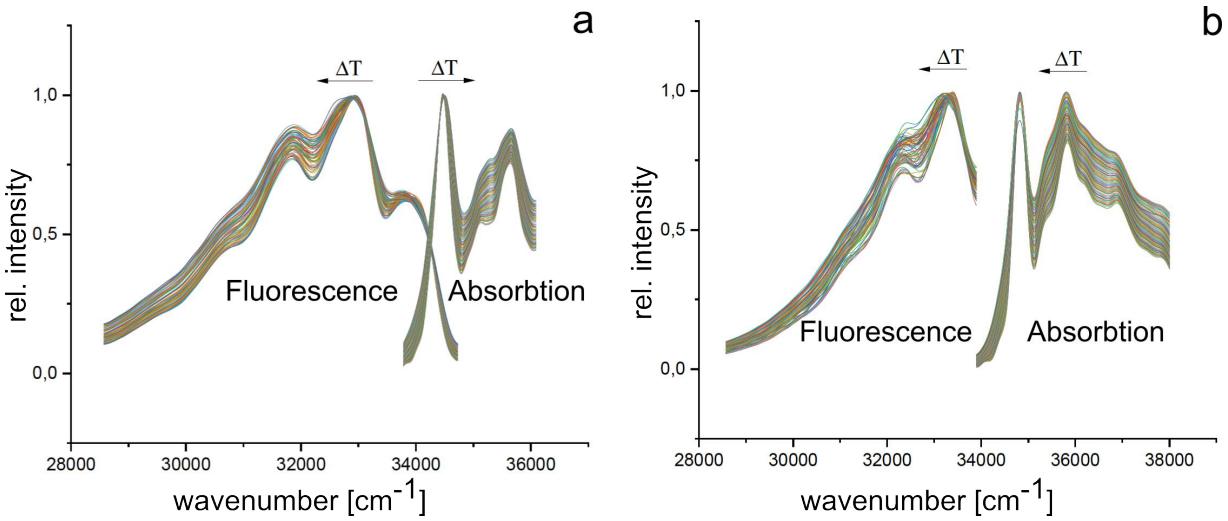

Figure 8.4.: Shift of the fluorescence and absorption spectra of 12-DCB (a) and 13-DCB (b) with varying temperature.

Lippert and Mataga derived an equation for evaluating the change of the dipole moment from solvatochromic shifts in different solutions:

$$\tilde{\nu}_A - \tilde{\nu}_F = -\frac{2(\mu_e - \mu_g)^2}{4\pi\varepsilon_0 hca^3} \cdot F_{LM} + const. \tag{8.2}$$

where $\tilde{\nu}_A$ and $\tilde{\nu}_F$ are the wavenumbers of the maxima in absorption and fluorescence spectra, μ_g and μ_e are the ground and excited state dipole moment ε_0 is the vacuum permittivity, h the Planck constant, c the speed of light, a the Onsager cavity radius, and F_{LM} the solvent polarity function according to Lippert and Mataga[133], [39]:

$$F_{LM} = \frac{\varepsilon - 1}{2\varepsilon + 1} - \frac{n^2 - 1}{2n^2 + 1} \tag{8.3}$$

Using the experimentally determined cavity volume instead of the Onsager radius of the cavity, equation 8.2 becomes:

$$\tilde{\nu}_A(T) - \tilde{\nu}_F(T) = -\frac{2\,(\mu_e - \mu_g)^2}{3\varepsilon_0 hc} \cdot F_{LM}(T) + const. \tag{8.4}$$

$$F_{LM}(T) = \frac{1}{V(T)} \cdot \left[\frac{\varepsilon(T) - 1}{2\varepsilon(T) + 1} - \frac{n(T)^2 - 1}{2n(T)^2 + 1} \right] \tag{8.5}$$

The plot of $\tilde{\nu}_A(T) - \tilde{\nu}_F(T)$ (equation 8.4) versus F_{LM} (8.5) yields the change of the dipole moment upon electronic excitation from the slope m_{LM}.

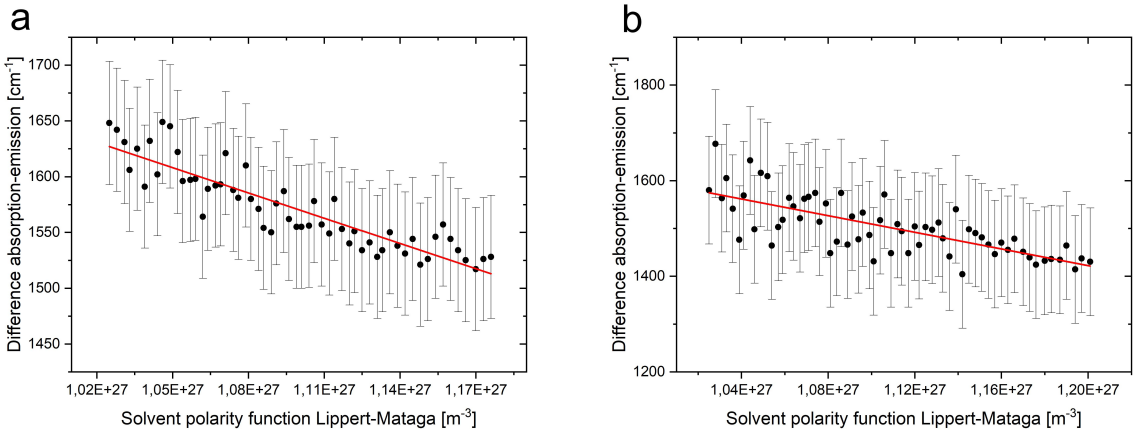

Figure 8.5.: Plot of $\tilde{\nu}_A(T) - \tilde{\nu}_F(T)$ versus F_{LM} for solutions of 12-DCB (a) and 13-DCB (b) in EA.

The second approach we will use here, has been introduced by Bilot and Kawski [43]. According to Bilot - Kawski a plot of the sum of fluorescence and absorption maxima vs. the solvent polarity function yield the excited state dipole moment, given that the ground state dipole is known:

$$\tilde{\nu}_A(T) + \tilde{\nu}_F(T) = -\frac{2\left(\mu_e^2 - \mu_g^2\right)}{3\varepsilon_0 hc} \cdot F_{BK}(T) + const. \tag{8.6}$$

$$F_{BK}(T) = \frac{1}{V(T)} \cdot \left[\frac{2n(T)^2 + 1}{n(T)^2 + 2} \cdot \left(\frac{\varepsilon(T) - 1}{\varepsilon(T) + 1} - \frac{n(T)^2 - 1}{n(T)^2 + 2} \right) + \frac{3\left(n(T)^4 - 1\right)}{\left(n(T)^2 + 2\right)^2} \right] \tag{8.7}$$

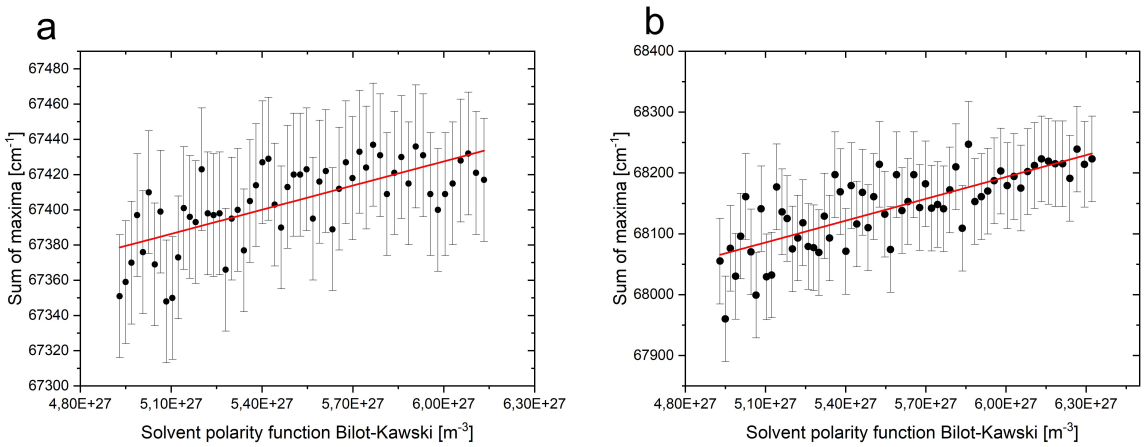

Figure 8.6.: Plot of $(\tilde{\nu}_A + \tilde{\nu}_F)$ versus $F_{BK}(T)$ for solutions of 12-DCB (a) and 13-DCB (b) in EA.

Table 8.3 summarizes the ground and excited state dipole moments of 12-DCB and 13-DCB from the LM and BK treatment, described above and compares it to the results of SCS-CC2/cc-pVTZ *ab initio* calculations and to independent experimental determinations of the ground state dipole from microwave Stark spectra [252]. Additionally, the dipole moment of BN has been determined using the above procedure and is compared for the ground and the excited state to the results of electronic Stark spectroscopy from the group of Pratt [250].

Table 8.3.: Dipole moments in Debye obtained from the method of Lippert-Mataga and of Bilot-Kawski compared to those from SCS-CC2/cc-pVTZ calculations for the ground (S_0) and lowest excited singlet states (S_1, S_2), and to independent determinations from evaluation of MW Stark [252] and UV Stark spectra [250].

	BN			12-DCB			13-DCB		
	S_0	S_1	S_2	S_0	S_1	S_2	S_0	S_1	S_2
SCS-CC2	4.43	4.52	4.93	6.95	6.88	7.27	4.18	4.11	4.04
MP2	4.43	-	-	6.98	-	-	4.18	-	-
ADC(2)	-	4.52	5.02	-	6.90	7.29	-	4.11	4.14
MP2 (COSMO)	5.45	-	-	10.04	-	-	5.87	-	-
ADC(2) (COSMO)	-	5.50	5.42	-	8.88	8.63	-	5.27	4.94
Exp.(MW)	4.48[250]	4.57[250]	-	6.82[252]	-	-	3.99[252]	-	-
Exp.(LM)	-	6.8(8)	-	-	11.0(1)	-	-	8.5(2)	-
Exp.(BK)	-	4.42[154]	-	-	6.88(1)	-	-	4.33(3)	-

8.6. Discussion

Prior to the discussion of the experimental results and their comparison to the theoretical calculations we have to express a caveat about solvation effects on excited state dipole moments from thermo- or solvatochromic shifts. At first sight it seems plausible to compare gas phase dipole moments from Stark spectroscopy with those from *ab initio* calculations of the isolated species and dipole moments from solvatochromic shifts to *ab initio* calculations which contain solvation effects like the Conductor-like Screening Model (COSMO) or the Polarizable Continuum Model (PCM). This however, is not correct, since the solvent polarity functions defined by Lippert - Mataga, Bilot - Kawski, McRae, Bakhshiev, and Chamma – Viallet, to name only the most popular, establish a correlation between the solvent shifts of fluorescence or absorption transitions and the dipole moment of the **unpolarized** molecule. Hence, the so determined dipole moments will resemble more the results from *ab initio* calculations of the isolated species than of that of solvation models, which return the values of the **polarized** molecule.
Since COSMO is not available for CC2 wave functions, we first assessed the ground state dipole moments of he isolated molecules by MP2 and the excited states dipoles by ADC(2) and compared them to the respective CC2 values, cf. Table 8.3. All calculations have been performed using Dunning's triple-ζ cc-pVTZ basis set. The close agreement of the dipole moments (as well as rotational constants and excitation energies, etc.) shows that the level of theory is adequate for a calculations of the molecular parameters.
As has been shown previously, the results for excited state dipole moments from application of the original Lippert - Mataga theory are inferior to those from the modified Bilot - Kawski ansatz [184]. For 1,2-DCB, using BK, we find a value of 6.88 D in the S_1 state, in perfect agreement with the SCS-CC2/cc-pVTZ and the ADC(2)/cc-pVTZ calculated values, while the respective ADC(2) COSMO value for EA as solvent is by 2 Debye too large, cf. Table 8.3. The value from a evaluation using LM theory is 11.0 D, far from what can be expected.

For 1,3-DCB, BK theory yields 4.33 D in good agreement with the SCS-CC2 and ADC(2) values of the isolated molecule of 4.11 D), while again the LM value of 8.5 D is about a factor of two too high. As for 1,2-DCB, the ADC(2) COSMO value is considerably too high (5.27 D).
The additivity of bond dipole moments has made the concept of the dipole moment so successful in chemistry. Textbook examples are the isomeric dichloro- and difluorobenzenes in which vector addition allows for a semi-quantitative assessment of the molecular dipole moments form the dipole of the monosubstituted chloro- and fluorobenzenes [19], [246].

However, for the excited state of *cis*- and *trans*-3-aminophenol the additivity rule has been shown to yield unsatisfactory results [258].
BN has a ground state dipole moment of 4.48 D [250]. The C-N groups in 1,2-dicyanobenzene form an angle α of 61.4° [259]. Vectorial addition yields a dipole moment of $\mu_{12} = 2cos(\alpha/2) \cdot \mu = 7.70$ Debye. However, the experimental value is 6.82 Debye [252] (SCS-CC2 calculated: 6.95 D), deviating by 13% from the value obtained by vector addition.
For 1,3-DCB (α=120°) one obtains from vectorial addition a value $\mu_{13} = 4.48$ D, which differs from the experimental value of 3.99 D [252] by 11%. Deviations from vector additivity in the electronic ground state can be attributed to inductive effects on neighboring bonds, which is larger for the neighboring CN groups in 1,2-DCB.
For the excited state of 1,2-DCB, the dipole moment from applying BK theory is 6.88 D (SCS-CC2 calculated: 6.88 D), vector addition using the BN excited state dipole of 4.57 D from ref. [250] yields a value of 7.86 D, which means a deviation of 14% from the experiment. For 1,3-DCB we obtain 4.33 D from BK theory and 4.57 D from dipole addition (6% deviation).

8.7. Conclusion

The excited state dipole moments which are obtained from solvatochromic or thermochromic shifts have to be compared to the values of the isolated molecule. These might be from Stark experiments in the gas phase or in molecular beams or alternatively from *ab initio* calculations. The reason is that solvent shifts of fluorescence or absorption transitions are correlated to the dipole moment of the unpolarized molecule. Keeping this in mind, good agreement is obtained between the calculated and experimentally determined excted state dipole moments.
We were able to show that the deviations of the experimentally determined dipole moments for 1,2-DCB and 1,3-DCB from the results of an vector addition in the excited state are similar and in the order of what was found for the electronic ground state. The ground state deviations are similar to those for the textbook example dichlorobenzene. Thus, it is not generally impossible to deduce excited state dipole moments from vector addition of individual dipoles. This is, however, only true for compounds, which have two identical substituents and not for differing substituents like in 3-aminophenol (3AP) [258]. The reduced symmetry in 3-AP leads to a considerable amount of state mixing between the L_a- and L_b-states, which is not present in DCB.

8.8. Acknowledgements

Financial support of the Deutsche Forschungsgemeinschaft via grant SCHM1043/16-1 is gratefully acknowledged. Computational support and infrastructure was provided by the "Center for Information and Media Technology" (ZIM) at the Heinrich-Heine-University Düsseldorf.

8.9. Credit author statement

Matthias Zajonz: Methodology, data acquisition, evaluation, writing. Tim Oberkirch: Data acquisition, evaluation. Marie-Luise Hebestreit: Reviewing, writing. Mirko Matthias Lindic: Software. Christof Hättig: ab initio calculations. Michael Schmitt: Supervision, conceptualization, ab initio calculations, writing, reviewing and editing.

8.10. Own Share

The content of this chapter has already been published in the *Journal of Photochemistry and Photobiology A: Chemistry*, **452**, 115589, 2024 under the title *Excited state dipole moments of two dicyanobenzene isomers from thermochromic shifts and ab initio calculations* written by Matthias Zajonz, Tim Oberkirch, Marie-Luise Hebestreit, Mirko Matthias Lindic, Christof Hättig and Michael Schmitt.

My own share of this publication is about 70% and consists of writing - original draft, software, methodology, investigation, formal analysis.

9. Publication on n-Cyanoindoles

Lippert-Mataga Treatment Fails in Predicting Excited State Dipole Moments in n-Cyanoindoles (n=2,3,4,5,6).†

Matthias Zajonz[a], Marie-Luise Hebestreit[a], Peter Gilch[b], Christof Hättig[c], and Michael Schmitt[a*]

[a]Heinrich-Heine-Universität, Institut für Physikalische Chemie I, Arbeitsgruppe für Hochauflösende Spektroskopie, D-40225 Düsseldorf, Germany, E-mail:mschmitt@hhu.de
[b]Heinrich-Heine-Universität, Institut für Physikalische Chemie II, Arbeitsgruppe Femtosekundenspektroskopie, D-40225 Düsseldorf, Germany
[c] Ruhr-Universitaet Bochum, Lehrstuhl für Theoretische Chemie, D-44780 Bochum, Germany

9.1. Abstract

The dipole moments of six positional isomers of n-cyanoindole in their lowest electronically excited singlet states have been determined from thermochromic shifts of the absorption and emission spectra in solution and are compared to the results of dipole moment determination from rotationally resolved electronic Stark spectra in the gas phase and to *ab initio* calculations. A good agreement with the theory can be obtained for the solvent polarity function of Bilot and Kawski, while the by far more popular and widely used solvent polarity function of Lippert and Mataga completely fails to describe the changes of dipole moment upon electronic excitation.

9.2. Introduction

Dipole moments are among the most important physical parameters of molecules. They relate with the state of aggregation of substances and strongly affect solubilities and reactivities. Whereas the dipole moment of the molecular ground state is easily accessible through measurement of the permittivity, the determination of the dipole of short-lived species, like molecules in their excited states, or photochemical transients is far more challenging [6]. Knowledge of the change of modulus and orientation of molecular dipole moments following an electronic excitation of fluorophores is crucial for the characterization of the respective excited states. Furthermore, this knowledge is important for improving the performance of organic light emitting diodes (OLEDS) [260], [261]. Here, the charge transfer state of thermally activated delayed fluorescent (TADF) emitters are stabilized by the interaction of the excited state dipole moment of the TADF emitter and the ground state dipole of the host. Large dipole moments of the host are capable of lowering the energy of the lowest excited singlet state, thus reducing the gap to the lowest triplet state [262]. Engineering the host and TADF dipole moments can enhance delayed fluorescence quantum yields of the TADF emitters, which increases the external quantum efficiency of these devices.

The abstraction of charge distribution in molecules as electric dipole moment, is one of the basic concepts in chemistry, since it was originally introduced by Max Reinganum in 1903 [30] and later, independently by Peter Debye in 1905 [32]. An appealing aspect of this concept, is the idea of bond dipoles, which can be added up in a vectoral manner in order to result in a microscopically interpretable picture of the origin of molecular dipole moments [263], [264]. Although, Bader had shown that it is wrong to assume that any bond moment would point along the line joining the atoms which are connected by the chemical bond [265], the concept is still sufficiently accurate for non-vibrating molecules in their electronic ground states. For electronically excited states, however, neither magnitude nor direction of the dipole moment can be deduced from simple vector addition of bond dipole moments [258], [6].
Due to its inherent accuracy, gas phase electronic Stark spectroscopy became the gold standard for the determination of molecular dipole moments in electronically excited states [266], [267], [268], [269], [270]. In the time-domain, electric field induced quantum beats in the exponential decay after pulsed laser excitation can be used for determination of dipole moments in the excited state [271], [272]. However, despite their accuracy, methods for determining the dipole moments in excited states in the gas phase are limited to molecules

with sufficiently large vapor pressure in order to transfer them to the gas phase. The most severe obstacle is that many molecules are thermally labile, and cannot be vaporized without decomposition. Until now, this problem remains unresolved, since the inherently large spectral resolution, which is needed to resolve the rovibronic lines in the electric field, requires continuous laser beams, and thus prohibits the use of pulsed laser desorption techniques, mainly due to the small duty cycle. Apart from this restriction, the resolution, which is needed to resolve even the zerofield electronic spectra of large molecules, comes to a limit for molecules with rotational constants on the order of a few MHz [6]. Therefore, solution based spectroscopic techniques, with randomly oriented molecules have found widespread applications. Electro-absorption spectroscopy has been pioneered in the 60s of the 20th century by Ramsay and Liptay [273]. It is applicable for various electronic states, even if their absorption spectra are overlapping. The group of Fessenden pioneered excited state dipole moments from time-resolved changes in photoinduced microwave dielectric absorption [274]. A very popular method for the determination of excited state dipole moments is based upon the solvatochromic shift of absorption and emission spectra through the so-called Lippert-Mataga (LM) equation [133], [39], [275], [276]. The derivation of the LM equation is based on Onsager's reaction field theory [36], which assumes that the fluorophore is represented by a point dipole, located in the centre of a spherical cavity. The radius of the cavity, formed by the homogeneous and isotropic solvent with the permittivity ϵ is called the Onsager radius.

However, the use of solvatochromic shifts has some shortcomings with regard to the exact determination of dipole moments [277], [278], [154]. Most severely, variation of the solvent does not only change the permittivity ϵ and refractive index n, but also influences other parameters that influence the shift within the spectra, such as the affinity to form hydrogen bonds. In order to overcome the problems connected with the use of different solvents, the thermochromic method has been introduced, which utilizes the temperature dependence of permittivity and refractive index [151], [149]. Our research group has started investigations of molecules, which can be studied simultaneously by electronic Stark spectroscopy in the gas phase and by thermochromic spectroscopy in solution [184], [156], [279], [280]. This way we seek a better understanding of basic concepts of thermochromism and an improvement of excited state dipole moment determination.

Dipole moments in electronically excited states are important indicators for the nature of the excited states. For example, the lowest two excited singlet states with $\pi\pi^*$-character of indole and substituted indoles are commonly labelled by L_a and L_b, following the nomenclature of Weber [281], which is an extension of the original Platt nomenclature for cata-condensed hydrocarbons [257]. These states can be distinguished on the basis of

their considerable different dipole moments.

Tryptophan is widely used as an (intrinsic) fluorescence sensor, since as natural amino acid, it introduces only small changes in its protein environment. However, there are several draw-backs, which motivated the search for similar fluorophores. One of the draw-backs is the complex decay kinetics, and the spectral overlap with other natural chromophores [5], another the small dependence of the spectrum and the quantum yield (QY) to the surrounding [282]. Many attempts concentrated on the different isomeric cyanotryptophans, which have favourable fluorescence properties [283], [284], [285], [286], [287].

In order to understand the basic photophysical properties, Hilaire *et al.* studied the solvent dependence of fluorescence life times and QYs of six isomeric cyanoindoles (CI) [282]. A thorough theoretical study of solvent effects on CI fluorescent probes was presented by Abou-Hatab and Matsika [288]. In our group, the excited state structures, dipole moments, and fluorescence life times of isolated 2-CI [132], 3-CI [129], 4-CI [130], [289], and 5-CI [290], [291] were studied in cold molecular beams by means of rotationally resolved electronic Stark spectroscopy and Franck-Condon analyses. Binary water clusters of 2-CI [292], 3-CI [293], [294], 5-CI [295] have been investigated under cold molecular beam conditions.

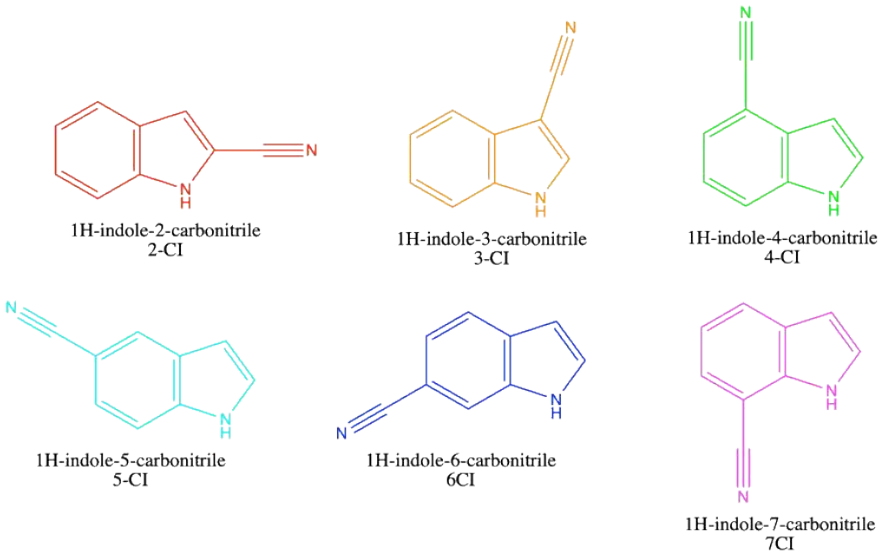

Figure 9.1.: The six different constitutional isomers of n-cyanoindole, n = 2-7.

In the present contribution a detailed analysis of the excited state dipole moments of all six positional isomers of cyanoindole, shown in Figure 9.1 will be given and compared to the results of quantum mechanical computations.

9.3. Results and Discussion

Absorption and fluorescence emission spectra of the six isomeric cyanoindoles (cf. Figure 9.1) in ethyl acetate solution are presented in Figure 9.2. The emission maxima shift to higher wavenumber according to $7-CI < 4-CI < 5-CI < 6-CI < 2-CI < 3-CI$.

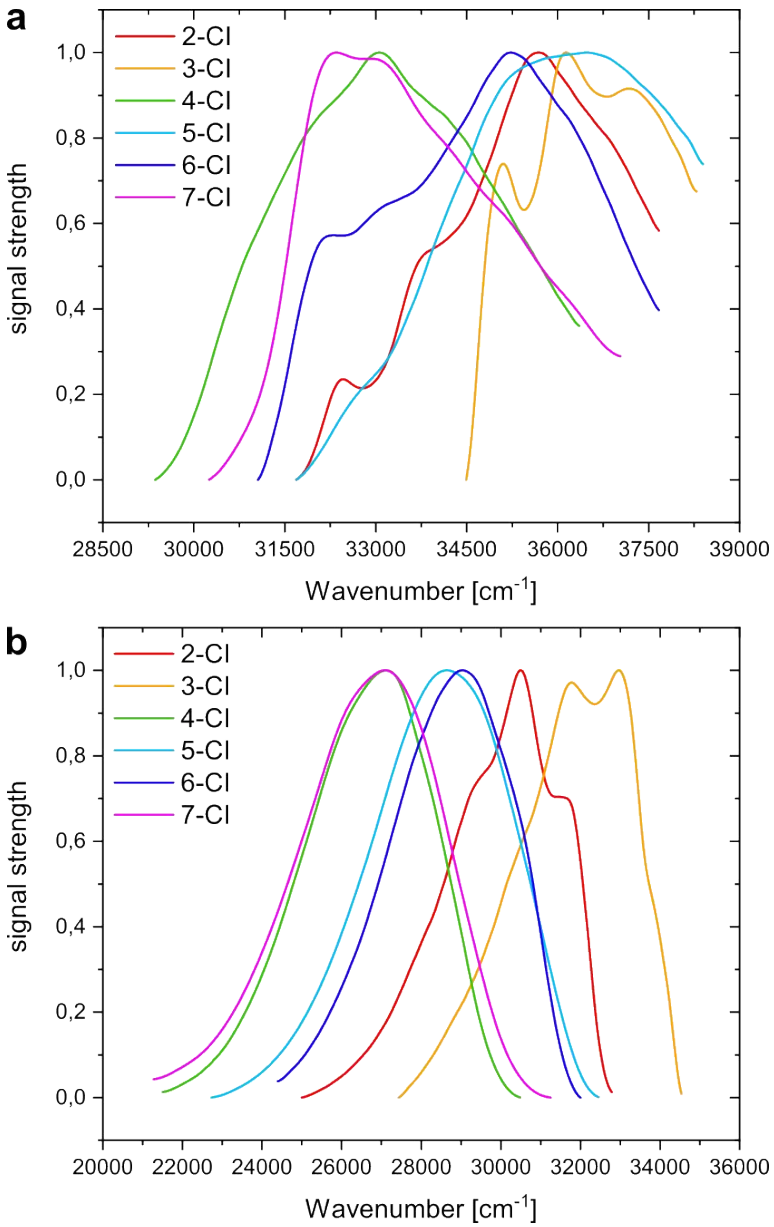

Figure 9.2.: Normalized fluorescence absorption (**a**) and emission (**b**) spectra of the six different isomers of cyanoindole in ethyl acetate solution.

Dipole moments in ground and excited singlet state

We determined the change of the permanent dipole moments of the six isomers of CI upon electronic excitation from the thermochromic shifts of absorption and emission spectra in ethyl acetate and compared them to the dipole moments from rotationally resolved electronic Stark spectroscopy in the gas phase, where available. The thermochromic shifts of absorption and emission spectra of 2-CI are shown in Figure 9.3. The spectral data of all other isomers are given in the online supporting information. In order to obtain the excited state dipole moments in solution, the variation of the permittivity ϵ of the used solvent ethyl acetate with temperature was determined, and the refractive index n of the solvent was investigated with regard to variation of temperature and wavelength. In previous studies, the refractive index n_D determined at 589,3 nm was used. However, since the absorption as well as the emission of the investigated CIs is below about 330,0 nm and the refractive indices enter the calculations in second power, the wavelength dependence of n should not be neglected.

It was found that there is a mutual influence between temperature and wavelength dependence. For the refractive index, a 3D fit was applied, in which the wavelength dependence of the refractive index n was modeled using the Sellmeier equation [88].

Using the relation derived independently by Lippert [133] and Mataga [39] the change of the dipole moment upon electronic excitation can be obtained from equation 9.1. It is assumed that dipole vectors are oriented equally in ground and excited states.

$$\Delta\mu(LM) = \sqrt{\frac{3m_{LM}\epsilon_0 hc}{2}} \tag{9.1}$$

where m_{LM} is the slope of the plot of the difference of the absorption and emission maxima $\tilde{\nu}_A(T) - \tilde{\nu}_E(T)$ *vs.* the so-called solvent polarity function (SPF) $F_{LM}(T)$:

$$\tilde{\nu}_A(T) - \tilde{\nu}_E(T) = \frac{2(\mu_e - \mu_g)^2}{3\epsilon_0 hc} \cdot F_{LM}(T) + const. \tag{9.2}$$

The original SPF of LM has been modified by replacing the Onsager radius with the (experimentally determined) cavity volume, which is a function of the temperature like the index of refraction and the permittivity [101], [155]:

$$F_{LM}(T) = \frac{1}{V(T)}\left[\frac{\epsilon(T)-1}{2\epsilon(T)+1} - \frac{1}{2}\left(\frac{n(T)^2-1}{2n(T)^2+1}\right)\right] \tag{9.3}$$

Following Bilot and Kawski (BK) [135], [134], the excited state dipole moment can be obtained from the relation:

$$\mu_e(BK) = \sqrt{\mu_g^2 + \frac{3m_{BK}\epsilon_0 hc}{2}} \tag{9.4}$$

where m_{BK} is obtained from the slope of a plot of the sum of the absorption and emission maxima $\tilde{\nu}_A(T) + \tilde{\nu}_E(T)$ *vs.* the SPF $F_{BK}(T)$:

$$\tilde{\nu}_A(T) + \tilde{\nu}_F(T) = -\frac{2(\mu_e^2 - \mu_g^2)}{3\epsilon_0 hc} \cdot F_{BK}(T) + const. \tag{9.5}$$

The solvent polarity function of Bilot and Kawski $F'_{BK}(T)$ is defined as:

$$F'_{BK}(T) =$$

$$\frac{1}{V(T)}\left(\frac{\left(\frac{\epsilon(T)-1}{2\epsilon(T)+1} - \frac{n(T)^2-1}{2n(T)^2+1}\right)}{\left(1-\frac{2\alpha n(T)^2-1}{\alpha^3 2n(T)^2+1}\right)^2\left(1-\frac{2\alpha\epsilon(T)-1}{\alpha^3 2\epsilon(T)+1}\right)} + 2\frac{\frac{n(T)^2-1}{2n(T)^2+1}\left(1-\frac{\alpha n(T)^2-1}{\alpha^3 2n(T)^2+1}\right)}{\left(1-\frac{2\alpha n(T)^2-1}{\alpha^3 2n(T)^2+1}\right)^2}\right) \tag{9.6}$$

Compared to the original LM Ansatz, BK additionally considered the influence of the polarizability α of the solute on the state energies. LM expanded the state energies in a series including the permanent dipole moment and the reaction field according to the first order Stark effect, while BK expanded the series up to the second term, including the static electron polarizability and the squared reaction field according to the second order Stark effect. If the static polarizability of the solvent in equation 9.6 is considered to be zero, equation 9.5 equals the original LM equation 9.2 using the solvent polarity

function 9.3. Although the polarizability α of the fluorophore is not known explicitly in many cases, a good approximation, which holds for many molecules has been given by Kawski for the ratio of polarizability and cube of the Onsager radius as $\frac{\alpha}{a^3} \approx 0,5$. This approximation yields the solvent polarity function, which is used in the following:

$$F_{BK}(T) = \frac{1}{V(T)}\left(\frac{2n(T)^2+1}{n(T)^2+2}\left(\frac{\epsilon(T)-1}{\epsilon(T)+1} - \frac{n(T)^2-1}{n(T)^2+2}\right) + \frac{3(n(T)^4-1)}{(n(T)^2+2)^2}\right) \tag{9.7}$$

For the determination of the cavity volume $V(T)$, the density of eleven solutions of each cyanoindole isomer in ethyl acetate with different mole fractions were measured. The molar cavity volumes V_m at the respective temperatures were determined from the slope of the plot of the inverse density of the solution *vs.* the mass fraction w of the solute, cf. equation 9.7

$$\frac{1}{\rho} = \frac{1}{\rho^*} + \left(\frac{V_m}{M_m} - \frac{1}{\rho^*}\right) \cdot w \tag{9.8}$$

with ρ as density of the solution, ρ^* as density of the solvent, V_m and M_m as molar volume and molar mass of the solute, and w as mass fraction of the solute in the solution. Figure 1 of the online supporting material shows the plot of the inverse density of the solution $\frac{1}{\rho}$ *vs.* the mass fraction w at 293,15 K, Figure 2 of the online supporting material shows the dependence of the individual cavity volumes from the temperature in the range between 267,15 and 343,15 K for the solution of 2-CI in EA. Using the so determined cavity volumes, the change of the dipole moments upon electronic excitation is determined from equations 9.1 according to Lippert-Mataga and the absolute excited state dipole moment from 9.5 according to Bilot-Kawski. Figure 9.4 presents the plots of $\tilde{\nu}_A(T) - \tilde{\nu}_E(T)$ *vs.* the SPF of Lippert and Mataga and of $\tilde{\nu}_A(T) + \tilde{\nu}_F(T)$ *vs.* the SPF of Bilot and Kawski. Obviously, the correlation in the BK plot is much better than for LM. The same holds true for the BK and LM plots of all other CI isomers, which are presented in the online supplementary material.

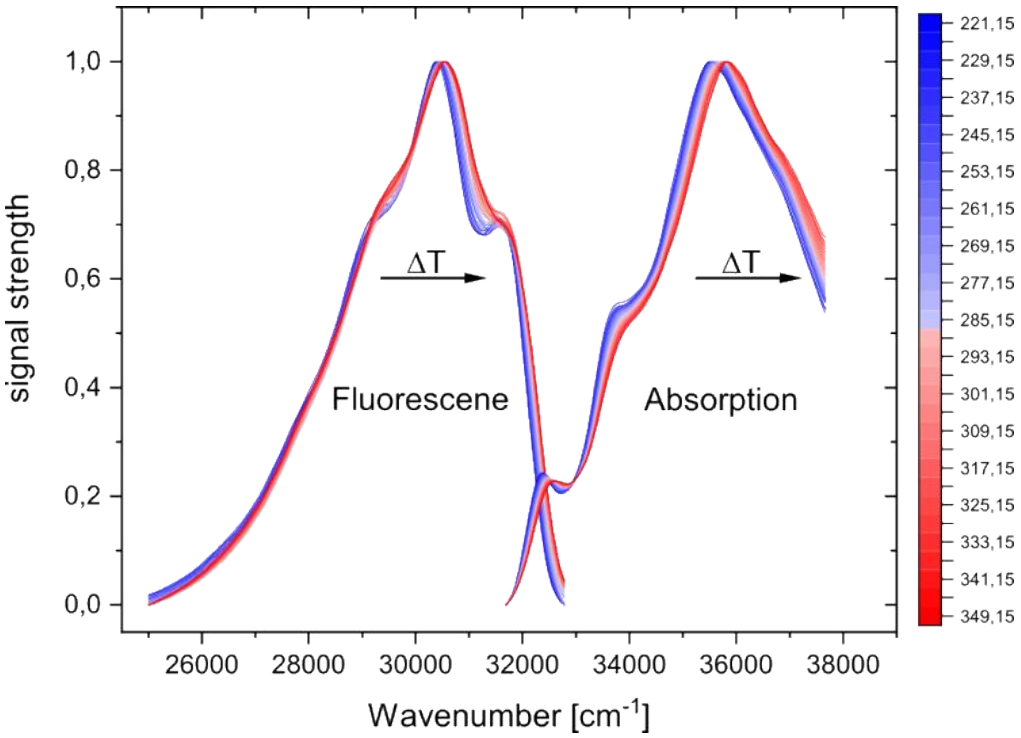

Figure 9.3.: Temperature dependent fluorescence and absorption measurements of 2-cyanoindole.

The changes of the dipole moments of all cyanoindoles in EA solution using the modified Lippert-Mataga equation $\Delta\mu^S(LM)$ and the excited state dipole from the Bilot-Kawski model $\mu^S(BK)(S_1)$ are summarized in Table 9.1, and are compared to those from rotationally resolved electronic Stark spectroscopy of the isolated, cold molecules [132], [129], [130], [143]. One has to keep in mind, that LM directly yields the change of the dipole moment upon electronic excitation $\Delta\mu$ without prior knowledge of the ground state dipole moment μ_g. The BK model however, yields the (absolute) excited state dipole moment μ_e assuming a known ground state dipole moment. This difference is due to the fact that the slope of a linear plot of the difference of the absorption and emission maxima $\tilde{\nu}_A(T) - \tilde{\nu}_E(T)$ *vs.* $F_{LM}(T)$ of LM is proportional to $(\mu_e - \mu_g)^2$ (cf. Figure 9.4 a), while plotting of the sum of absorption and emission maxima $\tilde{\nu}_A(T) + \tilde{\nu}_E(T)$ *vs.* $F_{BK}(T)$ of BK yields a straight line with a slope, which is proportional to $(\mu_e^2 - \mu_g^2)$ (Figure 9.4 c). As a test, we also plotted $F_{LM}(T)$ of LM *vs.* the sum of absorption and emission maxima $\tilde{\nu}_A(T) + \tilde{\nu}_E(T)$ (Figure 9.4 b). This plot even shows no linear dependence and is discarded in the following.

The ground state dipole moments, which are needed for the determination of the excited state dipole moment according to BK

$$\mu_e(BK) = \sqrt{\mu_g^2 + \frac{3m_{BK}\epsilon_0 hc}{2}} \tag{9.4}$$

are taken from the respective gas phase values, where applicable (2-,3-,4-,5-CI), and from *ab initio* calculations for 6-CI and 7-CI, cf. Table 9.1.

For comparison, the absolute values and the changes of the dipole moments from SCS-CC2/cc-pVTZ calculations of the isolated molecules $\Delta\mu^{calc}$ are given in Table 9.1 as well. Both ground and excited state dipole moments from Stark spectroscopy for 2-CI, 3-CI, 4-CI, and 5-CI are in general good agreement with the *ab initio* calculated values. Thus, we are confident, that the SCSCC2/cc-pVTZ calculated excited state dipole moments of 6-CI and 7-CI, the two positional isomers, for which the Stark measurements of the isolated species are still lacking, will be similarly accurate.

The absolute values for the excited state dipole moments in EA solution according to BK are in very good agreement with gas phase and *ab initio* values for the exception of 4-CI for which the experimental S_1 dipole moment in EA solution is by 0,93 D too low. According to the *ab initio* calculations (see next section), 4-CI is the isomer with the smallest energy gap between S_1 and S_2 state. The observed S_1-state is the L_a in this case. The small gap to the S_2 (L_b) state allows for considerable mixing of the two states in the strong reaction field of the solvent and mixes the (smaller) L_b dipole moment with that of the L_a. Recently, we have shown how state mixing between S_1 and S_2 state in 2,3-benzofuran can be induced by the reaction field of the solvent [280]. In benzimidazole we encountered the situation that the lower state with small dipole moment 'steals' dipole moment from the upper state, which has the larger dipole moment. In 4-CI the situation is reversed, since here the S_1 has the larger dipole moment, explaining part of the discrepancy. However, it has to be mentioned that also the gas phase dipole moment of 4-CI from electronic Stark measurement is by 0,5 D smaller than the calculated one. Since the electric field strength of the Stark field amounts only to 400 Vcm ($4 \cdot 10^4$ V/m), electronic mixing should be weak compared to the reaction field of the solvent cage in the solution, which is in the order of $10^9 - 10^{10}$ V/m [280].

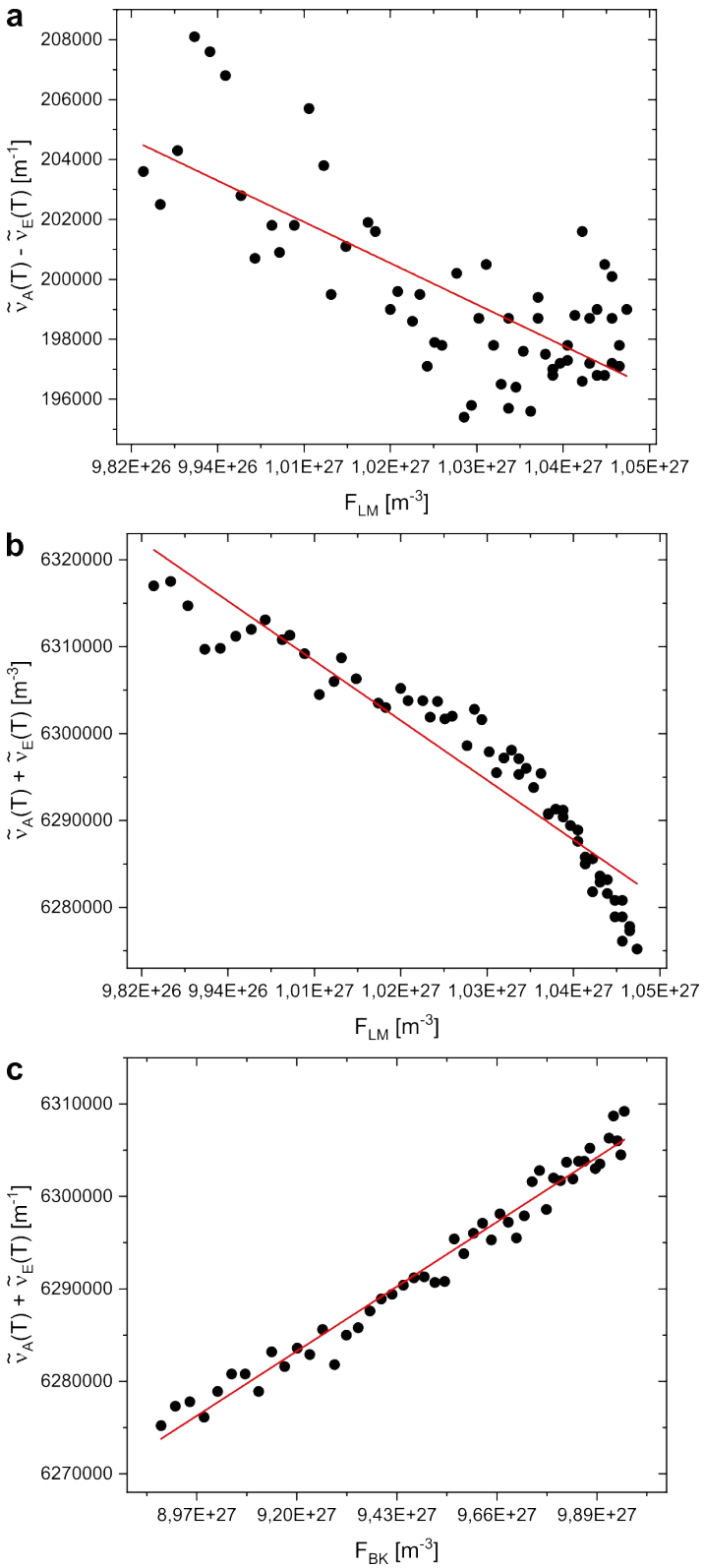

Figure 9.4.: Plots of $\tilde{\nu}_A(T) - \tilde{\nu}_E(T)$ *vs.* the SPF of Lippert and Mataga **(a)**, of $\tilde{\nu}_A(T) + \tilde{\nu}_F(T)$ *vs.* the SPF of vs. Lippert and Mataga **(b)**, and vs. the SPF of Bilot and Kawski **(c)** for 2-CI dissolved in EA.

Quantum Chemical Calculations

The relative stability of the six isomeric cyanoindoles, calculated at the SCS-CC2/cc-pVTZ level of theory is shown in Figure 9.5, along with the adiabatic excitation energies (including zero-point energy at the level of theory used for optimization) to the lowest excited singlet states. The most stable conformer is 3-CI, followed by 7-CI, which is only 40 cm^{-1} less stable than the former one. Relative to the most stable 3-CI conformer, the remaining cyanoindoles are by 157 (4-CI), 268 (5-CI), 309 (6-CI), and 887 cm^{-1} (2-CI) less stable.

The calculated ground state dipole moments of the isolated n-CIs differ by more than a factor of 2. The smallest ground state dipole moment is calculated for 7-CI (3.40 D), the largest for 5-CI (7.08 D). The four n-CIs for which Stark measurement in the gas phase are available, show a very close agreement between experiment and theory, cf. Table 9.1. We assume that this is also the case for 6-CI and 7-CI, for which we still do not have the experimental Stark results.

In the electronic ground state, the dipole moments can be rationalized by vector addition of the indole chromophore dipole vector and the dipole of the cyano group. Figure 9.6 shows the calculated ground state dipole moment vector of the individual n-CIs (red straight arrow), the ground state dipole vector of the indole chromophore (blue dashed arrow), which is shifted with its tail to the tail of the n-CI vector and the result of the vector subtraction (green bold vector). The resulting vector points in each case in the direction of the cyano group, independent of the substitution position. This is surprising, since the dipole moment of the cyano group is large and the indole moiety is easily polarizable. This should lead to an induced dipole moment in the indole moiety of the CNs, which then should spoil the dipole additivity. An example for this, is the large dipole of the water moiety in the hydrogen bonded phenol (H_2O) cluster, which induces an additional dipole moment in the indole chromophore [296].

The utilization of LM and BK theory requires the dipole moments in ground and excited state to have the same orientation. Figure 9.7 shows all S_0 and S_1 dipole moment orientations from the SCSCC2 calculations. With the exception of 4-CI all excited state dipoles are aligned along the respective ground state moments. For the electronically excited singlet states, we have to distinguish between the L_a and the L_b labelled states. For 2-CI the lower state is calculated to be the L_b-state with a dipole moment of 4,95 D in fair

Table 9.1.: Electronic nature of the lowest excited singlet state in the isolated n-CI, ground state ($\mu^S(S_0)$) and excited state ($\mu^S(S_1)$) dipole moments in ethyl acetate solution, ground state ($\mu^G(S_0)$) and excited state ($\mu^G(S_1)$) dipole moments in the gas phase, and SCS-CC2/cc-pVTZ calculated dipole moments of the ground state ($\mu^{calc}(S_0)$) and excited state ($\mu^{calc}(S_1)$). The changes of dipole moments are defined as $\Delta\mu = \mu(S_1) - \mu(S_0)$. All dipole moments are given in units of Debye D. Uncertainties of the last digit is given in parentheses.
[a] From Ref. [132]. [b] From Ref. [129]. [c] From Ref. [130]. [d] From Ref. [290]. [e] $\Delta\mu^S$ (BK) calculated from the difference of the BK excited state dipole moment μ^S (BK) (S_1) to *ab initio* calculated ground state dipole moment μ^{calc} (S_0).

	2-CI	3-CI	4-CI	5-CI	6-CI	7-CI
S_1 nature	L_b	L_b	L_a	L_a/L_b	L_b	L_b
μ^G (S_0)	3,71(1)[a]	5,90(1)[b]	6,31(1)[c]	7,14(4)[d]	-	-
μ^{calc} (S_0)	3,56	5,89	6,39	7,08	5,98	3,40
μ^G (S_1)	5,21(1)[a]	5,35(1)[b]	8,92(1)[c]	8,17(3)[d]	-	-
μ^S (BK) (S_1)	4,57(3)	5,20(4)	7,99(14)	8,29(5)	7,15(4)	4,46(19)
μ^{calc} (S_1)	4,95	5,39	9,42	7,63	7,20	4,74
$\Delta\mu^S$ (LM)	+1,57(14)	+2,23(10)	+4,5(18)	+5,14(12)	+3,97(9)	+5,04(26)
$\Delta\mu^S$ (BK)[e]	+1,01(3)	-0,69(4)	+1,60(14)	+1,15(5)	+1,17(4)	+1,06(14)
$\Delta\mu^G$	+1,50(2)[a]	-0,55(2)[b]	+2,61(2)[c]	+1,03(7)[d]	-	-
$\Delta\mu^{calc}$	+1,39	-0,50	+3,03	+0,55	+1,22	+1,34

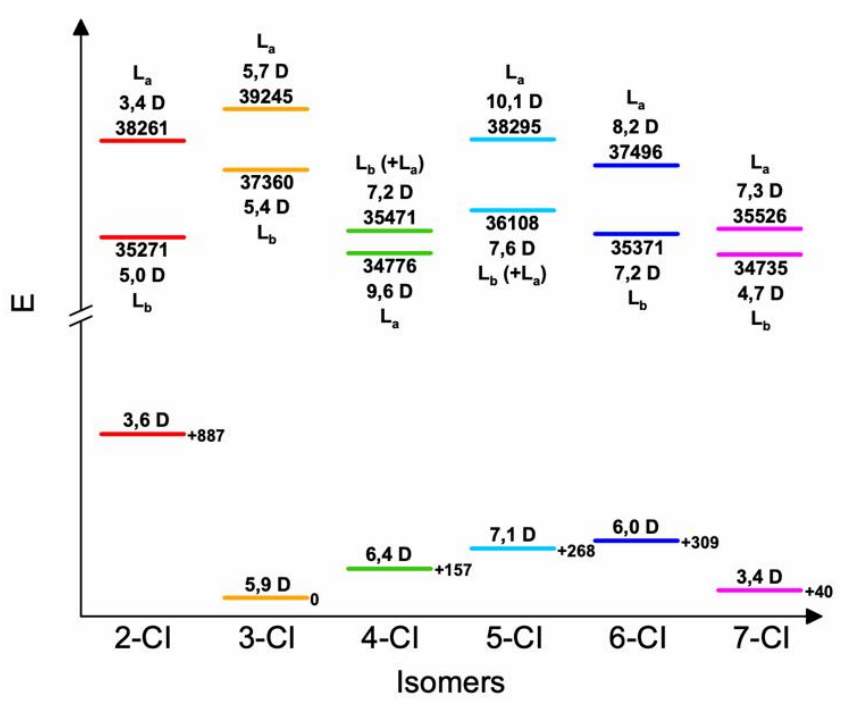

Figure 9.5.: *Ab initio* (SCS-CC2/cc-pVTZ) calculated ground state energies (in wavenumber units, relative to the most stable 3-cyanoindole), adiabatic excitation for excitation to the lowest two excited singlet states energies (in wavenumber units), their respective dipole moments (in Debye D) and the electronic nature (L_a or L_b) of the respective excited state.

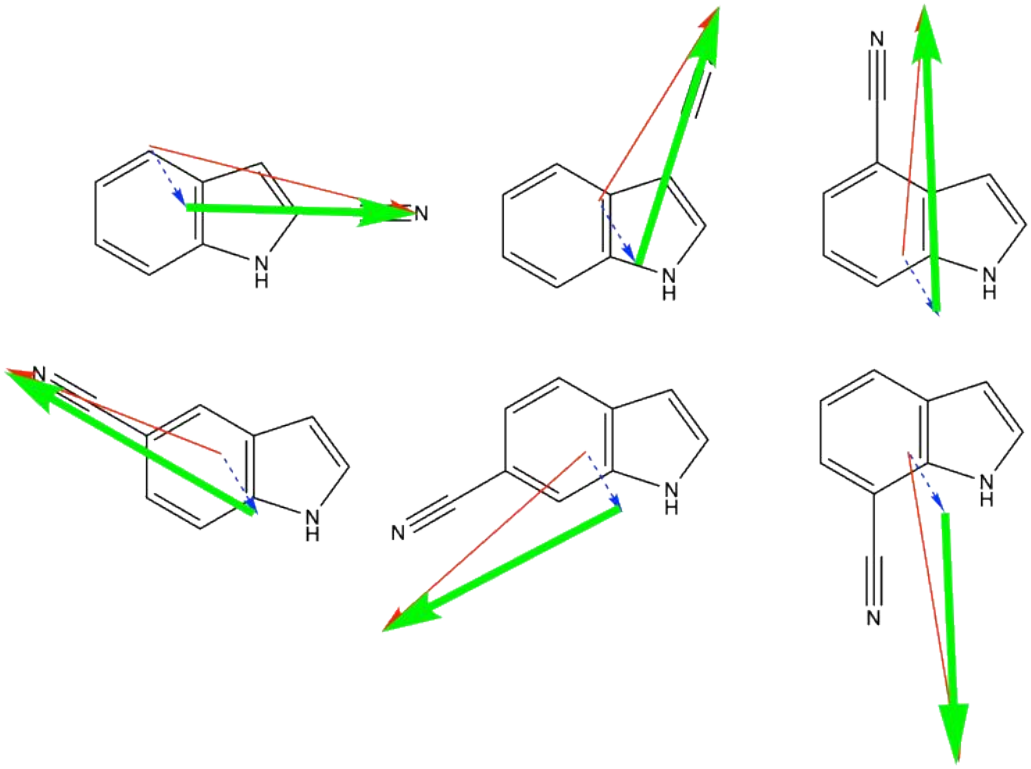

Figure 9.6.: Vector subtraction of the calculated ground state dipole of the individual n-CIs (red straight arrow), the ground state dipole vector of the indole chromophore (blue dashed arrow) and the resulting difference vector (green bold vector), which represents the dipole of the cyano group. The dipole moment vectors have been drawn in the chemical convention from positive to negative partial charge.

agreement with the experimental value from gas phase Stark measurements 5,21 D.

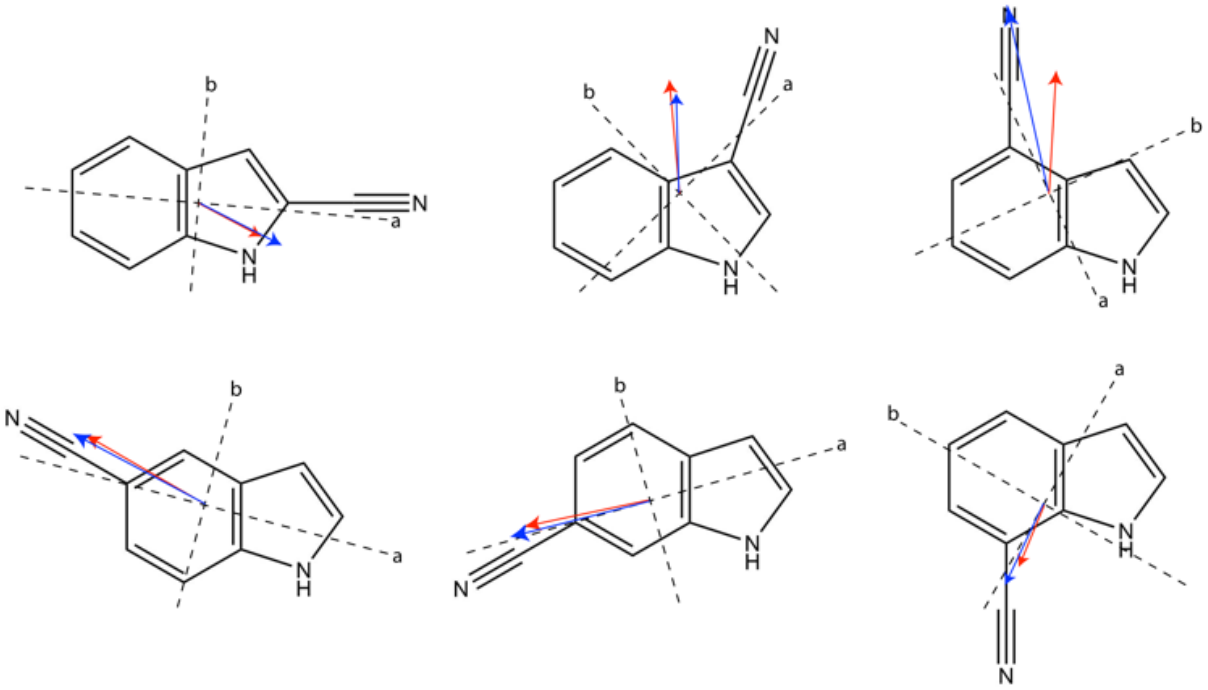

Figure 9.7.: Ground and excited state dipole moments from the SCS-CC2/cc-pVTZ calculations, along with the inertial axes a and b. The dipole moment vectors have been drawn in the chemical convention from positive to negative partial charge.

The adiabatic excitation energy to the lowest excited singlet state of 2-CI has been calculated to be 35271 cm^{-1}. Since the transition is mostly composed of LUMO $\leftarrow$ HOMO-1 and LUMO + 1 $\leftarrow$ HOMO, the resulting excited state can be classified as L_b-state. This was also confirmed by an analysis of the orientation of the transition dipole moment [132], which is in line with an assignment as L_b-state. The following state, calculated to be 2990 cm^{-1} higher as the L_b-state can be classified to be of L_a-character. This is the largest L_a-L_b gap in the series of the cyanoindoles. The calculated dipole moment of the lower excited state is larger than that of the upper state. This is surprising, since the L_a-state in indole and substituted indoles is considered to have a larger dipole moment than the L_b-state.

The energy gap between the excited singlet states of 3-CI is substantially smaller (1885 cm^{-1}) however, with the same energetic ordering of the excited states as for 2-CI. The dipole moments for the S_0 (5,9 D), the L_b (5,4 D) and the upper excited L_a-state (5,7 D)

are nearly the same.

4-CI has the smallest energy gap between L_a- and L_b-state (695 cm^{-1}), and, unlike as for 2-CI and 3-CI, the L_a is the lowest excited (S_1) state. However, the upper (S_2) state shows considerable mixing with the L_a-state. For 4-CI, the dipole moment of the (lower) L_a-state (9,6 D) is considerably larger than that of the L_b-state (7,2 D). The deviation of the excited state dipole orientation from that of the ground state is due to the fact, that the S_1-state is the L_a-state in 4-CI, with a strongly altered electron distribution.

For 5-CI an energy gap of 2187 cm^{-1} is calculated with the lower state being of mixed L_a/L_b character with a dipole moment of 7,6 D, and the upper state a pure L_a-state with a dipole moment of 10,1 D. The energy difference of the lower L_b-state (μ = 7,2 D) and the upper L_a-state (μ = 8,2 D) of 6-CI amounts to 2125 cm^{-1}.

6-CI has an S_1/S_2 energy gap of 2125 cm^{-1}, with the lower excited state being the L_b with a dipole moment of 7,2 D and the upper excited state the L_a with a dipole moment of 8,2 D.

7-CI shows a similarly small energy difference as 4-CI of 791 cm^{-1}. The lower L_b-state has a dipole moment of 4,7 D, the higher lying L_a-state of 7,3 D. Figure 9.5 summarizes for all isomers, the ground state energies (relative to the energy of the most stable isomer, 3-CI), the excitation energies to the lowest two excited singlet states and the dipole moments of all states involved.

9.4. Conclusions

Employment of the Lippert-Mataga equation using solvatochromic shifts has been criticized as to the different solute-solvent interactions, which tend to impede a straightforward dipole moment determination of excited states. While the use of thermochromic shifts avoids these pitfalls, the inherent weakness of the LM treatment is the neglect of solvent polarization. Therefore, LM theory employing thermochromic shifts of the absorption and fluorescence maxima, leads to values of the excited state dipole moment of all investigated cyanoindoles, which are neither in agreement with the results of *ab initio* calculations on the isolated molecule nor with experimental values from electronic Stark spectroscopy in the gas phase. However, dipole moments from BK theory closely match the experimental gas phase and theoretical values, cf. Figure 9.8.

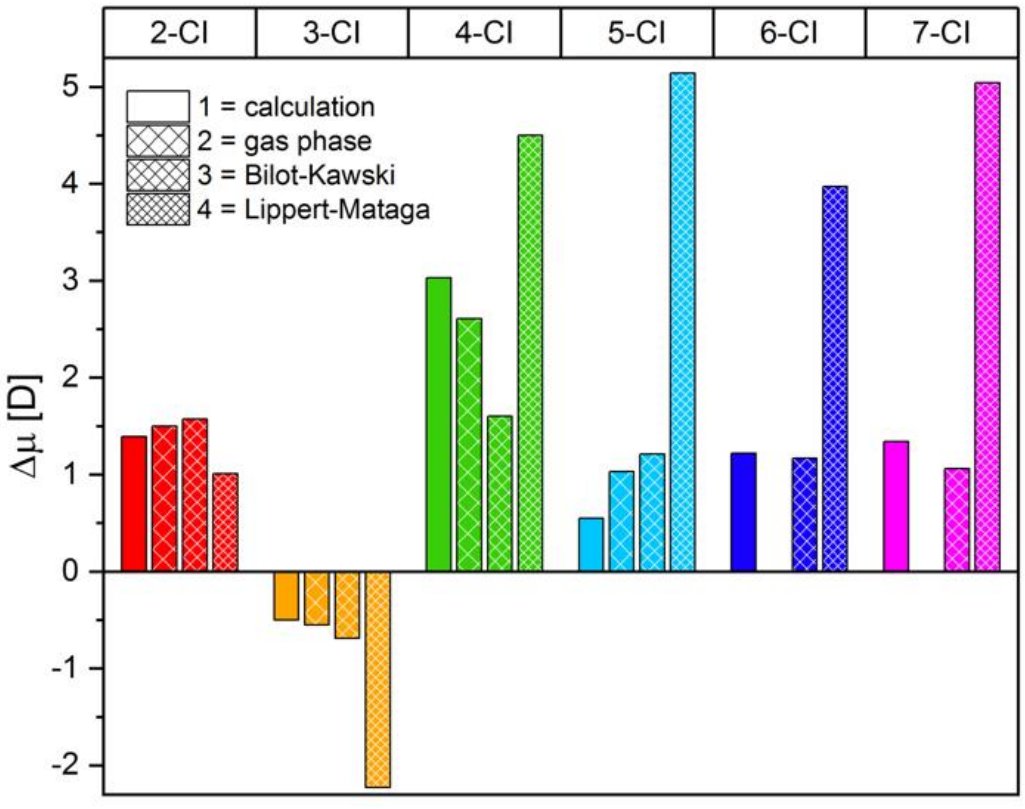

Figure 9.8.: Comparison of the change of dipole moment upon electronic excitation to the lowest excited singlet state from *ab initio* (SCS-CC2/cc-pVTZ) calculations, gas phase Stark spectroscopy, thermochromic shifts using the Bilot-Kawski and Lippert-Mataga formalism for all six cyanoindoles.

Modifications to the original Lippert-Mataga theory, which have been introduced by Bilot and Kawski, yield much more precise values for the absolute dipole moment in the lowest excited singlet states of the isomeric n-cyanoindoles and are in good agreement with the *ab initio* calculated excited state dipoles and (where available) also with the experimental ones from electronic Stark spectroscopy of the isolated molecules.

The later fact seems odd at first sight. LM and BK theories are used in order to determine the excited state dipole moments in solution, while we compare these dipoles to those of the isolated molecule. In order to compute dipole moments in solution, the conductor-like screening model (COSMO) [164] was used. Since COSMO for RI-CC2 calculations of the excited states is not yet implemented, we switched the dipole moment computations to (RI-)ADC(2) for the excited states and to (RI-)MP2 for the ground state.

At first, we compared the dipole moments from the respective CC2 calculations to those from MP2 (S_0) and ADC(2) (S_1 and S_2) for the isolated molecules. This comparison is shown in Table 9.2. The very close agreement between MP2 and CC2 for the ground state and ADC(2) and CC2 for the excited state shows, that the values from ADC(2) can indeed be used for the calculation of the excited state dipole moments in the COSMO model. We subsequently performed these COSMO calculations using an index of refraction $n = 1{,}3723$ and a permittivity $\epsilon = 6{,}080$ for EA and compared the theoretical to the experimental and to the *ab initio* calculated dipole moments of the isolated molecules.

Table 9.2.: Experimentally determined dipole moments from Stark spectroscopy of the isolated n-CIs in the ground (S_0) and excited states (S_1). MP2, CC2, ADC(2) calculations are performed with the cc-pVTZ basis set. COSMO calculations with $n = 1{,}3723$ and $\epsilon = 6{,}080$ are performed using MP2 for the ground state and ADC(2) for the excited state. All dipole moments are given in units of Debye D.

	2-CI	3-CI	4-CI	5-CI	6-CI	7-CI
Exp. (S_0)	3,71(1)	5,90(1)	6,31(1)	7,14(4)	-	-
CC2 (S_0)	3,56	5,89	6,39	7,08	5,98	3,40
MP2 (S_0)	3,53	5,87	6,36	7,06	5,93	3,37
COSMO (S_0)	4,24	7,49	8,06	8,87	7,38	4,12
Exp. (S_1)	5,21(1)	5,35(1)	8,92(1)	8,17(3)	-	-
CC2 (S_1)	4,95	5,39	9,42	7,63	7,20	4,74
ADC(2) (S_1)	5,04	5,43	9,46	7,73	7,26	4,75
COSMO (S_1)	6,80	6,83	12,59	13,88	13,43	6,43
μ^S (BK) (S_1)	4,57(3)	5,20(4)	7,99(14)	8,29(5)	7,15(4)	4,46(19)
μ^S (BK)^e	+1,01(3)	-0,69(4)	+1,60(14)	+1,15(5)	+1,17(4)	+1,06(14)
Exp. $\Delta\mu$	+1,50(2)	-0,55(2)	+2,61(2)	+1,03(7)	-	-
CC2 $\Delta\mu$	+1,39	-0,50	+3,03	+0,55	+1,22	+1,34
COSMO $\Delta\mu$	+2,56	-0,66	+4,53	+5,01	+6,05	+2,31

It is obvious that there is a close agreement between the excited state dipole moments of the isolated n-CIs form Stark spectroscopy and from *ab initio* theory but a rather large discrepancy to the values of the COSMO calculations.

This deviation can be expected, since the solvent polarity functions, defined by Lippert-Mataga and Bilot-Kawski, establish a correlation between the solvent shifts of fluorescence or absorption transitions and the dipole moment of the **unpolarized** molecule. Hence, the so determined dipole moments will resemble more the results from *ab initio* calculations of the isolated species than of that of solvation models, which return the values of the **polarized** molecule.
To have a closer look into the discrepancies of the LM SPF, we computed the (vertical) absorption and emission energies with COSMO (ADC(2)/cc-pVTZ), using the temperature dependent permittivities and indices of refraction. Then the resulting SPF of LM and BK were plotted *vs.* the difference and the sum of the absorption and emission maxima. The results are shown in Figure 9.9. It is obvious that the plot according to LM does not even result in a straight. BK however shows a nearly linear dependence. The excited state dipole moment determined from the slope of the synthetic BK plot amounts to 4,19 D, close to the experimental BK value of 4,57 D.
Although criticism of the determination of excited state dipoles on the basis of solvatochromic (and thermochromic) shifts has been expressed early by Lombardi [297], the number of studies, which compare excited state dipole moments from thermochromic or solvatochromic shifts to those from other methods, is quite limited.

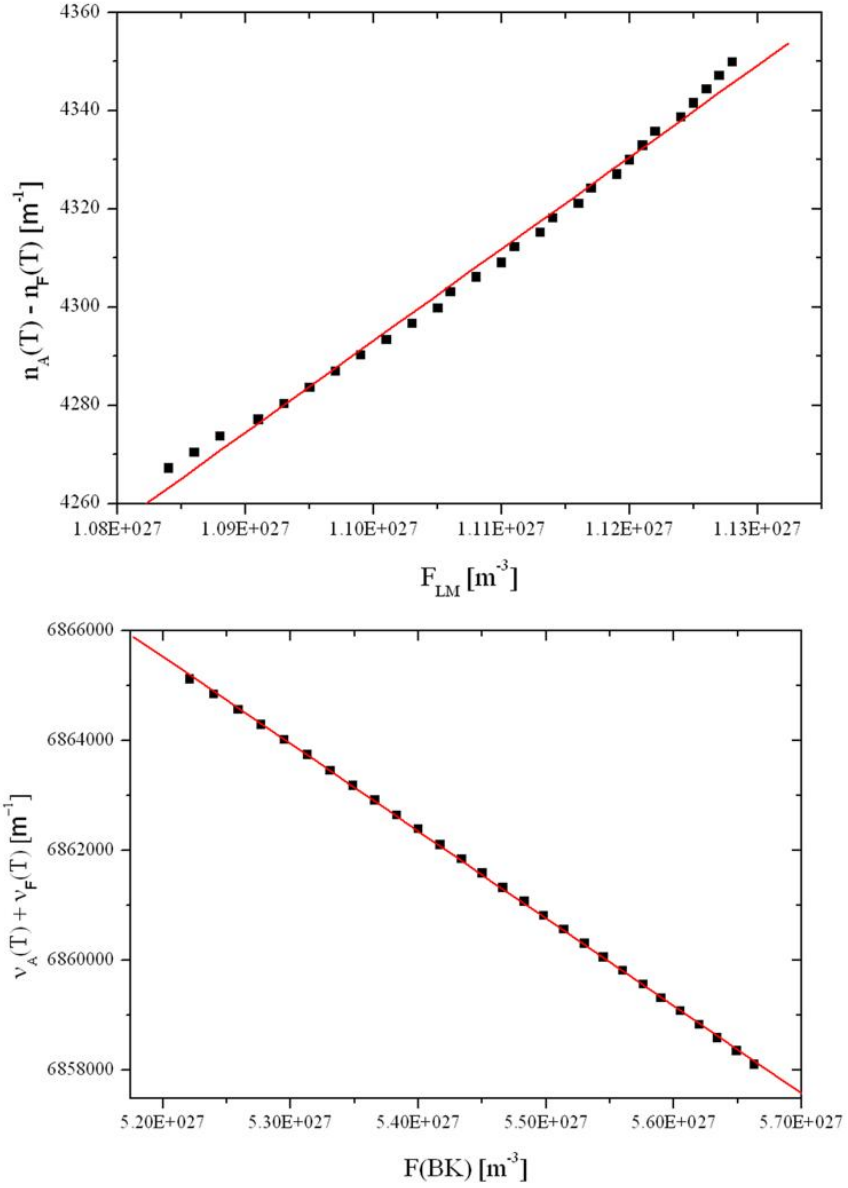

Figure 9.9.: *Ab initio* CC2/cc-pVTZ calculated difference and sum of absorption and fluorescence emission maxima plotted vs. the SPF of LM and BK.

From the current study we infer, that the Bilot-Kawski method for determination of excited state dipole moments gives reliable values, in cases in which the lowest excited states are not too close, and their dipole moments do not differ much. Otherwise, the strong electric field from the solvent cavity leads to an effective electronic mixing of the excited states and thus influences the value of the dipole moment under consideration. 7-CI seems

to be an exception, which will be investigated by gas-phase Stark spectroscopy in the near future in our group. The much more frequently used Lippert-Mataga method suffers from various deficiencies, the most serious one is the neglect of solvent polarity effects. It therefore fails to reproduce the excited state dipole moments from rotationally resolved electronic Stark spectra. Most investigations on electric dipole moment changes upon electronic excitation, compare results from different solvation models like Lippert-Mataga, Bilot-Kawski, Bakhshiev [298], Kawski-Chamma-Viallet [136], [45], and Reichardt [299]. However, a critical assessment of the reliability of the model chosen, can only be given by comparison to dipole determination using rovibronically line resolved spectroscopic Stark techniques.

9.5. Acknowledgements

Financial support of the Deutsche Forschungsgemeinschaft (SCHM1043/16-1) is gratefully acknowledged.

9.6. Credit author statement

Matthias Zajonz: Methodology, data acquisition, evaluation, writing. Marie-Luise Hebestreit: Reviewing, writing. Peter Gilch: Reviewing. Christof Hättig: ab initio calculations. Michael Schmitt: Supervision, conceptualization, ab initio calculations, writing, reviewing and editing.

9.7. Own Share

The content of this chapter will be published in the Angewandte Chemie International Edition under the title *Lippert-Mataga treatment Fails in Predicting Excited State Dipole Moments in n-Cyanoindoles (n = 2,3,4,5,6)* written by Matthias Zajonz, Marie-Luise Hebestreit, Peter Gilch, Christof Hättig and Michael Schmitt.

My own share of this publication is about 70% and consists of writing - original draft, data acquisition, evaluation, software, methodology, investigation, formal analysis.

10. Publication on n-Methylindoles

Excited State Dipole Moments of n-Methylindoles from Thermochromic Shifts.[†] To be submitted.

Matthias Zajonz[a], Marie-Luise Hebestreit[a], Michael Schmitt[a*]

[a]Heinrich-Heine-Universität, Institut für Physikalische Chemie I,
Arbeitsgruppe für Hochauflösende Spektroskopie,
D-40225 Düsseldorf, Germany, E-mail:mschmitt@hhu.de

10.1. Abstract

The excited state dipole moments of six positional isomers of methylindole have been determined from thermochromic shifts of the absorption and fluorescence emission spectra in ethylacetate solution and compared to the results of *ab initio* calculations.

10.2. Introduction

Electronically excited states of substituted indoles have been the focus of spectroscopic and theoretical investigations for decades. Solvatochromic studies of the dipole moments have been performed in order to examine the excited state dipoles of the two lowest excited singlet states that are designated as L_a and L_b [300], [301], [302], [303]. We use the L_a/L_b nomenclature, which follows the convention for cata-condensed hydrocarbons given by Platt [257] and was later modified by Weber to cover the case of indole, which actually lacks the necessary symmetry [281], and is in a physical sense meaningless. However, since it is used frequently, we will follow this convention in the context of this work. The barrier to internal rotation in the electronic ground state of seven methylindoles (1-MI to 7-MI) has been studied using internal rotation and ^{14}N nuclear quadrupole coupling [304]. Rotationally resolved electronic spectra of the electronic origin bands of 1-, 3-

and 5-methylindole have been investigated in the groups of Pratt [305] and Meerts [306]. The dipole moment of 3-MI in its L_a-state has been determined by Stark absorption spectroscopy of 3-MI doped into a polymethylmethacrylate film [307]. Hebestreit *et al.* determined the dipole moment of 6-MI in the ground and lowest excited singlet state (L_b) from rotationally resolved Stark spectroscopy in a molecular beam [308]. The He (I) photoelectron spectra of 1-, 2-, 3-, 4- and 6-MI have been reported by Güsten *et al.* [309]. Lin *et al.* studied the methyl substitution effect of 3-MI and 5-MI cations using mass analyzed threshold ionization spectroscopy [310]. Polarized two-photon fluorescence excitation spectra of 3-MI and 5-MI in cyclohexane and butanol solutions have indicated the onset of L_a absorption [311].

10.3. Computational Methods

10.3.1. Quantum chemical calculations

Structure optimizations were performed employing a Dunning's correlation-consistent polarized valence triple zeta (cc-pVTZ) basis set from the TURBOMOLE library [158], [254]. The equilibrium geometries of the electronic ground and the lowest excited singlet states were optimized using the approximate coupled cluster singles and doubles model (CC2) employing the resolution-of-the-identity (RI) approximation [170], [160], [161]. For the structure optimizations spin-component scaling (SCS) modifications to CC2 were taken into account [162]. Vibrational frequencies and zero-point corrections to the adiabatic excitation energies were obtained from numerical second derivatives using the NumForce script [163].

10.4. Experimental Methods

To determine the cavity volume of the methylindoles dissolved in ethyl acetate a high-precision density meter from Anton Paar (model: DMA 4500) was used for the density measurements. For this purpose, a concentration series was prepared for each constitutional isomer of the methylindole and measured in a temperature range from 265.15 to 343.15 K with an increment of 2 K. The spectroscopic measurements were carried out in a self-constructed cell using two spectrometers from Varian. A Varian Cary 50 Scan UV-Visible was used for absorption measurements and a Cary Eclipse Fluorescence for emission measurements. The measurements were made on a scale of 225.15 K to 343.15 K with an increment of 2 K. For the determination of the refractive indices of the solvent, a

refractometer from Anton Paar (model: Abbemat MW) was used, whereby measurements were made on a temperature scale from 283.15 K to 343.15 K with an increment of 1 K. At each temperature refractive indices were determined at 5 different wavelengths.

10.5. Results and Discussion

Prior to a comparison of the experimental values with the quantum chemical calculations that will be presented later, it is necessary to make four preliminary comments.

(i) Despite the fact that the method for determination of the dipole moments in the ground state, from absorption and emission maxima shifts as proposed by Demissie, has previously been identified as having limited accuracy, the experimental values for the dipole moments in the ground state were also calculated using this method, for comparison.

(ii) Second, the behavior of the cavity volume of the dissolved methylindoles in response to temperature fluctuations and the temperature-plotted curves of the maxima exhibit some anomalous characteristics. An attempt was made to address the anomalies in the cavity volumes, employing a nonlinear fit, in contrast to the conventional linear fit, to determine the cavity volumes.

(iii) A comparison of the dipole moments of the ground state, calculated according to the method proposed by Demissie, with the values obtained from the quantum chemical calculations reveals that the experimental values derived from this calculation method, when considered along with the quantum chemical calculations and values, are more accurately described as a fortuitous conjecture than as a meaningful calculation method.

(iv) Comparison of the experimental values for the dipole moments in the excited state with values from quantum chemical calculations demonstrates the superiority of the Bilot and Kawski methodology over other calculation methods. These findings corroborate those of previous publications.

Furthermore, the calculation method proposed by Lippert and Mataga is inherently limited in its ability to accurately assess the difference between the ground and excited states. This is particularly evident in cases where the calculated difference is extremely small or even negative, as observed in this study. This is because the calculated values from this method often overestimate the dipole moment, which is in contrast to the findings of

earlier publications from the research group.

It should also be noted that the absorption and emission maxima at 293.15 K of the constitutional isomers of methylindoles with 3-MeI < 2-MeI < 6-MeI < 5-MeI < 4-MeI < 7-MeI follow the inverse order of the absorption and emission maxima of cyanoindoles. This aspect is of interest because the two substituent groups, i.e. the cyano group and the methyl group, exert opposing effects on the electron density distribution within the molecule. The cyano group introduces a negative charge, whereas the methyl group introduces a positive charge. These effects are observed for the same basic building block.

10.5.1. Computational Results

Table 10.1.: SCS-CC2/cc-pVTZ calculated rotational constants, dipole moments and methyl torsional barriers of 2- to 7-methylindole in the ground (doubly primed) and excited state (singly primed).

	2-MI	3-MI	4-MI	5-MI	6-MI	7-MI
A''/MHz	3790	2604	2162	3417	3559	2139
B''/MHz	989	1266	1484	1030	1041	1514
C''/MHz	788	856	885	790	802	891
μ''_a/D	2.06	-1.78	1.94	-0.06	0.63	-0.10
μ''_b/D	-1.17	1.04	-0.48	-1.95	1.92	2.32
μ''_c/D	0.01	0.00	-0.01	-0.08	0.02	0.02
μ''/D	2.53	2.06	2.00	1.95	2.02	2.32
A'/MHz	3645	2564	2092	3317	3311	2093
B'/MHz	978	1245	1467	1033	1027	1484
C'/MHz	775	842	867	799	788	873
μ'_a/D	2.36	-1.99	1.50	-0.25	0.35	0.01
μ'_b/D	-0.94	0.64	-1.01	-1.49	2.00	1.99
μ'_c/D	0.01	0.00	0.00	-0.60	0.03	0.02
μ'/D	2.54	2.09	1.81	1.63	2.04	1.99
ΔA/MHz	-145	-40	-70	-100	-248	-100
ΔB/MHz	-9	-2	-17	+3	-14	-30
ΔC/MHz	-13	-14	-18	+9	-14	-18
$\Delta\mu_a$/D	0.09	-0.20	-0.43	-0.19	-0.28	0.11
$\Delta\mu_b$/D	0.23	-0.40	-0.53	0.45	0.09	-0.33
$\Delta\mu_c$/D	0.00	0.00	0.00	0.00	0.00	0.00
$\Delta\mu$/D	0.02	-0.02	-0.19	-0.32	0.01	0.33

In the following an overview of the maxima of the absorption and emission measurements of the six methylindoles in ethyl acetate at 293.15 K is given. Depending on the position

Table 10.2.: SCS-CC2/cc-pVTZ computed vertical excitation energies and oscillator strengths, of 2- to 7-MI.

	2-MI		3-MI		4-MI		5-MI		6-MI		7-MI	
	ν_{fi}	f	ν_{fi}	f	ν_{fi}	f	ν_{fi}	f	ν_{fi}	f	ν_{fi}	f
$\pi\pi^*$ (L_b)	352802		35580		35804		35097		35630		35290	

of the methyl group the following order with increasing wavenumber results for absorption: 3-MeI < 2-MeI < 6-MeI < 5-MeI < 4-MeI < 7-MeI, whereby this order is also found for emission.

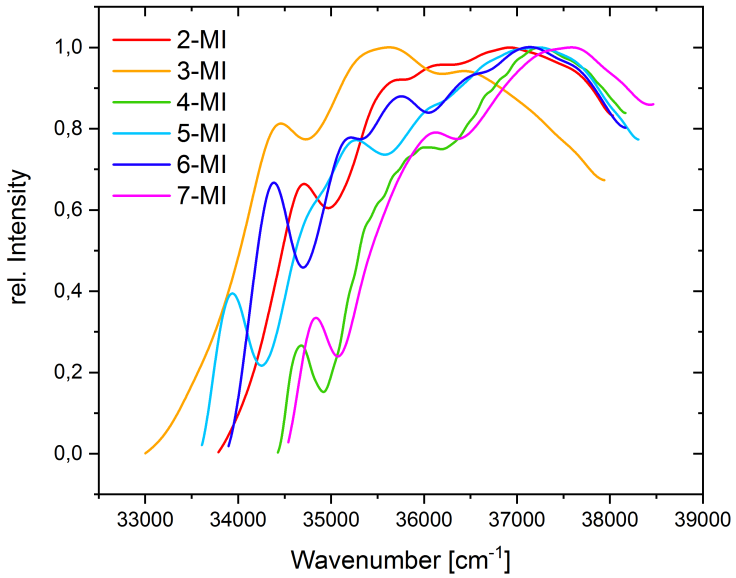

Figure 10.1.: Normalized absorption spectra of the six different isomers of methylindole in ethyl acetate solution.

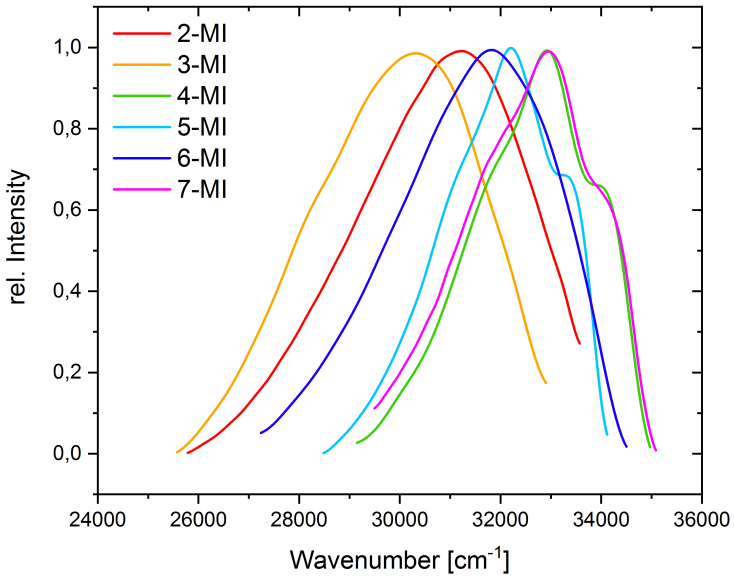

Figure 10.2.: Normalized fluorescence emission spectra of the six different isomers of methylindole in ethyl acetate solution.

This sequence of absorption and emission maxima was also found in an earlier study carried out by our group, where the individual positions on the indole ring were occupied by a cyano group instead of a methyl group. The determination of the dipole moments of the methylindole isomers dissolved in ethyl acetate was carried out via thermochromic shifts of the absorption and emission spectra. For this purpose, the known equations of Lippert and Mataga [39], Bilot and Kawski [154], [43] are used. However, the original equations were adapted accordingly so that the cavity volume was used instead of the Onsager radius and the refractive index used was also adapted. The adjustment of the refractive indices used was necessary because the original equations always use the refractive index of the Sodium-D-line, n_D = 589.3 nm, but the investigated isomers of methylindole absorb as well as emit in a range of approximately 265 - 350 nm. To address this issue, the data from the wavelength- and temperature-dependent measurements of the refractive indices were plotted in a 3D diagram and the equations for determining the dipole moment were adjusted. The plot in the 3D diagram was based on the Sellmeier equation [88].

Lippert-Mataga:

$$\tilde{\nu}_A(T) - \tilde{\nu}_E(T) = \frac{2(\mu_e - \mu_g)^2}{3\varepsilon_0 hc} \cdot F_{LM}(T,\lambda) + const.$$

$$F_{LM}(T,\lambda) = \frac{1}{V(T)}\left[\frac{\varepsilon(T)-1}{2\varepsilon(T)+1} - \frac{1}{2}\left(\frac{n(T,\lambda)^2-1}{2n(T,\lambda)^2+1}\right)\right] \tag{10.1}$$

$$\Delta\mu(LM) = \mu_e - \mu_g = \sqrt{\frac{3m_{LM}\varepsilon_0 hc}{2}}$$

where $\tilde{\nu}_{A/E}$ describes the maxima of adsorption or emission, $\mu_{e/g}$ the dipole moment in the ground state or in the electronically excited state, V describes the cavity volume, ε the permittivity, n is the refractive index, F_{LM} is the solvent polarity function of the corresponding equation and m_{LM} is the slope of the respective plot of the difference of the maxima against the corresponding solvent polarity function.

Demissie:

$$\tilde{\nu}_{A/E}(T) = \tilde{\nu}^0_{A/E} - \frac{2\mu_{g/e}(\mu_e - \mu_g)}{3\varepsilon_0 hc} \cdot F_i(T,\lambda)$$

$$F_{LM}(T,\lambda) = \frac{1}{V(T)}\left[\frac{\varepsilon(T)-1}{2\varepsilon(T)+1} - \frac{1}{2}\frac{n^2(T,\lambda)-1}{2n^2(T,\lambda)+1}\right]$$

$$F_{BK}(T,\lambda) = \frac{1}{V(T)}\left[\frac{2n^2(T,\lambda)+1}{n^2(T,\lambda)+2}\left(\frac{\varepsilon(T)-1}{\varepsilon(T)+2} - \frac{n^2(T,\lambda)-1}{n^2(T,\lambda)+2}\right)\right. \tag{10.2}$$

$$\left. + \frac{3(n^4(T,\lambda)-1)}{(n^2(t,\lambda)+2)^2}\right]$$

$$\mu_{g/e} = \sqrt{\frac{3\varepsilon_0 hc \cdot m^2_{A/E}}{2(m_E - m_A)}}$$

where $\tilde{\nu}_{A/E}$ describes the maxima of adsorption or emission, $\mu_{e/g}$ the dipole moment in the ground state or in the electronically excited state, V describes the cavity volume, ε the permittivity, n is the refractive index, F_i is the solvent polarity function of the corresponding equation whereby the solvent polarity function can accord to Lippert-Mataga or Bilot-Kawski and $m_{A/E}$ is the slope of the respective plot of the maxima from absorption or emission against the corresponding solvent polarity function.

Bilot-Kawski:

$$\tilde{\nu}_A(T) - \tilde{\nu}_E(T) = \frac{2(\mu_e^2 - \mu_g^2)}{4\pi\varepsilon_0 hc} \cdot F_{BK}(F,\lambda) + const.$$

$$\tilde{\nu}_A(T) + \tilde{\nu}_E(T) = \frac{2(\mu_e^2 - \mu_g^2)}{3\varepsilon_0 hc} \cdot \Phi_{BK}(F,\lambda) + const.$$

$$F_{BK}(T,\lambda) = \frac{1}{V(T)}\left[\frac{2n^2(T,\lambda)+1}{n^2(T,\lambda)+2} \cdot \left(\frac{\varepsilon(T)-1}{\varepsilon(T)+2} - \frac{n^2(T,\lambda)-1}{n^2(T,\lambda)+2}\right)\right] \tag{10.3}$$

$$\Phi(T,\lambda) = F_{BK}(T,\lambda) + \frac{1}{V(T)}\left(\frac{3(n^4(T,\lambda)-1}{(n^2(T,\lambda)+2)^2}\right)$$

$$\mu_e = \sqrt{\mu_g^2 + \frac{3m_{BK}hc\varepsilon_0}{2}}$$

where $\tilde{\nu}_{A/E}$ describes the maxima of adsorption or emission, $\mu_{e/g}$ the dipole moment in the ground state or in the electronically excited state, V describes the cavity volume, ε the permittivity, n is the refractive index, F_{BK} and Φ is the solvent polarity function of the corresponding equation and m_{BK} is the slope of the respective plot of the difference of the maxima against the corresponding solvent polarity function.

The cavity volume $V(T)$ was calculated from the aforementioned measurements as well as the plot of inverse density against the mass fraction using the following formula:

$$\frac{1}{\rho} = \frac{1}{\rho^*} + \left(\frac{V_m}{M_m} - \frac{1}{\rho^*}\right) \cdot w \tag{10.4}$$

where ρ is the density of the solution, ρ^* the density of the solvent, V_m the molar cavity volume, M_m the molar mass of the solute and w the mass fraction of the solute.

10.5.2. Experimental Results

Table 10.3.: Calculated values from the experimental data of n-methylindole.

	$F(T,n)_{LM}$	$F(T)_{LM}$	$F(T,n)_{BK}$	$F(T)_{BK}$	$\Phi(T,n)_{BK}$	$\Phi(T)_{BK}$
2-MeI	12,2(5)	6,32(12)	4,68(13)	1,74(17)	3,96(8)	3,56(3)
3-MeI	8,84(28)	11,88(43)	3,45(20)	3,67(21)	3,83(9)	3,31(6)
4-MeI	9,00(25)	6,25(16)	2,24(14)	0,98(12)	0,94(17)	1,33(8)
5-MeI	12,6(3)	11,3(3)	4,59(6)	4,46(11)	2,26(7)	2,88(4)
6-MeI	12,3(3)	7,20(13)	4,92(10)	8,53(12)	3,70(4)	2,248(9)
7-MeI	14,5(4)	14,4(4)	4,53(10)	5,75(12)	3,02(12)	3,79(3)

10.6. Conclusion

The findings indicate that the methodology proposed by Demissie for calculating the dipole moments in the ground state is unsuitable for application, as the resulting values are not aligned with the comparative data. As is often the case, the dipole moments in the excited state are significantly overestimated by the Lippert and Mataga calculation method and the Bilot and Kawski method is the preferred option. It is evident that the method of determining dipole moments in solution is a reliable approach. However, for verification and validation, this method still necessitates the integration of values derived from quantum chemical calculations and gas phase measurements. An intriguing approach is the comparison of molecules with an identical molecular backbone but differing substituents, which exert varying effects on the electron density distribution of the molecule. Moreover, it can be observed, in light of other published works, that thermochromic methods can be

readily employed, but should be used with caution in instances of anomalous behaviour of the molecule in solution, as evidenced by the non-linear relationships observed in all cases.

10.7. Acknowledgements

Financial support of the Deutsche Forschungsgemeinschaft via grant SCHM1043/16-1 is gratefully acknowledged. Computational support and infrastructure was provided by the "Center for Information and Media Technology" (ZIM) at the Heinrich-Heine-University Düsseldorf.

10.8. Own Share

My own share of this publication is about 70% and consists of writing - original draft, data acquisition, evaluation, software, methodology, investigation, formal analysis.

11. Results on Refractive Indices

On determining the temperature and wavelength dependent refractive indices.†

Matthias Zajonz[a], Michael Schmitt[a*]

[a]Heinrich-Heine-Universität, Institut für Physikalische Chemie I,
Arbeitsgruppe für Hochauflösende Spektroskopie,
D-40225 Düsseldorf, Germany, E-mail:mschmitt@hhu.de

11.1. Abstract

The temperature and wavelength dependence of the refractive index behaviour of various solvents was examined and fitted using a 3-dimensional fit. A modified form of the Sellmeier equation was used, which also takes the temperature component into account through the extension. All empirical parameters used in the fit were determined and show a good correlation with the temperature- and wavelength-dependent measured values in the examined range.

11.2. Introduction

In numerous publications and in the course of everyday scientific work, the refractive index is frequently taken for granted and is not subject to further scrutiny. It is well established that the refractive index is a function of the temperature. However, when applied to specific problems, it is frequently overlooked that the refractive index is also dependent on the wavelength. For example, numerous publications on the determination of the dipole moment in solution can be referenced [133], [149], [150] and more, where the standard value n_D is employed despite the fact that the molecules under investigation absorb and emit at low wavelengths and the refractive index is included in the calculation in the second power. Furthermore, the refractive index, as a central and fundamental optical

property of materials, plays a pivotal role in a number of fields, including optics, photonics, telecommunications and sensor technology [312], [313], [314], [315]. The objective of this paper is to examine the temperature and wavelength dependence of the refractive indices as well as the mutual influence of the two dependencies in a range of solvents, with the intention of providing a foundation for further research in the area.

11.3. Experimental Methods

The refractive index is determined by means of a Abbemat MW refractometer, manufactured by Anton Paar. The temperature scale for each solvent to be examined begins at 283.15 K, with an increment of 1 K. The measurement is conducted as closely as possible to the respective boiling point for each solvent to be examined. The measurement at the available wavelengths (486.1 nm, 513.9 nm, 531.9 nm, 589.3 nm and 632.9 nm) was always conducted with a delay following the temperature setting.

11.4. Systems

In the course of the study, solvents that are readily accessible were selected for examination. In addition, water, which is an ubiquitous solvent, was also subjected to analysis. The individual liquids examined are presented in the following table.

Table 11.1.: Solvents studied, including some of their properties.

	Formula	Polarity	Boiling Point [K]
Cyclohexane	C_6H_{12}	non-polar / aprotic	353,15
Ethanol	C_2H_6O	polar / protic	351,15
Isopropanol	C_3H_8O	polar / protic	355,15
Water	H_2O	polar / protic	373,15
Ethyl acetate	$C_4H_8O_2$	polar / aprotic	350,15

11.5. Results and Discussion

The empirical fit values were calculated in accordance with the equation below (cf. 11.1), which is a modified form of the Sellmeier equation [88].

$$n(\lambda, T) = \sqrt{1 + \sum_{i=1}^{3} \frac{B_i}{1 - \frac{C_i}{\lambda^2}}} \cdot \left(p_0 + p_1 \left(\frac{T}{K} \right) + p_2 \left(\frac{T}{K} \right)^2 + p_3 \left(\frac{T}{K} \right)^3 \right) \tag{11.1}$$

The Sellmeier equation was modified to account for wavelength dependence and the interdependency of wavelength dependence and temperature dependence. This modification bears resemblance to the equation established by Wei *et al.* [89]. The specific empirical parameters of the solvents under examination are presented in the following table 11.2.

Table 11.2.: Empirical parameters of the 3D fit of the modified Sellmeier equation of the respective solvent examined.

Parameter	Cyclohexane	Ethanol	Isopropanol	Water	Ethyl acetate
B_1	0,7256	0,8347	0,8647	0,8647	0,8136
B_2	0,1706	0,0977	0,0778	0,1736	0,1158
B_3	0,1283	0,1044	0,1056	0,0176	0,1077
C_1 $[nm^2]$	7156,1	8541,0	8395,3	8911,7	8621,7
C_2 $[nm^2]$	19821,7	7515,3	7378,1	13487,9	7201,5
C_3 $[nm^2]$	12585,3	15104,0	14977,7	27236,9	16549,1
p_3	$-1,06 \cdot 10^{-9}$	$-1,65 \cdot 10^{-9}$	$-1,73 \cdot 10^{-9}$	$-2,06 \cdot 10^{-9}$	$-1,52 \cdot 10^{-9}$
p_2	$8,11 \cdot 10^{-7}$	$1,15 \cdot 10^{-6}$	$9,65 \cdot 10^{-7}$	$1,04 \cdot 10^{-9}$	$1,30 \cdot 10^{-6}$
p_1	$-5,82 \cdot 10^{-4}$	$-5,25 \cdot 10^{-4}$	$-4,08 \cdot 10^{-4}$	$-1,49 \cdot 10^{-4}$	$-5,04 \cdot 10^{-4}$
p_0	1,1227	1,0444	1,0362	0,99878	1,2236

The results of the 3D fit were subjected to graphical processing and are presented in the following figures (cf. 11.1 to 11.4). The correlation between the fitted curve and the measured values is satisfactory, both within the examined range of wavelengths and temperatures.

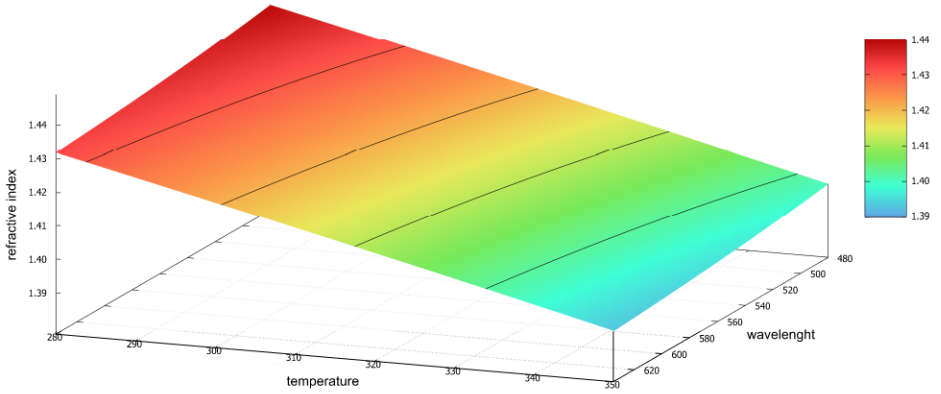

Figure 11.1.: Graphical representation of the refractive index of cyclohexane as a function of temperature and wavelength.

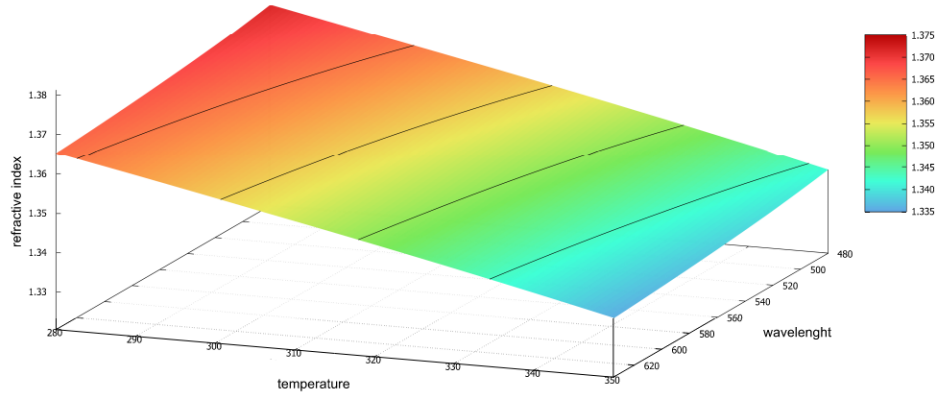

Figure 11.2.: Graphical representation of the refractive index of ethanol as a function of temperature and wavelength.

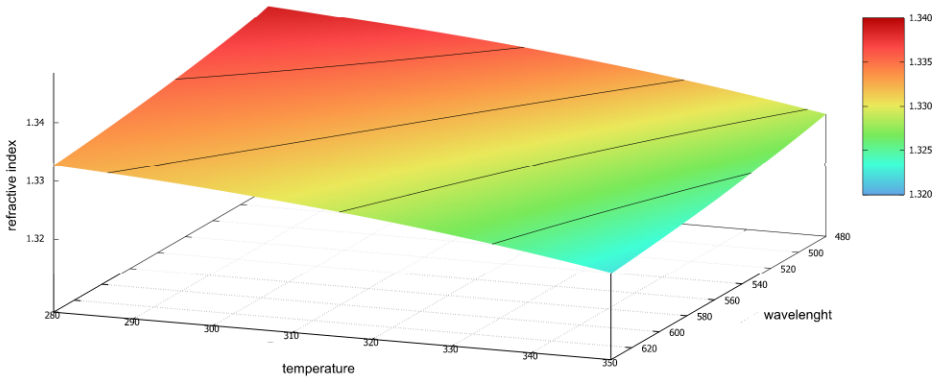

Figure 11.3.: Graphical representation of the refractive index of water as a function of temperature and wavelength.

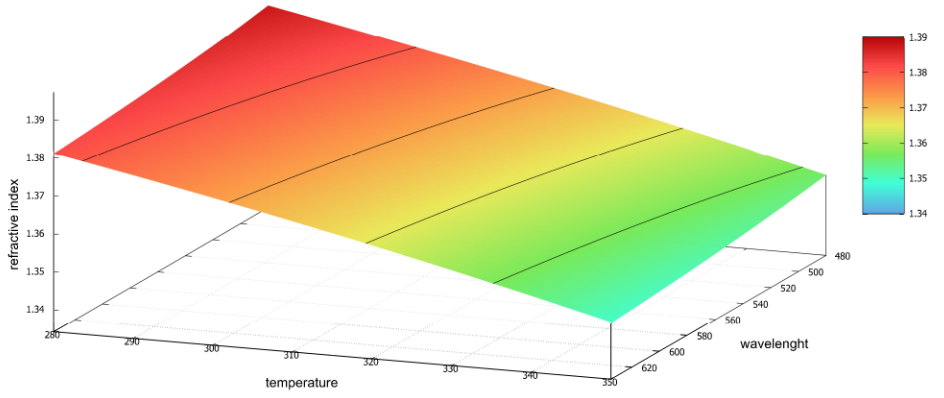

Figure 11.4.: Graphical representation of the refractive index of isopropanol as a function of temperature and wavelength.

11.6. Conclusion

It can be concluded that this is a viable method for determining the temperature and wavelength dependence, and that the equation that was set up is valid. The determination of empirical parameters enables a preliminary estimation of refractive indices with regard to temperature and wavelength dependence, which fall outside the technically limited measuring range. Any shortcomings or discrepancies from the actual values are attributable to the approximations that are inherent to the methodology. It is recommended that the parameters be refined by measuring more than five wavelengths and by covering a broader temperature range. In conclusion, the predictions of the refractive indices can be used with confidence.

11.7. Acknowledgements

The financial support of the Deutsche Forschungsgemeinschaft through grant SCHM1043/16-1 is gratefully acknowledged. Computational support and infrastructure was provided by the "Center for Information and Media Technology" (ZIM) at the Heinrich-Heine-University Düsseldorf.

11.8. Own Share

My own share of this publication is about 70% and consists of writing - original draft, data acquisition, evaluation, software, methodology, investigation, formal analysis.

12. Summary

The aim of the present dissertation is to further develop and more precisely investigate, as well as gain deeper understanding of, the determination of the dipole moment in both the ground state and the electronically excited state in the liquid phase, employing methods of thermochromism. Furthermore, the understanding of the interaction between the solvent and the solvate is to be elucidated and examined in greater detail. To verify and determine relevant data, High-Resolution-Laser-Induced Fluorescence Stark spectroscopy is employed, as well as quantum chemical *ab initio* calculations, CC2/cc-pVTZ level of theory, for the determination of molecular parameters and COSMO for the interaction between solvent and solvate. The molecules employed in this investigation were indole derivatives, which permitted the examination of the impact of diverse substituents on molecular parameters. This included the investigation of substituents with opposing effects, such as those observed in n-cyanoindoles and n-methylindoles. Furthermore, benzene derivatives with cyano groups as a substituents were examined in order to establish a connection with the indole derivatives to a certain extent.

The theoretical foundations that introduce the topic are discussed in chapter 3, where the crucial parameter of the refractive index is also examined in more detail. Additionally, the change within the formula for determining the temperature-dependent refractive index is discussed, with consideration of the wavelength dependence of the refractive index. Subsequently, an in-depth analysis of the interaction between solvents and solvates is conducted, with a particular focus on the understanding of this interaction as a pivotal aspect. This facilitates a more comprehensive comprehension of dipole moment determination in solution, thereby paving the way for the development of novel determination approaches and calculation methods. The following chapter 4 addresses the subject of quantum chemical calculation methods, wherein it is determined that the incorporation of COSMO theory is a highly suitable approach. Subsequently, closing the expanded theoretical part, Chapter 5 deals with the calculation methods employed in this dissertation. This chapter corroborates the findings of Chapter 9 that the Lippert and Mataga calculation method is unsuccessful. Furthermore, this chapter elucidates that the approach

of distinct determination, devoid of consideration for the mutual relationship, of the dipole moments in the ground state and in the electronically excited state according to the method of Demissie, despite its appealing nature, nevertheless yields inadequate results in the majority of cases. This is particularly evident when determining the dipole moments in the ground state. The sole genuine enhancement or alteration to the calculation methodologies introduced by Demissie is the utilisation of the actual cavity volume in lieu of the Onsager radius. This is evident from both the theoretical considerations and the ongoing criticism of the Onsager radius in the literature pertinent to the subject matter. These conclusions are corroborated by the present work and by earlier publications of the research group. As demonstrated in Chapter 6, the experimental setup shown illustrates the significant investment of resources required to ascertain the dipole moment of the excited state.

The conclusion of chapter 8 is that, although it initially appears reasonable to compare dipole moments derived from measurements in the gas phase of Stark spectroscopy with *ab initio* calculations of the isolated species and dipole moments derived from measurements in the liquid phase of solvatochromic or thermochromic shifts with *ab initio* calculations that include solvation models, this is not a valid approach. Nevertheless, a closer examination reveals that the most prevalent and extensively utilized calculation techniques, which were also employed in the investigation of 1,2-DCB and 1,3-DCB, establish a correlation between the shifts for unpolarized molecules. Consequently, the calculated dipole moments should be compared with the ab initio calculations of the isolated species. Furthermore, the significant divergence between the Lippert and Mataga approach and the modified Bilot and Kawski approach is once again apparent. As previously mentioned, these findings are evident in the calculation for 1,2-DCB according to the Bilot and Kawski approach, which yields a value of 6,88 D in the S_1 state. This value exhibits a high degree of agreement with the calculation according to the SCS-CC2/cc-pVTZ and ADC(2)/cc-pVTZ theory. These findings are further corroborated by the results obtained using the ADC(2) COSMO theory, which are 2,0 D greater than the expected value, and additionally by the calculations according to the Lippert and Mataga approach, where the result is 11,0 D and thus clearly exceeds the anticipated outcome. The results for 1,3-DCB exhibit a similar trend. The value of 4,33 D obtained from the Bilot and Kawski approach aligns with the predictions of the SCS-CC2 and ADC(2) theories. However, the calculated value from the Lippert and Mataga approach is significantly higher, and the result from the ADC(2) COSMO theory also deviates considerably. The consideration of the vector addition of individual bond dipoles to determine the dipole moments of 1,2-DCB and 1,3-DCB is found to have limited validity in the underestimated case, with

an average deviation of approximately 10%. In conclusion, the dipole moments obtained from the liquid phase should be compared with those of the isolated molecule, as there is a correlation between the dipole moment of the unpolarised molecule and the transitions. Vector addition can be employed to determine the dipole moment in the excited state under certain conditions.

The fundamental insights derived from Chapter 9 indicate that the wavenumber of the emission of the n-cyanoindoles exhibits an increasing trend from 7-CI via 4-CI, 5-CI, 6-CI, and 2-CI, culminating in 3-CI. Furthermore, the proposed alteration to the function used to describe the temperature-dependent refractive indices with regard to wavelength dependence is supported by the evidence, given that the absorption and emission of the n-CIs is observed below 330,0 nm and the refractive index within the solvent polarity functions is represented by the second power. The function is modelled using a three-dimensional fit, which follows the Sellmeier equation as described in the theoretical section of this work. It has been demonstrated on numerous occasions that the correlation of the Bilot and Kawski plot is markedly superior to that of the Lippert and Mataga plot. In essence, the calculated dipole moments from the liquid phase demonstrate a high degree of concordance with the corresponding *ab initio* calculations. However, the 4-CI, with a deviation of 0,98 D, represents an exception to this rule. As evidenced by the *ab initio* calculations, the 4-CI exhibits the narrowest gap between the S_1 and S_2 states, wherein the former corresponds to L_a and the latter to L_b. The narrow gap between the two states allows for significant interconversion between them, which contributes to the discrepancy between the *ab initio* calculation and the calculation from the liquid phase. This is corroborated by the values obtained in the gas phase, although a discrepancy of 0,5 D persists between the experimental data and the *ab initio* calculations. This discrepancy can be attributed to the diminished strength of the Stark field when applied in the gas phase, as compared to its intensity created in solution. The relative stabilities of the six constitutional isomers are determined using the SCS-CC2/cc-pVTZ theory. The 3-CI is characterised as the most stable conformer, while the 2-CI is identified as the least stable. The calculated ground-state dipole moments exhibit a discrepancy of over two orders of magnitude, with the 7-CI displaying the lowest value and the 5-CI exhibiting the highest. The outcome of the vector addition for the ground state of the n-CI is noteworthy, as it does not result in an induced dipole moment within the indole moiety. Upon aligning the dipole moments of the ground state and the excited state, it was observed that all n-CIs, with the exception of the 4-CI, exhibited a similar behaviour. In conclusion, despite the circumvention of the shortcomings of the Lippert and Mataga calculation

method through the utilisation of thermochromic methods, the aforementioned calculation method ultimately fails due to the complete neglect of solvent polarisation. Additionally, the Bilot and Kawski calculation method has once again demonstrated superior results.

The results of the methylindoles investigated also show, as already mentioned, that on the one hand the method according to Demessie for the calculation of the ground state dipole moments should rather not be applied, since the calculated ground state dipole moment values do not agree with the quantum chemical calculations and if they do, it is probably more a matter of luck than that these values are based on a solid scientific basis. This may be due to the fact that the solvent polarity functions used are designed to calculate dipole moments in the electronically excited state and thus assume a known value, which of course is derived from other methods of determination, and on the other hand they derive their calculation basis from the change during electronic excitation, which cannot be easily reversed as these are not isoenergetic processes. On the other hand, certain values of the dipole moments in the electronically excited state show, as already shown in previous publications, that the calculation methods according to Bilot and Kawski give better results and that the method according to Lippert and Mataga overestimates these values extremely. It is also interesting to note that when using the same basic building block of the molecule, but with different substituents that have opposite effects on the electron density distribution within the molecule, the order of the absorption and emission maxima is reversed when positioned at the same point in the molecule. This leads to the conclusion that by observing the effects on the electron density distribution, general conclusions can be drawn about the electron density distribution with respect to the dipole moments, although this aspect requires further research. However, it should be noted that the known methods should be used with caution if the molecule behaves abnormally or unusually in solution, which also explains the delay in publishing the results.

In principle, some relevant conclusions can be drawn from the theoretical consideration alone, which can be confirmed to a certain extent by experimental results. It is evident that the utilisation of thermochromic methodologies offers considerable benefits, as these maintain all potential parameters, that is, all potential effects of the interaction between the solvent and the solvate, constant and modify them to a certain extent in a uniform manner across the temperature range. The requisite shifts within the absorption and emission spectra can be adequately generated by varying the temperature. Furthermore, the retention of a solvent permits the targeted selection of this solvent, thereby reducing the complexity of the interaction between solvent and solvate. This, in turn,

enables a more precise description of the interaction. Furthermore, it is evident that a precise comprehension of the interaction between solvent and solvate represents a pivotal foundation for the accurate formation of the highly pertinent solvent polarity function. Even minor alterations to the solvent polarity functions, such as the incorporation of cavity volume in lieu of Onsager radius and the incorporation of wavelength-dependent refractive index considerations, markedly enhance the precision of the calculated results, as per the established methodologies for determining dipole moments in solution. The significance of an accurate solvent polarity function is further confirmed by the consistent superiority of the Bilot and Kawski calculation method over the Lippert and Mataga calculation method.

In conclusion, the results of this dissertation demonstrate that determining dipole moments in the liquid phase via thermochromic methods is a superior approach compared to solvatochromic methods. This methodology represents a significant advancement in the determination of dipole moments of molecules in solution. The combination of this method with quantum chemical *ab initio* calculations and with the determination of dipole moments in the gas phase using High-Resolution-Laser-Induced-Fluorescence-Spectroscopy significantly expands the scope for determining molecular properties and for enhancing the method itself. The detailed examination of solvent polarity functions also offers benefits not only in relation to this methodology but also in broader contexts across diverse fields of application.

13. Outlook

A consideration of the research domain explored in this dissertation reveals a number of intriguing avenues and prospective avenues for further investigation which will be discussed below. This outlook is predicated on the author's deliberations, which, on the one hand, pertain to the retention of the measurement methodology while concomitantly investigating novel systems and, on the other hand, to potential approaches for modifying the measurement methodology itself.

An intriguing avenue for further exploration within the domain of measurement methodology is the examination of the same molecules, but utilising an alternative solvent. This approach may facilitate the identification of a more optimal solvent, thereby enabling a more comprehensive investigation into the influence of the solvent on the dissolved molecule. Moreover, the investigation of larger molecules and molecules with TADF properties represents a potential avenue for further exploration, as initiated by the working group. The investigation of larger molecules also indicates a potential avenue for further research, whereby the entire large molecule is measured, along with the smaller molecules that constitute it. A combined analysis of the two measurements could then be conducted to ascertain whether the parameters of the large molecules can be determined from the individual smaller components. This may permit the proposition that variations of a large molecular entity may not be required to be carried out through direct measurement of the large molecule. Instead, the initial step may be to measure the component, thereby enabling the effect of the exchange to be deduced.

Another interesting approach, contingent on the solubility of the molecule under investigation, would be to measure it via thermochromic methods using, for instance, propylene glycol (melting point: -59 $°C$ [316]), ethylene glycol (melting point: -12 $°C$ [317]) or glycerol (melting point: 18 $°C$ [318]), which on occasion do not crystallise directly at near the respectiv melting point but form clear, highly viscous liquids, thereby practically immobilising the dissolved molecule. It should be noted, however, that the aforementioned measurements are to be carried out at temperatures approximately corre-

sponding to the respective melting points in order to allow the immobilisation effects to be exploited fully and to prevent the results being distorted as a result of high temperatures.

Furthermore, it would be beneficial to consider whether a reduction in the data volume, specifically the number of measuring points at different temperatures, could offer a notable advantage. Ultimately, the slope of the plot of the spectral shifts against the solvent polarity function is of paramount importance in the calculation methods. Therefore, a reduction in the amount of data would facilitate the identification of the essential trend and mitigate the impact of fluctuations in the measurement conditions, given that absolute control of the solution behaviour is unfeasible. Concurrently, this would minimise the measurement and evaluation effort, thereby enabling a more expeditious evaluation and determination.

Although the benefits of determining dipole moments in solution using thermochromic methods are evident, a potential avenue for future research could be the integration of thermochromic and solvatochromic techniques to enhance the differences between the individual measurement points of the absorption and emission spectra. This approach could facilitate a more distinct separation of the absorption and emission bands. The following research approach could be undertaken: The molecule to be examined is dissolved in a solvent of choice and the temperature is initiated at a low temperature. Subsequently, the temperature is increased while simultaneously introducing another solvent, in accordance with the requisite solubility and shift direction, and the measuring point is recorded. Subsequently, additional measuring points are recorded in accordance with the aforementioned methodology, with the sole variation being an increase in the concentration of the added solvent. This, in turn, gives rise to an increase in the complexity of the solvent polarity function and the determination of the effects of the interaction between the solvent and the solvate. Nevertheless, the spectral shift can be amplified through the judicious selection of solvents. By concurrently reducing the number of measurement points as previously outlined, the requisite effort can be confined to a reasonable scope.

The central point of future research in this area is the detailed investigation of the individual relevant variables or parameters of the solvent polarity function and, of course, the solvent polarity functions themselves. Such an understanding could also prove useful in other research areas. It is therefore of great importance to conduct a thorough investigation of the refractive indices, taking into account all factors that may influence them, as well as to investigate the permittivity in a similar manner. This is crucial for providing an

accurate description of the spectral shifts and thus for determining dipole moments in solution. A comprehensive and detailed compilation of the solvent polarity functions, which has already facilitated incremental improvements through ongoing research, is a crucial element in accurately determining the quantities under investigation. The realisation of this research direction could be characterised by the development of a new solvent polarity function, the modification or improvement of existing solvent polarity functions, or the application of existing solvent polarity functions within calculation methods. It is important to note, however, that according to the current state of research, a universal solvent polarity function is not feasible due to the significant differences in the effects of various solvents. Consequently, a separate or modified solvent polarity function would be necessary for each class of solvent. A comprehensive understanding of the interaction between the solvent and the solvate is pivotal to advancing the methodology within this field of research.

14. List of Publications and Conference Contributions

Publications

- Mirko Matthias Lindic, **Matthias Zajonz**, Marie-Luise Hebestreit, Michael Schneider, W. Leo Meerts, Michael Schmitt: Excited state dipole moments of anisole in gas phase and solution. Journal of Photochemistry & Photobiology A: Chemistry **365** (2018) 213-219

- Mirko Matthias Lindic, **Matthias Zajonz**, Marie-Luise Hebestreit, Michael Schneider, W. Leo Meerts, Michael Schmitt: Additional data for evaluation of the excited statedipole moments of anisole. Data in Brief **21** (2018) 313-315

- Mirko Matthias Lindic, **Matthias Zajonz**, Charlotte Gers-Panther, Thomas J.J. Müller, Michael Schmitt: The excited state dipole moment of 2-[(4-methoxyphenyl)-ethynyl]-3-(1-methyl-1H-indol-3-yl)-quinoxaline from thermochromic shifts. Spectrochimica Acta Part A: Molecular and Biomolecular Spectroscopy **228** (2020) 117574

- Mirko Matthias Lindic, **Matthias Zajonz**, Marie-Luise Hebestreit, Michael Schneider, W. Leo Meerts, Michael Schmitt: Determination of excited state dipole moments in solution via thermochromic methods. MethodsX **7** (2020) 101101-1 - 101101-12

- **Matthias Zajonz**, Tim Oberkirch, Marie-Luise Hebestreit, Mirko Matthias Lindic, Christof Hättig, Michael Schmitt: Excited state dipole moments of two dicyanobenzene isomers from thermochromic shifts and ab initio calculations. Journal of Photochemistry and Photobiology A: Chemistry **452** (2024) 115589

- **Matthias Zajonz**, Marie-Luise Hebestreit, Peter Gilch, Christof Hättig, and Michael Schmitt: Lippert-Mataga Treatment Fails in Predicting Excited State Dipole Moments in n-Cyanoindoles (n=2,3,4,5,6). To be published in Angewandte Chemie International Edition.

- **Matthias Zajonz**, Marie-Luise Hebestreit, Michael Schmitt: Excited State Dipole Moments of n-Methylindoles from Thermochromic Shifts. To be published in Journal of Molecular Spectroscopy.

Conference Contributions

- **Poster: Matthias Zajonz**, Mirko Lindic, Marie-Luise Hebestreit and Michael Schmitt. Determination of dipole moments in the electronically excited state of quinoxaline via thermochromic methods. 34th European Congress on Molecular Spectroscopy, Coimbra, Portugal 08/2018

- **Poster: Matthias Zajonz**, Tim Oberkirch, Mirko Lindic and Michael Schmitt. Investigation of quadrupole moment effects on the determination of excited state dipole moments in solution. Frühjahrstagung der Deutschen Physikalischen Gesellschaft, Rostock, Germany 03/2019

Bibliography

[1] Bernreuther, W.; Suzuki, M. The electric dipole moment of the electron. *Reviews of Modern Physics* **1991**, *63*, 313–340.

[2] Borchers, H. J. The CPT-theorem in two-dimensional theories of local observables. *Communications in Mathematical Physics* **1992**, *143*, 315–332.

[3] Greaves, H.; Thomas, T. On the CPT theorem. *Studies in History and Philosophy of Science Part B: Studies in History and Philosophy of Modern Physics* **2014**, *45*, 46–65.

[4] Shindler, A. Flavor-diagonal CP violation: the electric dipole moment. *The European Physical Journal A* **2021**, *57*.

[5] Lakowicz, J. R. *Principles of Fluorescence Spectroscopy*, 3rd ed.; Springer: New York, NY, U.S.A., 2010; Vol. 954.

[6] Schmitt, M.; Meerts, L. In *Frontiers and Advances in Molecular Spectroscopy*, 1st ed.; Laane, J., Ed.; Elsevier Science, 2017.

[7] Abeywickrama, C.; Premaratne, M.; Gunapala, S. D.; Andrews, D. L. Impact of a charged neighboring particle on Förster resonance energy transfer (FRET). *Journal of Physics: Condensed Matter* **2019**, *32*, 095305.

[8] Penfold, T. J.; Dias, F. B.; Monkman, A. P. The theory of thermally activated delayed fluorescence for organic light emitting diodes. *Chemical Communications* **2018**, *54*, 3926–3935.

[9] Uoyama, H.; Goushi, K.; Shizu, K.; Nomura, H.; Adachi, C. Highly efficient organic light-emitting diodes from delayed fluorescence. *Nature* **2012**, *492*, 234–238.

[10] Huang, T.; Jiang, W.; Duan, L. Recent progress in solution processable TADF materials for organic light-emitting diodes. *Journal of Materials Chemistry C* **2018**, *6*, 5577–5596.

[11] Teng, J.-M.; Wang, Y.-F.; Chen, C.-F. Recent progress of narrowband TADF emitters and their applications in OLEDs. *Journal of Materials Chemistry C* **2020**, *8*, 11340–11353.

[12] Bryden, M. A.; Zysman-Colman, E. Organic thermally activated delayed fluorescence (TADF) compounds used in photocatalysis. *Chemical Society Reviews* **2021**, *50*, 7587–7680.

[13] Xiao, Y.; Wang, H.; Xie, Z.; Shen, M.; Huang, R.; Miao, Y.; Liu, G.; Yu, T.; Huang, W. NIR TADF emitters and OLEDs: challenges, progress, and perspectives. *Chemical Science* **2022**, *13*, 8906–8923.

[14] E., S. K.; Berti, L.; Medintz, I. L. Materialien für den resonanten Fluoreszenzenergietransfer (FRET): über klassische Donor-Akzeptor-Kombinationen hinaus. *Angewandte Chemie* **2006**, *118*, 4676–4704.

[15] Shrestha, D.; Jenei, A.; Nagy, P.; Vereb, G.; Szöllősi, J. Understanding FRET as a Research Tool for Cellular Studies. *International Journal of Molecular Sciences* **2015**, *16*, 6718–6756.

[16] Valchanov, G.; Ivanova, A.; Tadjer, A.; Chercka, D.; Baumgarten, M. Understanding the Fluorescence of TADF Light-Emitting Dyes. *The Journal of Physical Chemistry A* **2016**, *120*, 6944–6955.

[17] Olivier, Y.; Moral, M.; Muccioli, L.; Sancho-García, J.-C. Dynamic nature of excited states of donor–acceptor TADF materials for OLEDs: how theory can reveal structure–property relationships. *Journal of Materials Chemistry C* **2017**, *5*, 5718–5729.

[18] Naqvi, B. A.; Schmid, M.; Crovini, E.; Sahay, P.; Naujoks, T.; Rodella, F.; Zhang, Z.; Strohriegl, P.; Bräse, S.; Zysman-Colman, E.; Brütting, W. What Controls the Orientation of TADF Emitters? *Frontiers in Chemistry* **2020**, *8*.

[19] Atkins, P.; de Paula, J. *Physical Chemistry*; W. H. Freeman, 2006; p 1072.

[20] Ahmadivand, A.; Semmlinger, M.; Dong, L.; Gerislioglu, B.; Nordlander, P.; Halas, N. J. Toroidal Dipole-Enhanced Third Harmonic Generation of Deep Ultraviolet Light Using Plasmonic Meta-atoms. *Nano Letters* **2018**, *19*, 605–611.

[21] Kuzyk, *Characterization Techniques and Tabulations for Organic Nonlinear Optical Materials*; CRC Press LLC, 2018.

[22] Quéméner, G.; Bohn, J. L. Strong dependence of ultracold chemical rates on electric dipole moments. *Physical Review A* **2010**, *81*, 022702.

[23] Graf, A.; Liehm, P.; Murawski, C.; Hofmann, S.; Leo, K.; Gather, M. C. Correlating the transition dipole moment orientation of phosphorescent emitter molecules in OLEDs with basic material properties. *J. Mater. Chem. C* **2014**, *2*, 10298–10304.

[24] Würfel, U.; Seßler, M.; Unmüssig, M.; Hofmann, N.; List, M.; Mankel, E.; Mayer, T.; Reiter, G.; Bubendorff, J.; Simon, L.; Kohlstädt, M. How Molecules with Dipole Moments Enhance the Selectivity of Electrodes in Organic Solar Cells – A Combined Experimental and Theoretical Approach. *Advanced Energy Materials* **2016**, *6*.

[25] Li, M.; Zhou, Y.; Zhang, J.; Song, J.; Bo, Z. Tuning the dipole moments of non-fullerene acceptors with an asymmetric terminal strategy for highly efficient organic solar cells. *Journal of Materials Chemistry A* **2019**, *7*, 8889–8896.

[26] Santra, P. K.; Palmstrom, A. F.; Tanskanen, J. T.; Yang, N.; Bent, S. F. Improving Performance in Colloidal Quantum Dot Solar Cells by Tuning Band Alignment through Surface Dipole Moments. *The Journal of Physical Chemistry C* **2015**, *119*, 2996–3005.

[27] Ji, X.; Wang, T.; Fu, Q.; Liu, D.; Wu, Z.; Zhang, M.; Woo, H. Y.; Liu, Y. Deciphering the Effects of Molecular Dipole Moments on the Photovoltaic Performance of Organic Solar Cells. *Macromolecular Rapid Communications* **2023**, *44*.

[28] Privado, M.; de la Cruz, P.; Malhotra, P.; Sharma, G. D.; Langa, F. Influence of the dipole moment on the photovoltaic performance of polymer solar cells employing non-fullerene small molecule acceptor. *Solar Energy* **2021**, *221*, 393–401.

[29] Maxwell, J. C. A treatise on electricity and magnetism. *Clarendon Press* **1873**, *2*, 3408–3425.

[30] Reinganum, M. Über Molekularkräfte und elektrische Ladungen der Moleküle. *Annalen der Physik* **1903**, 354 – 359.

[31] Debye, P. J. W. Der Lichtdruck auf Kugeln von beliebigem Material. Ph.D. thesis, Ludwig-Maximilians Universität München, 1908.

[32] Debye, P. Einige Resultate einer kinetischen Theorie der Isolatoren. *Physikalische Zeitschrift* **1912**, 9.

[33] Stark, J. Beobachtungen über den Effekt des elektrischen Feldes auf Spektrallinien. I. Quereffekt. *Annalen der Physik* **1914**, *348*, 965–982.

[34] Lo Surdo, A. Sul Fenomeno Analogo A Quello Di Zeeman Nel Campo Elettrico. *Il Nuovo Cimento* **1914**, *7*, 335–337.

[35] Kirkwood, J. G. Theory of Solutions of Molecules Containing Widely Separated Charges with Special Application to Zwitterions. *The Journal of Chemical Physics* **1934**, *2*, 351–361.

[36] Onsager, L. Electric Moments of Molecules in Liquids. *Journal of American Chemistry* **1936**, *58*, 1482 – 1493.

[37] Ooshika, Y. Absorption Spectra of Dyes in Solution. *Journal of the Physical Society of Japan* **1954**, *9*, 594 – 602.

[38] Lippert, E.; Moll, F. The influence of the solvent on the electronic spectra of intramolecular ionic aromatic compounds. *Zeitschrift fuer Elektrochemie und Angewandte Physikalische Chemie (1954), 58* **1954**, *58*, 718 – 724.

[39] Mataga, N.; Kaifu, Y.; Koizumi, M. Solvent effects upon fluorescence spectra and the dipole moments of excited molecules. *Bulletin of the Chemical Society of Japan* **1956**, *29*, 465 – 470.

[40] Bayliss, N. S. The Effect of the Electrostatic Polarization of the Solvent on Electronic Absorption Spectra in Solution. *The Journal of Chemical Physics* **1950**, *18*, 292–296.

[41] McRae, E. G. Theory of Solvent Effects on Molecular Electronic Spectra. Frequency Shifts. *Journal of Physical Chemistry (1957), 61* **1957**, *61*, 562 – 572.

[42] Bakhshiev, N. G. Universal Intermolecular Interactions and Their Effect on the Position of the Electronic Spectra of Molecules in Two-Component Solutions. V. Dependence of the Spectra on the Electrical Properties, Dimensions, and Structure of the Molecules Under Stud. *Optics and Spectroscopy* **1962**, *13*, 24.

[43] Bilot, L.; Kawski, A. Zur Theorie des Einflusses von Lösungsmitteln auf die Elektronenspektren der Moleküle. *Z. Naturforschung, 17 a, 621-627 [1962]* **1962**,

[44] Kawski, A.; Bilot, L. Spectroscopic Determination of Electrical Dipole Moments of Aromatic Compounds in the First Excited Singlet State. *Acta Phys. Pol* **1964**, *26*, 41–45.

[45] Chamma, A.; Viallet, P. Determination du moment dipolaire d'une molecule dans un etat excite singulet. *CR Acad Sci Paris Ser C* **1970**, *270*, 1901–1904.

[46] Reichardt, C. *Solvents and Solvent Effects in Organic Chemistry - Empirical Parameters of Solvent Polarity*; John Wiley & Sons, Ltd, 2002; Chapter Chapter 7, pp 389–469.

[47] Czekalla, J.; Wick, G. Die Bestimmung von absoluten Übergangsmomentrichtungen und von Dipolmomenten angeregter Moleküle aus Messungen des elektrischen Dichroismus. II. Ergebnisse. *Zeitschrift für Elektrochemie, Berichte der Bunsengesellschaft für physikalische Chemie* **1961**, *65*, 727–734.

[48] Gryczynski, I.; Kawski, A. Temperaturabhängigkeit der statischen Dielektrizitätskonstante und des optischen Brechungsindex von Flüssigkeit (Auswertung zur Bestimmung des elektrischen Dipolmomentes im Anregungszustand). *Z. Naturforschung* **1975**, *30 a*, 287–291.

[49] Suppan, P.; Tsiamis, C. Temperature effects in solvatochromic shifts. *Journal of the Chemical Society, Faraday Transactions 2* **1981**, *77*, 1553.

[50] Hallidy, L. A.; Topp, M. R. Time-resolved fluorescence spectroscopy of 2-amino-7-nitrofluorene in two-solvent solutions. *The Journal of Physical Chemistry* **1978**, *82*, 2415–2419.

[51] Badea, M. G.; Brand, L. *Enzyme Structure Part H*; Elsevier, 1979; pp 378–425.

[52] Pulay, P.; Fogarasi, G.; Pang, F.; Boggs, J. E. Systematic ab initio gradient calculation of molecular geometries, force constants, and dipole moment derivatives. *Journal of the American Chemical Society* **1979**, *101*, 2550–2560.

[53] Suppan, P. Invited review solvatochromic shifts: The influence of the medium on the energy of electronic states. *Journal of Photochemistry and Photobiology A: Chemistry* **1990**, *50*, 293–330.

[54] Sim, F.; Salahub, D. R.; Chin, S. The accurate calculation of dipole moments and dipole polarizabilities using Gaussian - based density functional methods. *International Journal of Quantum Chemistry* **1992**, *43*, 463–479.

[55] De Proft, F.; Martin, J. M.; Geerlings, P. On the performance of density functional methods for describing atomic populations, dipole moments and infrared intensities. *Chemical Physics Letters* **1996**, *250*, 393–401.

[56] Swart, M.; van Duijnen, P. T.; Snijders, J. G. Mean polarizabilities of organic molecules. A comparison of Restricted Hartree Fock, Density Functional Theory and Direct Reaction Field results. *Journal of Molecular Structure: THEOCHEM* **1998**, *458*, 11–17.

[57] Tomasi, J.; Mennucci, B.; Cancès, E. The IEF version of the PCM solvation method: an overview of a new method addressed to study molecular solutes at the QM ab initio level. *Journal of Molecular Structure: THEOCHEM* **1999**, *464*, 211–226.

[58] Santoro, F.; Barone, V.; Lami, A.; Improta, R. The excited electronic states of adenine-guanine stacked dimers in aqueous solution: a PCM/TD-DFT study. *Physical Chemistry Chemical Physics* **2010**, *12*, 4934.

[59] Pedone, A.; Barone, V. Unraveling solvent effects on the electronic absorption spectra of TRITC fluorophore in solution: a theoretical TD-DFT/PCM study. *Physical Chemistry Chemical Physics* **2010**, *12*, 2722.

[60] Rebane, A.; Drobizhev, M.; Makarov, N.; Beuerman, E.; Tillo, S.; Hughes, T. New all-optical method for measuring molecular permanent dipole moment difference using two-photon absorption spectroscopy. *Journal of Luminescence* **2010**, *130*, 1619–1623.

[61] Takaya, T.; Hamaguchi, H.-o.; Iwata, K. Femtosecond time-resolved absorption anisotropy spectroscopy on 9,9′-bianthryl: Detection of partial intramolecular charge transfer in polar and nonpolar solvents. *The Journal of Chemical Physics* **2009**, *130*.

[62] Kovalenko, A. *Springer Handbook of Electrochemical Energy*; Springer Berlin Heidelberg, 2017; pp 95–139.

[63] Asada, T.; Ando, K.; Sakurai, K.; Koseki, S.; Nagaoka, M. Efficient approach to include molecular polarizations using charge and atom dipole response kernels to calculate free energy gradients in the QM/MM scheme. *Physical Chemistry Chemical Physics* **2015**, *17*, 26955–26968.

[64] Brunk, E.; Rothlisberger, U. Mixed Quantum Mechanical/Molecular Mechanical Molecular Dynamics Simulations of Biological Systems in Ground and Electronically Excited States. *Chemical Reviews* **2015**, *115*, 6217–6263.

[65] Rodriquez, M. B.; Shelton, D. P. What is measured by hyper-Rayleigh scattering from a liquid? *The Journal of Chemical Physics* **2018**, *148*.

[66] Pandey, R.; Umapathy, S. Solvent-induced changes on the polarity of the triplet excited state of 2-chlorothioxanthone: From time-resolved absorption and resonance Raman spectroscopies. *Chemical Physics* **2014**, *428*, 175–180.

[67] Backus, E. H. G.; Cyran, J. D.; Grechko, M.; Nagata, Y.; Bonn, M. Time-Resolved Sum Frequency Generation Spectroscopy: A Quantitative Comparison Between Intensity and Phase-Resolved Spectroscopy. *The Journal of Physical Chemistry A* **2018**, *122*, 2401–2410.

[68] Marciniak, H.; Auerhammer, N.; Ricker, S.; Schmiedel, A.; Holzapfel, M.; Lambert, C. Reduction of the Fluorescence Transition Dipole Moment by Excitation Localization in a Vibronically Coupled Squaraine Dimer. *The Journal of Physical Chemistry C* **2019**, *123*, 3426–3432.

[69] Gryczynski, Z. K.; Gryczynski, I. *Practical Fluorescence Spectroscopy*; CRC Press, 2019.

[70] Adhikari, S.; Orrit, M. Progress and perspectives in single-molecule optical spectroscopy. *The Journal of Chemical Physics* **2022**, *156*.

[71] Simpson, G. J.; García-López, V.; Boese, A. D.; Tour, J. M.; Grill, L. Directing and Understanding the Translation of a Single Molecule Dipole. *The Journal of Physical Chemistry Letters* **2023**, *14*, 2487–2492.

[72] Smit, R.; Ristanović, Z.; Deperasińska, I.; Kozankiewicz, B.; Orrit, M. Probing the in-plane dipole moment vector between ground and excited state of single molecules by the Stark effect. *ChemPhysChem* **2024**, *25*.

[73] Wedler, G. *Lehrbuch der physikalischen Chemie*, 5th ed.; Wiley - VCH, 2010; Vol. 1072.

[74] Kasha, M. Characterization Of Electronic Transitions In Complex Molecules. *Discussions Of Faraday Society* **1950**,

[75] Brancatto, G.; Signore, G.; Neyroz, P.; polli, D.; Cerullo, G.; Abbandonato, G.; Nucara, L.; Barone, V.; Beltram, F.; Bizzarri, R. Dual Fluorescence through Kashas Rule Breaking: An Unconventional Photomechanism for Intracellular Probe Design. *The Journal Of Physical Chemistry B* **2015**, *119*, 6144 – 6154.

[76] Boyd, R. W.; Lukishova, S. G.; Zadkov, V. N. In *Quantum Photonics: Pioneering Advances and Emerging Applications*; Boyd, R. W., Lukishova, S. G., Zadkov, V. N., Eds.; Springer, 2019.

[77] Longfellow, R. J.; Moss, D. B.; Parmenter, C. S. Rovibrational Level Mixing below and within the Channel Three Region of S1 Benzene. *The Journal of Physical Chemistry* **1988**, *92*, 5438 – 5449.

[78] Jablonski, A. Über das Entstehen der breiten Absorptions- und Fluoreszenzbanden in Farbstofflösungen. *Zeitschrift für Physik* **1931**, *73*, 460 – 469.

[79] Gryczynski, I.; Kawski, A. Temperaturabhängigkeit der statischen Dielektrizitätskonstante und des optischen Brechungsindexes von Flüssigkeiten: (Auswertung zur Bestimmung des elektrischen Dipolmomentes im Anregungszustand). *Zeitschrift fur Naturforschung - Section A Journal of Physical Sciences* **1975**, *30*, 287–291.

[80] Eichler, H.-J. et al. In *Lehrbuch der Experimentalphysik - Optik - Wellen- und Teilchenoptik*; Niedrig, H., Ed.; de Gruyter, 2004.

[81] Hecht, E. *Optics*; Addison Wesley, 2002; p 698.

[82] Yariv, A. *Photonics*; Oxford University Press, 2006; p 848.

[83] Pedrotti, F. L.; Pedrotti, L. S.; Bausch, W.; Schmidt, H. In *Optik für Ingenieure - Grundlagen*; Pedrotti, F. L., Ed.; Springer Verlag - Heidelberg, 2002.

[84] Born, M.; Wolf, E. *Principles of optics*; Cambridge University Press, 1999; p 952.

[85] Baker, J. *50 Schlüsselideen Physik*; Spektrum Akademischer Verlag, 2009; pp 60–63.

[86] Conduitt, J. *Opticks or A treatise of the reflections, refractions, inflections and colours of light*; Dover Publications, 1979; p 406.

[87] Cauchy, A.-L. La Refraction et la Reflexion de la Lumiere. *Bulletin de Ferussae* **1830**, *14*, 6–10.

[88] von Sellmeier, W. Zur Erklärung der abnormen Farbenfolge im Spectrum einiger Substanzen. *Annalen der Physik und Chemie* **1871**, *143*, 272 – 282.

[89] Wei, J.; Murray, J. M.; Barnes, J. O.; Krein, D. M.; Schunemann, P. G.; Guha, S. Temperature dependent Sellmeier equation for the refractive index of GaP. *Optical Materials Express* **2018**, *8*, 485.

[90] Griffiths, D. J.; Schroeter, D. F. *Introduction to Quantum Mechanics*, 3rd ed.; Cambridge University Press, 2018; p 508.

[91] Pauli, W. Pauli exclusion principle. *Naturwiss* **1924**, *12*, 741.

[92] Hund, F. Chemical binding. *Transactions of the Faraday Society* **1929**, *25*, 646–648.

[93] Levine, I. *Quantum Chemistry*; Pearson Education, Limited, 2013.

[94] Zeeman, P. The Effect of Magnetisation on the Nature of Light Emitted by a Substance. *Nature* **1897**, *55*, 347–347.

[95] Voigt, W. Ueber das elektrische Analogon des Zeemaneffectes. *Annalen der Physik* **1901**, *309*, 197–208.

[96] Wilke, M. Influence of different substituents on the character of electronically excited states. Ph.D. thesis, Heinrich - Heine Universitaet Duesseldorf, 2017.

[97] Sager, H. In *Fourier-Transformation - Beispiele, Aufgaben, Anwendungen*, 1st ed.; Heim, T. A., Ed.; 1. Auflage; vdf Hochschulverlag AG an der ETH Zürich, 2012.

[98] Linder, B.; Hoernschemeyer, D. Cavity Concept in Dielectric Theory. *The Journal of Chemical Physics* **1967**, *46*, 784–790.

[99] Ehrenson, S. Cavity boundary effects within the onsager theory for dielectrics. *Journal of Computational Chemistry* **1981**, *2*, 41–52.

[100] Luo, Y.; Agren, H.; Mikkelsen, K. V. Unique determination of the cavity radius in Onsager reaction field theory. *Chemical Physics Letters* **1997**, *275*, 145 – 150.

[101] Demissie, E. G.; Mengesha, E. T.; Woyessaa, G. W. Modified solvatochromic equations for better estimation of ground and excited state dipole moments of p-aminobenzoicacid (PABA): Accounting for real shape over hypothetical spherical solvent shell. *Journal of Photochemistry and Photobiology A: Chemistry* **2016**, *337*, 184 – 191.

[102] Prabhumirashi, L. S. On estimating excited state dipole moments from solvent effects on electronic absorption spectra - drawbacks and improvement in the procedure. *Spectrochemica Acta* **1983**, *39A*, 91 – 92.

[103] Prabhumirashi, L. Reply to the comment of P. Suppan. *Spectrochimica Acta Part A: Molecular Spectroscopy* **1985**, *41*, 1355–1356.

[104] Suppan, P. Excited-state dipole moments from absorption/fluorescence solvatochromic ratios. *Chemical Physics Letters* **1983**, *94*, 272–275.

[105] Planck, M. *Das Princip der Erhaltung der Energie*; Druck und Verlag von B.G. Teubner, Leipzig, 1887.

[106] Lorentz, H. A. *The Theory of Electrons and Its Applications to the Phenomena of Light and Radiant Heat.*; Leiden University, 1909.

[107] Lorenz, L. Über die refractionsconstante. *Ann. Phys* **1880**, *11*, 70–103.

[108] Kirkwood, J. G. The Dielectric Polarization of Polar Liquids. *The Journal of Chemical Physics* **1939**, *7*, 911–919.

[109] Fröhlich, H. *Theory of dielectrics : dielectric constant and dielectric loss*; Oxford: Clarendon press., 1949.

[110] Reichardt, C. *Solvents and solvent effects in organic chemistry*; Wiley-VCH, 2003; p 629.

[111] Josten, M. D.; Schaad, L. Hydrogen bonding. *New York* **1974**, 599.

[112] Huggins, M. L. 50 Years of Hydrogen Bond Theory. *Angewandte Chemie International Edition in English* **1971**, *10*, 147–152.

[113] Latimer, W. M.; Rodebush, W. H. Polarity and ionization from the standpoint of the Lewis theory of valence. *Journal of the American Chemical Society* **1920**, *42*, 1419–1433.

[114] Suppan, P. Solvent effects on the energy of electronic transitions: experimental observations and applications to structural problems of excited molecules. *Journal of the Chemical Society A: Inorganic, Physical, Theoretical* **1968**, 3125.

[115] West, W.; Geddes, A. The effects of solvents and of solid substrates on the visible molecular absorption spectrum of cyanine dyes. *The Journal of Physical Chemistry* **1964**, *68*, 837–847.

[116] Nicol, M. F. Solvent Effects on Electronic Spectra. *Applied Spectroscopy Reviews* **1974**, *8*, 183–227.

[117] Kawski, A. Solvent-shift effect on electronic spectra and excited-state dipole moments. *Progress in photochemistry and photophysics* **1992**, *5*, 1–47.

[118] Bayliss, N. S.; McRae, E. G. Solvent Effects In Merocyanine Spectra. *Journal of the American Chemical Society* **1952**, *74*, 5803–5804.

[119] Bayliss, N. S.; McRae, E. G. Solvent Effects in Organic Spectra: Dipole Forces and the Franck - Condon Principle. *Journal of Physical Chemistry, 1954, 58 (11)* **1954**, *58*, 1002 – 1006.

[120] Cabannes, J. Spectroscopy applied to molecular physics. *Reports on Progress in Physics* **1944**, *10*, 378–417.

[121] Gordy, W. Microwave spectroscopy. Introductory paper: quadrupole couplings, dipole moments and the chemical bond. *Discussions of the Faraday Society* **1955**, *19*, 14–29.

[122] Hassell, W.; Magee, M.; Tucker, S.; Walker, S. New microwave procedure for determining dipole moments and relaxation times. *Tetrahedron* **1964**, *20*, 2137–2155.

[123] Scharpen, L. H.; Laurie, V. W. Microwave spectroscopy. *Analytical Chemistry* **1972**, *44*, 378–384.

[124] Buckingham, A. D.; Disch, R. L. The quadrupole moment of the carbon dioxide molecule. *Proceedings of the Royal Society of London. Series A. Mathematical and Physical Sciences* **1963**, *273*, 275–289.

[125] Dows, D. A.; Buckingham, A. Electric field-induced spectra. *Journal of Molecular Spectroscopy* **1964**, *12*, 189–197.

[126] Rodrigues, S. V.; Maiti, A.; Reis, H.; Baumann, W. Electro optical emission measurements on a non-conjugated bichromophoric donor-acceptor molecule. *Molecular Physics* **1992**, *75*, 953–960.

[127] Baumann, W.; Bischof, H.; Fröhling, J.-C.; Brittinger, C.; Rettig, W.; Rotkiewicz, K. Considerations on the dipole moment of molecules forming the twisted intramolecular charge transfer state. *Journal of Photochemistry and Photobiology A: Chemistry* **1992**, *64*, 49–72.

[128] Wilke, J. Rotationally resolved electronic Stark Spectroscopy. Ph.D. thesis, Heinrich - Heine Universitaet Duesseldorf, 2016.

[129] Schneider, M.; Hebestreit, M.-L.; Lindic, M.; Parsian, H.; Torres-Boy, A. Y.; Álvarez Valtierra, L.; Meerts, L.; Kühnemuth, R.; Schmitt, M. Rotationally resolved electronic spectroscopy of 3-cyanoindole and the 3-cyanoindole–watercomplex. *Physical Chemistry Chemical Physics* **2018**, *20*, 23441–23452.

[130] Hebestreit, M.-L.; Schneider, M.; Lartian, H.; Betz, V.; Heinrich, M.; Lindic, M.; Choi, M. Y.; Schmitt, M. Structures, dipole moments and excited statelifetime of isolated 4-cyanoindole in its groundand lowest electronically excited singlet states. *Physical Chemistry Chemical Physics* **2019**, *21*, 14766–14774.

[131] Schneider, M. Structures, dipoles and dynamics of large molecules in their excited singlet states. Ph.D. thesis, Heinrich - Heine Universitaet Duesseldorf, 2019.

[132] Hebestreit, M.-L.; Lartian, H.; Henrichs, C.; Kühnemuth, R.; Meerts, W. L.; Schmitt, M. Excited state dipole moments and lifetimes of 2-cyanoindole from rotationally resolved electronic Stark spectroscopy. *Physical Chemistry Chemical Physics* **2021**, *23*, 10196–10204.

[133] Lippert, E. Dipolmomente und elektronstrukturen von angeregten Zuständen. *Zeitschrift für Naturforschung 10A* **1955**, 541 – 545.

[134] Bilot, L.; Kawski, A. Notizen: Dipolmomente einiger Phthalimid-Derivate im ersten angeregten Singulettzustand. *Zeitschrift für Naturforschung A* **1963**, *18*, 256–256.

[135] Bilot, L.; Kawski, A. Der Einfluß des Lösungsmittels auf die Elektronenspektren lumineszierender Moleküle. *Zeitschrift für Naturforschung* **1963**, *18a*, 10 – 15.

[136] Kawski, A.; Bilot, L. Der Wellenzahl von elecktronenbanden lumineszierenden Molekuele. *Acta Phys Polon* **1966**, *29*, 507–518.

[137] Khitrova, G.; Berman, P. R.; Sargent, M. Theory of pump–probe spectroscopy. *Journal of the Optical Society of America B* **1988**, *5*, 160.

[138] Stock, G.; Domcke, W. Model studies on the time-resolved measurement of excited-state vibrational dynamics and vibronic coupling. *Chemical Physics* **1988**, *124*, 227–238.

[139] Pollard, W. T.; Lee, S.-Y.; Mathies, R. A. Wave packet theory of dynamic absorption spectra in femtosecond pump–probe experiments. *The Journal of Chemical Physics* **1990**, *92*, 4012–4029.

[140] Yan, Y. J.; Mukamel, S. Femtosecond pump-probe spectroscopy of polyatomic molecules in condensed phases. *Physical Review A* **1990**, *41*, 6485–6504.

[141] Hammon, S.; Kümmel, S. Pump-probe photoemission simulated in real time: Revealing many-particle signatures. *Physical Review A* **2021**, *104*, 012815.

[142] Brand, C. Shaping and Modelling Electronically Excited States of Indoles. Ph.D. thesis, Heinrich - Heine Universitaet Duesseldorf, 2013.

[143] Wilke, J.; Wilke, M.; Brand, C.; Meerts, W. L.; Schmitt, M. On the Additivity of Molecular Fragment Dipole Moments of 5-Substituted Indole Derivatives. *Chem Phys Chem* **2016**, *17*, 2736–2743.

[144] Debye, P. J. W. In *Polare Molekeln*; Hirzel, S., Ed.; Leipzig: S. Hirzel, 1929; Vol. 1.

[145] Sack, H. *Ergebnisse der exakten naturwissenschaften*; Springer Berlin Heidelberg, 1929; pp 307–366.

[146] Hantzsch, A. Über die Halochromie und »Solvatochromie« des Dibenzalacetons und einfacher Ketone, sowie ihrer Ketochloride. *Berichte der deutschen chemischen Gesellschaft (A and B Series)* **1922**, *55*, 953–979.

[147] El-Ayaan, U.; Murata, F.; Fukuda, Y. Thermochromism and Solvatochromism in Solution. *Chemical Monthly* **2001**, *132*, 1279–1294.

[148] Marini, A.; Munoz-Losa, A.; Biancardi, A.; benedetta Mennucci, What is Solvatochromism? *Journal of Physical Chemistry* **2010**, *114*, 17128 – 17135.

[149] Suppan, P. Thermochromic Shifts of the Fluorescnce Spectra of 4-N,N-Dimethylaminobenzonitril in Solution. *Journal of Luminescence* **1985**, *33*, 29–32.

[150] Kawski, A.; Kuklinski, B.; Bojarski, P. Thermochromic Shifts of Absorption and Fluorescence Spectra and Excited State Dipole Moment of PRODAN. *Z. Naturforschung* **2000**, *55a*, 550–554.

[151] Kawski, A.; Kukliński, B.; Bojarski, P.; Diehl, H. Ground and Excited State Dipole Moments of LAURDAN Determined from Solvatochromic and Thermochromic Shifts of Absorption and Fluorescence Spectra. *Zeitschrift für Naturforschung A* **2000**, *55*, 817–822.

[152] Kawski, A. On the Estimation of Excited - State Dipole Moments from Solvatochromic Shifts of Absorption and Fluorescence Spectra. *Zeitschrift für Naturforschung 57a, 255–262 (2002)* **2002**, *57a*, 255 – 262.

[153] Kawski, A.; Kuklinski, B.; Bojarski, P. Thermochromic Absorption, Fluorescence Band Shifts and Dipole Moments of BADAN and ACRYLODAN. *Z. Naturforschung* **2002**, *57a*, 716–722.

[154] Kawski, A.; Kuklinski, B.; Bojarski, P. Dipole moment of aniline in the excited S1 state from thermochromic effect on electronic spectra. *Chemical Physics Latters* **2005**, *415*, 251–255.

[155] Lindic, M. M.; Zajonz, M.; Gers-Panther, C.; Müller, T. J.; Schmitt, M. The excited state dipole moment of 2-[(4-methoxyphenyl)ethynyl]-3-(1-methyl-1H-indol-3-yl)-quinoxaline from thermochromic shifts. *Spectrochimica Acta Part A: Molecular and Biomolecular Spectroscopy* **2019**,

[156] Lindic, M. M.; Zajonz, M.; Hebestreit, M.-L.; Schneider, M.; Meerts, W. L.; Schmitt, M. Determination of excited state dipole moments in solution via thermochromic methods. *MethodsX* **2020**, *7*, 101101.

[157] Zajonz, M.; Oberkirch, T.; Hebestreit, M.-L.; Lindic, M. M.; Hättig, C.; Schmitt, M. Excited state dipole moments of two dicyanobenzene isomers from thermochromic shifts and ab initio calculations. *Journal of Photochemistry and Photobiology A: Chemistry* **2024**, *452*, 115589.

[158] Ahlrichs, R.; Bär, M.; Häser, M.; Horn, H.; Kölmel, C. Electronic structure calculations on workstation computers: The program system turbomole. *Chemical Physics Letters* **1989**, *162*, 165 – 253.

[159] Hättig, C.; Weigend, F. CC2 excitation energy calculations onlarge molecules using the resolution of theidentity approximation. *The Journal of Chemical Physics* **2000**, *113*, 5154 – 5161.

[160] Hättig, C.; Köhn, A. Transition moments and excited-state first-order properties in the coupled-clustermodel CC2 using the resolution-of-the-identity approximation. *The Journal of Chemical Physics* **2002**, *117*, 6939 – 6951.

[161] Hättig, C. Geometry optimizations with the coupled-cluster model CC2 using the resolution-of-the-identity approximation. *The Journal of Chemical Physics* **2003**, *118*, 7751 – 7761.

[162] Hellweg, A.; Grün, S. A.; Hättig, C. Benchmarking the performance of spin-component scaled CC2 in ground and electronically excited states. *Physical Chemistry Chemical Physics* **2008**, *10*, 4119.

[163] Deglmann, P.; Furche, F.; Ahlrichs, R. An efficient implementation of second analyticalderivatives for density functional methods. *Chemical Physics Letters* **2002**, *362*, 511 – 518.

[164] Klamt, A.; Schüürmann, G. COSMO: a new approach to dielectric screening in solvents with explicit expressions for the screening energy and its gradient. *J. Chem. Soc., Perkin Trans. 2* **1993**, 799–805.

[165] Schäfer, A.; Klamt, A.; Sattel, D.; Lohrenz, J. C. W.; Eckert, F. COSMO Implementation in TURBOMOLE: Extension of an efficient quantum chemical code towards liquid systems. *Physical Chemistry Chemical Physics* **2000**, *2*, 2187–2193.

[166] Lunkenheimer, B.; Köhn, A. Solvent Effects on Electronically Excited States Using the Conductor-Like Screening Model and the Second-Order Correlated Method ADC2. *Journal of Chemical Theory and Computation* **2012**, *9*, 977–994.

[167] Christiansen, O.; Koch, H.; Jørgensen, P. The second-order approximate coupled cluster singles and doubles model CC2. *Chemical Physics Letters* **1995**, *243*, 409–418.

[168] Pabst, M. Uebergangsmomente zwischen angeregten Zustaenden mit der RI-CC2-Methode: Implementierung und Anwendung auf Triplett-Excimere. Ph.D. thesis, 2011.

[169] Vahtras, O.; Almlöf, J.; Feyereisen, M. Integral approximations for LCAO-SCF calculations. *Chemical Physics Letters* **1993**, *213*, 514–518.

[170] Hättig, C.; Weigend, F. CC2 excitation energy calculations on large molecules using the resolution of the identity approximation. *The Journal of Chemical Physics* **2000**, *113*, 5154–5161.

[171] Grimme, S. Improved second-order Møller–Plesset perturbation theory by separate scaling of parallel- and antiparallel-spin pair correlation energies. *The Journal of Chemical Physics* **2003**, *118*, 9095–9102.

[172] Klamt, A.; Jonas, V. Treatment of the outlying charge in continuum solvation models. *The Journal of Chemical Physics* **1996**, *105*, 9972–9981.

[173] Aggarwal, K.; Khurana, J. M. Synthesis, photophysical studies, solvatochromic analysis and TDDFT calculations of diazaspiro compounds. *Spectrochimica Acta Part A: Molecular and Biomolecular Spectroscopy* **2015**, *143*, 288 – 297.

[174] Jozefowicz, M.; Milart, P.; Heldt, J. R. Determination of ground and excited State dipole moments of 4,5'-diaminol[1,1':3',1"-terphenyl]-4',6'-dicarbonitrile using solvatochromic method and quantum-chemical calculations. *Spectrochimica Acta Part A: Molecular and Biomolecular Spectroscopy* **2009**, *74*, 959 – 963.

[175] Sheppard, S. E. The Effects of Environment and Aggregation on the Absorption Spectra of Dyes. *Reviews of Modern Physics* **1942**, *14*, 303–340.

[176] Bayliss, N. S. The effect of the electrostatic polarization of the solvent on electronic absorption spectra in solution. *Journal of Chemical Physics (1950), 18, 292-6* **1950**, *18*, 292 – 296.

[177] Brooker, L. G. S.; Keyes, G. H.; Sprague, R. H.; VanDyke, R. H.; VanLare, E.; VanZandt, G.; White, F. L.; Cressman, H. W. J.; Dent, S. G. Color and Constitution. X.[1] Absorption of the Merocyanines[2]. *Journal of the American Chemical Society* **1951**, *73*, 5332–5350.

[178] Simpson, W. T. A Mathematical Treatment of the Color of the Merocyanine Dyes. *Journal of the American Chemical Society* **1951**, *73*, 5359–5363.

[179] Bakhshiev, N. G.; Knyazhanskii, M. I.; Minkin, V. I.; Osipov, O. A.; Saidov, G. V. Experimental Determination of the Dipole Moments of Organic Molecules in Excited Electronic States. *Russian Chemical Reviews* **1969**, *38*, 740–754.

[180] Germer, H. A. Solvent interaction within the Hartree-Fock SCF molecular orbital formalism. *Theoretica Chimica Acta* **1974**, *34*, 145–155.

[181] Ågren, H.; Mikkelsen, K. V. Theory of solvent effects on electronic spectra. *Journal of Molecular Structure: THEOCHEM* **1991**, *234*, 425–467.

[182] Klamt, A. Calculation of UV/Vis Spectra in Solution. *The Journal of Physical Chemistry* **1996**, *100*, 3349–3353.

[183] Herbert, J. M. Dielectric continuum methods for quantum chemistry. *WIREs Computational Molecular Science* **2021**, *11*.

[184] Lindic, M. M.; Zajonz, M.; Hebestreit, M.-L.; Schneider, M.; Meerts, W. L.; Schmitt, M. Excited state dipole moments of anisole in gas phase and solution. *Journal of Photochemistry and Photobiology A: Chemistry* **2018**, *365*, 213–219.

[185] Pavia, D. L. *Introduction to Spectroscopy*; Brooks Cole, 2008; p 752.

[186] Einstein, A. Über einen die Erzeugung und Verwendung des Lichtes betreffenden heuristischen Gesichtspunkt. *Annalen der Physik* **1905**, 132 – 148.

[187] Gasnjani, S. Untersuchung von Photodioden für hohe Datenraten in optischen Empfängerschaltungen. M.Sc. thesis, Technische Universität Graz, 2015.

[188] Lindic, M. Evaluation of Ground- and Excited State Dipole Moments via Thermochromic Fluorescence Spectroscopy - Studies with Improved Solvation Effect Approximation. M.Sc. thesis, Heinrich-Heine-Universität Düsseldorf, 2018.

[189] Lindic, M. Dipole moment determination of large chromophores in solution. Ph.D. thesis, Heinrich - Heine Universitaet Duesseldorf, 2021.

[190] Göttinger, C.; Meyer, K. L.; Weichel, W.; Müller, W.; Raftery, B.; Radbruch, A. Cell-Cooling in Flow Cytometry by Peltier Elements. *Journal of Quantitative Cell Science* **1986**, *7*, 295 – 297.

[191] Bauer, A. Thermoelektrizität - Vorlesungsskript, Ludwig-Maximilians-Universität München.

[192] MacDonald, D. K. C.; Tuomi, D. Thermoelectricity: An Introduction to the Principles. *Journal of The Electrochemical Society* **1963**, *110*, 206C.

[193] MacDonald, D. K. C. *Thermoelectricity*; Dover Publications, 2006; p 144.

[194] Pelster, R.; Pieper, R.; Hüttl, I. Thermospannung - Viel Genutzt Und Fast Immer Falsch Erklärt! *Physik und Didaktik in Schule und Hochschule* **2005**, 10 – 22.

[195] Stabinger, H. Density Measurement using modern oscillating transducers. *South Yorkshire Trading Standards Unit, Sheffield* **1994**,

[196] Furtado, A.; Batista, E.; Spohr, I.; Filipe, E. Measurment of density using oscillation-type density meters calibration, traceability and uncertainties. 2009.

[197] Sze, S. M.; Ng, K. K. *Physics of Semiconductor Devices*; Wiley and Sons, Incorporated, John, 2006.

[198] Pieterse, J.-W.; Kafka, J. D.; Sheng, S. S.; Jr., W. L. N. US Patent 5,696,780, Frequency conversion system. 1997.

[199] Koechner, W. *Solid-State Laser Engineering (Springer Series in Optical Sciences)*; Springer, 2006; p 748.

[200] Eichler, H. J.; Eichler, J. *Laser Bauformen, Strahlführung, Anwendungen*; Springer Vieweg. in Springer Fachmedien Wiesbaden GmbH, 2015.

[201] Meschede, D. *Optik, Licht und Laser*; Vieweg+Teubner Verlag / GWV Fachverlage, Wiesbaden, 2008; p 568.

[202] Sirah Laser und Plasmatechnik GmbH. Matisse User's Guide Version 1.12.

[203] Boyd, R. W. *Nonlinear optics*; Academic Press, 2008; p 613.

[204] Demtroeder, W. *Experimentalphysik 2 Elektrizitaet und Optik*; Springer Spektrum, 2018; p 466.

[205] Demtroeder, W. *Laserspektroskopie*; Springer-Verlag, 1993; p 636.

[206] Gerstenkorn, S.; Luc, P. Atlas du Spectre d'Absorption de la Molecule d'Iodine. **1978**,

[207] Scoles, G., Ed. *Atomic and molecular beam methods*; Oxford University Press, 1988.

[208] Schmitt, M. *Hochaufloesende elektronische Spektroskopie an Molekuelen und Clustern. Habilitationsschrift*; 2000.

[209] Haken, H.; Wolf, H. C. *Molekülphysik und Quantenchemie. Einführung in die experimentellen und theoretischen Grundlagen (Springer-Lehrbuch)*; Springer Verlag, 1998; p 565.

[210] Ono, L.; Majima, T.; Hamamoto, Y.; Norizawa, K.; Yoshida, K.; Itoh, A. Preliminary Study of Gas Cluster Ion Beam Source. *Department of Nuclear Engineering, Kyoto University* **2023**,

[211] Ludwig Bergmann, C. S. In *Lehrbuch Der Experimentalphysik / Gase, Nanosysteme, Flüssigkeiten*; Kleinermanns, K., Ed.; Walter De Gruyter Inc, 2005; p 1105.

[212] Kochanowska-Karamyan, A. J.; Hamann, M. T. Marine Indole Alkaloids: Potential New Drug Leads for the Control of Depression and Anxiety. *Chemical Reviews* **2010**, *110*, 4489–4497.

[213] Patil, S. A.; Patil, R.; Miller, D. D. Indole molecules as inhibitors of tubulin polymerization: potential new anticancer agents. *Future Medicinal Chemistry* **2012**, *4*, 2085–2115.

[214] Kaushik, N.; Kaushik, N.; Attri, P.; Kumar, N.; Kim, C.; Verma, A.; Choi, E. Biomedical Importance of Indoles. *Molecules* **2013**, *18*, 6620–6662.

[215] Sravanthi, T.; Manju, S. Indoles — A promising scaffold for drug development. *European Journal of Pharmaceutical Sciences* **2016**, *91*, 1–10.

[216] Kim, G. H.; Lampande, R.; Im, J. B.; Lee, J. M.; Lee, J. Y.; Kwon, J. H. Controlling the exciton lifetime of blue thermally activated delayed fluorescence emitters using a heteroatom-containing pyridoindole donor moiety. *Materials Horizons* **2017**, *4*, 619–624.

[217] Ryoo, C. H.; Cho, I.; Han, J.; hoon Yang, J.; Kwon, J. E.; Kim, S.; Jeong, H.; Lee, C.; Park, S. Y. Structure Property Correlation in Luminescent Indolo[3,2-b]indole (IDID) Derivatives: Unraveling the Mechanism of High Efficiency Thermally Activated Delayed Fluorescence (TADF). *ACS Applied Materials &amp Interfaces* **2017**, *9*, 41413–41420.

[218] Ai, Q.; Chai, J.; Lou, W.; Liu, T.; Wang, D.; Deng, C.; Wang, C.; Li, G.; Liu, X.; Liu, Z.; Zhang, Q. Efficient and Stable Organic Light-Emitting Diodes Employing Indolo[2,3-b]indole-Based Thermally Activated Delayed Fluorescence Emitters. *ACS Applied Materials Interfaces* **2019**, *12*, 6127–6136.

[219] Bandini, M.; Eichholzer, A. Catalytic Functionalization of Indoles in a New Dimension. *Angewandte Chemie International Edition* **2009**, *48*, 9608–9644.

[220] Somei, M.; Yamada, F.; Kurauchi, T.; Nagahama, Y.; Hasegawa, M.; Yamada, K.; Teranishi, S.; Sato, H.; Kaneko, C. The Chemistry of Indoles. CIII. Simple Syntheses of Serotonin, N-Methylserotonin, Bufotenine, 5-Methoxy-N-methyltryptamine, Bufobutanoic Acid, N-(Indol-3-yl)methyl-5-methoxy-N-methyltryptamine, and Lespedamine Based on 1-Hydroxyindole Chemistry. *Chemical and Pharmaceutical Bulletin* **2001**, *49*, 87–96.

[221] Semenov, B. B.; Granik, V. G. Chemistry of N-(1H-indol-3-ylmethyl)-N,N-dimethylamine (Gramine): A Review. *Pharmaceutical Chemistry Journal* **2004**, *38*, 287–310.

[222] Sasidharan, R.; Manju, S. L.; Uçar, G.; Baysal, I.; Mathew, B. Identification of Indole-Based Chalcones: Discovery of a Potent, Selective, and Reversible Class of MAO-B Inhibitors. *Archiv der Pharmazie* **2016**, *349*, 627–637.

[223] Barden, T. C. *Topics in Heterocyclic Chemistry*; Springer Berlin Heidelberg, 2010; pp 31–46.

[224] Chappuis, C. J.-F.; Huber, R.; Niclass, Y.; Starkenmann, C. Simulating latrine conditions to assess perfume performance against malodour. *Flavour and Fragrance Journal* **2018**, *33*, 313–321.

[225] Mindt, M.; Kashkooli, A. B.; Suarez-Diez, M.; Ferrer, L.; Jilg, T.; Bosch, D.; dos Santos, V. M.; Wendisch, V. F.; Cankar, K. Production of indole by Corynebacterium glutamicum microbial cell factories for flavor and fragrance applications. *Microbial Cell Factories* **2022**, *21*.

[226] Ye, K.-X.; Fan, T.-T.; Keen, L. J.; Han, B.-N. A Review of Pigments Derived from Marine Natural Products. *Israel Journal of Chemistry* **2018**, *59*, 327–338.

[227] Namgung, S.; Park, H. A.; Kim, J.; Lee, P.-G.; Kim, B.-G.; Yang, Y.-H.; Choi, K.-Y. Ecofriendly one-pot biosynthesis of indigo derivative dyes using CYP102G4 and PrnA halogenase. *Dyes and Pigments* **2019**, *162*, 80–88.

[228] Nitha, P. R.; Soman, S.; John, J. Indole fused heterocycles as sensitizers in dye-sensitized solar cells: an overview. *Materials Advances* **2021**, *2*, 6136–6168.

[229] Andreani, A.; Rambaldi, M. Indole derivatives as agrochemicals. *Journal of Heterocyclic Chemistry* **1988**, *25*, 1519–1523.

[230] Ma, Q.; Zhang, X.; Qu, Y. Biodegradation and Biotransformation of Indole: Advances and Perspectives. *Frontiers in Microbiology* **2018**, *9*.

[231] Yan, W.; Zhao, S. S.; Ye, Y. H.; Zhang, Y. Y.; Zhang, Y.; Xu, J. Y.; Yin, S. M.; Tan, R. X. Generation of Indoles with Agrochemical Significance through Biotransformation by Chaetomium globosum. *Journal of Natural Products* **2019**, *82*, 2132–2137.

[232] Lee, J.-H.; Lee, J. Indole as an intercellular signal in microbial communities. *FEMS Microbiology Reviews* **2010**, *34*, 426–444.

[233] Chu, W.; Zere, T. R.; Weber, M. M.; Wood, T. K.; Whiteley, M.; Hidalgo-Romano, B.; Valenzuela, E.; McLean, R. J. C. Indole Production Promotes Escherichia coli Mixed-Culture Growth with Pseudomonas aeruginosa by Inhibiting Quorum Signaling. *Applied and Environmental Microbiology* **2012**, *78*, 411–419.

[234] Li, G.; Young, K. D. Indole production by the tryptophanase TnaA in Escherichia coli is determined by the amount of exogenous tryptophan. *Microbiology* **2013**, *159*, 402–410.

[235] Rappoport, Z. *The chemistry of the cyano group*; Interscience Pub., 1970; p 1044.

[236] Exner, O.; Mach, I. Polarization and apparent dipole moments of some symmetrical molecules. *Collection of Czechoslovak Chemical Communications* **1991**, *56*, 406–410.

[237] Murthy, S. S. N.; Gangasharan,; Nayak, S. K. Novel differential scanning calorimetric studies of supercooled organic liquids. *Journal of the Chemical Society, Faraday Transactions* **1993**, *89*, 509.

[238] Frenzel, F.; Borchert, P.; Anton, A. M.; Strehmel, V.; Kremer, F. Charge transport and glassy dynamics in polymeric ionic liquids as reflected by their inter- and intramolecular interactions. *Soft Matter* **2019**, *15*, 1605–1618.

[239] Zhang, W.; Meng, N.; Sun, R.; Li, C. Determination and Correlation of Vapor–Liquid Equilibrium Data for the Ethyl Acetate + Hexamethyl Disiloxane System at 101.3 kPa. *Journal of Chemical & Engineering Data* **2011**, *56*, 5078–5080.

[240] Pintos, M.; Bravo, R.; Baluja, M. C.; Andrade, M. I. P.; Roux-Desgranges, G.; Grolier, J.-P. E. Thermodynamics of alkanoate + alkane binary mixtures. Concentration dependence of excess heat capacities and volumes. *Canadian Journal of Chemistry* **1988**, *66*, 1179–1186.

[241] Venkatesan, D.; Amarnath D., J.; Krishna, T. S.; Biswas, P.; Dey, R. Densities, viscosities and excess parameters of octanol with alkyl(C1 – C4) acetates at varying temperatures. *Journal of Molecular Liquids* **2020**, *299*, 112221.

[242] Shirke, R.; Chaudhari, A.; More, N.; Patil, P. Temperature dependent dielectric relaxation study of ethyl acetate — Alcohol mixtures using time domain technique. *Journal of Molecular Liquids* **2001**, *94*, 27–36.

[243] Brockmann, U.; Stockhausen, M. Dielectric relaxation spectroscopy of electrolyte solutions: $ZnCl_2$ in N-methyl-2-pyrrolidone, tetramethylurea and ethylacetate. *Berichte der Bunsengesellschaft für physikalische Chemie* **1996**, *100*, 1163–1168.

[244] Yaws, C. L.; Narasimhan, P. K. *Thermophysical Properties of Chemicals and Hydrocarbons*; Elsevier, 2009; Chapter Chapter 19, pp 672–682.

[245] Dimroth, K.; Reichardt, C.; Siepmann, T.; Bohlmann, F. Ueber Pyridinium-N-phenol-betaine und ihre Verwendung zur Charakterisierung der Polaritaet von Loesungsmitteln. *Justus Liebigs Annalen der Chemie* **1963**, *661*, 1–37.

[246] Gossauer, A. *Structure and Reactivity of Biomolecules : An Introduction into Organic Chemistry*; Wiley-VCH, p 683.

[247] McGuire, B. A.; Burkhardt, A. M.; Kalenskii, S.; Shingledecker, C. N.; Remijan, A. J.; Herbst, E.; McCarthy, M. C. Detection of the aromatic molecule benzonitrile ($c-C_6H_5CN$) in the interstellar medium. *Science* **2018**, *359*, 202–205.

[248] Chitarra, O.; Lee, K. L. K.; Buchanan, Z.; Melosso, M.; McGuire, B. A.; Goubet, M.; Pirali, O.; Martin-Drumel, M.-A. Hunting the relatives of benzonitrile: Rotational spectroscopy of dicyanobenzenes. *Astronomy Astrophysics* **2021**, *652*, A163.

[249] McGuire, B. A.; Loomis, R. A.; Burkhardt, A. M.; Lee, K. L. K.; Shingledecker, C. N.; Charnley, S. B.; Cooke, I. R.; Cordiner, M. A.; Herbst, E.; Kalenskii, S.; Siebert, M. A.; Willis, E. R.; Xue, C.; Remijan, A. J.; McCarthy, M. C. Detection of two interstellar polycyclic aromatic hydrocarbons via spectral matched filtering. *Science* **2021**, *371*, 1265–1269.

[250] Borst, D. R.; Korter, T. M.; Pratt, D. On the additivity of bond dipole moments. stark effect studies of the rotationally resolved electronic spectra of aniline, benzonitrile and aminibenzonitrile. *Chemical Physical Latters* **2001**, *350*, 485 – 490.

[251] Lide, D. R. Microwave Spectrum and Structure of Benzonitrile. *The Journal of Chemical Physics* **1954**, *22*, 1577–1578.

[252] Sato-Toshima, T.; Sakiyama, M.; Seki, S. Thermochemical Estimation of Destabilization Energies of 1,2-, 1,3-, and 1,4-Dicyanobenzenes Due to Interactions between Substituents. Appendix: Dipole Moments in Solution of the Dicyanobenzenes. *Bulletin of the Chemical Society of Japan* **1980**, *53*, 2762–2767.

[253] TURBOMOLE V7.5.1 2017, a development of University of Karlsruhe and Forschungszentrum Karlsruhe GmbH, 1989–2007, TURBOMOLE GmbH, since 2007; available from http://www.turbomole.com.

[254] Dunning, T. H. J. Chem. Phys. 90, 1007 (1989); 1989 American Institute of Physics.Gaussian basis sets for use in correlatedmolecular calculations. I. The atoms boronthrough neon and hydrogen. *The Journal of Chemical Physics* **1989**, *90*, 1007 – 1023.

[255] Weigend, F.; Häser, M. RI-MP2: first derivatives and global consistency. *Theoretical Chemistry Accounts: Theory, Computation, and Modeling (Theoretica Chimica Acta)* **1997**, *97*, 331–340.

[256] Hättig, C. *Response Theory and Molecular Properties (A Tribute to Jan Linderberg and Poul Jørgensen)*; Elsevier, 2005; pp 37–60.

[257] Platt, J. R. Classification of Spectra of Cata-Condensed Hydrocarbons. *The Journal of Chemical Physics* **1949**, *17*, 484–495.

[258] Reese, J. A.; Nguyen, T. V.; Korter, T. M.; Pratt, D. W. Charge Redistribution on Electronic Excitation. Dipole Moments of *cis*- and *trans*-3-Aminophenol in Their S_0 and S_1 Electronic States. *Journal of the American Chemical Society* **2004**, *126*, 11387–11392.

[259] Fronczek, F. R. Experimental Crytal Structure Determination. *CCDC* **2014**, 967891.

[260] Deng, C.; Zheng, S.; Wang, D.; Yang, J.; Yue, Y.; Li, M.; Zhou, Y.; Niu, S.; Tao, L.; Tsuboi, T.; Zhang, Q. Improving the Stability of Green Thermally Activated Delayed Fluorescence OLEDs by Reducing the Excited-State Dipole Moment. *The Journal of Physical Chemistry C* **2019**, *123*, 29875–29883.

[261] Wada, Y.; Kaji, H. Dipole Moment in the Excited State: An Important Property for TADF Hosts. *Chem* **2018**, *4*, 2018–2019.

[262] Ihn, S.-G. et al. Dipole Moment- and Molecular Orbital-Engineered Phosphine Oxide-Free Host Materials for Efficient and Stable Blue Thermally Activated Delayed Fluorescence. *Advanced Science* **2021**, *9*.

[263] Exner, O. *Dipole moments in Organic chemistry*; Thieme, 1975; p 156.

[264] Williams, D. E. Representation of the molecular electrostatic potential by atomic multipole and bond dipole models. *Journal of Computational Chemistry* **1988**, *9*, 745–763.

[265] Bader, R. F. Atoms in molecules. *Accounts of chemical research* **1985**, *18*, 9–15.

[266] Freeman, D. E.; Klemperer, W. Electric Dipole Moment of the 1A2 Electronic State of Formaldehyde. *The Journal of Chemical Physics* **1966**, *45*, 52–57.

[267] Lombardi, J. R.; Campbell, D.; Klemperer, W. Electric Dipole Moment of the $n - \pi^*$ Singlet State of HCOF. *The Journal of Chemical Physics* **1967**, *46*, 3482–3486.

[268] Korter, T. M.; Borst, D. R.; Butler, C. J.; Pratt, D. W. Stark Effects in Gas-Phase Electronic Spectra. Dipole Moment of Aniline in Its Excited S1 State. *Journal of the American Chemical Society* **2000**, *123*, 96–99.

[269] Nguyen, T. V.; Pratt, D. W. Permanent electric dipole moments of four tryptamine conformers in the gas phase: A new diagnostic of structure and dynamics. *The Journal of Chemical Physics* **2006**, *124*.

[270] Wilke, J.; Wilke, M.; Meerts, W. L.; Schmitt, M. Determination of ground and excited state dipole moments via electronic Stark spectroscopy: 5-methoxyindole. *The Journal of Chemical Physics* **2016**, *144*.

[271] Brieger, M.; Hese, A.; Renn, A.; Sodeik, A. The dipole moment of 7LiH in the electronically excited a $1\sigma+$ state. *Chemical Physics Letters* **1980**, *76*, 465–468.

[272] Ohta, N.; Tanaka, T. Stark quantum beats and electric dipole moment in the S1 state of pyrimidine vapor. *The Journal of Chemical Physics* **1993**, *99*, 3312–3319.

[273] Liptay, W. *Excited States*; Elsevier, 1974; pp 129–229.

[274] Samanta, A.; Fessenden, R. W. Excited-State Dipole Moment of 7-Aminocoumarins as Determined from Time-Resolved Microwave Dielectric Absorption Measurements. *The Journal of Physical Chemistry A* **2000**, *104*, 8577–8582.

[275] Abe, T.; Iweibo, I. Comparison of the excited-state dipole moments and polarizabilities estimated from solvent spectral shifts with those from electrooptical measurements. *Bulletin of the Chemical Society of Japan* **1985**, *58*, 3415–3422.

[276] Abe, T. Estimation of Angles between the Ground-and Excited-State Dipole Moments from Solvent Spectral Frequency Shifts. *Bulletin of the Chemical Society of Japan* **1991**, *64*, 3224–3228.

[277] Lombardi, J. R. Solvatochromic Shifts: A Reconsideration. *The Journal of Physical Chemistry A* **1998**, *102*, 2817–2823.

[278] Lombardi, J. R. Solvatochromic Shifts Reconsidered: Field-Induced Mixing in the Nonlinear Region and Application to Indole. *The Journal of Physical Chemistry A* **1999**, *103*, 6335–6338.

[279] Lindic, M. M.; Schmitt, M. Ground and excited state dipole moments of 1-methylindole from thermochromic shifts in absorption and emission spectra. *Journal of Photochemistry and Photobiology A: Chemistry* **2021**, *406*, 112984.

[280] Lindic, M. M.; Oberkirch, T. A.; Tatchen, J.; Schmitt, M. The excited state effective dipole moment of 2,3-benzofuran from thermochromic shifts in absorption and emission spectra. *Journal of Photochemistry and Photobiology A: Chemistry* **2021**, *419*, 113476.

[281] Weber, G. Fluorescence-polarization spectrum and electronic-energy transfer in tyrosine, tryptophan and related compounds. *Biochemical Journal* **1960**, *75*, 335–345.

[282] Hilaire, M. R.; Mukherjee, D.; Troxler, T.; Gai, F. Solvent dependence of cyanoindole fluorescence lifetime. *Chemical Physics Letters* **2017**, *685*, 133–138.

[283] Markiewicz, B. N.; Mukherjee, D.; Troxler, T.; Gai, F. Utility of 5-Cyanotryptophan Fluorescence as a Sensitive Probe of Protein Hydration. *The Journal of Physical Chemistry B* **2016**, *120*, 936–944.

[284] Hilaire, M. R.; Ahmed, I. A.; Lin, C.-W.; Jo, H.; DeGrado, W. F.; Gai, F. Blue fluorescent amino acid for biological spectroscopy and microscopy. *Proceedings of the National Academy of Sciences* **2017**, *114*, 6005–6009.

[285] Talukder, P.; Chen, S.; Roy, B.; Yakovchuk, P.; Spiering, M. M.; Alam, M. P.; Madathil, M. M.; Bhattacharya, C.; Benkovic, S. J.; Hecht, S. M. Cyanotryptophans as Novel Fluorescent Probes for Studying Protein Conformational Changes and DNA–Protein Interaction. *Biochemistry* **2015**, *54*, 7457–7469.

[286] Acharyya, A.; Ahmed, I. A.; Gai, F. *Chemical Tools for Imaging, Manipulating, and Tracking Biological Systems: Diverse Methods for Optical Imaging and Conjugation*; Elsevier, 2020; pp 191–215.

[287] van Wilderen, L. J. G. W.; Brunst, H.; Gustmann, H.; Wachtveitl, J.; Broos, J.; Bredenbeck, J. Cyano-tryptophans as dual infrared and fluorescence spectroscopic labels to assess structural dynamics in proteins. *Physical Chemistry Chemical Physics* **2018**, *20*, 19906–19915.

[288] Abou-Hatab, S.; Matsika, S. Theoretical Investigation of Positional Substitution and Solvent Effects on n-Cyanoindole Fluorescent Probes. *The Journal of Physical Chemistry* **2019**, *123*, 7424–7435.

[289] Henrichs, C.; Reineke, M.; Hebestreit, M.-L.; Schmitt, M. Excited state structure of isolated 4-cyanoindole from a combined Franck-Condon and rotational constants analysis†. *Journal of Molecular Structure* **2021**, *1223*, 129241.

[290] Oeltermann, O.; Brand, C.; Engels, B.; Tatchen, J.; Schmitt, M. The structure of 5-cyanoindole in the ground and the lowest electronically excited singlet states, deduced from rotationally resolved electronic spectrascopy and ab initio theory. *Physical Chemistry Chemical Physics* **2012**, *14*, 10266 – 10270.

[291] Wilke, J.; Wilke, M.; Brand, C.; Meerts, W. L.; Schmitt, M. On the Additivity of Molecular Fragment Dipole Moments of 5-Substituted Indole Derivatives. *ChemPhysChem* **2016**, *17*, 2736–2743.

[292] Henrichs, C.; Zimmermann, S.; Hebestreit, M.-L.; Schmitt, M. Excited state structure of isolated 2-cyanoindole and the binary 2-cyanoindole-$(H_2O)1$ cluster from a combined Franck-Condon and rotational constants fit. *Journal of Molecular Structure* **2021**, *1233*, 130055.

[293] Min, A.; Ahn, A.; Moon, C. J.; Lee, J. H.; Choi, M. Y.; Kim, S. K. Conformational structures of 3-cyanoindole-(H_2O) n (n = 0–2) by UV–UV hole-burning and IR-dip spectroscopy. *Chemical Physics Letters* **2014**, *614*, 263–268.

[294] Ahn, A.; Min, A.; Moon, C. J.; Lee, J. H.; Choi, M. Y. Conformational structures of 3-cyanoindole-(H_2O) (n= 0–2): Franck–Condon simulations. *Chemical Physics Letters* **2014**, *616–617*, 55–60.

[295] Min, A.; Moon, C. J.; Ahn, A.; Lee, J. H.; Kim, S. K.; Choi, M. Y. Electronic and vibrational spectroscopic studies of jet-cooled 5-cyanoindole and its water clusters, 5CI–(H_2O) , (n= 0–2). *Chemical Physics Letters* **2016**, *658*, 63–70.

[296] Kang, C.; Korter, T. M.; Pratt, D. W. Experimental measurement of the induced dipole moment of an isolated molecule in its ground and electronically excited states: Indole and indole–H_2O. *The Journal of Chemical Physics* **2005**, *122*.

[297] Lombardi, J. R. On the comparison of solvatochromic shifts with gas phase Stark effect measurements. *Spectrochimica Acta Part A: Molecular Spectroscopy* **1987**, *43A*, 1323–1324.

[298] Bakshiev, N. Opt. i. Spektroscopiya, 16, 821 - 832. *Spectry* **1964**, *16*, 446.

[299] Reichardt, C. Solvatochromic dyes as solvent polarity indicators. *Chemical Reviews* **1994**, *94*, 2319–2358.

[300] Lami, H.; Glasser, N. Indole's solvatochromism revisited. *The Journal of Chemical Physics* **1986**, *84*, 597–604.

[301] Catalan, J.; Diaz, C. First reported evidence that solvent polarity induces an $\leftrightarrow$ inversion in the indole chromophore. *Chemical Physics Letters* **2003**, *368*, 717–723.

[302] Roy Meech, S.; Phillips, D.; Lee, A. G. On the nature of the fluorescent state of methylated indole derivatives. *Chemical Physics* **1983**, *80*, 317–328.

[303] Mataga, N.; Torihashi, Y.; Ezumi, K. Electronic structures of carbazole and indole and the solvent effects on the electronic spectra. *Theoretica Chimica Acta* **1964**, *2*, 158–167.

[304] Gurusinghe, R. M.; Tubergen, M. J. Probing the Electronic Environment of Methylindoles using Internal Rotation and 14N Nuclear Quadrupole Coupling. *The Journal of Physical Chemistry A* **2016**, *120*, 3491–3496.

[305] Korter, T. M.; Pratt, D. W. Perturbations of the Fully Resolved Electronic Spectra of Large Molecules by the Internal Rotation of Attached Methyl Groups. Influence of Complex Formation. *The Journal of Physical Chemistry B* **2001**, *105*, 4010–4017.

[306] Remmers, K.; Jalviste, E.; Mistrik, I.; Berden, G.; Meerts, W. L. Internal rotation effects in the rotationally resolved $S_1(1Lb) \leftarrow S$ origin bands of 3-methylindole and 5-methylindole. *The Journal of Chemical Physiscs* **1998**, *108*, 8436–8445.

[307] Jalviste, E.; Ohta, N. Stark absorption spectroscopy of indole and 3-methylindole. *The Journal of Chemical Physics* **2004**, *121*, 4730–4739.

[308] Hebestreit, M.-L.; Boeschen, H.; Lartian, H.; Meerts, W. L.; Schmitt, M. Rotationally resolved electronic spectroscopy of 6-methylindole: Structures, transition moments, and permanent dipole moments of ground and excited singlet states. *Journal of Molecular Structure* **2022**, *1252*, 132053.

[309] Guesten, H.; Klasinc, L.; Ruscic, B. Photoelectron Spectroscopy of Heterocycles. Indene Analogs. *Zeitschrift für Naturforschung A* **1976**, *31*, 1051–1056.

[310] Lin, J. L.; Zhang, S.; Tzeng, W. B. Mass analyzed threshold ionization spectroscopy of 5-methylindole and 3-methylindole cations and the methyl substitution effect. *The Journal of Chemical Physics* **2004**, *120*, 5057–5063.

[311] Rehms, A. A.; Callis, P. R. Resolution of La and Lb bands in methyl indoles by two-photon spectroscopy. *Chemical Physics Letters* **1987**, *140*, 83–89.

[312] Iadicicco, A.; Cusano, A.; Cutolo, A.; Bernini, R.; Giordano, M. Thinned Fiber Bragg Gratings as High Sensitivity Refractive Index Sensor. *IEEE Photonics Technology Letters* **2004**, *16*, 1149–1151.

[313] Wu, D. K. C.; Kuhlmey, B. T.; Eggleton, B. J. Ultrasensitive photonic crystal fiber refractive index sensor. *Optics Letters* **2009**, *34*, 322.

[314] Xu, Y.; Bai, P.; Zhou, X.; Akimov, Y.; Png, C. E.; Ang, L.; Knoll, W.; Wu, L. Optical Refractive Index Sensors with Plasmonic and Photonic Structures: Promising and Inconvenient Truth. *Advanced Optical Materials* **2019**, *7*.

[315] Haque, E.; Anwar Hossain, M.; Namihira, Y.; Ahmed, F. Microchannel-based plasmonic refractive index sensor for low refractive index detection. *Applied Optics* **2019**, *58*, 1547.

[316] Lopatin, P. V.; Safonov, V. P.; Litvinova, T. P.; Yakimenko, L. M. Use of nonaqueous solvents to prepare injection solutions. *Pharmaceutical Chemistry Journal* **1972**, *6*, 724–733.

[317] Cagli, E.; Liu, H.; Khokhar, V.; Klemm, A.; Gurkan, B. E. Thermal and Physical Properties of CO_2-Reactive Binary Mixtures. *Journal of Chemical & Engineering Data* **2024**, *69*, 2676–2687.

[318] Rahman, M. S.; Roy, R.; Montoya, C.; Halim, M. A.; Raynie, D. E. Acidic and basic amino acid-based novel deep eutectic solvents and their role in depolymerization of lignin. *Journal of Molecular Liquids* **2022**, *362*, 119751.

List of Figures

List of Tables

A. Supplementary Material

A.1. Supplementary to Chapter 8

Table A.1.: BN S_0 Cartesian geometry SCS-CC2/cc-pVTZ in Bohr.

Atom	Coord.	Coord.	Coord.
C	-2.78510654770674	-2.07397750633172	-0.00065638075952
C	-4.42875347346047	-0.00804503610364	-0.00114161991966
C	-3.46690471856425	2.45064639688674	-0.00001425616521
C	-0.86421300721344	2.85337827870892	0.00150320470105
C	0.78113285107767	0.77684988581654	0.00216486312777
C	-0.17918850347953	-1.69238657251163	0.00100631905167
H	-0.09886703159991	4.74846723526785	0.00204796449615
C	3.46838289495843	1.18228296287141	0.00414988914905
N	5.66533762592656	1.51419454678022	0.00579956504093
H	1.11028336797262	-3.27800376127567	0.00144379229260
H	-3.52947024630032	-3.97765916621049	-0.00160163398738
H	-6.45047468652260	-0.31264041714134	-0.00239734149034
H	-4.73917791142724	4.05041180873632	-0.00023279499364

Table A.2.: BN S_1 Cartesian geometry SCS-CC2/cc-pVTZ in Bohr.

Atom	Coord.	Coord.	Coord.
C	-2.81882372	-2.11700850	-0.00048833
C	-4.51341269	-0.02083650	-0.00121486
C	-3.51202220	2.48186886	-0.00016552
C	-0.84081978	2.90529195	0.00161647
C	0.87321873	0.79101519	0.00224672
C	-0.14142142	-1.73469400	0.00108574
H	-0.08978350	4.80415232	0.00263939
C	3.51590234	1.18929455	0.00393692
N	5.72381514	1.52187732	0.00539745
H	1.13593269	-3.32780224	0.00145631
H	-3.54772897	-4.02492541	-0.00117734
H	-6.53110558	-0.32496986	-0.00243232
H	-4.77077043	4.09025498	-0.00082907

Table A.3.: 1,2-DCB S_0 Cartesian geometry SCS-CC2/cc-pVTZ in Bohr.

Atom	Coord.	Coord.	Coord.
C	-1.76136993584408	-3.08553848136883	-0.00125216169287
C	-3.40378917198719	-1.01846939426014	-0.00223791973210
C	-2.44537006647503	1.43453680022069	-0.00142234288063
C	0.17029432468794	1.83574345515735	0.00035197609187
C	1.82670071742784	-0.24905734040993	0.00126924639286
C	0.84477449264884	-2.70630514109007	0.00045842493087
C	1.14010439017613	4.37094888511429	0.00091320011091
C	4.51557724408673	0.12302622171904	0.00277326408232
N	6.72338842412715	0.37852234093099	0.00409968039785
H	2.13287668582981	-4.29241035650265	0.00104113957373
H	-2.50640565498574	-4.98845734212972	-0.00174515357645
H	-5.42585895758141	-1.31420621752522	-0.00347376120147
H	-3.69917836560351	3.04787369676728	-0.00212044340227
N	1.88825587349248	6.46379287337696	0.00134485090532

Table A.4.: 1,2-DCB S_1 Cartesian geometry SCS-CC2/cc-pVTZ in Bohr.

Atom	Coord.	Coord.	Coord.
C	-1.79459378	-3.14203629	-0.00102214
C	-3.46636883	-1.03799223	-0.00230502
C	-2.48229849	1.46272525	-0.00183238
C	0.20720942	1.91157300	0.00029037
C	1.90910650	-0.23014792	0.00106041
C	0.86397094	-2.74873436	0.00069407
C	1.14388436	4.41147350	0.00148075
C	4.55591872	0.11719280	0.00234520
N	6.77591682	0.36291593	0.00317173
H	2.15257104	-4.33353432	0.00166772
H	-2.52756418	-5.04688898	-0.00132081
H	-5.48759182	-1.32139982	-0.00369522
H	-3.73476458	3.07624258	-0.00300516
N	1.88460389	6.51861087	0.00247048

Table A.5.: 1,3-DCB S_0 Cartesian geometry SCS-CC2/cc-pVTZ in Bohr.

Atom	Coord.	Coord.	Coord.
C	-2.80666610751423	-2.04946650542469	-0.00064100359475
C	-4.45321616241570	0.00696643910282	-0.00098049997365
C	-3.47865793858830	2.47113954441300	0.00016912246305
C	-0.86654817029450	2.87970431317228	0.00177497808409
C	0.76632801654785	0.80008965868088	0.00219344527393
C	-0.20013908172486	-1.66724445707898	0.00097831815956
H	-0.11727906658131	4.78051867633879	0.00258032113735
C	3.45394517862840	1.20162055716263	0.00394336990390
N	5.65203864273856	1.52415037791587	0.00542192393974
H	1.08747062851035	-3.25403663924710	0.00152843264221
H	-3.55491692917682	-3.95063930199778	-0.00181359667044
H	-6.47684503635626	-0.27717364798105	-0.00227574254022
C	-5.17227170765364	4.59632817688265	-0.00055147183291
N	-6.56307040562063	6.32883116564012	-0.00131805253561

Table A.6.: 1,3-DCB S_1 Cartesian geometry SCS-CC2/cc-pVTZ in Bohr.

Atom	Coord.	Coord.	Coord.
C	-2.82429873	-2.09483701	-0.00064664
C	-4.52330928	-0.00633258	-0.00109996
C	-3.53420817	2.51895181	0.00011439
C	-0.84607036	2.93211000	0.00198379
C	0.83959485	0.79781331	0.00235577
C	-0.15759619	-1.72429623	0.00101694
H	-0.09853285	4.83214066	0.00307530
C	3.48514361	1.20604467	0.00394087
N	5.69075692	1.54406597	0.00524157
H	1.12207080	-3.31406069	0.00126576
H	-3.57207011	-3.99502386	-0.00163238
H	-6.54324247	-0.29749125	-0.00232293
C	-5.19206987	4.62066501	-0.00074223
N	-6.57599629	6.37103855	-0.00154071

A.2. Supplementary to Chapter 10

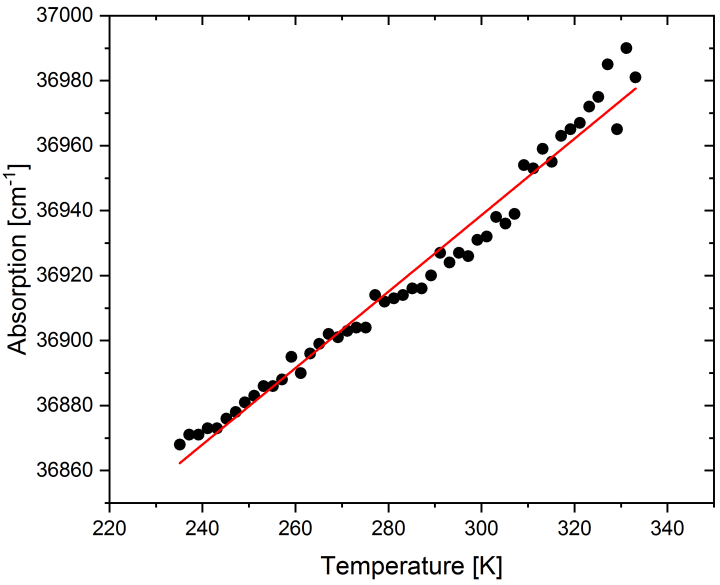

Figure A.1.: Absorption maxima of 2-methylindole and its fit function.

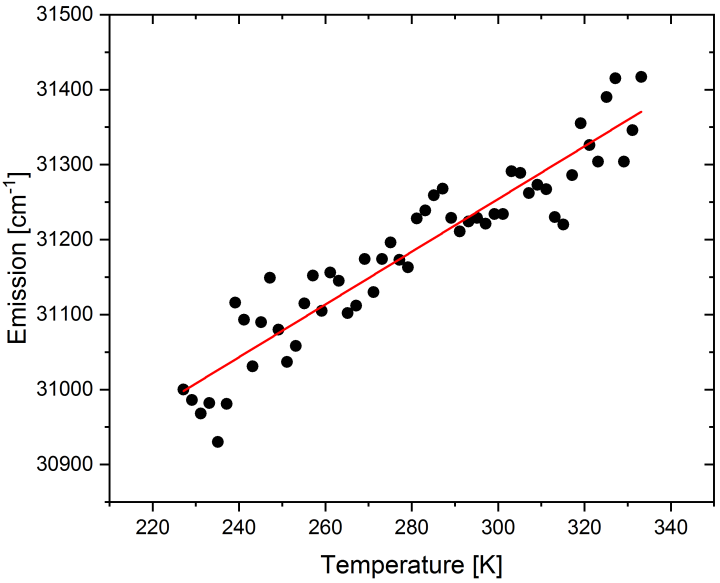

Figure A.2.: Emission maxima of 2-methylindole with fit function.

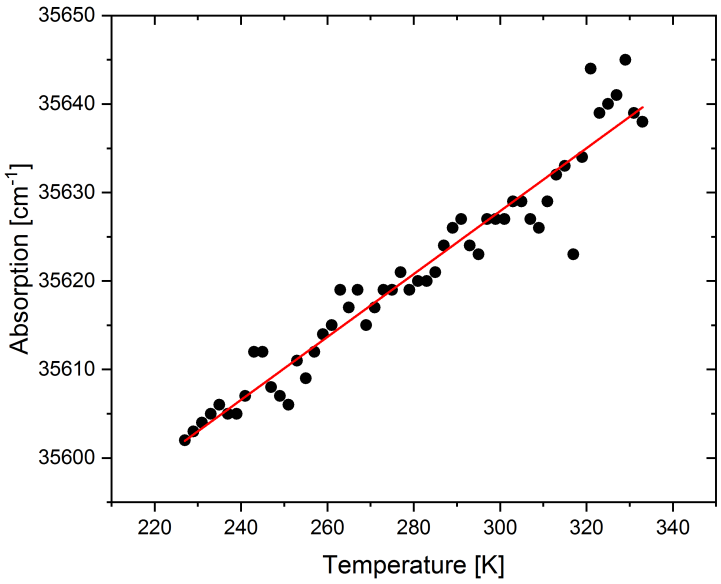

Figure A.3.: Absorption maxima of 3-methylindole and its fit function.

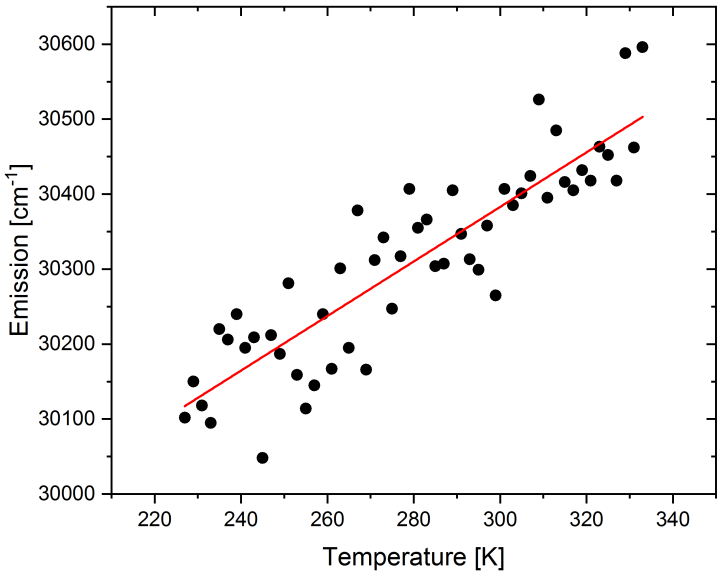

Figure A.4.: Emission maxima of 3-methylindole with fit function.

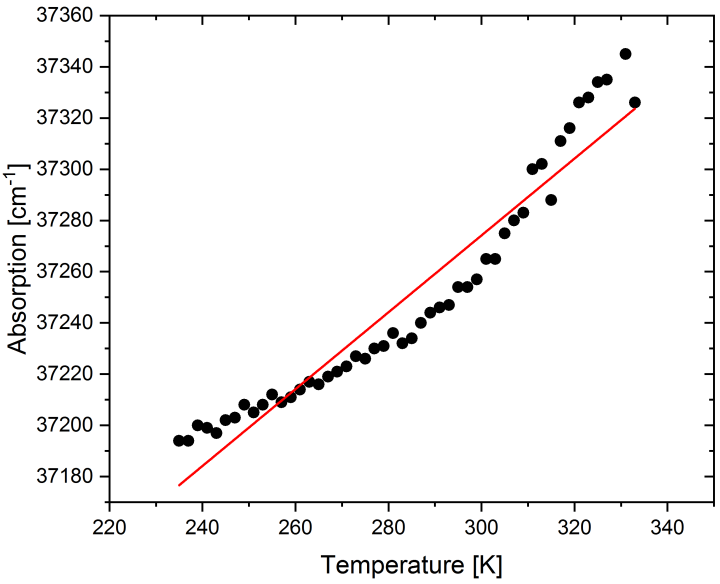

Figure A.5.: Absorption maxima of 4-methylindole and its fit function.

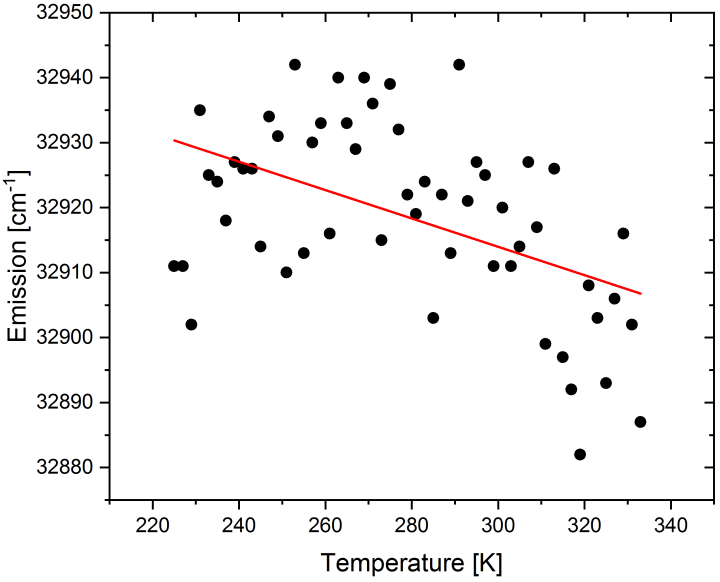

Figure A.6.: Emission maxima of 4-methylindole with fit function.

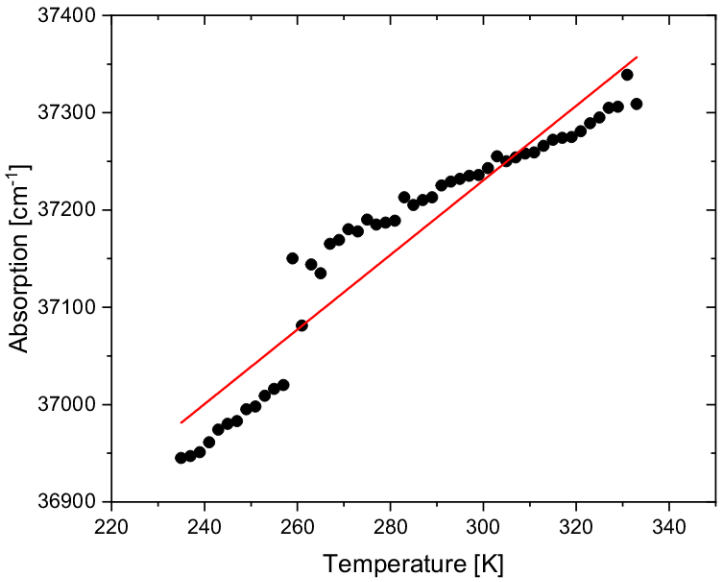

Figure A.7.: Absorption maxima of 5-methylindole and its fit function.

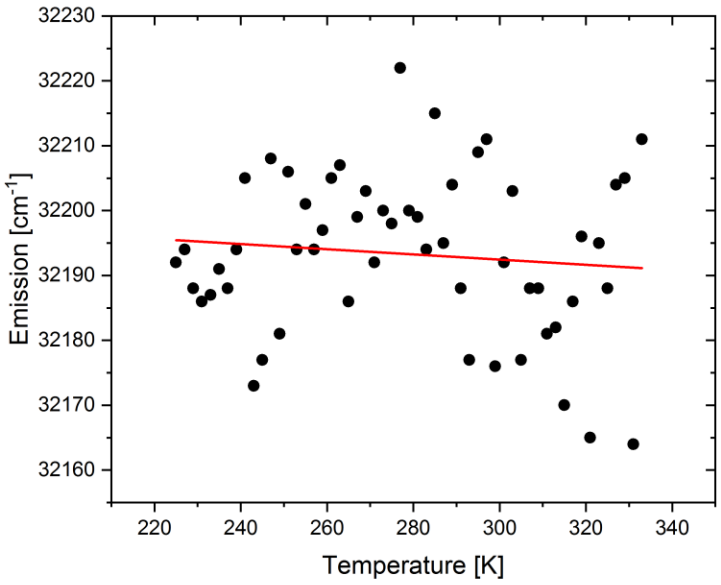

Figure A.8.: Emission maxima of 5-methylindole with fit function.

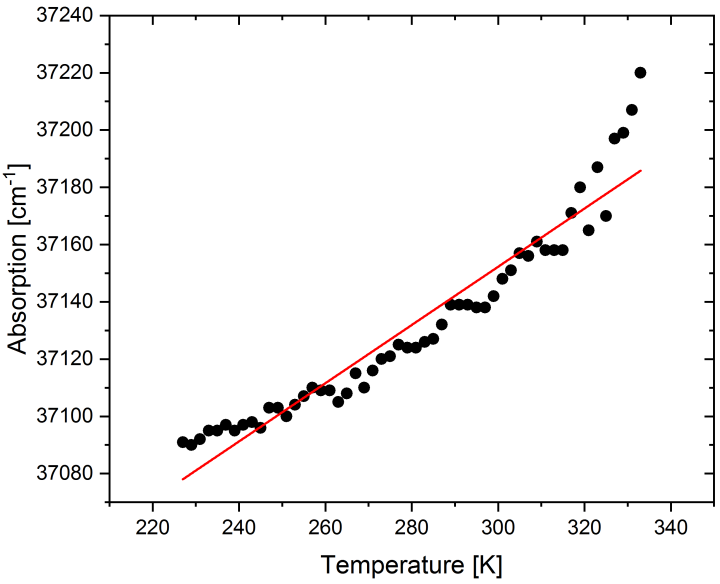

Figure A.9.: Absorption maxima of 6-methylindole and its fit function.

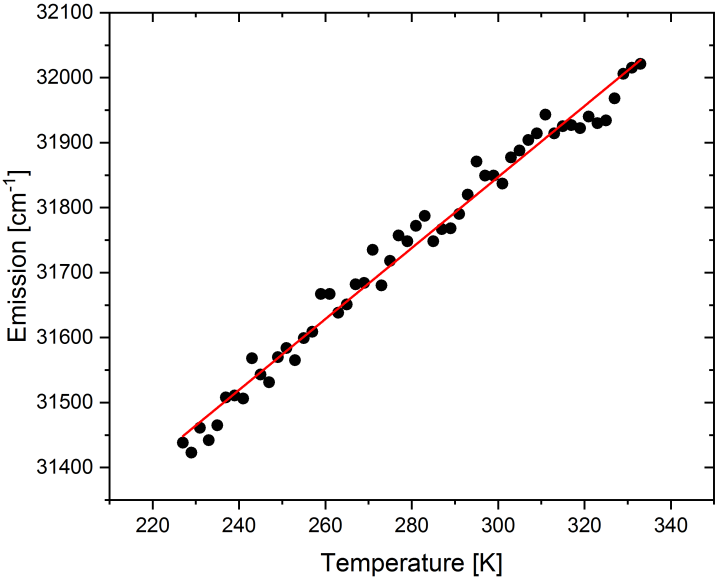

Figure A.10.: Emission maxima of 6-methylindole with fit function.

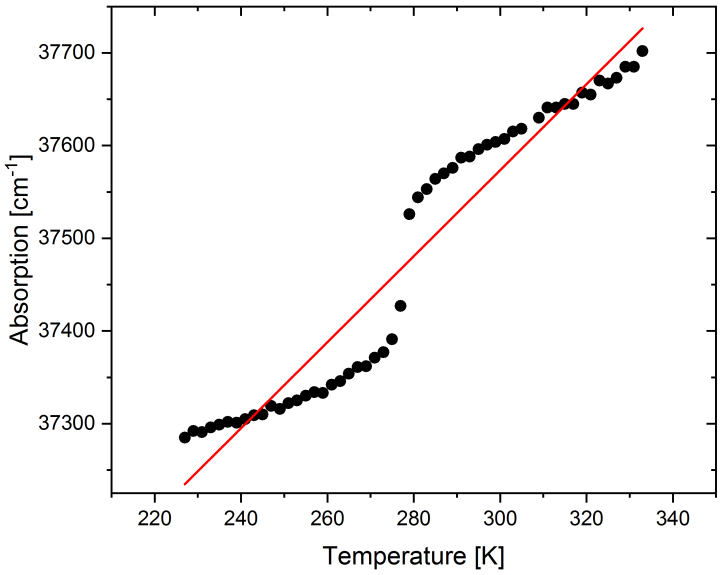

Figure A.11.: Absorption maxima of 7-methylindole and its fit function.

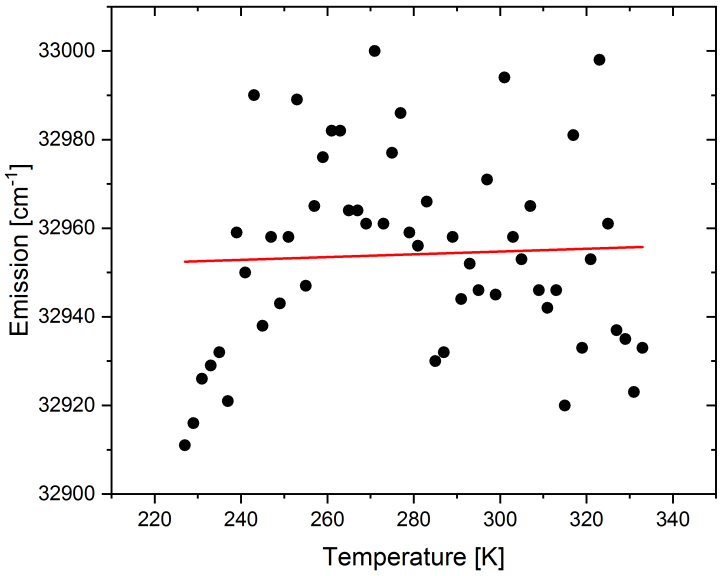

Figure A.12.: Emission maxima of 7-methylindole with fit function.